Photochemical Synthesis of Dihydroquinolinones and their Investigation Toward Macrocycle Synthesis via Ring Expansion.

By

CHIPO MAGURA

(MGRCHI001)

SUBMITTED TO THE UNIVERSITY OF CAPE TOWN

In fulfilment of the requirements for the degree

MSc Chemistry

FACULTY OF SCIENCE

UNIVERSITY OF CAPE TOWN

DATE OF SUBMISSION: 24-02-2023

SUPERVISOR: DR. WADE F. PETERSEN

CO-SUPERVISOR: DR. MARWAAN RYLANDS

DEPARTMENT: CHEMISTRY

UNIVERSITY OF CAPE TOWN

DECLARATION

I, *Chipo Magura*, hereby declare that the work on which this dissertation/thesis is based is my original work (except where acknowledgements indicate otherwise) and that neither the whole work nor any part of it has been, is being, or is to be submitted for another degree in this or any other university.

I empower the university to reproduce for the purpose of research either the whole or any portion of the contents in any manner whatsoever.

Signature: ……. Signed by candidate

Date: …24-02-2023…….

DEDICATION

In loving memory of my beautiful mother. I am ever grateful for her undying love which continues to inspire me to be the best person I can be.

ACKNOWLEDGEMENTS

My sincere gratitude and appreciation go to my supervisor Dr Wade F. Petersen for his guidance and support that have helped me grow as a scientist.

Many thanks to my co-supervisor Dr Marwaan Rylands for teaching, guiding and encouraging me.

My sincere appreciation goes to the Peterson Research Group and the Hunter Research Group for being pleasant colleagues and great exchange of ideas in the group meetings.

Thank you to the Royal Society (FLR\R1\190531;FCG\R1\201007) and the University of Cape Town for financial assistance.

To my dad, thank you for your loving support, thank you for always cheering me on. Your faith in me inspires me to keep going.

To my siblings, thank you for your encouragement and providing laughter when I needed it.

To my dear friends Ruvimbo and Alice, thank you for being the people I could lean on and thank you for the fun times.

To my Cape Town church family, I count myself blessed to have come to known each of you. Thank you for lending an ear, for support, love and care. Thank you for the adventures.

To my beloved husband, thank you for being my best friend, you have been and continue to be there for me when I need you. Thank you for supporting me, encouraging me and holding my hand through this journey. I truly appreciate your love and I love you!

Most importantly, I thank God for being a constant source of comfort and strength. You have seen me through it all and kept your promise to never leave me nor forsake me.

ABSTRACT

Graphical: An efficient triplet energy transfer process catalysed by an iridium photocatalyst for the synthesis *N*-unsubstituted 3,4-dihydroquinolin-2(1*H*)-ones, featuring a formal C(sp^2)-H/C(sp^3)-H hydroarylation is reported. The 3,4-dihydroquinolin-2(1*H*)-one products were subsequently investigated as novel substrates in a Successive Ring Expansion (SuRE) macrocyclization protocol to effect the synthesis of the next generation of therapeutic macrocycles that could be used in fighting the African disease burden of illnesses such as tuberculosis and malaria.

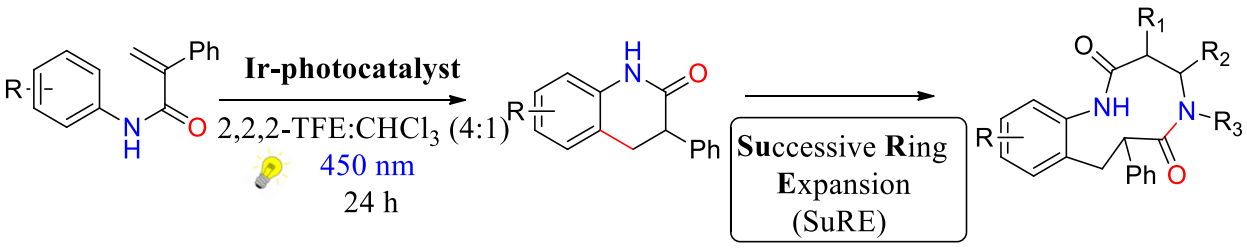

There are several macrocyclic drugs that are currently on the market. As representative examples, erythromycin and azithromycin are currently approved antibiotics. Macrocycles are also used to treat other infectious diseases, for example, natamycin and amphotericin B are used as antifungal agents and ivermectin is used as an antiparasitic agent.[1] The synthesis of macrocyclic compounds is typically done using an end-to-end macrocyclization approach. However, challenges arise due to competing intermolecular reactions leading to the use of high dilution conditions. It is therefore important that synthetic chemists develop general and modular methods for their synthesis in order to produce the next generation of therapeutic macrocyclic drugs. One such method is the **Su**ccessive **R**ing **E**xpansion (SuRE) protocol developed by Unsworth and co-workers at the University of York, offering an innovative and straightforward way to access such compounds. With this methodology, a cyclic starting material such as a lactam, is coupled to a *N*-protected β-amino acid fragment which is then deprotected to yield the ring-expanded cyclic product following rearrangement.

Given our group's interest in the development of dihydroquinolinones (DHQs) and realizing that their suitability for SuRE had not yet been investigated, we recognised an opportunity to collaborate with the Unsworth group, as it would enable the synthesis of more diversely functionalised macrocyclic molecules. Visible-light mediated triplet energy transfer has enabled the synthesis of *N*-substituted DHQs by our group and others through a formal C(sp^2)-H/C(sp^3)-H hydroarylation.[2–5] However, none of these methods have reported such syntheses producing the *N*-unsubstituted DHQ

— which is required for the SuRE. Thus we first set out to optimise this photochemical cyclisation to enable the direct formation of *N*-unsubstituted DHQs. Gratifyingly, this reaction was successfully developed, requiring the use of an iridium photocatalyst, and was able to provide a diverse range of unprotected DHQs that could be investigated in the SuRE

In application towards the synthesis of macrocycles using the SuRE methodology, a model DHQ was first investigated. Unfortunately, in the event, the *N*-unsubstituted DHQ was obtained instead of the ring-expanded product.After facing this challenge, **C**onjugate **A**ddition or **R**ing **E**xpansion (CARE) method, also developed by the Unsworth and co-workers was considered[6], however the acylation to generate the key starting material was unsuccessful. To overcome the acylation, and in a third strategy (returning to a SuRE approach), we thought to replace the amide linker with an alkyl chain instead and effect a SuRE macrocyclization following a Staudinger deprotection in the presence of triphenylphosphine. The intermediate was successfully synthesised, and while a trial reaction revealed promising results, this is still under investigation. Analysis of the product mixture by NMR suggested the desired product formation, however residual triphenylphosphine oxide (TPPO) complicated this analysis. Time constraints prevented further investigation, however methods to remove or avoid the formation of TPPO will be a topic of future work.

Since our direct DHQ synthesis requires an expensive iridium photocatalyst, we considered a demethylation strategy for the synthesis of *N*-unsubstituted DHQs from *N*-methyl DHQs — as these can be accessed using inexpensive thioxanthone photosensitisers.[3] A related demethylation of amides was reported by Yi *et al* using a Cu catalyst and NFSI as an oxidant[7] and in our attempt to use this procedure to produce the unprotected DHQ, we obtained the unsaturated quinolinone, instead. Quinolinones are important biological molecules and are used as antiviral, anticancer, antiulcer, and antihistaminic agents in medicinal chemistry, and thus we were very pleased with this result. These relatively mild oxidation conditions also offer opportunities for late-stage functionalization.[8] Ultimately, through the use of photocatalysis, we could develop this oxidation chemistry to avoid the need for a metal — favouring a thioxanthone photosensitiser over a copper catalyst, and the reaction could be conducted at ambient temperature, rather than at 80 ^{o}C as per Yi *et al*'s conditions. This methodology is of great importance because existing methods for this transformation make use of expensive transition metals such as Pd[8–10] and Pt[11] or require even higher temperatures.[12]

Table of Contents

DECLARATION.....2
Dedication.....3
Acknowledgements.....4
Abstract.....5
List of Tables.....8
List of Abbreviations.....9
CHAPTER 1: INTRODUCTION.....12
1.0 Introduction to Macrocycles and their Importance.....12
1.1 African Disease Burden.....17
1.2 Macrocycles in Drug Discovery: Advantages and Disadvantages.....19
1.3 Synthesis of Macrocycles.....20
Chapter 2: DHQs.....29
2.0 Importance of DHQs.....29
2.2 Approaches to the Photochemical Synthesis of Dihydroquinolinones (DHQs).....32
2.3 Results and Discussion.....32
2.3.1 Synthesis of Acrylanilides.....32
2.3.2 Catalyst Screening and Optimization for the Formation of DHQs.....37
Chapter 3: Macrocycle Synthesis via SuRE.....45
3.1 Results and Discussion.....45
3.2 Future Work and Considerations.....61
Chapter 4: Quinolinones.....63
4.1 A Serendipitous Discovery.....63
4.2 Results and Discussion.....63
4.2.1 Preliminary Studies.....63
4.2.2 Catalyst Screen and Optimization.....65
4.3 Conclusions and Recommendations.....73
Chapter 5: Experimental.....74
General procedures.....74
2.0 Synthesis of Acrylanilides and β-lactams.....75
2.1 Synthesis of DHQs.....80
3.0 Synthesis of Medium-Sized Rings.....86
3.1 Synthesis Starting from β-keto Esters.....86
3.2 Synthesis Starting from Lactams.....89
4.0 Synthesis of quinolinones.....93
6.0 References.....98
Appendices.....105

LIST OF TABLES

Table 1: Optimisation Studies.....38
Table 2. Optimisation Studies.....66

LIST OF ABBREVIATIONS

2CMPI	2-Chloro-1-methylpyridinium iodide
2-CTX	2-Chorothioxanthone
2D-NMR	Two-dimensional nuclear magnetic resonance spectroscopy
2-iPrTX	2-Isopropylthioxanthone
2-ITX	2-Iodothioxanthone
4CzIPN	1,2,3,5-Tetrakis(carbazol-9-yl)-4,6-dicyanobenzene
ACN	Acetonitrile
AIDS	Acquired Immunodeficiency Syndrome
Ar	Aromatic
β	Beta
Bn	Benzyl
Boc	Tert-butoxycarbonyl
CARE	Conjugated Addition and/Ring Expansion
COSY	Correlated Spectroscopy
Covid-19	Coronavirus disease
CuDMP	$[Cu(DMP)_2Cl]Cl$
DBU	1,8-Diazabicyclo[5.4.0]undec-7-ene
DCM	Dichloromethane
dd	doublet of doublets
ddt	doublet of doublet of triplets
DHQ	Dihydroquinolinone
DIPEA	*N*,*N*-Diisopropylethylamine
DMAP	4-Dimethylaminopyridine
DMF	*N*,*N*-Dimethylformamide
DMSO	Dimethylsulfoxide
DNA	Dioxyribonucleic acid
EDR	Extensively Drug Resistant
EnT	Energy transfer
eq.	Equivalence
EtOAc	Ethyl acetate
EtOH	Ethanol

Fmoc	Fluorenylmethyloxycarbonyl
h	Hour(s)
HAT	Hydrogen Atom Transfer
HIV	Human Immunodeficiency Virus
HMBC	Heteronuclear Multiple Bond Correlation
HOMO	Highest Occupied Molecular Orbital
HRMS	High Resolution Mass Spectrometry
HSQC-DEPT	Heteronuclear Single Quantum Coherence-Distortionless Enhancement by Polarization Transfer
$IrdCF_3$	$Ir[dF(CF_3)ppy]_2(dtppy)PF_6$
ISC	Intersystem crossing
J	Coupling constant
LCMS	Liquid Chromatography Mass Spectrometry
LED	Light Emitting Diode
LUMO	Lowest Unoccupied Molecular Orbital
m	multiplet
MDR	Multi-Drug Resistant
Me	Methyl
MeOD	Deuterated methanol
MeOH	Methanol
min	Minute(s)
m/z	Mass to charge ratio
nBuLi	n-Butyllithium
NFSI	*N*-Fluorobenzenesulfonimide
NHSI	*N*-(Phenylsulfonyl)benzenesulfonamide
NMR	Nuclear Magnetic resonance
NSI	Benzenesulfonamide, N-(phenylsulfonyl)-, ion(1-)
PET	Petroleum ether
ppm	Parts per million
PT	Proton Transfer

q	quartet
RCM	Ring Closing Metathesis
R_f	Retention factor
RT	Room Temperature
s	singlet
S_0	Ground state
S_1	Singlet state
SET	Single Electron Transfer
SuRE	Successive Ring Expansion
t	Triplet
T_1	Triplet state
TB	Tuberculosis
TEA	Triethylamine
TFE	Trifluoroethanol
THF	Tetrahydrofuran
TLC	Thin Layer Chromatography
TMS	Trimethylsilane
TPO	Triphenylphosphine oxide
TPP	Triphenylphosphine
UN	United Nations
UV	Ultraviolet
WHO	World Health Organisation

CHAPTER 1: INTRODUCTION

1.0 Introduction to Macrocycles and their Importance

Macrocyclic compounds are generally described as cyclic molecules with ≥ 12-memberedrings.[13–16]There are many naturally occurring and synthetic examples of macrocycles (**Figure 1**). Naturally occurring macrocycles can be found from terrestrial and marine sources with some having more than 50 atoms in their cyclic framework — ring sizes greater than 35 rarely occur in nature, but the most common scaffolds have 14, 16 and 18 atoms in their rings.

This preference to form even-numbered macrocycles in nature, mentioned in the previous paragraph, was studied, but yielded inconclusive results because of the complexity and high number of biosynthetic pathways. Favoured mechanisms of macrocyclizations have been identified in non-ribosomal and polyketide synthases and it is possible that the preference for even-numbered macrocycles is a result of the specificity of these biosynthetic pathways. However, the same preference for an even number of atoms has been observed in laboratory synthesis of macrolactones and macrocyclic alpha-nitrile imines. This preference was in line with the formation of less strained rings, favourable cyclization reactions and minimal transannular reactions.[17] The ring strain is more significant in smaller ring sizes (11-13 membered rings).[14]

Macrocycles can be classified as either *natural* or *synthetic* with each having subclasses of peptidic and non-peptidic macrocycles.[18] Examples of natural product macrocycles are erythromycin and rapamycin which are used as antibiotics (**Figure 1A**). Erythromycin is a macrolide used in the treatment of bacterial infections and was originally isolated from *Streptomyces erythraeus.*[13] Rapamycin is produced by the bacterium *Streptomyces hygroscopicus* and is used as an immunosuppressant. Examples of synthetic macrocycles are crown ethers, cyclosporine and ocreotide (**Figure 1B**).[14] Crown ethers were the first subclass of synthetic macrocycles and found use in the recognition of metal ions. Ocreotide is an octapeptide which imitates somatostatin, a hormone that is responsible for inhibiting growth hormones, thus making ocreotide suitable for the treatment of tumors that produce growth hormones. Cyclosporine is a natural product from the fungus *Tolypocladium inflatum GAMS* and it is used as an immunosuppressant.[13]

A)

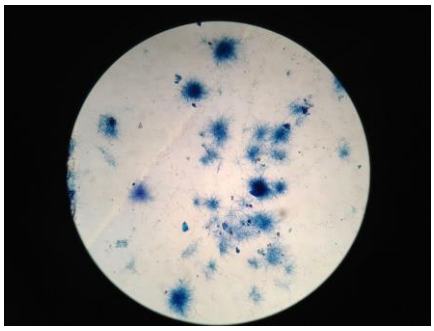

Streptomyces erythraeus
blue-dyed bacteria

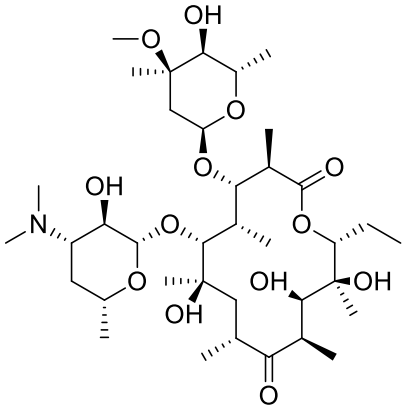

Erythromycin

Colonies of *Streptomyces hygroscopicus*

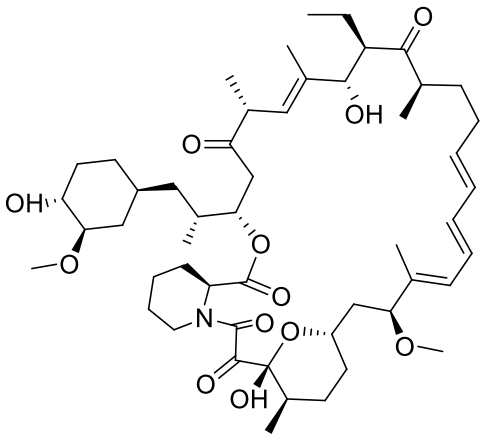

Rapamycin

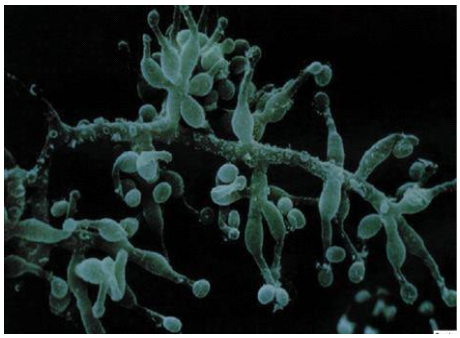

Tolypocladium inflatum

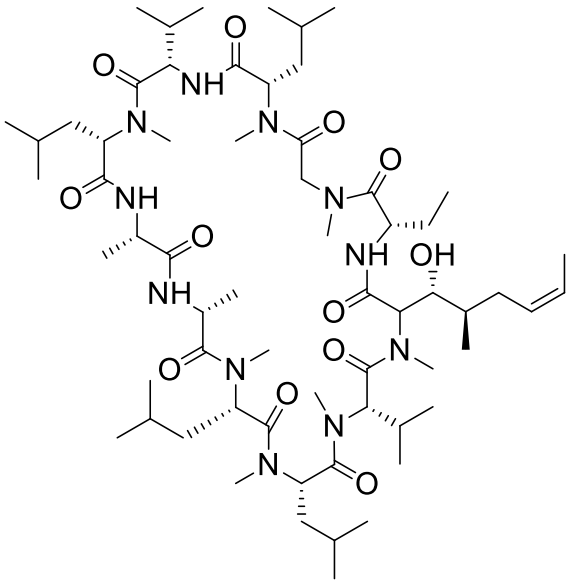

Cyclosporine A

Figure 1: A) Examples of natural macrocycles.

B)

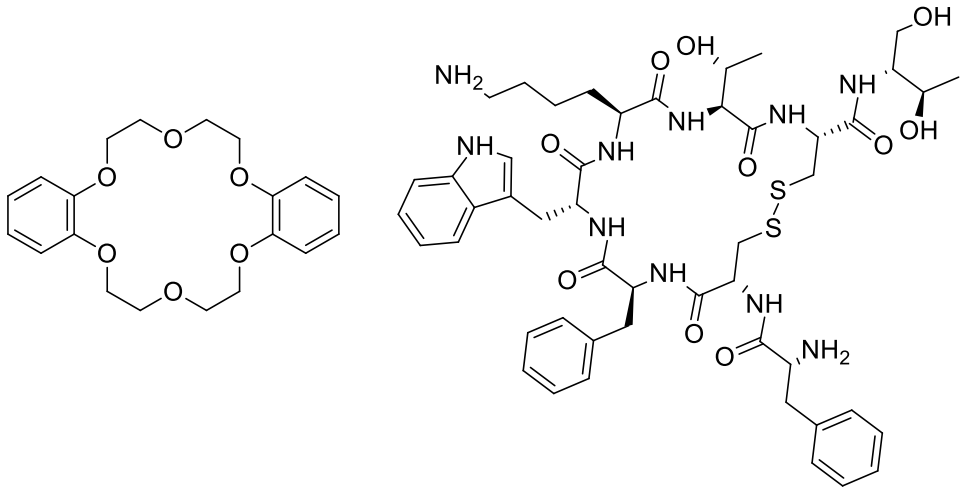

Dibenzo-18-crown-6 Ocreotide

Figure 2: B) Examples of synthetic macrocycles.

Macrocycles have wide applications in various fields such as medicinal chemistry, catalysis, materials science, chiral sensing, supramolecular chemistry, self-assembly, nanotechnology, natural product synthesis and more.[19] Of particular interest is their application in medicinal chemistry.[20] There are over 100 marketed macrocyclic drugs with proven success.[13] According to a study conducted on 74 macrocyclic drugs currently on the market, more than 50% are used to fight infectious diseases, mostly those caused by bacteria.[21] As examples, natamycin and amphotericin B are used as antifungal agents and ivermectin is used as an antiparasitic agent (**Figure 2**).[15]

Cyclic peptides have also been shown to have high therapeutic potentials because of their resistance to both exo and endo proteases which are responsible for the breaking down of protein via hydrolysis of the peptide bonds to form polypeptides and amino acids.[22] Proteases are vital to the reproductive cycle of some viruses such as HIV, thus inhibition of proteases by macrocyclic peptides such as simeprevir (**Figure 3**) demonstrates the possibility of using them as antiviral agents. Macrocycles also find use as chemotherapeutic agents, for example, dactinomycin and epothilone B (**Figure 3**).[15] About 13.5% of 74 macrocyclic drugs considered are used in the treatment of cancer. The remaining 32.4% have varying uses including treatment of cardiovascular diseases, and various applications in gynaecology and immunology.[21]

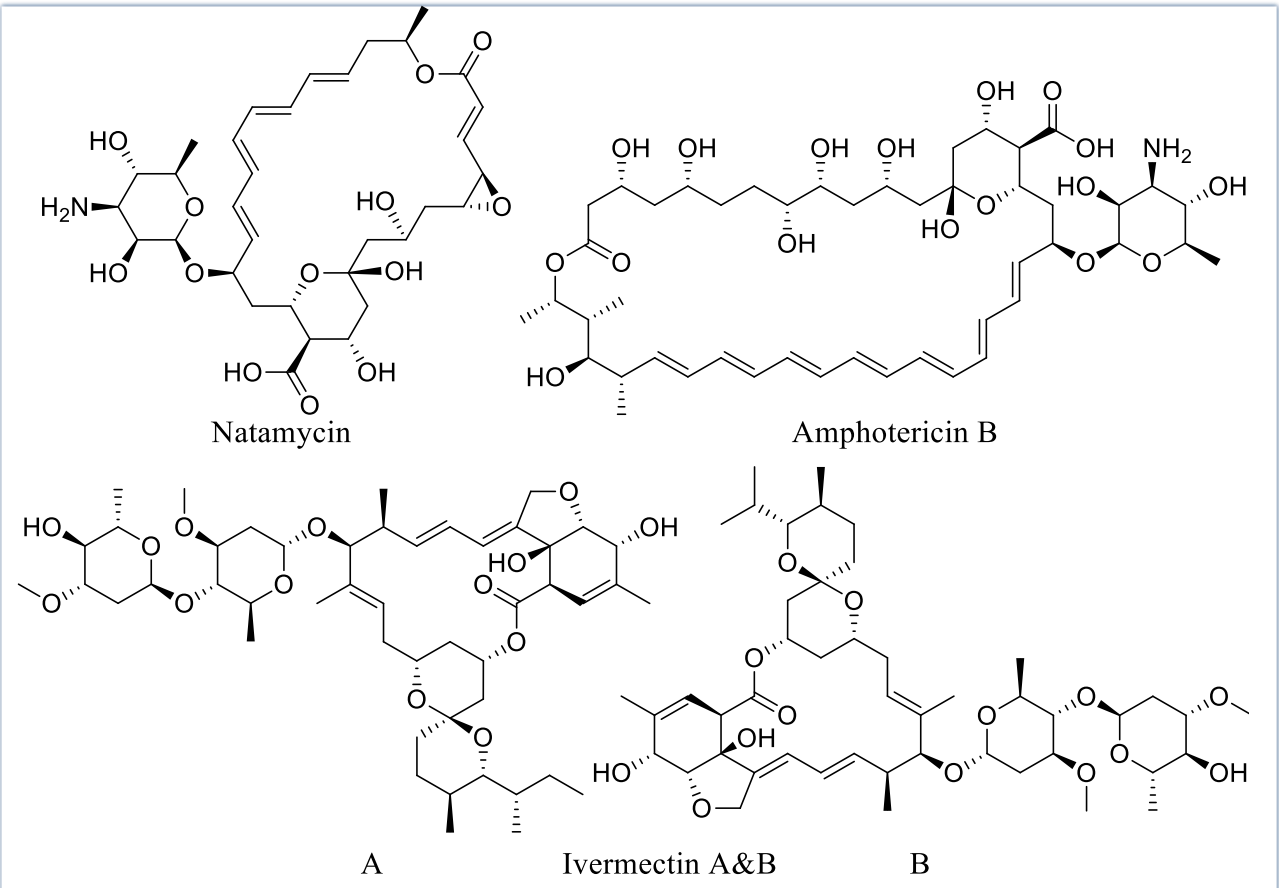

Figure 3: Examples of approved antifungal and antiparasitic macrocyclic drugs.

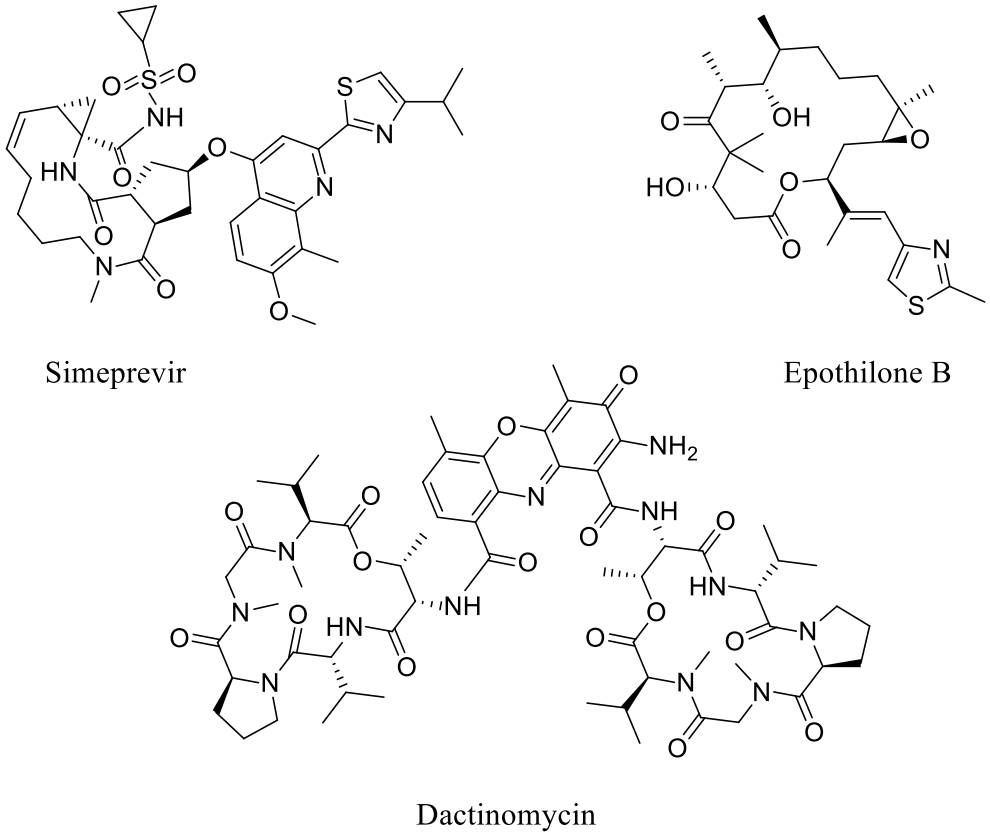

Figure 4: Examples of approved antiviral and anti-cancer macrocyclic drugs.

Studies are still ongoing to discover more macrocyclic drug leads. A macrocyclic spectrum selective kinase inhibitor for chemotherapy has been discovered.[23] A macrocyclic compound for the treatment of rheumatoid arthritis has also been identified.[24] A natural macrocycle, Nannocystin A (**Figure 4**) which acts against myxobacteria and prohibits proliferation was discovered and characterized. This 21-membered macrocyclic scaffold has nine stereo centres and studies showed that the high activity was dependent on the epoxide moiety.[25]

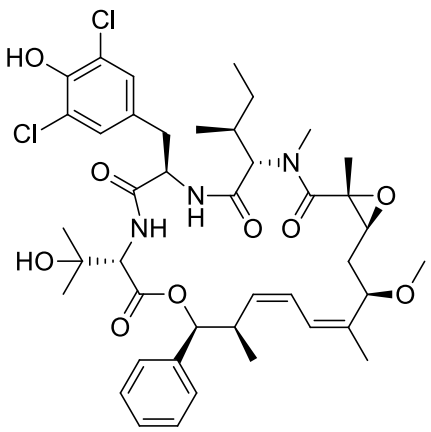

Figure 5: Nannocystin A.

1.1 African Disease Burden

Africa is the second largest continent with a population of approximately 1.4 billion people — about 45 people per km^2. Many parts of Africa are affected by extreme hunger and poverty. Eradicating hunger and poverty is one of the UN's millennium development goals for Africa.[26] Hunger and poverty create a fertile environment for the transmission of deadly airborne diseases such as tuberculosis (TB). Africa bears a significant portion of the world's disease burden alongside poor countries in Asia and Latin America.[27]

Tuberculosis, a disease caused by *Mycobacterium tuberculosis*, is included in the top 10 causes of death world-wide. Tuberculosis is the greatest cause of death by only one infectious agent, even more than HIV/AIDS. It is estimated that 10 million people (globally) were ill due to TB infection in 2019. Of these, an estimated 1.2 million died from those who were HIV negative. An additional 208 000 died from those who were HIV positive. The WHO African region contributed 25% of the global total of TB deaths. South Africa contributed 3.6% to the estimated global cases in 2019 placing it in the top eight countries. It is hard to control this disease because it is airborne and mostly affects the poor communities and many people also have latent TB. Genetic mutations and poor compliance to treatment regimens give rise to drug resistance. Poor compliance is in part due to the lengthy periods of treatment as well as usage of a combination of drugs. Current TB medications last for six months for drug-susceptible TB to 20 months or even more for Multi-Drug Resistant (MDR) TB.[28] There has been a substantial increase in cases of Extensively-Drug Resistant (EDR) TB in South Africa since 2000.[29] Globally, 206 030 people were detected to have Multi-Drug Resistant MDR-TB in 2019 which was a 10% increase from the previous year. The global success rate for the treatment of MDR-TB is around 57%. Further challenges to treatment include the limited number of paediatric formulations and that TB medication in HIV positive people is often complexed by drug-to-drug interactions.[28]

On the other hand, the number of malaria cases has decreased over the years. Although fewer regions still struggle with this disease, malaria eradication remains a top priority. Malaria is caused by parasites, the most common and widespread in sub-Saharan Africa being the *Plasmodium falciparum.*[30,31] The estimated global total of malaria cases in 2019 was 229 million. The WHO African region contributed 94% of the cases. 409 000 deaths were recorded globally, with Africa having the highest contribution (about 92%). Drug resistance has been on the increase since the 1980s when chloroquine resistance was detected. Artemisinins, which are usually used in the treatment of malaria are still being used effectively in most parts of Africa. However drug resistance has been detected in Southeast Asia and potential resistance has been identified in Angola.[31,32] Artemisinin drug resistance has been linked to PfKelch13 mutations.[25]

In a nutshell, there has been a lot of investment over several decades to eradicate TB and malaria, but these still contribute significantly to the African continent's disease burden. A major contributing factor has been the development of drug resistance. Drug resistance develops when microbes such as bacteria, parasites, viruses, and fungi stop responding to treatments. There are various mechanisms by which this happens as pictured in **Figure 5**. A change in the drug target which can be brought about by genetic mutation, drug uptake inhibition as a result of a change in the cell wall protein, breaking down of the drug by enzymes resulting in inactivation or the cell activates efflux pumps thereby preventing an accumulation of the drug within the cell. It is therefore vital and urgent that new drug scaffolds are developed to combat drug resistance.

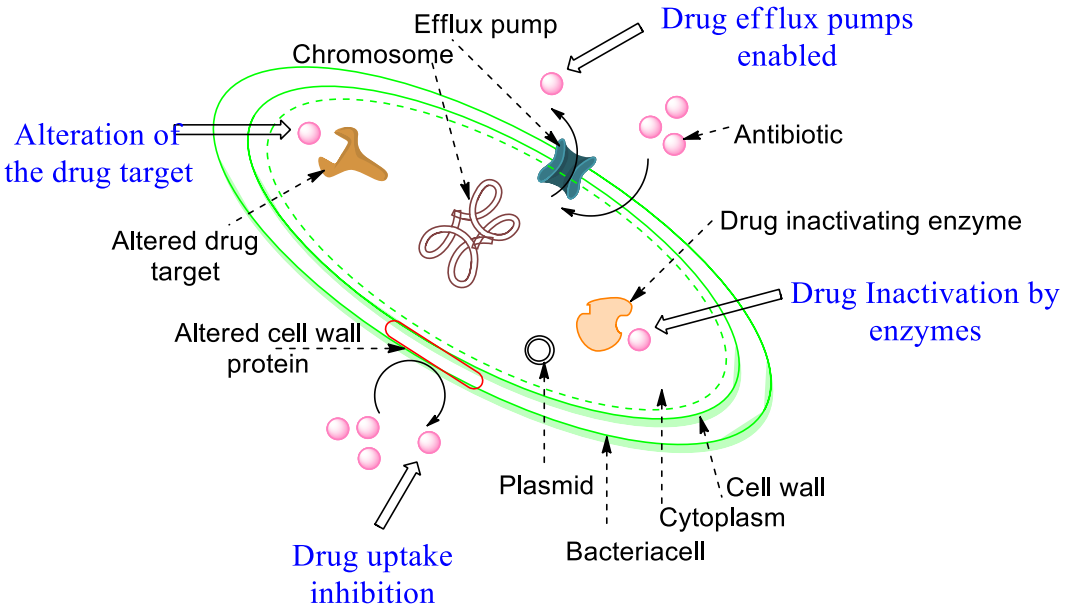

Figure 6: Mechanisms of antimicrobial drug resistance.[89]

1.2 Macrocycles in Drug Discovery: Advantages and Disadvantages

Although macrocycles are some of the most successful drugs, they make up a very small fraction of the drugs available on the market. A study of one retailer in the United States showed that macrocycles made up only 3% of the marketed drugs in 2016.[33]

Disadvantages

Of those macrocycles which are being marketed, most are natural product derivations. The pharmaceutical industry has been reluctant to pursue macrocycles as drug leads for several reasons. The chief among these reasons being the challenges associated with their synthesis. Another common deterrent of macrocycles by drug discovery programs is that they typically do not adhere to Lipinski's rule of five[13] — a metric that aims to predict favourable and druggable qualities of potential compounds at an early stage. Peptide-based macrocycles have large and polar surface areas thus permeating cells and achieving good bioavailability is a challenging process.[14] While these difficulties have limited the exploration of macrocycles in drug discovery, there are several good properties associated with macrocycles that have enabled them to remain relevant in the field of medicinal chemistry.

Advantages

Macrocycles offer a good compromise between structural preorganization and flexibility. Their large size makes it possible to insert diverse binding elements at different positions thereby increasing their binding affinity to targets. This high affinity is due to a greater surface area relative to small molecules. The planar interface that the ring offers also allows for disruption of protein-protein interactions as they can easily intercalate with DNA. As a result of these structural features of macrocycles and their conformational flexibility, they offer an array of functional advantages such as high potency and selectivity.[15] Macrocycles offer diverse functionality and stereochemical complexity, although this complexity can sometimes present with unwanted toxicity.[13] In comparison to acyclic molecules of the same molecular weight, macrocycles possess a lower number of rotatable bonds which improves their bioavailability.[16] Other favourable properties of macrocycles, that make them more drug-like, include appreciable solubility, better lipophilicity, augmented membrane penetration, increased metabolic stability and desirable pharmacokinetic and pharmacodynamic properties.[3] The success of macrocycles already in use as drug molecules shows that they are well worth the effort of medicinal chemists despite the synthetic challenge that they pose.

In this context and given the aforementioned benefits and promise of macrocyclic compounds, we were interested to investigate whether we could devise new macrocyclic compounds relevant to the fight against the African disease burden.

1.3 Synthesis of Macrocycles

Macrocycles are generally considered challenging to make, contributing to their under-exploration. The most common approach to macrocycle synthesis is end-to-end cyclisation of linear precursors. Formation of large rings in this way requires that the two reacting ends of the linear precursor be in proximity — a process that has been a challenge for synthetic chemists because the number of possible conformations is large, and the entropy of activation disfavours the reaction. Entropic loss because of the ring closure can be compensated by high dilution methods or enthalpy gain if the product has more stable conformations. However, the key challenge of starting with linear precursors is the competing intermolecular reactions (**Figure 6**) which has resulted in the use of high dilution conditions in an effort to prevent intermolecular reactions. [14,15]We will briefly look at some of the methods that are used to synthesize macrocycles.

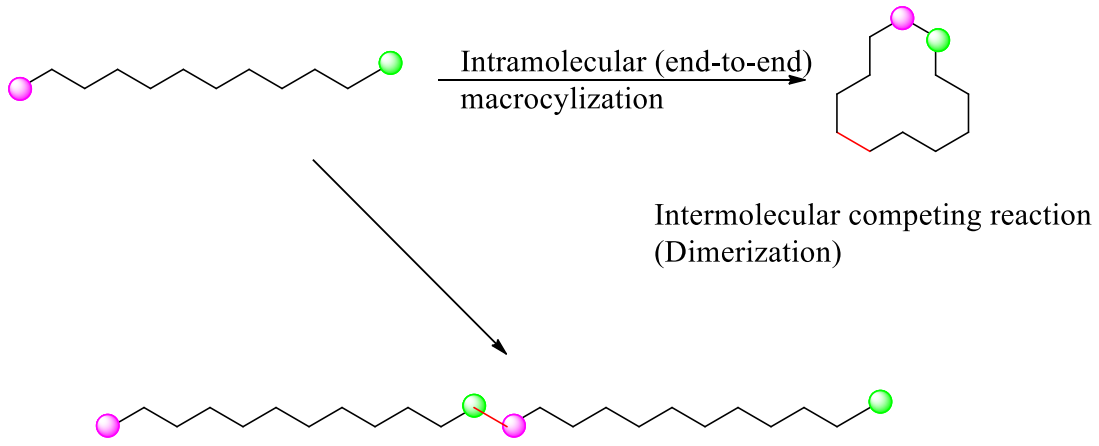

Figure 7: End-to-end macrocyclization and competing dimerization.[19]

Ring Closing Metathesis (RCM) makes use of an organometallic catalyst (usually a ruthenium carbene) to stimulate ring-closing metathesis in alkenes (**Figure 7**). A similar reaction can be applied to alkynes and is referred to as ring-closing alkyne metathesis. This reaction is generally versatile and flexible. It can be applied on various compounds as it has a high tolerance for other functionalities. It makes use of gentle reaction conditions as the catalysts are readily available and is adaptable to different ring sizes. The products are unsaturated and can thus be further exploited to add other functionalities. However, the products are produced in varying yields and usually as a combination of olefin stereoisomers. Furthermore, it can be challenging to set appropriate reaction conditions for

good yields while minimizing by-products and to remove the catalyst to acceptable pharmaceutical limits.[16,34]

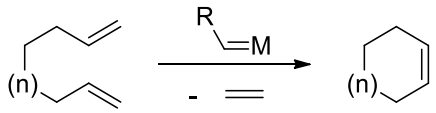

Figure 8: Ring Closing Metathesis.

Chemists are working on some of the challenges associated with RCM. A stereoselective RCM to yield *E*-macrocyclic alkenes using molybdenum monoaryloxide pyrrolide complex as the catalyst has been reported. It has been demonstrated that dienes which contain the *E*-alkenyl-B (pinacolato) group had the right steric and electronic properties for conversion to *E*-macrocyclic alkenes. The reactions gave yields with a maximum of 73% and *E/Z* ratios greater than 98/2. The practicality of this method was demonstrated by synthesis of an antibiotic called recifeiolide containing a 12-membered ring and an enzyme inhibitor known as pacritinib which possesses a 18-membered ring (**Figure 8**).[35]

The nature of the catalyst seems to have an effect on the *E/Z* ratios and thermodynamic stability in the synthesis of macrocycles using ruthenium catalysts.[36] The synthesis of steroidal 13 and 16 membered rings with Grubbs second generation catalyst has been achieved with preparatory reactions from readily available steroids affording the precursor dienes for the intramolecular metathesis. Heat was used on the catalyst to activate the reaction and the reaction yielded exclusively trans isomers at about 27% yield on average **(Figure 9**).[37] RCM has also been used in combination with other methods to afford macrocycles such as macrocyclic peptidomimetics using RCM and solid-phase synthesis[38] as well as thiazole-containing macrocycles synthesized with solid phase chemistry using Ru-catalysed RCM.[39]

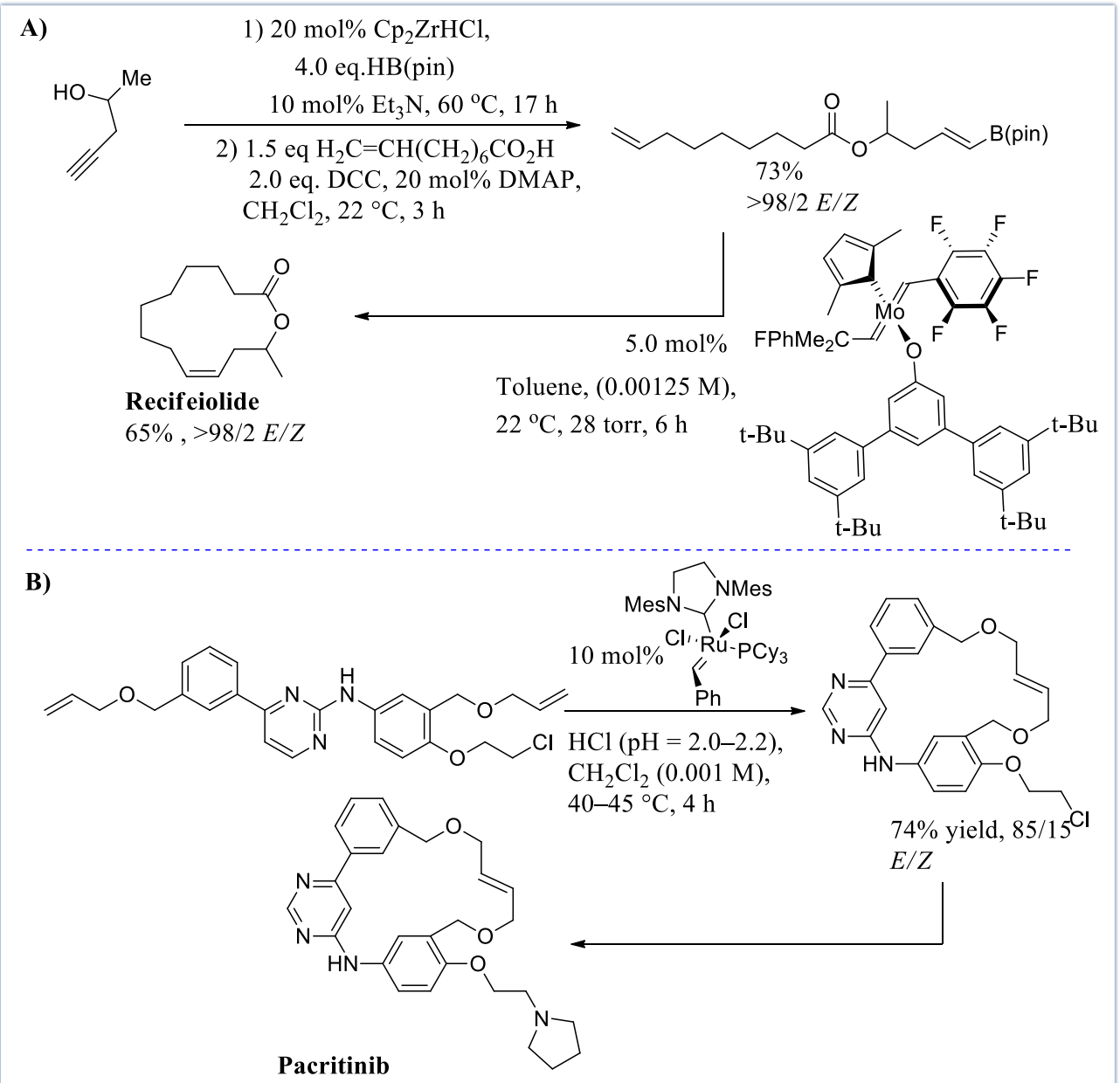

Figure 10: RCM synthesis of A) Recifeiolide. B) Pacritinib.

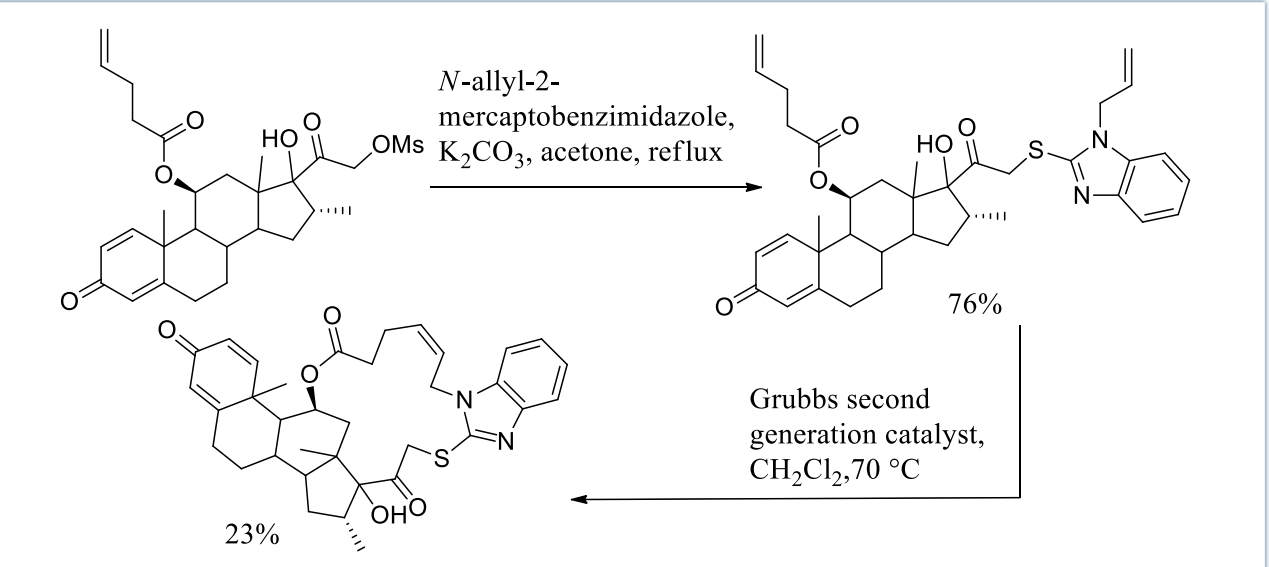

Figure 9: Synthesis of steroidal macrocycles using Grubbs second generation. catalyst.

To avoid high dilution conditions, scientists have explored pseudo-high dilution conditions such as solid phase synthesis where a solid support is used. In this approach, molecules are tethered covalently to a solid support and and the compound is made step by step. This can be done in a single vessel making use of selective protecting group chemistry. Besides the avoidance of high dilution, this method offers advantages such as high product purity and ease of product isolation. A similar method is DNA-templated synthesis in which the specificity of DNA is used to bring selected reactants into proximity (**Figure 10**). This method also avoids high dilution conditions.[13]

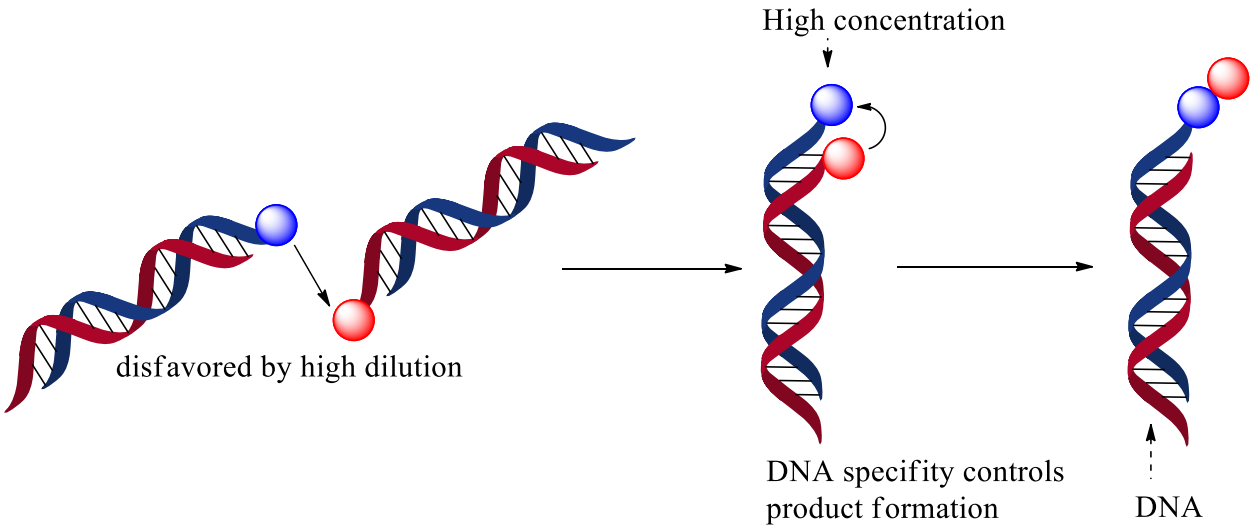

Figure 11: DNA-templated synthesis.[101]

Metal-templated chelation is also used to make macrocycles. Metal-templated chelation refers to the generation of two or more coordinate bonds connecting a polydentate ligand and a single central atom to an ion or molecule. The metal ion significantly increases the yield and directs the steric course. The metal ion can either favour the cyclization reaction or stabilize the formed macrocyle.[40] As an example, the formation of macrocyclic hydroxamic acids using Fe (III) as the coordinating metal has been reported (**Figure 11**).[41]

Another common method for the generation of macrocycles is direct lactonization of acids and alcohols (**Figure 12**) which usually involves three steps. The acid group is activated, the alcohol is converted into the preferred leaving group and then both reacting groups are activated at the same time.[3] This method is well-established, and the chemistry and methodologies are well-known. The reagents are readily available, and the linear precursors can be synthesized easily. The execution is straight forward, and the method can be applied to different ring sizes. However, not all target products are accessible and the reaction takes place under high dilution conditions.[16] As an example, the total synthesis of epothilone A using macrolactonization has been reported.[42]

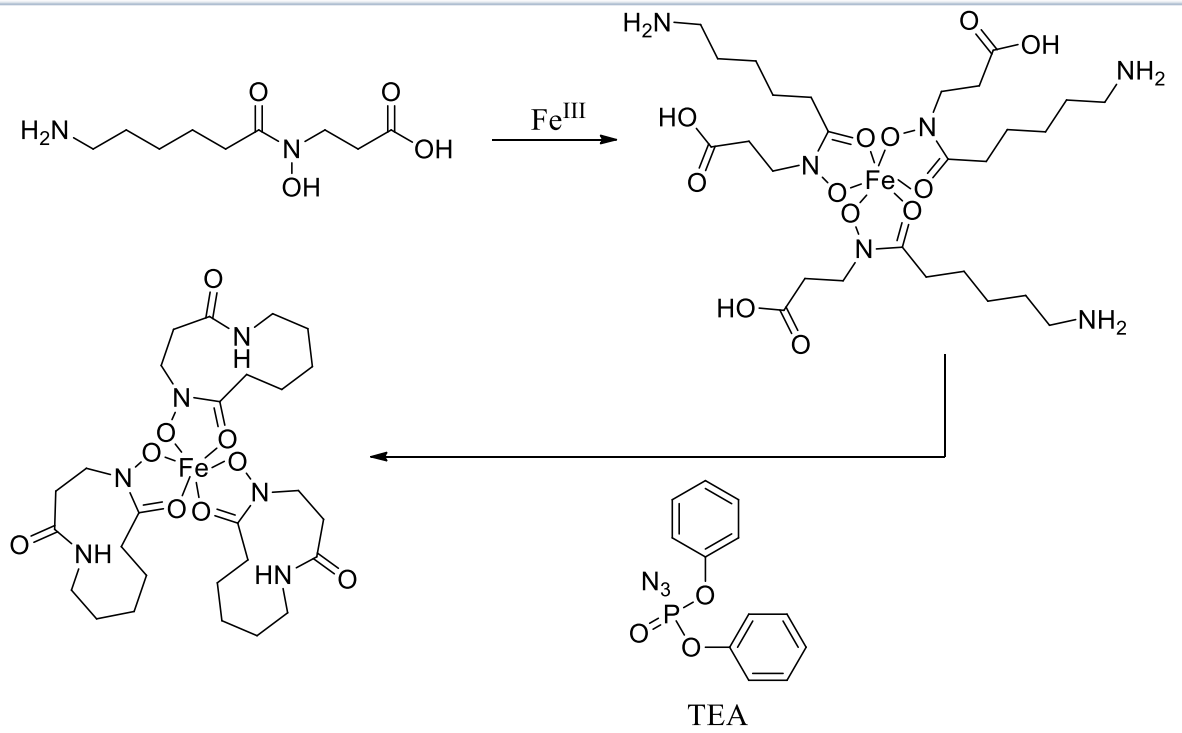

Figure 12: Metal-templated chelation synthesis of macrocyclic hydroxamic acids.

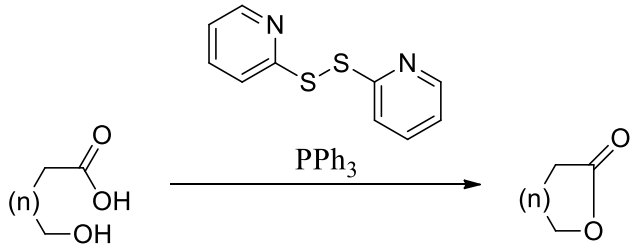

Figure 13: Macrolactonization for the formation of macrocycles.

There are several other reactions that are used to make macrocycles. These include multi-component reactions, although this approach has not been widely used. They involve a one pot process where a minimum of three reactants form a product which consists of substantial elements of the reactants involved.[43] An example of this is the one-pot four-component synthesis of macrocycles reported by Janvier and Bois-Choussy (**Figure 13**).[44]

Azide-alkyne reactions, where a cycloaddition is performed between alkynes and azides, have also been utilized in the making of macrocycles (**Figure 14**). Advantages of theses reactions include high yield under room temperature conditions, use of water as a solvent, the regioselectivity and high tolerance of various functional groups, as well as biocompatibility. However, it has a drawback due to the production of dimers and oligomers which are sometimes preferred over the monomeric products. Since these reactions always result in the formation of a triazole, the target compound can only be one in which a triazole is acceptable.

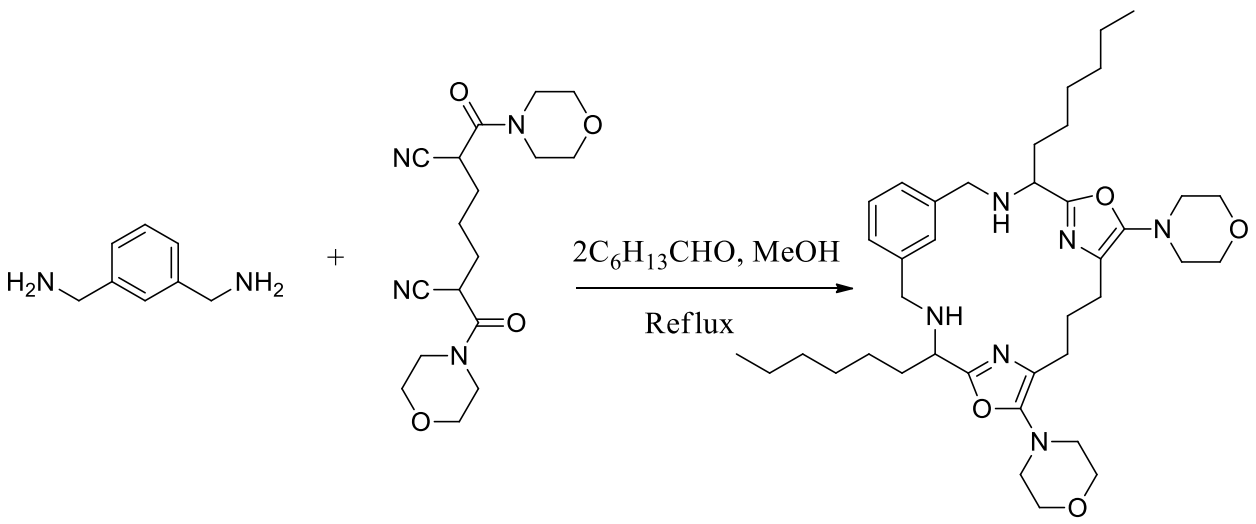

Figure 14: Multi-component reaction for the synthesis of macrocycles

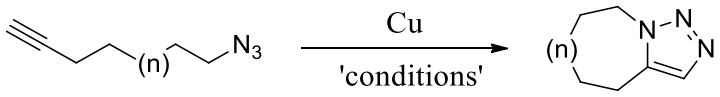

Figure 15: Click reaction.

1.7 Aims and Objectives: Partnership with the University of York

Ring-closing contraction sequences also find utility in the formation of macrocycles. In this approach, new rings are formed by rearrangement which leads to the loss of one or more carbon atoms from the original molecule.[45] Coupling reactions making use of transition metal catalysis have also been widely used in the synthesis of macrocycles with the generation of new C-C, C-N and C-O bonds.[15]

Unsworth and co-workers (University of York) reported using **S**uccessive **R**ing **E**xpansion (SuRE), an innovative synthetic strategy for the production of macrocycles starting from cyclic precursors (**Figure 15**). This method involves the addition of linear fragments to a cyclic molecule which encourages an intramolecular cyclization reaction which results in an expanded ring. The method avoids the use of a linear precursor thereby circumventing the problems of intermolecular reactions which have been traditionally prevented by using high dilution.[19] This is not a totally new concept and has been utilized in various other works.

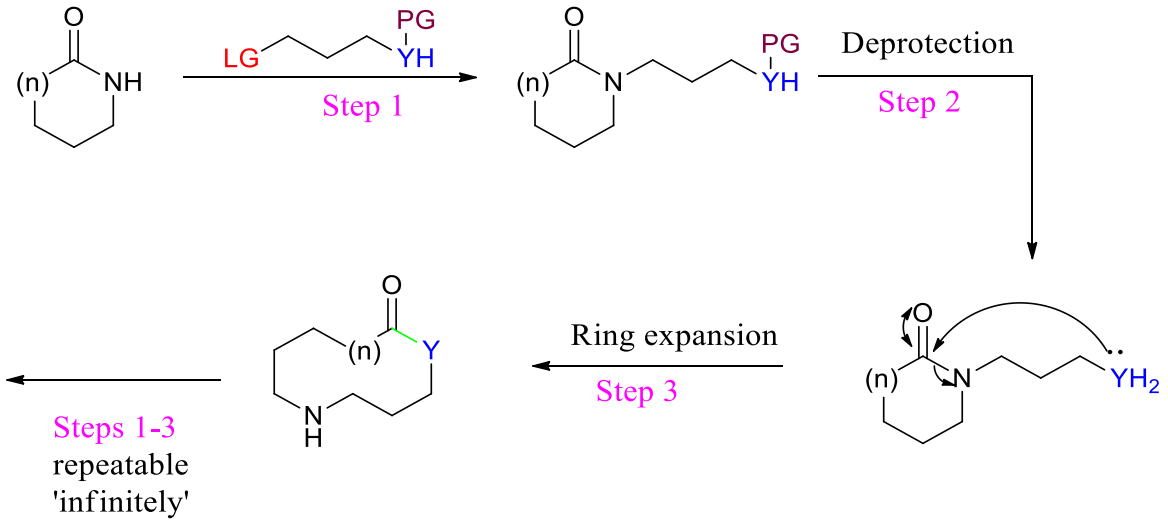

Figure 16: SuRE macrocyclization.

Thus far, cyclic β-keto esters and lactams have been utilized as starting materials to which various linear fragments were inserted to initiate an intramolecular cyclization reaction yielding a ring expanded product. The reacting motif is regenerated at each step and thus – in theory – the ring expansion can be repeated without end. A different linear fragment can be inserted at each step thus diverse structures can be made. The reactions using β-keto esters as starting materials work well with β-amino acid derivatives but more steps need to be taken for the removal of the labile β-keto ester motif to make them suitable for medicinal applications. However, when using lactams as the precursor, there is improved yield and substrate scope and the products are stable amides.[46] During

our study, Unsworth and co-workers were also able to improve the methodology for synthesizing macrocyclic peptides by using **C**onjugate **A**ddition/**R**ing **E**xpansion (CARE) (**Figure 16**). This method is much more versatile and allows for synthesis of more diversely functionalised macrocycles.

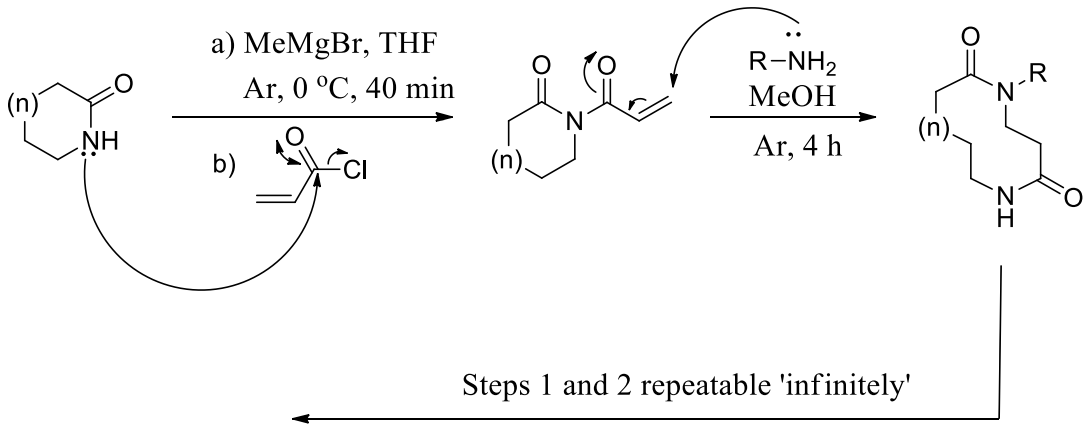

Figure 17: CARE macrocyclization.

Unsworth and co-workers created a virtual library based on the hydrolysis/decarboxylation of the ring expanded products that had β-keto ester moieties. They enumerated this library based on synthetic reactions based on the successful reactions done on a model 11-membered medium sized ring. Out of the 402 compounds that they generated, 200 of these had a lead-likeness score of zero.[47] This is the best possible score, with lead-likeness decreasing as this score increases.

Empowered by the results mentioned above, we envisioned that adding more functional groups around the macrocyclic peptides would increase their potential as medicinal drugs. After looking at some of the macrocyclic drugs that are currently being used in the treatment of TB, we realized that several contained a phenyl ring connected to an amide bond. Some of these macrocyclic drugs are shown in **Figure 17.**

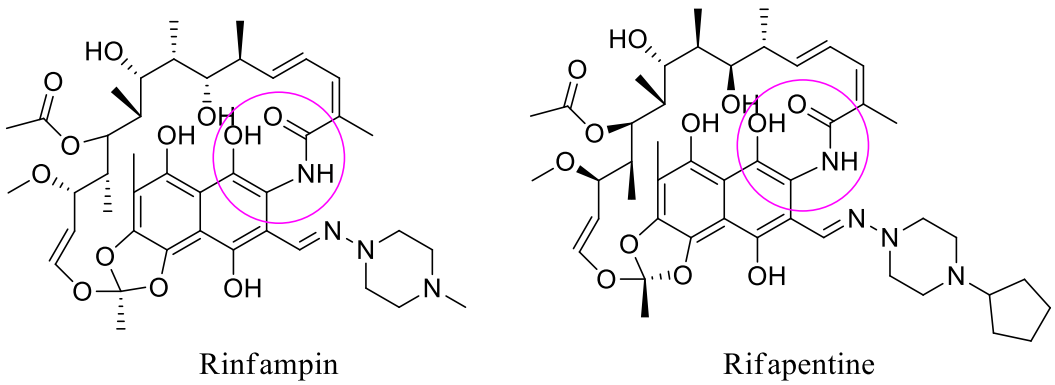

Rinfampin Rifapentine

Figure 18: Examples of macrocyclic drugs used in the treatment of TB showing an amide bonded to a phenyl ring (marked by the pink circle).

Our group had been working on the synthesis of *N*-methyl dihydroquinolinones (DHQs), and because of this interest, we recognized a collaborative opportunity with the Unsworth group. We envisioned that we could make *N*-unsubstituted DHQs and use these as starting materials for the SuRE synthesis which would enable us to access more diversely functionalised macrocyclic molecules (**Figure 18**).

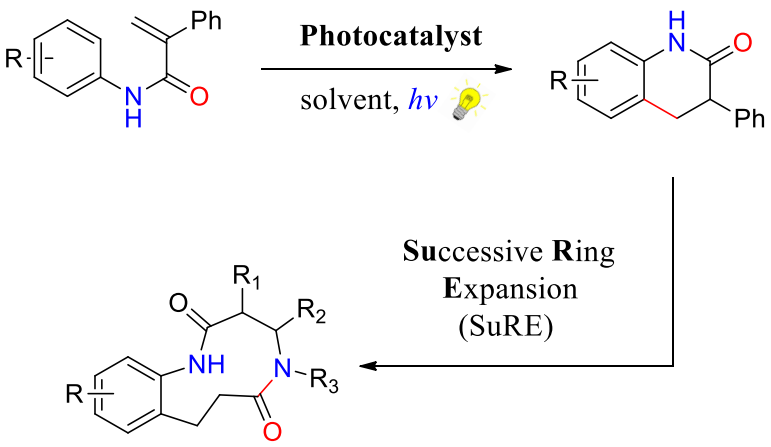

Figure 19: Synthetic strategy for this project.

The aim of this research is to develop a photochemical method for the synthesis of *N*-unsubstituted DHQs for investigating their application in the synthesis of diverse macrocyclic compounds via the SuRE method.

Objectives;

1. Explore methodologies for accessing *N*-unsubstituted DHQs using a photochemical pathway.
2. Synthesise and characterise a series of *N*-unsubstituted DHQs.
3. Evaluate *N*-unsubstituted DHQs as substrates in the SuRE reaction.
4. Assess the biological activity of ring expanded products from the SuRE reaction.

We have explained why DHQs are important for this project. The next chapter will explain why they are important in medicinal chemistry and approaches for their photochemical synthesis.

CHAPTER 2: DHQS

2.0 Importance of DHQs

Although the interest in DHQs for the purposes of this thesis has been the possibility of using them as starting material for accessing more functionalized and bioactive macrocycles, these compounds are useful in and of themselves. Certain DHQs have proven to be bioactive and can be found in nature.[48] Dihydroquinolin-2-ones are commonly found as part of polycyclic alkaloids such as excavatine B (**Figure 19**) which is extracted from the stems and leaves of *Clausena excavate*, while 4-arylDHQs are also usually isolated from fungus such as *Penicillium*. Furthermore, DHQs are used as antioxidants, cancer chemoprotective, antidepressants, antiradical agents and atypical antipsychotic medicines.[49] As a result, methodology for synthesizing DHQs is very important. One of the approaches involves photocatalysis which will be introduced next.

Leaves of *Clausena excavata*

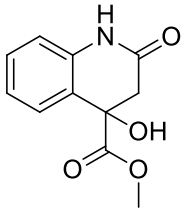

Excavatine B

Figure 20: Excavatine B and its source.[91]

2.1 Brief Introduction to Photocatalysis

Excited triplet states give access to reactivity modes that are not accessible in the ground states thereby making possible difficult synthetic transformations.[50,51] Accessing the excited triplet state was traditionally enabled through direct photoexcitation with harsh UV light as this is the region where most organic molecules will absorb. However, this has the disadvantage of lowering the selectivity, functional group tolerance and method application. As a result, visible-light-mediated photocatalysis was developed to access the triplet state under milder conditions.[52,53] The simplified Jablonski diagram in **Figure 20** illustrates photoexcitation of a catalyst from its ground state, S_0, to an excited state, S_1, and intersystem crossing (ISC) to the triplet state, T_1.

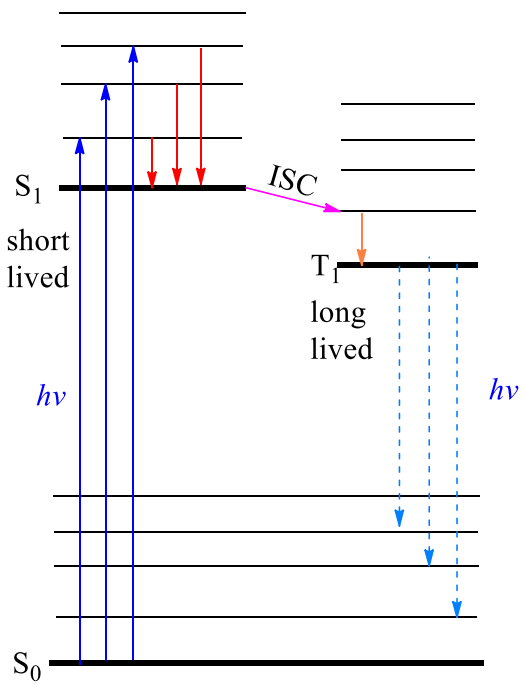

Figure 21: The Jablonski diagram.[92]

The field of visible-light-mediated photocatalysis has two distinct areas of study, namely, electron and energy transfer processes (**Figure 21**). Electron transfer catalysis, otherwise known as photoredox catalysis, makes use of the redox state of the excited molecule to prompt a single electron transfer event (SET). On the other hand, energy transfer (EnT) catalysis involves the deactivation of a donor molecule from its excited state to a lower energy state by energy transfer to an acceptor molecule, taking it to a higher energy state. Excited photocatalysts are referred to as either photoredox catalysts in the event of SET or photosensitisers in the event of EnT. However, it should be taken into account that many photoredox catalysts can act as powerful photosensitizers (and vice-versa) thus making the determination of their mode of action challenging.[54] As an example, ruthenium- and iridium-based photocatalysts have been predominantly used for SET applications, but are also suitable for EnT catalysis because of their ability to generate long-lived excited states as a result of their very high absorption of light and stability against degradation.[55]

There are three types of EnT processes. Namely, primitive EnT (emission-absorption mechanism), Forster resonance EnT (non-radiative donor-acceptor mechanism) and Dexter EnT (double electron transfer mechanism) (**Figure 22**).[56] The latter is predominant and most relevant within the framework of organic synthesis and will now be discussed further. The donor is photoexcited its singlet state where it then goes through intersystem crossing to its excited triplet state. This triplet state should ideally possess a long lifetime (μs to ms timescale), so that it has the opportunity to interact with the

acceptor molecule in a two-electron exchange mechanism where the donor molecule passess an electron to the LUMO of the acceptor molecule and receives a HOMO electron from the acceptor at the simultaniously. This results in an exchange of the excited state energy and spin multiplicity such that the excited triplet state of the acceptor is genrated while the ground state of the donor is regenerated.[57]

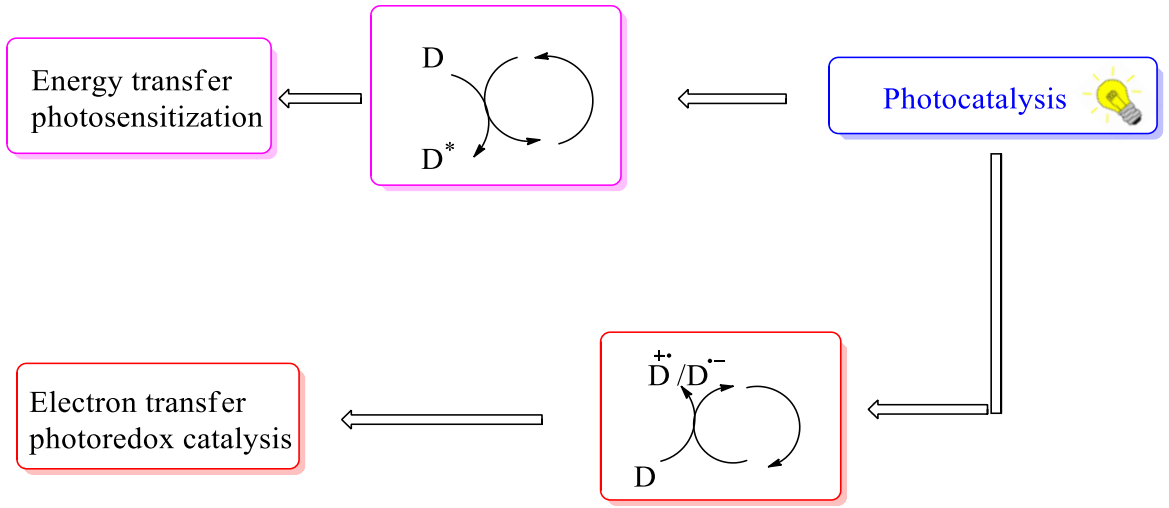

Figure 22: Electron (right) and energy transfer (left) processes of importance in photocatalysis.[54]

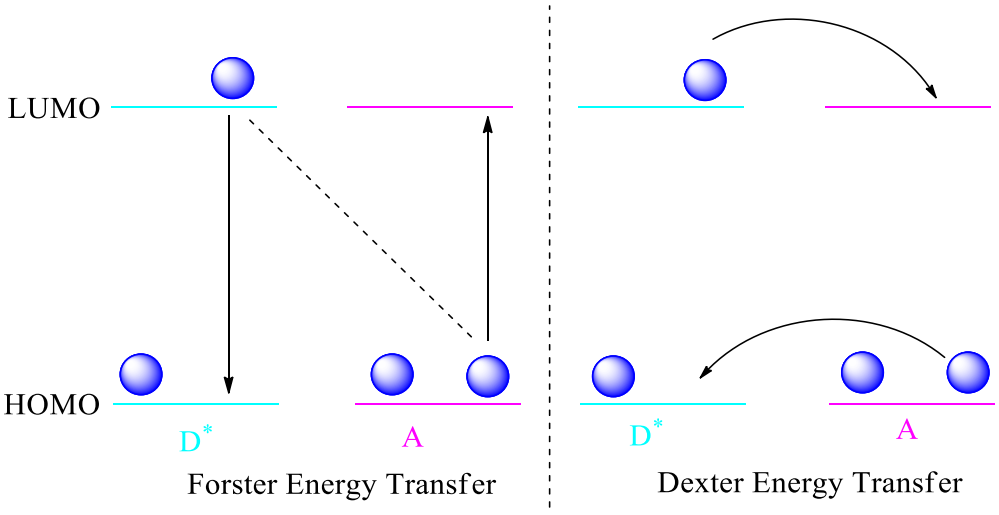

Figure 23: Types of EnT processes.[56]

2.2 Approaches to the Photochemical Synthesis of Dihydroquinolinones (DHQs)

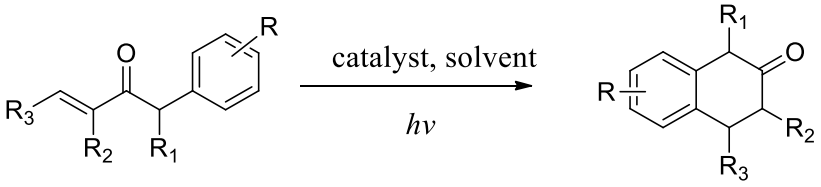

Figure 24: Previous work involving photochemical synthesis of *N*-substituted DHQs.[2–5]

The synthesis of the DHQ framework via a photochemical reaction was the initial object of this project. Visible-light mediated triplet energy transfer has enabled our group and others to perform a formal C(sp^2)-H/C(sp^3)-H hydroarylation to produce *N*-substituted DHQs (**Figure 23**).[2–5] However, none of these methods have reported such syntheses producing the *N*-unsubstituted DHQ — which is required for the SuRE, thus we first set out to optimise this photochemical cyclisation to enable the direct formation of *N*-unsubstituted DHQs.

Our group's photochemical cyclisation utilised thioxanthones as photosensitizers, namely 2-CTX, 2-ITX and 2-^{i}PrTx. At the time of reporting, the methodology had been optimized to work in a mixture of TFE and $CHCl_3$ at 450 nm.[2] It was later discovered that the reaction works well at 405 nm with greener solvents such as EtOH and ACN. As mentioned, these aforementioned methods however required *N*-protection (i.e. R^1 = Me), and considering our planned synthesis of macrocycles, we envisioned expanding the scope to the group's previous work to substrates in which R^1 = H.

2.3 Results and Discussion

2.3.1 Synthesis of Acrylanilides

Our studies commenced with the synthesis of model *N*-unsubstituted acrylanilide **2B**. To make this, standard amide coupling methodology was used as shown in the **Figure 24**. 2-Chloro-1-methylpyridinium iodide (2CMPI) was used as the coupling reagent. The yields were generally low (27% isolated) and were further lowered by formation of a β-lactam side product (**2A**) that was extremely challenging to separate from the desired acrylanilide due to the close R_f values. This necessitated the use of longer columns for the silica-gel column chromatography.

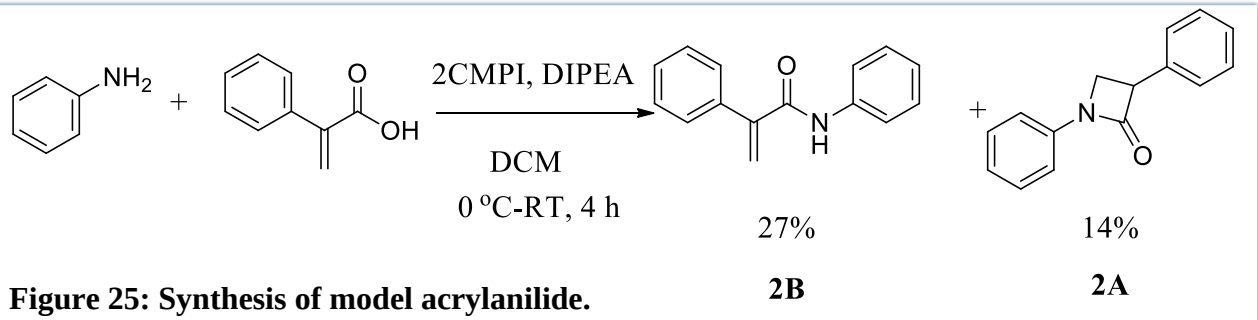

Figure 25: Synthesis of model acrylanilide.

The structure of the model compound, *N*,2-diphenylacrylamide (**2B**), was confirmed by ^{1}H-NMR spectroscopy as shown in **Figure 25**. The diagnostic peak for the formation of **2B** is the signal from H-7 a singlet at 10.32 ppm at RT in DMSO. This confirms the presence of a secondary amide. The other pertinent signals are alkenyl signals from H-10, singlets at 5.74 and 5.97 ppm. The aromatic signals are in the region 7.09-7.97 ppm. These results were in accordance with literature reports.[58]

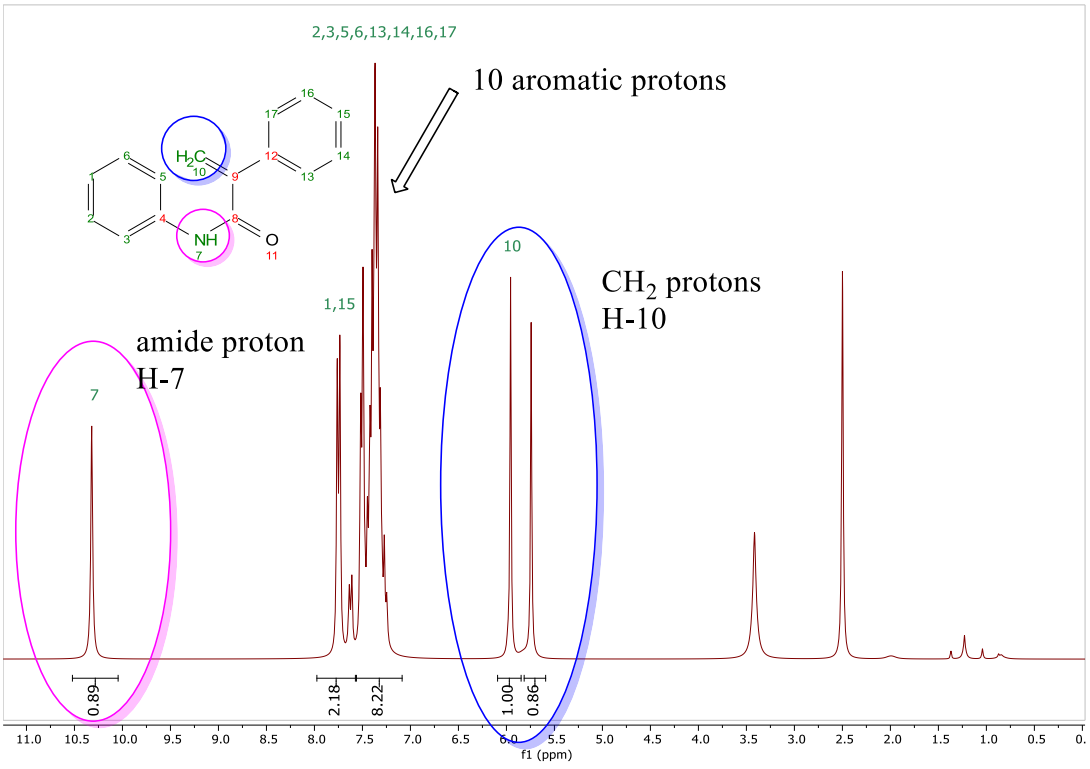

Figure 26: ^{1}H-NMR spectrum of Acrylanilide 2B.

In an effort to improve the yields of the acrylamide **2B**, we tried an acylation route (**Figure 26**). However, the yields obtained were lower than those obtained initially using the coupling agent, so we proceeded to use the initial method to synthesise other acrylanilides shown in **Figure 27**.

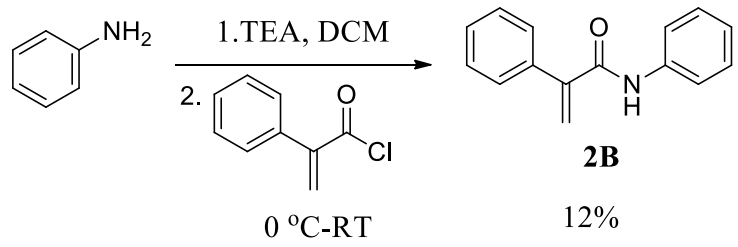

Figure 27: Method 2 for the synthesis of 2B.

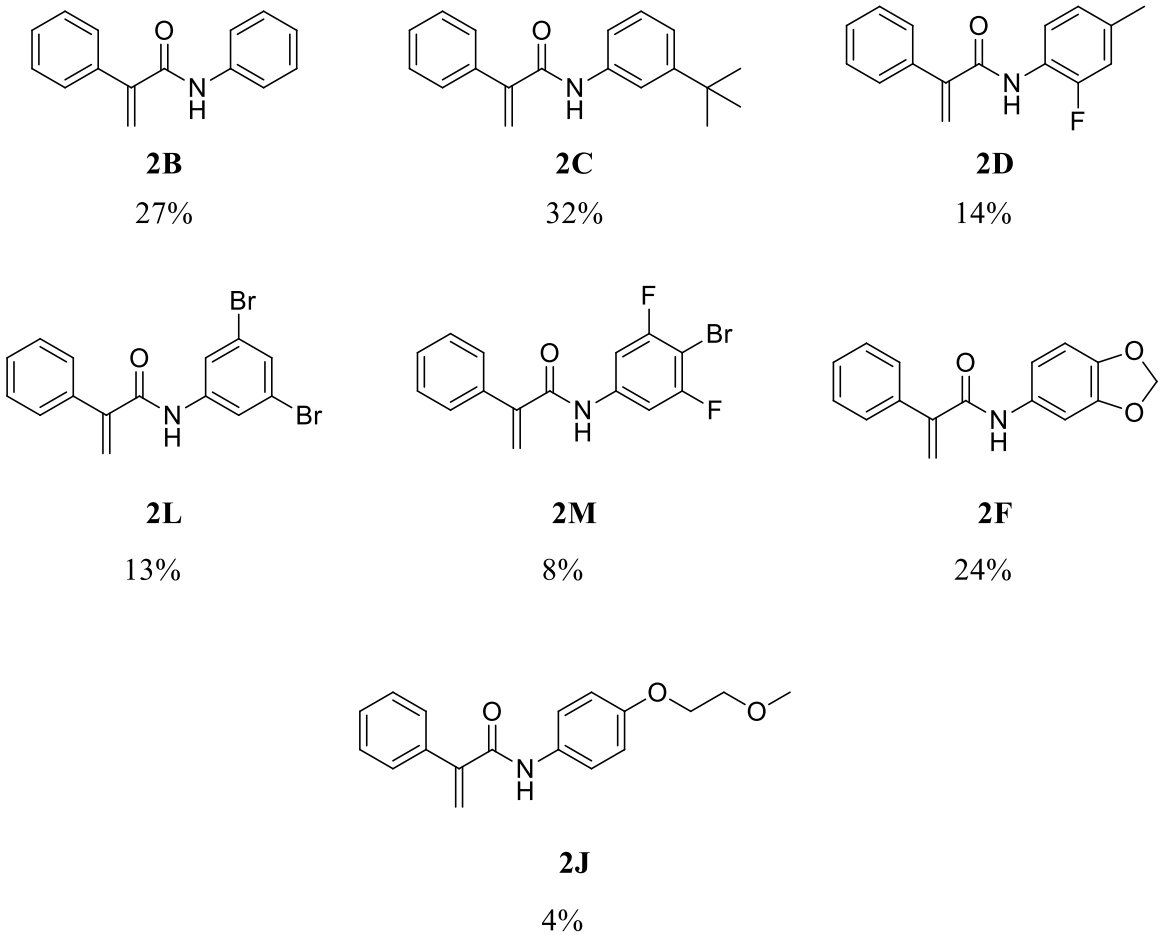

Figure 28: Substrate scope for acrylanilides.

The identity of the side product **2A** was also determined using NMR spectroscopy. The ^{1}H-NMR spectrum is shown in **Figure 28**. The spectrum featured the correct 10 aromatic signals in the region 7.01-7.49 ppm. A triplet and a doublet of doublets, consistent with the diastereotopic protons H-10, were observed at 4.11 ppm and 3.76 ppm, respectively and a doublet of doublets at 4.11 ppm for H-9.

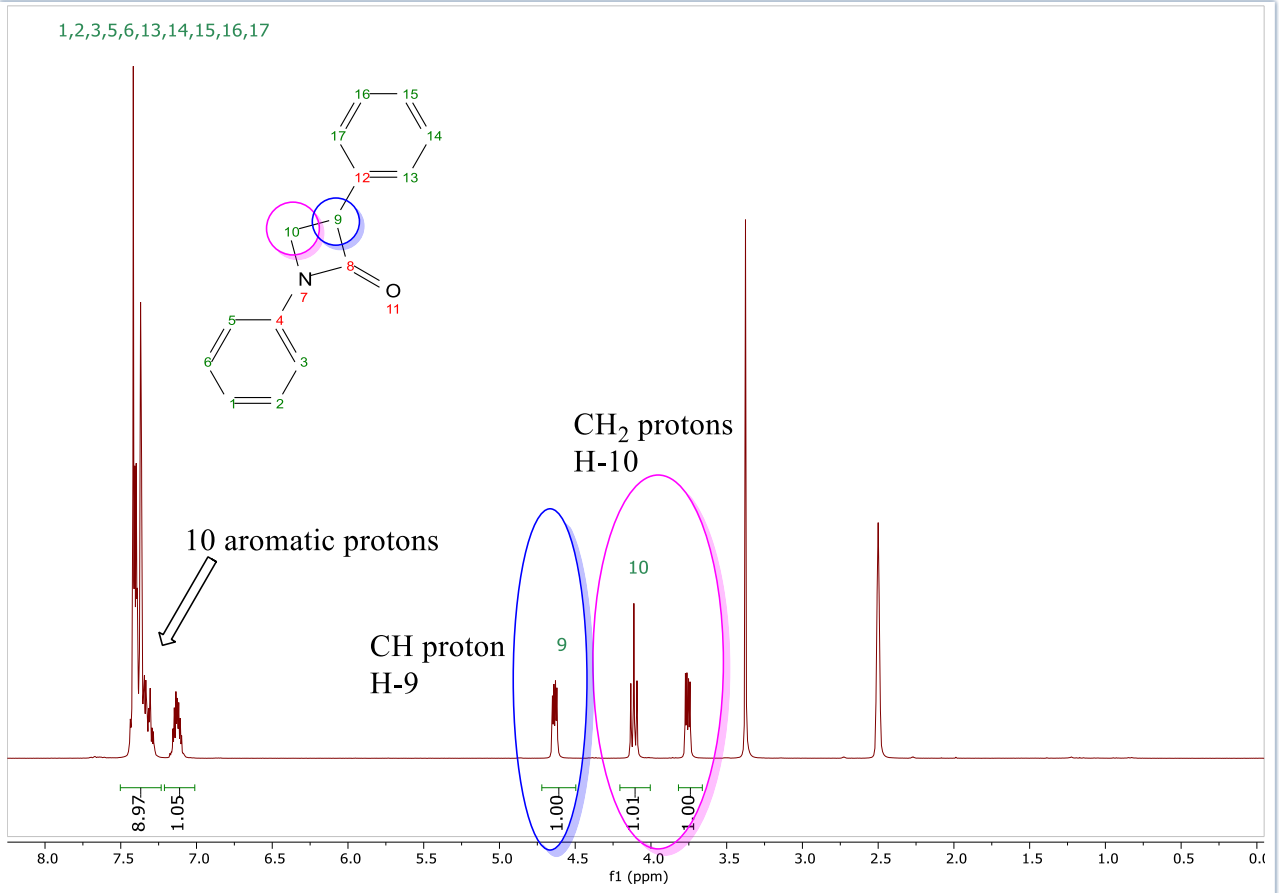

Figure 29: ^{1}H-NMR spectrum of side product 2A.

The ^{13}C-NMR of the suspected β-lactam (**Figure 29**) had the diagnostic peaks (two alkyl signals for C-9 and C-10) at 46.6 and 53.5 ppm, respectively. In addition, the carbonyl signal for C-8 at 165.3 ppm confirmed that an amide bond had been formed.

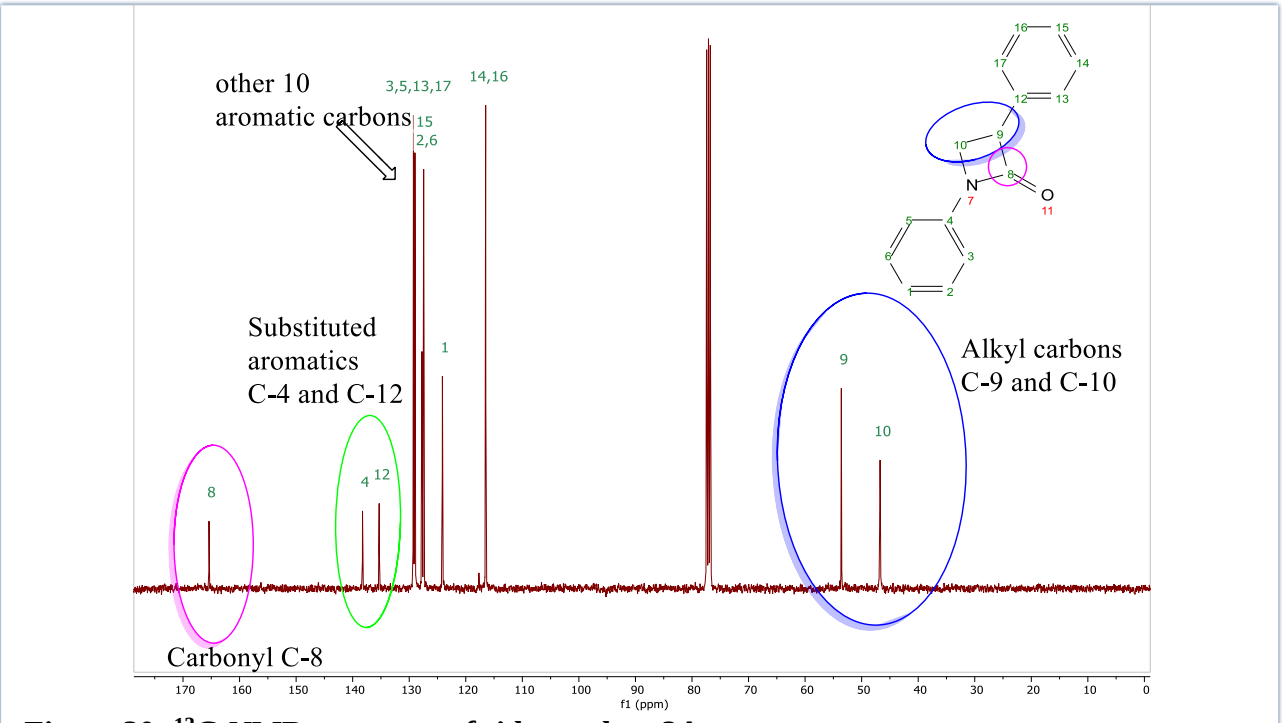

Figure 30: ^{13}C-NMR spectrum of side product 2A.

The ^{1}H-NMR and ^{13}C-NMR agreed with literature reports.[59] Furthermore, an HSQC-DEPT analysis of the side product enabled the assignment of the alkyl protons by revealing the CH_2 protons coded red in **Figure 30**.

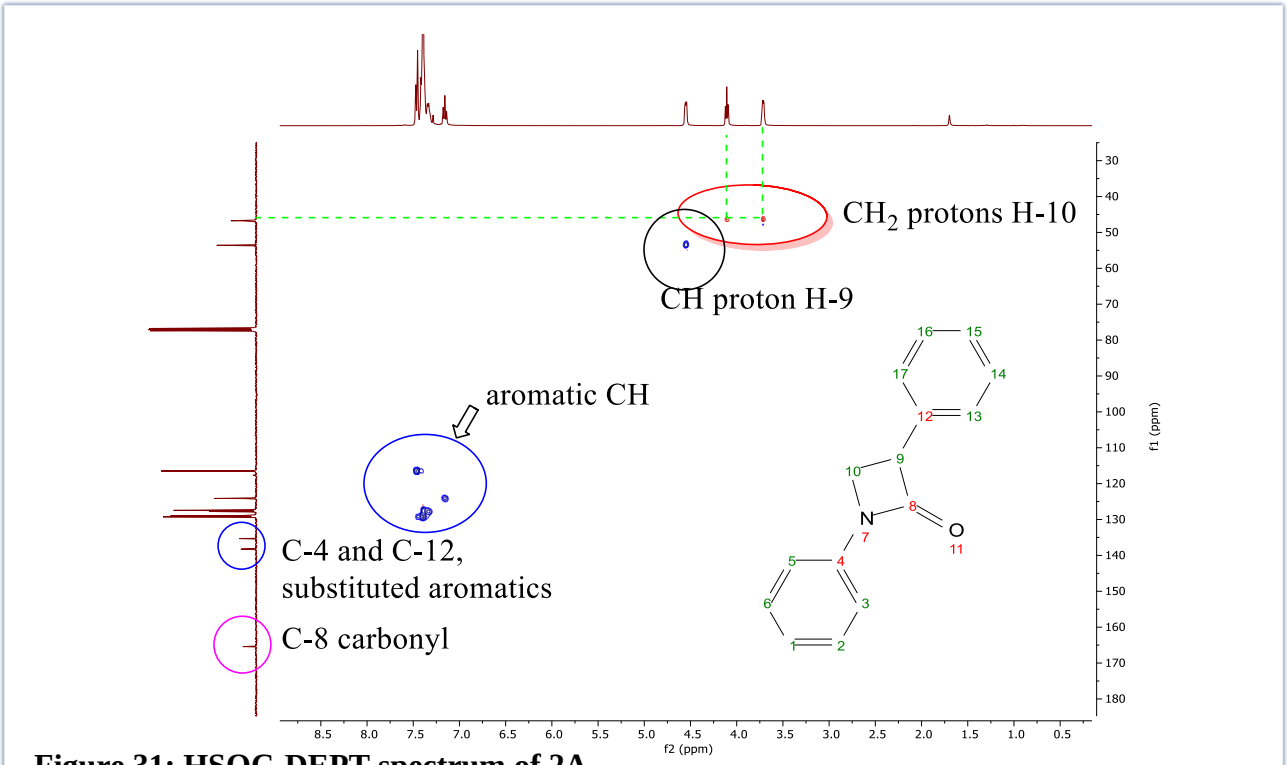

Figure 31: HSQC-DEPT spectrum of 2A.

While this side reaction was unexpected, we were pleased to discover that an old publication (1984) detailed the synthesis of β-lactams from β-amino acids under similar conditions.[60] No mechanism was provided in this report, but we proposed that a competing reaction was taking place once the acid had been activated with the 2-chloro-1-methylpyridinium iodide (2CMPI), producing intermediate **A2-3**. Thereafter, Michael addition affords β-amino acid (**A2-4**) which then undergoes a 4-exo-trig cyclization which is favoured according to Baldwin's rules (**Figure 31**).

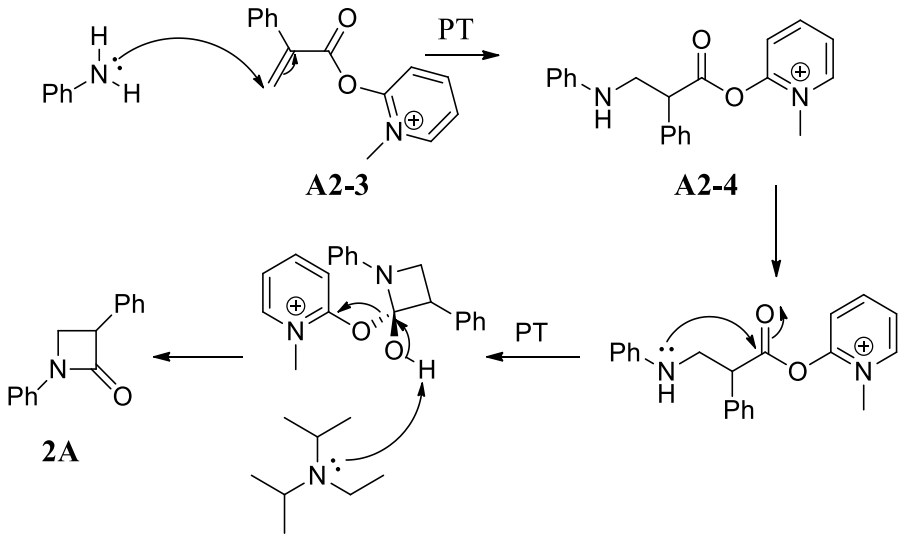

Figure 32: Proposed mechanism for the synthesis of 2A.

This result was quite interesting given the lower nucleophilicity of the aniline. Certainly, in the work by Huang *et al*, no aniline substituted β-lactams were formed. The full library β-lactam side-products isolated during our synthesis is shown in **Figure 32**. Although this was an interesting side-reaction, and despite the importance of β-lactams in medicinal chemistry, it was not the primary focus of our efforts and thus no further optimisation were carried out, but will be a topic of future work in our group.

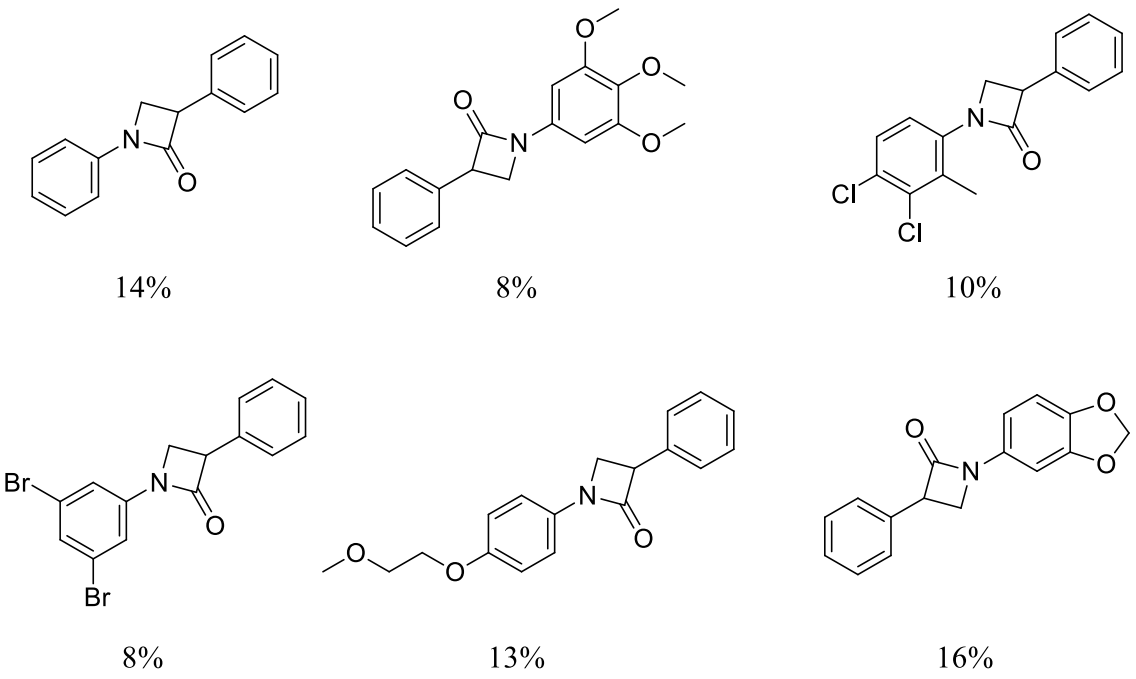

Figure 33: Isolated B-lactam side-products.

With acrylamide **2B** in hand, we proceeded to optimise the photochemical cyclisation to synthesise the target product **2N** as shown in **Figure 33**.

2.3.2 Catalyst Screening and Optimization for the Formation of DHQs

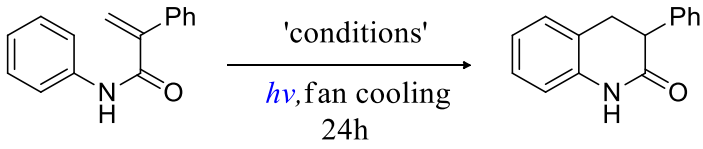

2B **2N**

Figure 34: Synthesis of model substrate 2N.

Table 1: Optimisation Studies

Entry	Photocatalyst	Catalyst mol%	Solvent	Nm light	Yield (%)
1	2-Chlorothioxanthone	20	TFE: $CHCl_3$ (4:1)	450	Not detected
2	2-Chlorothioxanthone	20	EtOH	405	trace
3	4CzIPN	20	TFE: $CHCl_3$ (4:1)	450	trace
4	Ir(*p*-F-ppy)$_3$	2	TFE: $CHCl_3$ (4:1)	450	Not detected
5	Ir[dF(CF_3)ppy]$_2$(dtppy)PF_6	2	TFE: $CHCl_3$ (4:1)	450	93
6	Ir[dF(CF_3)ppy]$_2$(dtppy)PF_6	2	DCM	450	trace
7	Ir[dF(CF_3)ppy]$_2$(dtppy)PF_6	2	$CHCl_3$	450	trace
8	Ir[dF(CF_3)ppy]$_2$(dtppy)PF_6	2	EtOAc	450	trace
9	Ir[dF(CF_3)ppy]$_2$(dtppy)PF_6	2	ACN	450	trace
10	Ir[dF(CF_3)ppy]$_2$(dtppy)PF_6	2	EtOH	450	trace
11	Ir[dF(CF_3)ppy]$_2$(dtppy)PF_6	2	TFE: $CHCl_3$ (4:1)	380	Not detected
12	Ir[dF(CF_3)ppy]$_2$(dtppy)PF_6	2	EtOH	380	Not detected

Various photocatalysts were attempted (**Table 1**); however, only Ir[dF(CF_3)ppy]$_2$(dtppy)PF_6 (IrdCF_3) in TFE:$CHCl_3$ was found to be suitable in accordance with our previous work, producing the desired product in 93% yield (entry 5). Interestingly, despite a strong absorbance of the photocatalysts at 380 nm (**Figure 34**), no reaction was observed using this light source (entry 12) with the same solvent system TFE:$CHCl_3$ (4:1). It is understood that the solvent can be the determining factor of the reaction outcome as it can influence the reaction rates, mechanisms, thermochemistry, and the photochemistry of excited states of solute molecules. This influence is often exerted through the solvent's polarity or viscosity and explicit solute-solvent interactions. The interactions can be nonspecific such as coulombic and van der Waals and specific such as hydrogen bonding and hydrophobic interactions.[61]

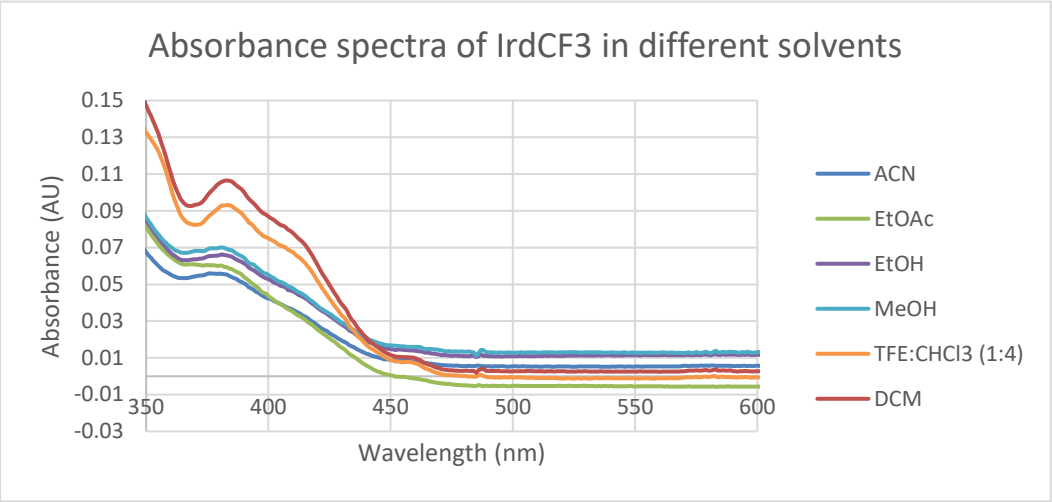

Figure 35: Absorbance spectra of $IrdCF_3$ in different solvents.

With our best conditions determined, we proceeded to produce a small library of DHQs, as shown in **Figure 35**, that we could use for our subsequent synthesis of macrocycles.

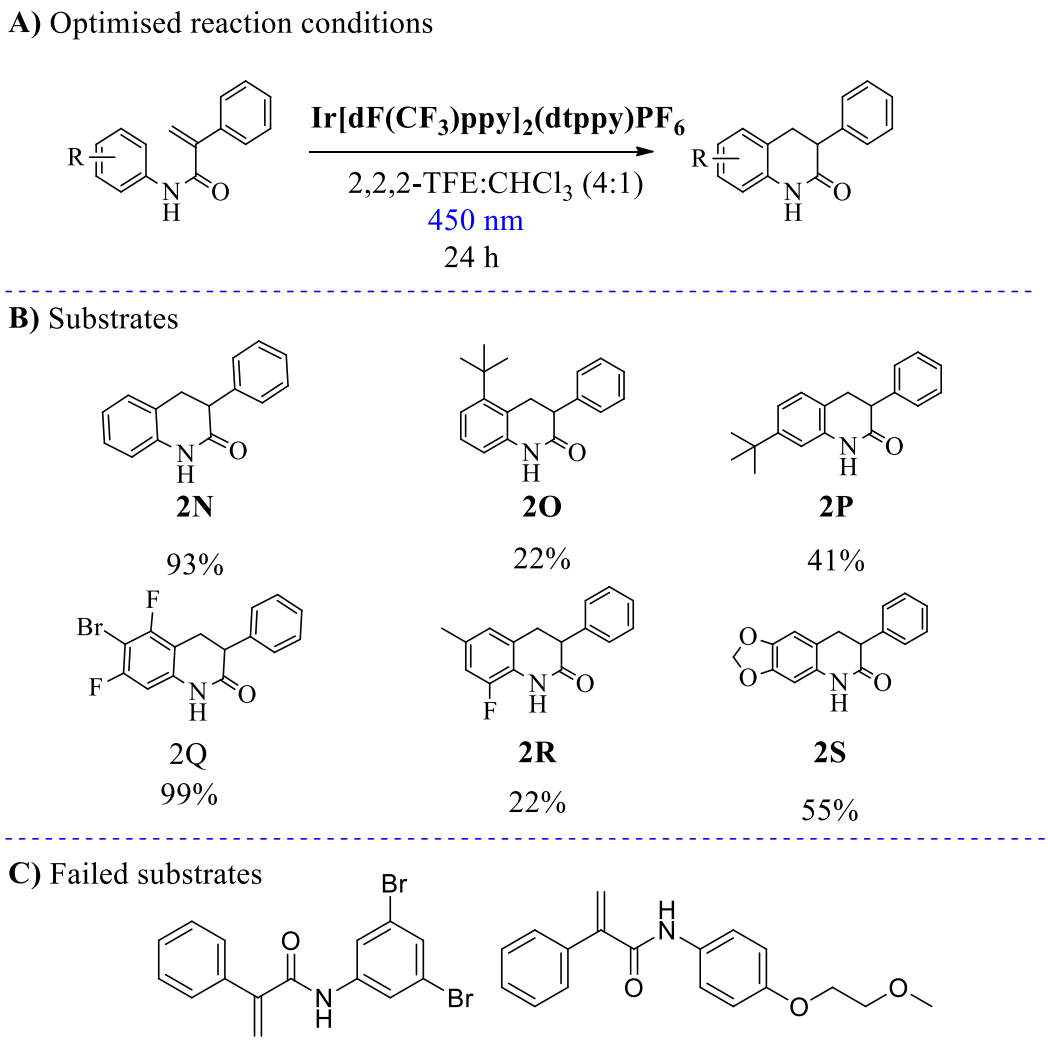

Figure 36: A) Optimised reaction conditions. B) Library of DHQs synthesised. C) Failed substrates

The model product **2N** was produced in 93% yield. The product was confirmed by ^{1}H-NMR and matched the literature reference.[62] The ^{1}H-NMR spectrum is shown below in **Figure 36**. The key diagnostic feature was the presence of alkyl signals at 3.86 ppm (dd) integrating for a single proton (H-5) and 3.22 ppm (m) integrating for two protons (H-6). The N-H of the amide (H-3) also shifted upfield from 10.32 ppm to 9.14 ppm (relative to the starting acrylamide) showing a reduction in the deshielding effect of the alkene. The aromatic region correctly integrated for nine protons. An overlay of the starting material **2B** and the product **2N** is given in **Figure 37** to provide a summary of the key changes and diagnostic points.

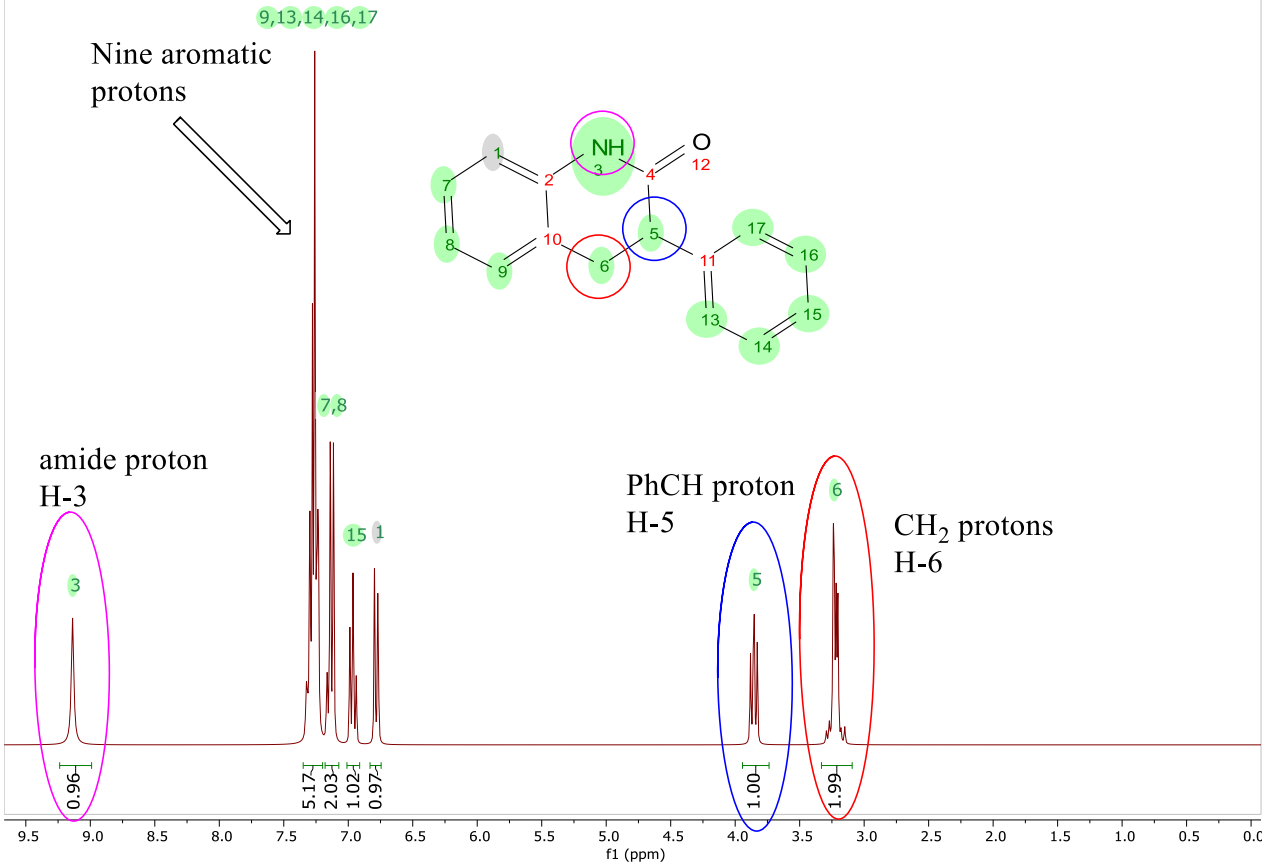

Figure 37: ^{1}H-NMR spectrum of 2N.

It is worth mentioning that carrying out the reaction with substrate **2C**, a 1:2 ratio of regioisomers **2O**:**2P**, was obtained, affording the corresponding DHQs in 22 and 41% yield, respectively (**Figure 38**) — a result consistent with placing the bulky *tert*-butyl group in a sterically less hindered environment for the major product.

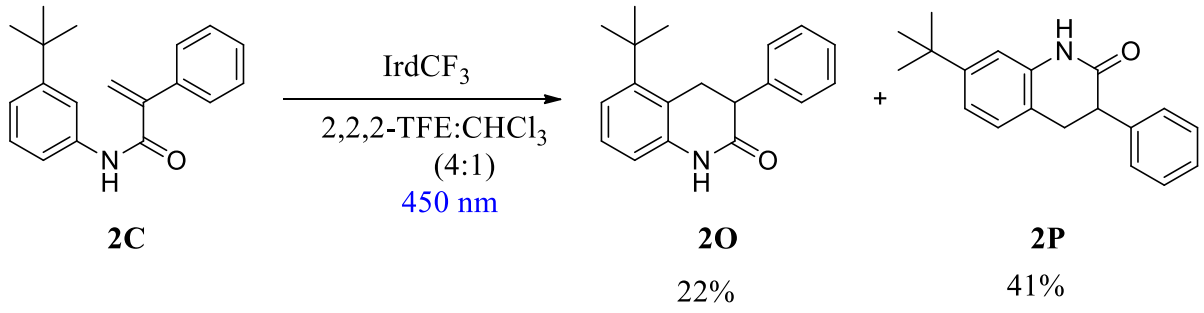

Figure 38: Synthesis of regioisomers 2O and 2P.

The overlayed ^{1}H-NMR spectra of **2O** and **2P** are shown in **Figure 39**. A key difference in the ^{1}H-NMR spectra is the difference in splitting pattern of the DHQ ring protons (H-9/H-10). It can be surmised that due the proximity of the bulky *tert*-butyl group to the CH_2 (H-10) protons in **2O**, the diastereotopic environment becomes more exaggerated, and this results in a more complex splitting pattern.

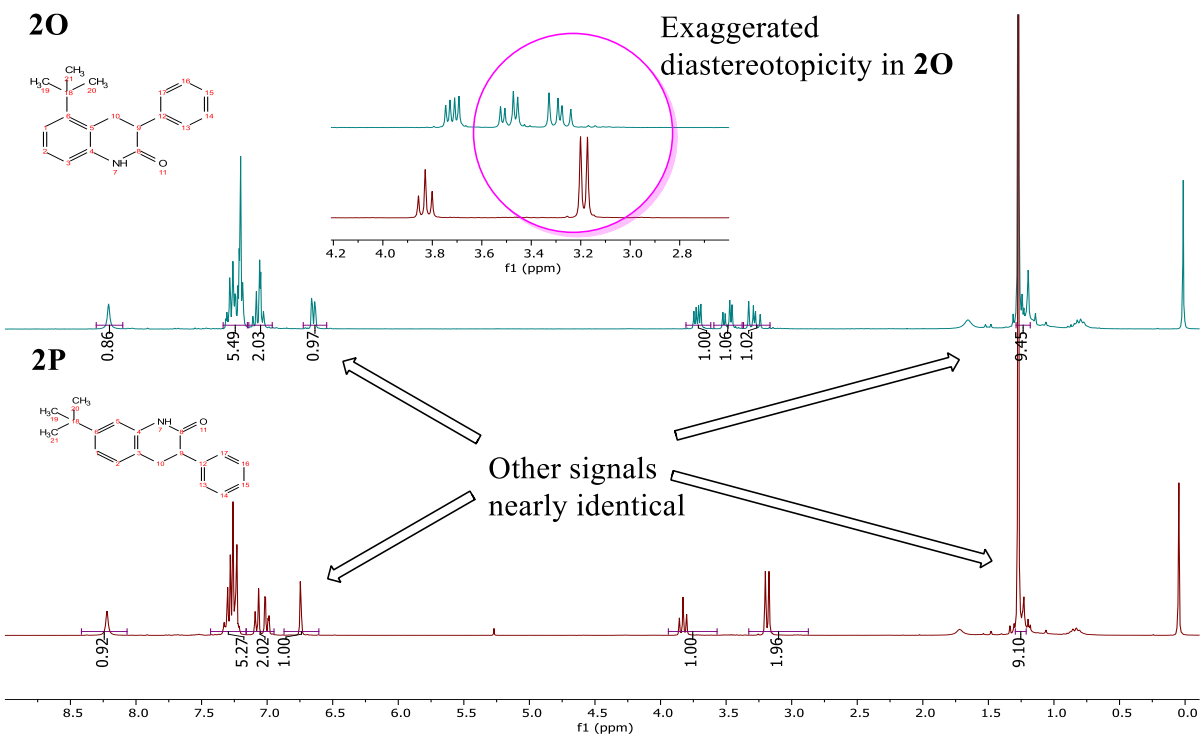

Figure 39: Overlayed ^{1}H-NMR spectra of 2O and 2P.

However, to conclusively assign **2O** and **2P** to their respective ^{1}H-NMR spectra, we proceeded to do an HMBC analysis (**Figure 40** and **41)**. The HMBC spectrum in **Figure 40** shows that the ^{1}H-NMR assignments for the two structures is correct. The absence of a cross peak between C-18, the substituted aromatic carbon of the *tert*-butyl group, and the CH_2 (H-10) protons, shows that the *tert*-butyl group is likely located more than 4 bonds away from the CH_2 protons as in **2P**.

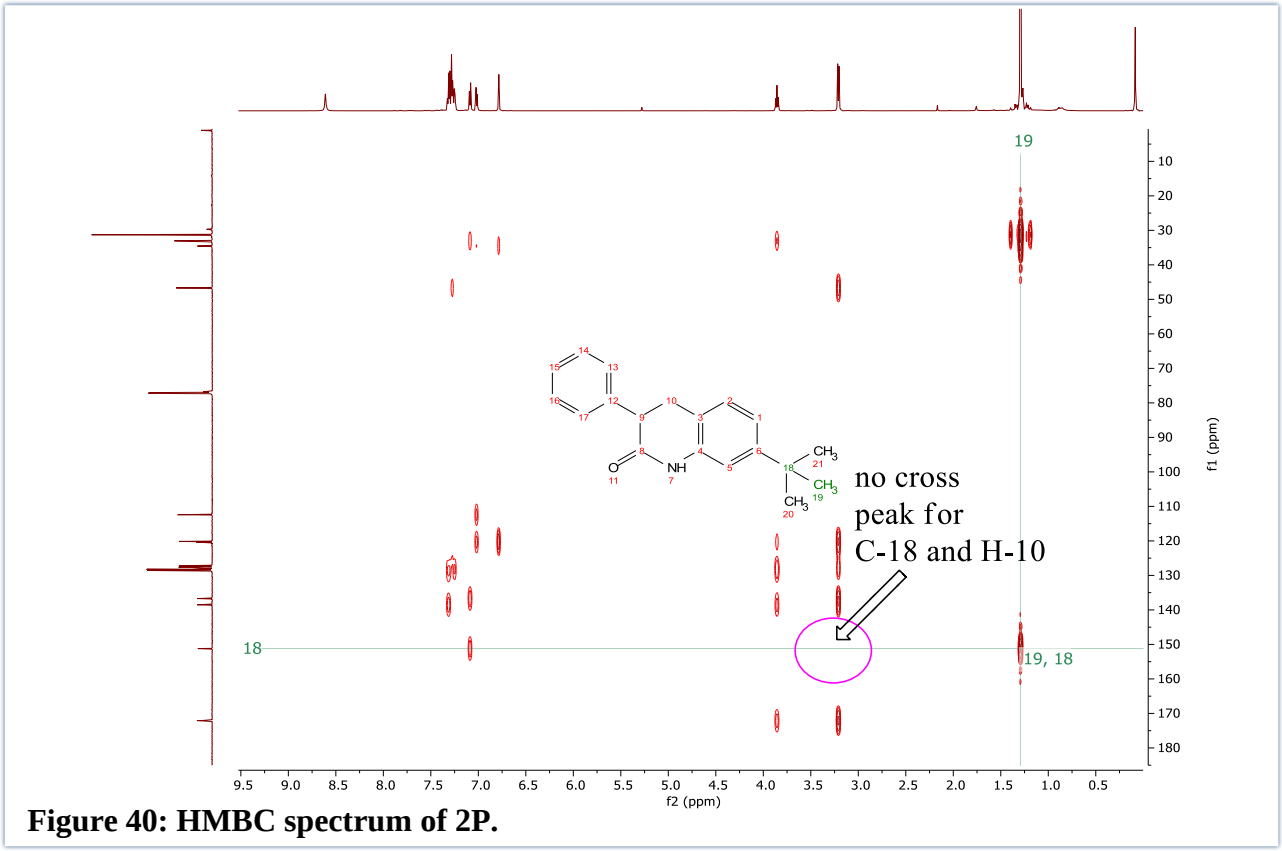

Figure 40: HMBC spectrum of 2P.

The key diagnostic feature in assigning the structure for structure **2O** is that the substituted aromatic carbon of the *tert*-butyl group, C-18, would have a cross peak with the CH_2 (H-10) protons as there are only 4 bonds between them. The two cross peaks are highlighted in yellow on **Figure 41**, providing definitive proof that the *tert*-butyl group is near the CH_2 protons as in **2O**.

The proposed mechanism for the DHQ synthesis can be viewed via two pathways, **A** and **B** as shown in **Figure 42**. The catalyst is photoexcited to its singlet state where it then undergoes intersystem crossing (ISC) to its triplet excited state. It then transfers this triplet energy to the acrylamide **2B**, which then goes to its triplet excited state. ^{3}**2B*** can follow pathway **A** and form a diradical species **A2-4** which forms the more stable diradical species **A2-5** that undergoes a [1,5]-H shift to form the *N*-unsubstituted DHQ **2N**. Alternatively, **2B** can undergo a 6π electrocyclization to form **A2-6**, and in a protic solvent, **A2-6** follows route **(i)** where it gets protonated by the solvent and tautomerizes to form the product **2N**. **A2-6** can also undergo direct [1,5]-H shift to form the product **2N** via route **(ii)**.

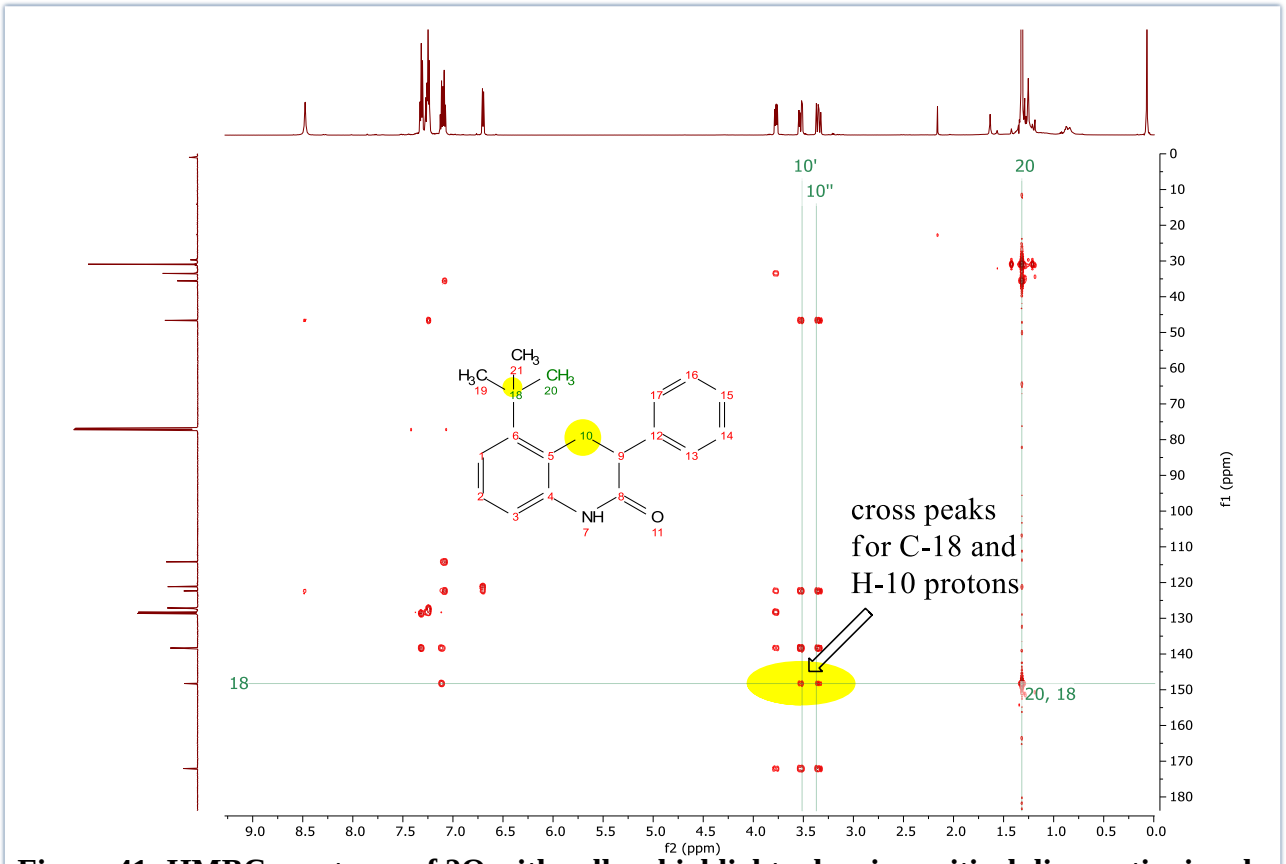

Figure 41: HMBC spectrum of 2O with yellow highlights showing critical diagnostic signals.

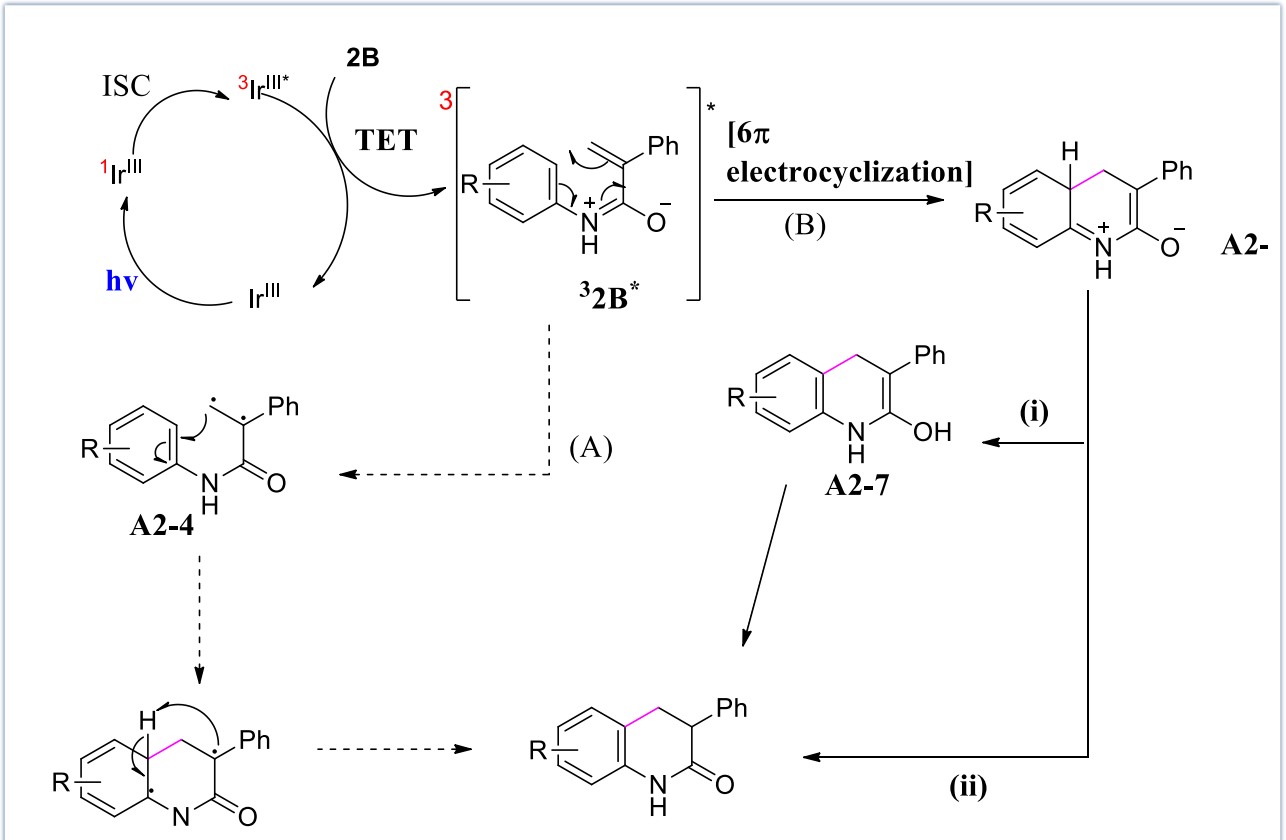

Figure 42: Proposed mechanism for the photochemical synthesis of *N*-unsubstituted DHQs.

With the photochemical reaction working to produce *N*-unsubstituted DHQs with moderate to good yields, we moved on to investigating their suitability as starting materials for SuRE macrocyclization.

CHAPTER 3: MACROCYCLE SYNTHESIS VIA SURE

It is worth noting that this part of the work — namely the application of the SuRE macrocyclization was due to be performed in the Unsworth laboratory as part of a student research exchange as they had the expertise in this area. Due to the Covid-19 restrictions and associated border closures, this travel could not occur. Therefore, in conjunction with developing methodology to make DHQs, we sought to understand the SuRE methodology and characterization of resulting products, based on model systems from the Unsworth laboratory (**Figure 43**) in order to become acquainted with various aspects of this approach. For example, the NMR spectroscopic characterization of macrocycles tends to be complicated by the presence of rotamers and tautomers as well as overlapping signals especially in the alkyl region. Also, literature has shown that macrocycles tend to adopt different conformations in different solvents. With the SuRE methodology itself, an extra complication is proving that cyclization has taken place and that the product obtained is not simply the deprotected intermediate of **B**. This is because the intermediate **B** and the cyclized product **D** have same number of protons and molecular mass. Thus, mass spectrometry and related techniques such as HRMS and LCMS alone cannot be used as confirmation.

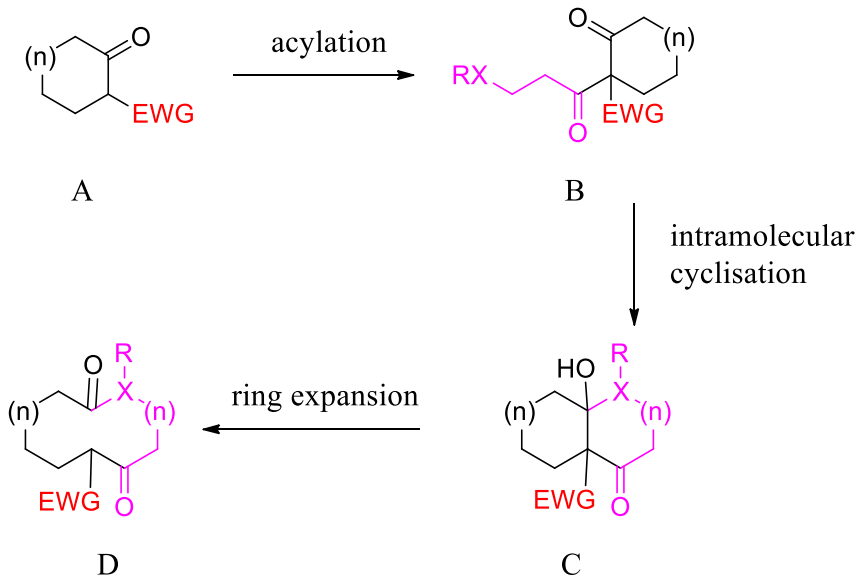

Figure 43: General scheme for SuRE macrocylization.

3.1 Results and Discussion

With this in mind, we considered that it would be helpful for us to start with molecules that Unsworth's group had already made and explore these with 2D-NMR to confirm cyclization. The SuRE methodology was initially developed using cyclic β-keto esters (**Figure 44A**) as starting materials and β-amino acids (**Figure 44B**), so we decided to follow this initial procedure.

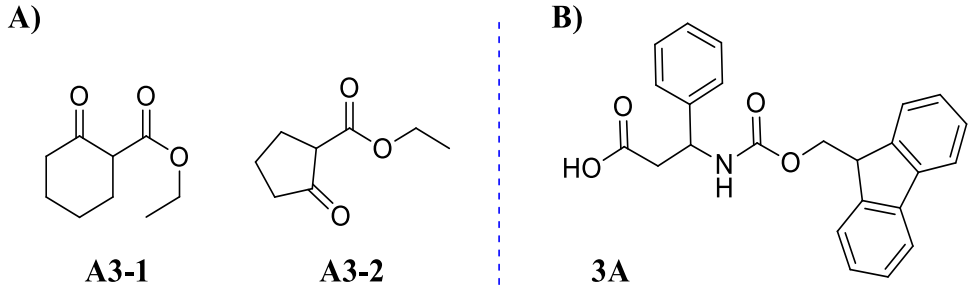

Figure 44: Model A) β-keto esters B) β-amino acids utilised by Unsworth and co-workers.

The first step was to prepare the Fmoc-protected amino-acid **3A (Figure 44B)** from (*S*)-3-amino-3-phenylpropionic acid (98%) (Please refer to chapter 5, section 3.1 for further details). The ^{1}H-NMR (400 Hz, DMSO) spectrum is shown in **Figure 45** below. Successful Fmoc protection was confirmed by the presence of Fmoc signals in the ^{1}H-NMR spectrum of the coupled product with the expected relative integration, i.e, an additional eight aromatic protons and a multiplet signal for the benzylic protons at 4.21–4.32 ppm integrating for two protons. The multiplet here is consistent with the diastereotopic nature of these signals with respect to the stereocentre of the amino acid at C-19 (according to the numbering below). In addition, there are no NH_2 proton signals; instead, a doublet at 7.93 ppm integrating for a single proton, pointed to the presence of an amide bond.

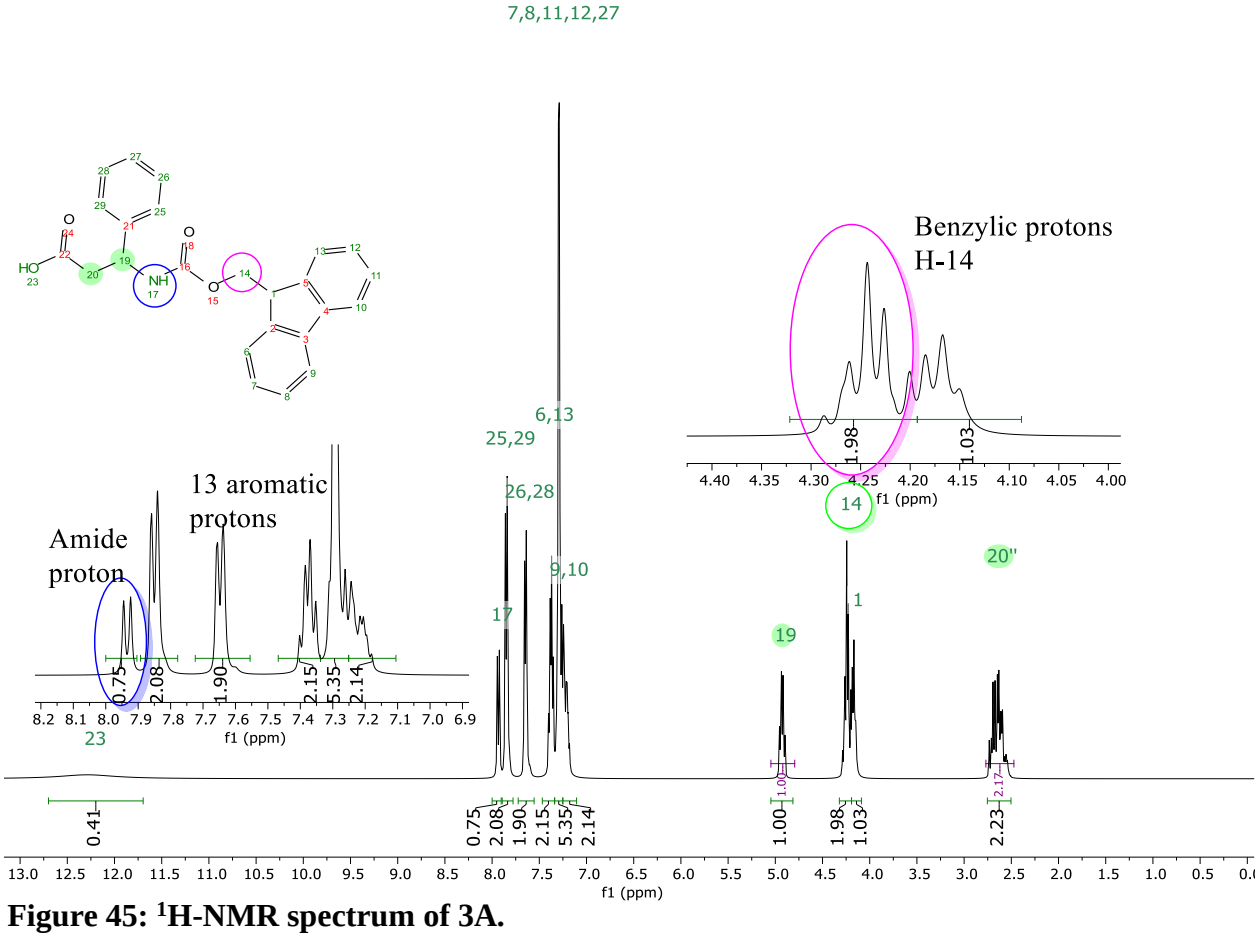

Figure 45: ^{1}H-NMR spectrum of 3A.

With **3A** in hand, we could now proceed to do the synthesis of the first model substrate **3C** as shown in **Figure 46**. To this end, **3A** was thus reacted with oxalyl chloride, with DMF as a catalyst, to afford the acid chloride **3A1**.

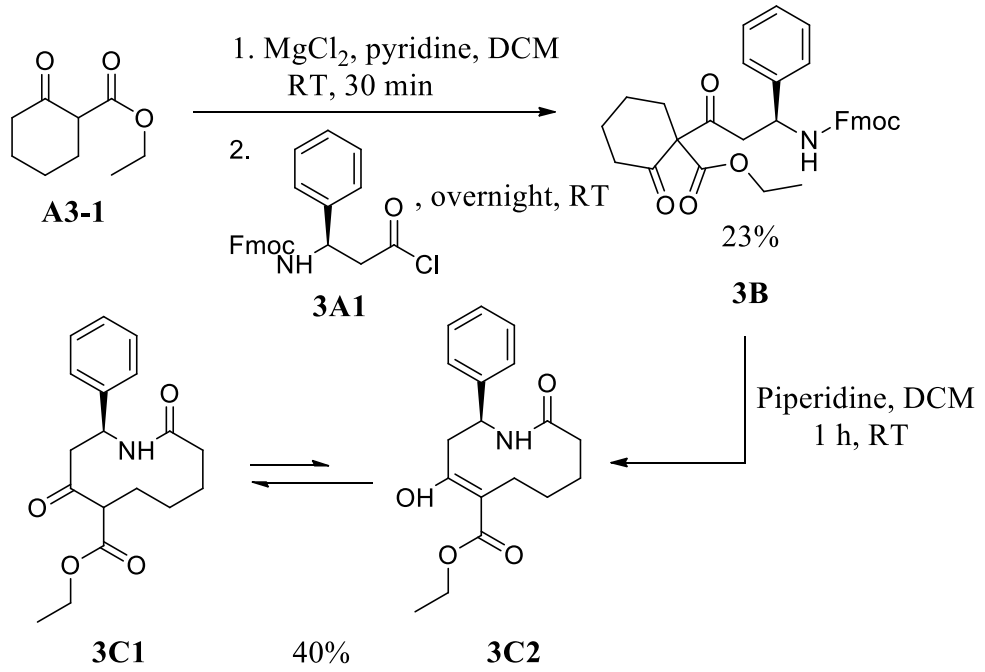

Figure 46: SuRE synthesis of 3C.

As a point of reference, commercially available 2-oxocyclohexane carboxylate, **A3-1**, was analysed by ^{1}H-NMR spectroscopy (300Hz, DMSO) as shown in **Figure 47** below. This starting material exists as a mixture of keto-enol tautomers (2:1) as evidenced by the singlet at 12.17 ppm (from the enol OH) and the ^{1}H signal at 3.55 (from the keto CH) in DMSO at room temperature.

The cyclic starting material, 2-oxocyclohexane carboxylate, **A3-1** was reacted with the freshly prepared acid chloride, **3A1** to afford **3B** via standard enolate chemistry as shown in **Figure 48** below. The formation of **3B** was confirmed by NMR spectroscopy.

An overlay of ^{1}H-NMR spectra of **A3-1**, **3A** and **3B** (**Figure 49**) showed that the CH proton signal at 3.59 ppm in the ^{1}H spectrum of 2-oxocyclohexane carboxylate, **A3-1**, was absent in **3B**. This suggested that a quaternary centre had formed as expected. This was then verified by HSQC. Furthermore, the PhCH proton signal which had been at 4.93 ppm in the Fmoc-amino-acid (**3A1**) appears at 4.98 ppm in **3B**. CH_2 proton signals which had previously appeared at 2.63 ppm in the Fmoc protected amino acid appear at 2.88 ppm and 3.05 ppm in **3B**. The signals appear more downfield because of greater deshielding.

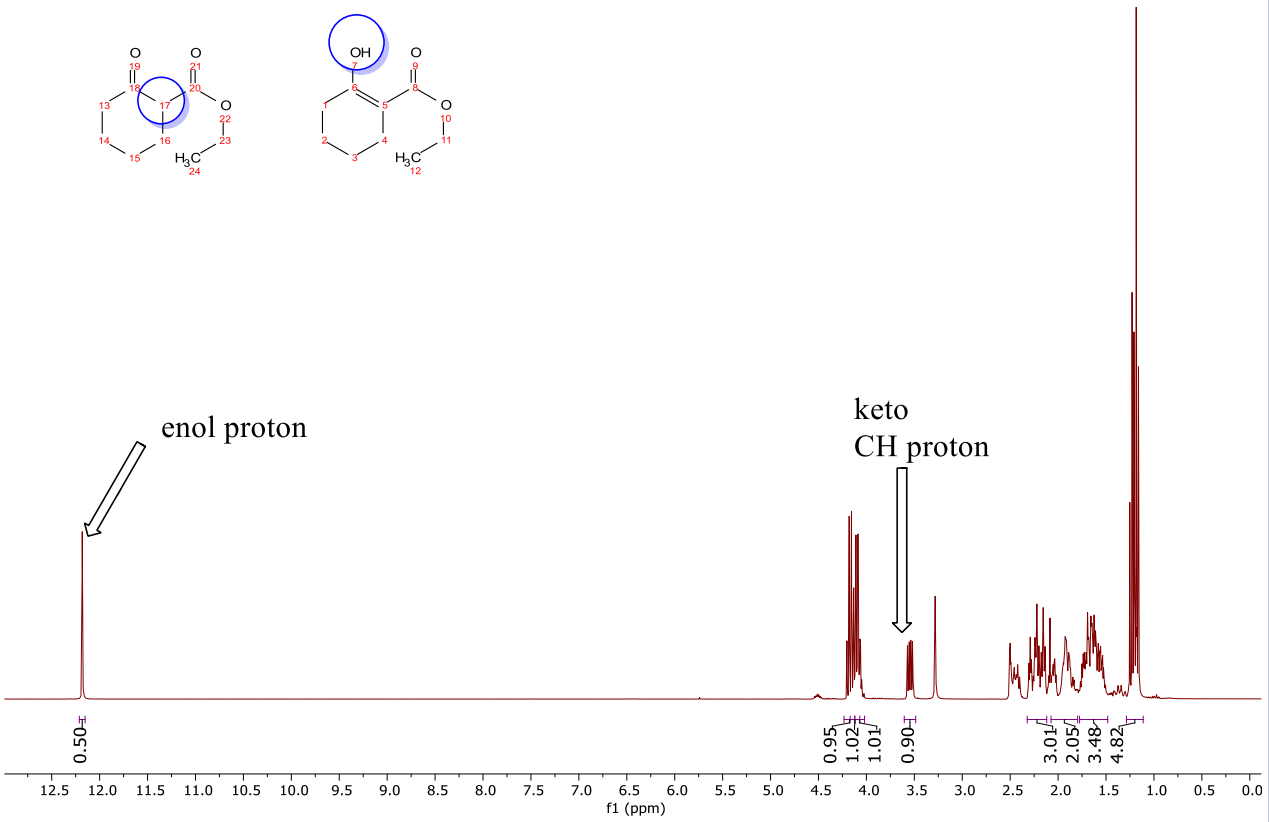

Figure 47: ^{1}H-NMR spectrum of A3-1.

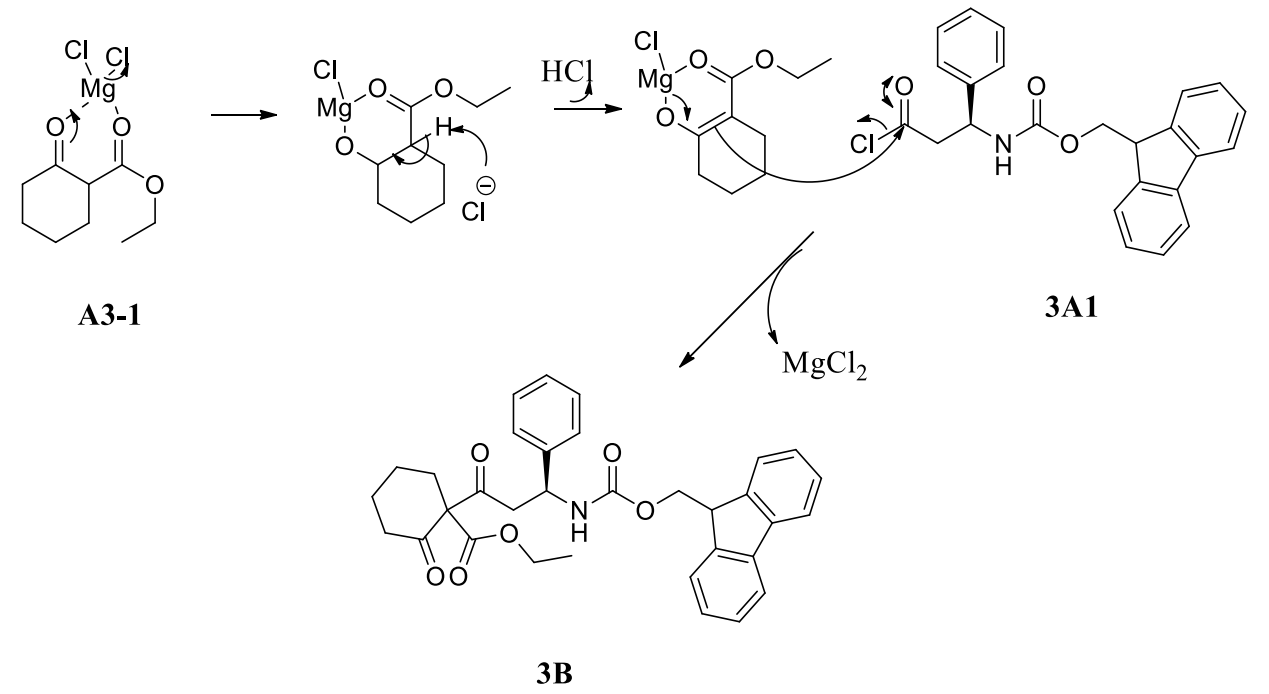

Figure 48: Mechanism for the formation of 3B.

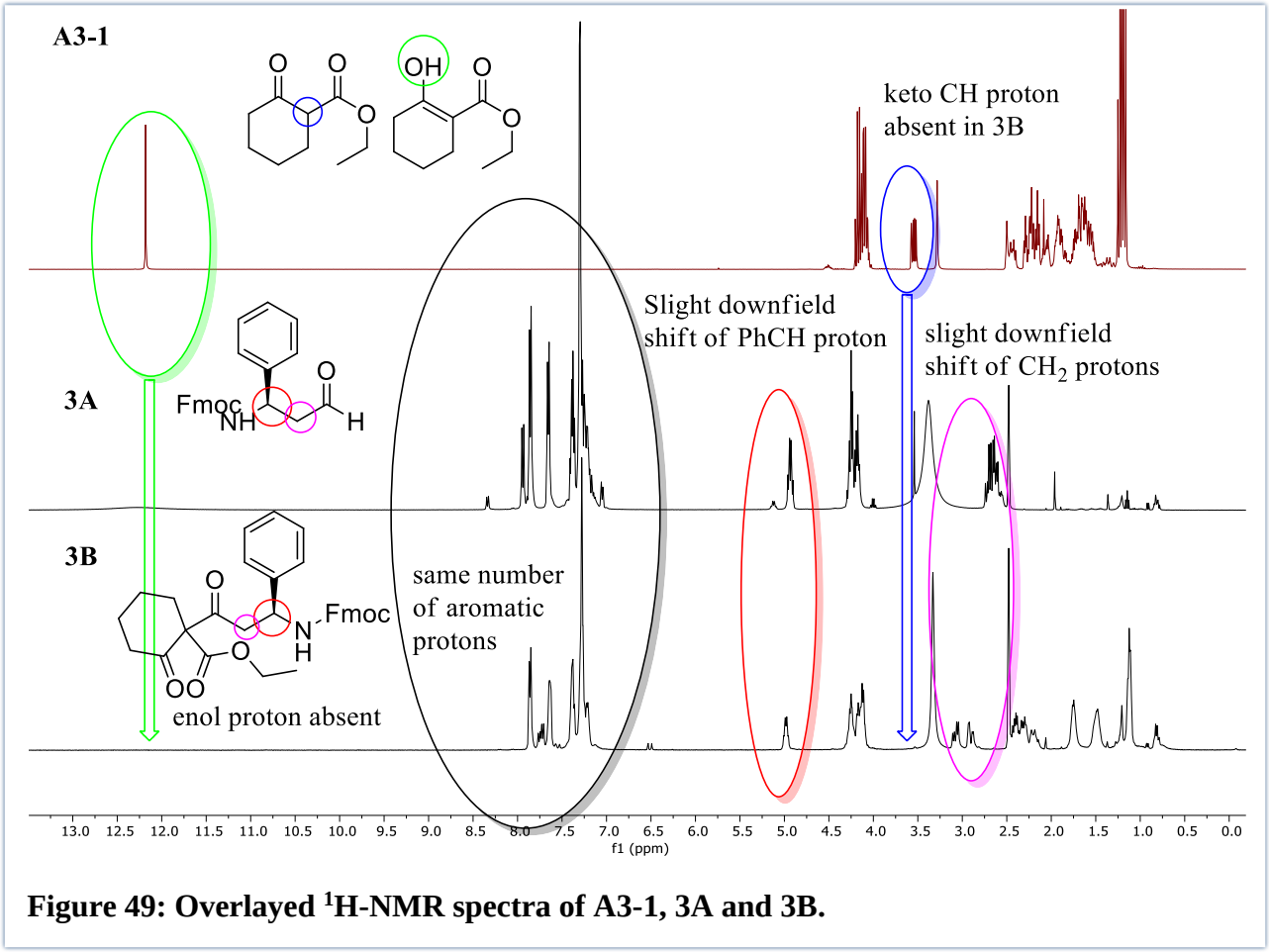

Figure 49: Overlayed ^{1}H-NMR spectra of A3-1, 3A and 3B.

One key diagnostic feature for the formation of **3B** is the existence of a quaternary carbon. In order to conclusively identify the quaternary carbon, we conducted an HSQC-DEPT analysis. The resultant spectra are shown in **Figure 50**, with quaternary carbon identifiable from not having any C-H correlations. Additionally, the spectra revealed the presence of two carbonyls, an ester and amide which are identifiable from their diagnostic chemical shifts, as well as the lack of C-H correlations in the HSQC spectra. Indeed, the ^{13}C-NMR on its own also shows this.

Compound **3B** was also subjected to 2D-NMR spectroscopic analysis. COSY and HMBC data allowed us to envision how the atoms are connected as shown in **Figure 51**. The spectra show that only one diastereomer was isolated at 23% yield, indicated by one set of signals in both ^{1}H and ^{13}C-NMR spectra. It was not beneficial to determine the stereochemistry at this point as it would be lost in the next transformation.

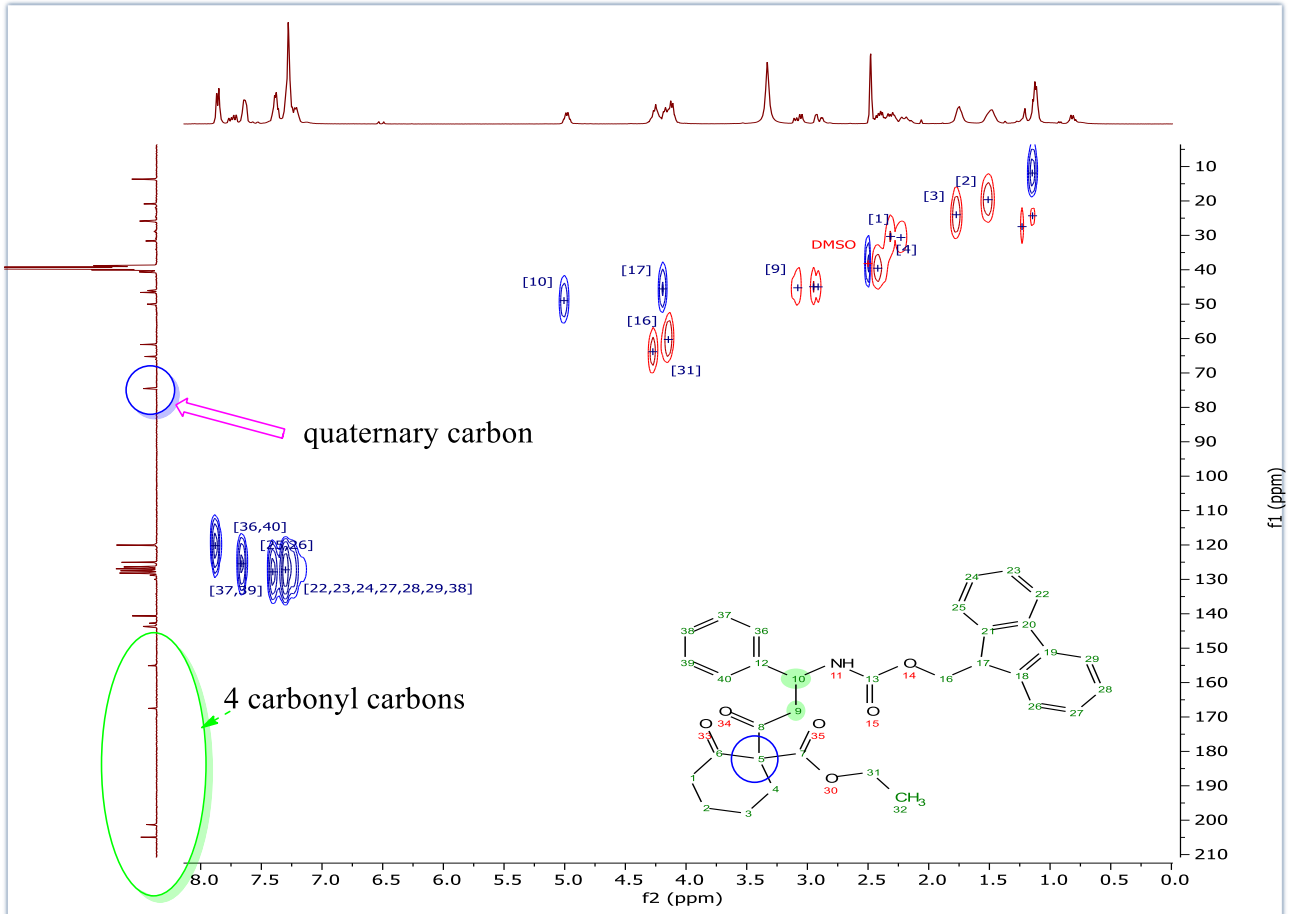

Figure 50: HSQC-DEPT spectra of 3B.

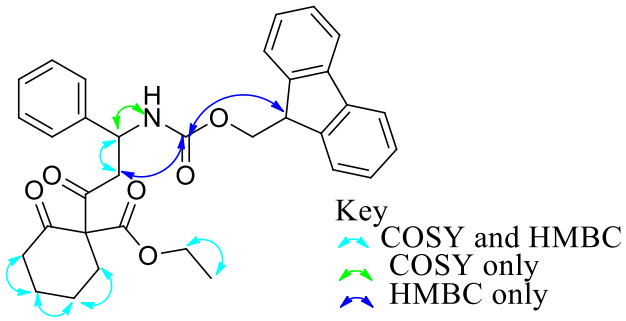

Figure 51: COSY and HMBC correlations of 3B.

The diastereomer **3B** was subsequently reacted with piperidine to deprotect the amine, allowing cyclization to occur (Please see chapter 5, section 3.1 for further details). The mechanism is shown in **Figure 52** below. The cyclized product, **3C** (existing as enol: keto tautomers; **3C1**:**3C2**) was obtained in 40% yield. The structure of the cyclized product, **3C**, was confirmed by ^{1}H-NMR, ^{13}C, HSQC and COSY data.

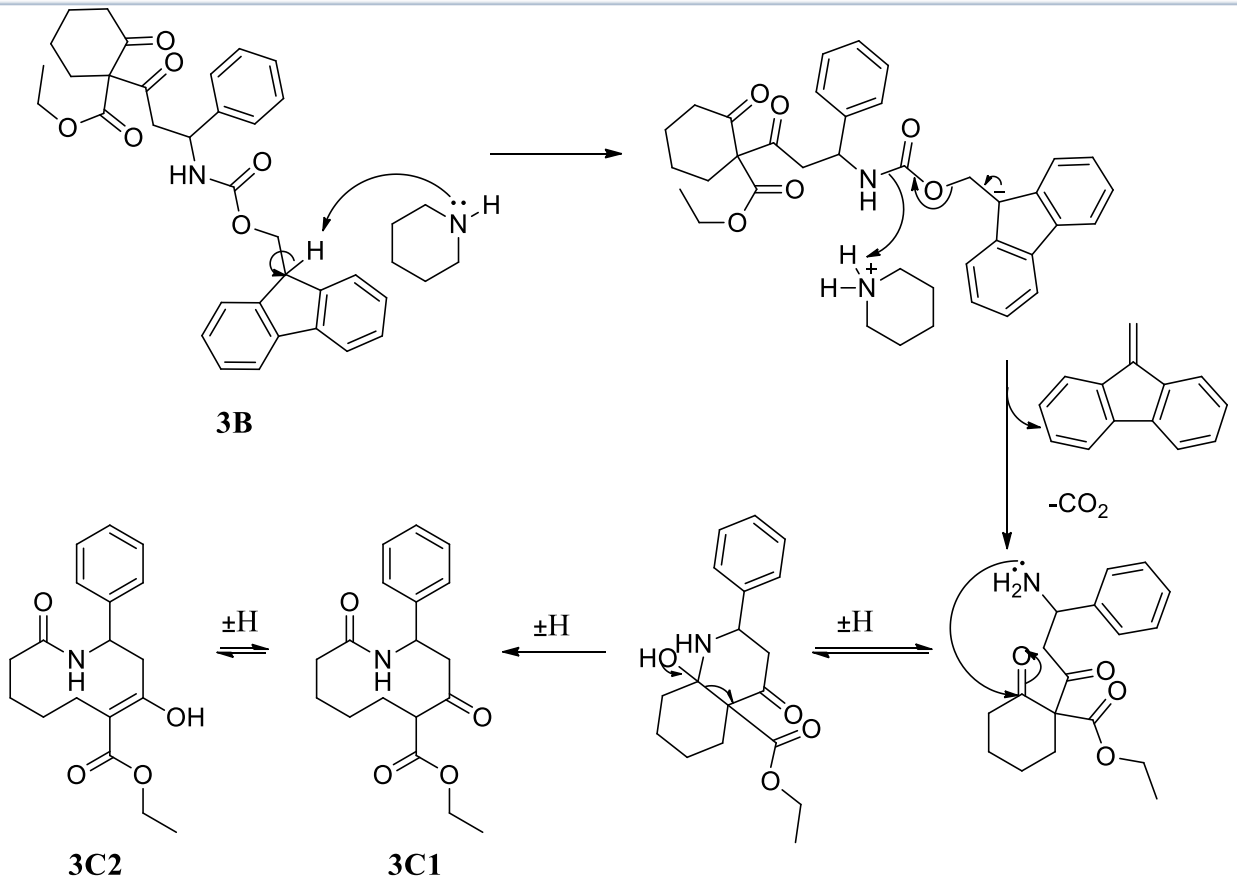

Figure 52: Mechanism of the deprotection of 3B to yield 3C.

An overlay of the ^{1}H-NMR spectra of **3B** and **3C** (**Figure 53)** showed that the Fmoc signals were absent in **3C**. The PhCH proton signal, which had been observed at 4.98 ppm in **3B**, can now be observed at 5.20 ppm in **3C**. This is consistent with the increased electrophilicity of the adjacent amide when compared the carbamate in **3B**, due to the absence of the resonance stabilisation by the oxygen atom. The CH_2 signals, which had appeared at 2.88 ppm and 3.05 ppm in **3B**, are observed at 2.65 ppm and 3.22 ppm in **3C**. Furthermore, a CH signal is observed at 4.35 ppm in **3C**, since the quaternary carbon in **3B** is now a tertiary centre in **3C** (only in the keto-form, **3C1**).

Although one diastereomer had been isolated for **3B**, the ^{1}H spectra of **3C** (**Figure 53**) indicated two sets of CH (H-7), PhCH (H-10), amide proton (H-4) signals and OH (H-13) signals. The CH (H-7) and PhCH (H-10) were confirmed as CH protons by phase from HSQC-DEPT, and the amide (H-4) and OH (H-13) were identified by lack of CH correlations. These observations suggest a mixture of diastereomers further compounded by apparent keto-enol-tautomerism. The two diastereomers could not be separated by flash chromatography as they appeared as a single spot on TLC. The diastereomeric ratio was calculated to be 4:1 in DMSO at RT using the relative integrals for the CH (H-7) signals. Using the relative integrals for the OH and CH signals, the keto-enol ratio was calculated to be 7:1 in DMSO at room temperature. The ^{13}C NMR spectrum shown in **Figure 54** had

the expected number of 18 carbon signals, although there were two sets of signals from the ester carbonyl (C-19) possibly due to the tautomers. The spectrum was comparable to literature.[47]

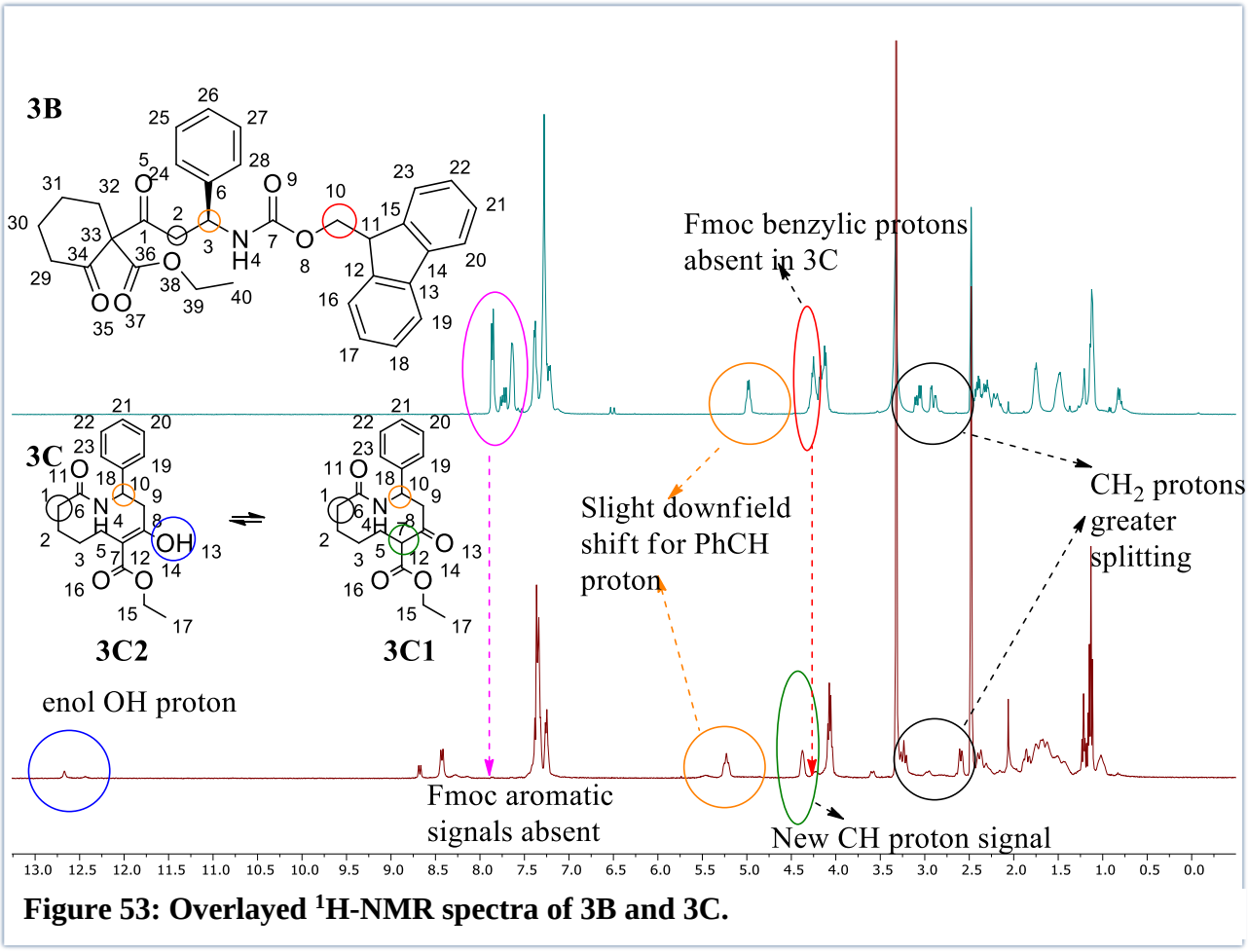

Figure 53: Overlayed ^{1}H-NMR spectra of 3B and 3C.

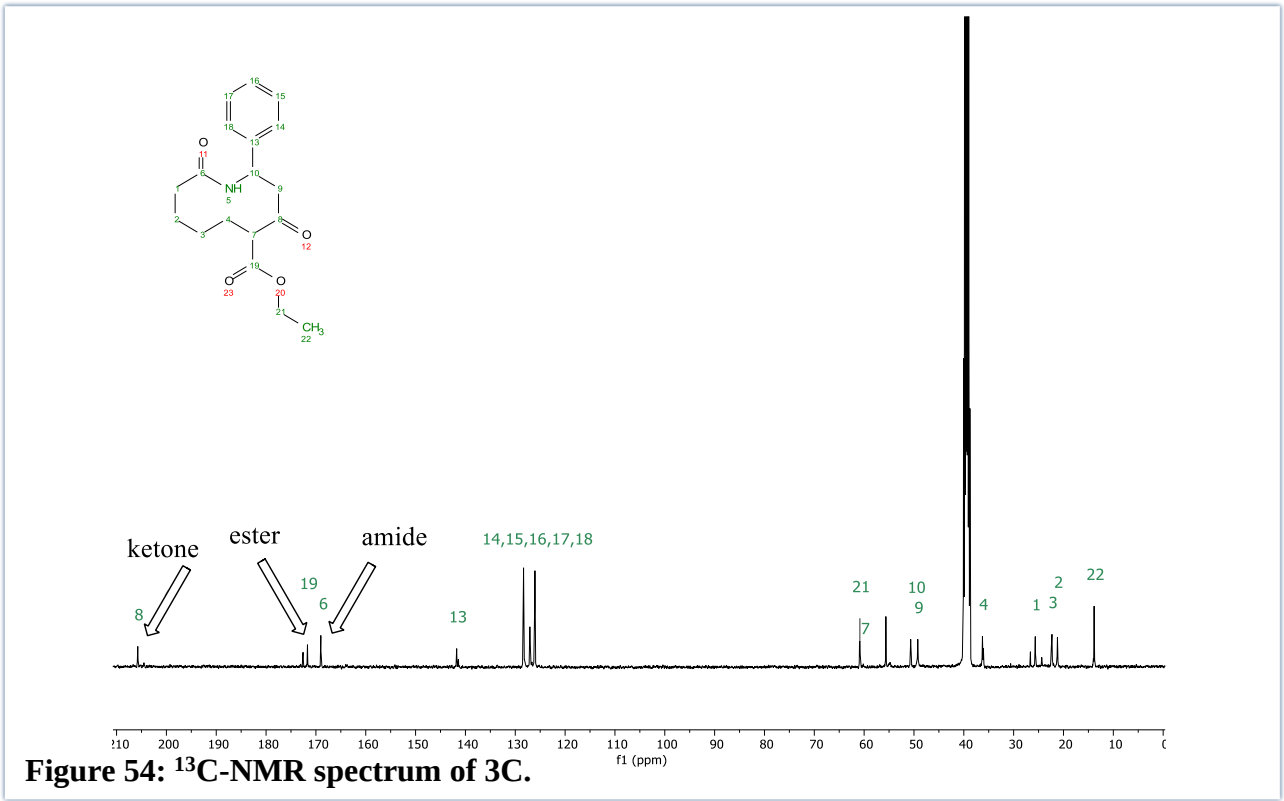

Figure 54: ^{13}C-NMR spectrum of 3C.

Compound **3C** was furthermore analysed using HSQC and COSY NMR spectroscopy experiments. COSY allowed us to confirm key assignments as shown in **Figure 55**. The absence of C-H correlations with the proton signal at 8.43 ppm and 8.66 ppm in the HSQC spectra allowed us to identify the amide proton.

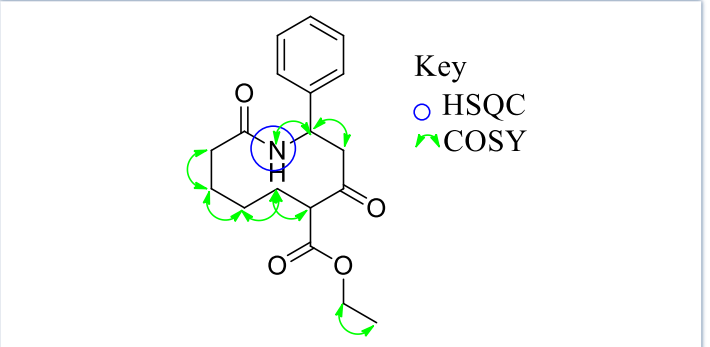

Figure 55: HSQC and COSY assignments of 3C.

The compound **3C** was subjected to HRMS analysis (**Figure 56**) to determine if the molecular weight matched. HRMS was used only as a secondary characterization tool because of the previously mentioned challenge that the deprotected intermediate would have the same molecular mass as the product. The calculated values were as follows; a) Chemical Formula: $C_{18}H_{23}NNaO_4$, b) Exact Mass: 340.1525, c) Molecular Weight: 340.3693, d) *m/z*: 340.1525 (100.0%), 341.1558 (19.5%), 342.1592 (1.8%). The experimental *m/z* ratio was 340.1525, thus the deviation from the calculated m/z ratio is zero.

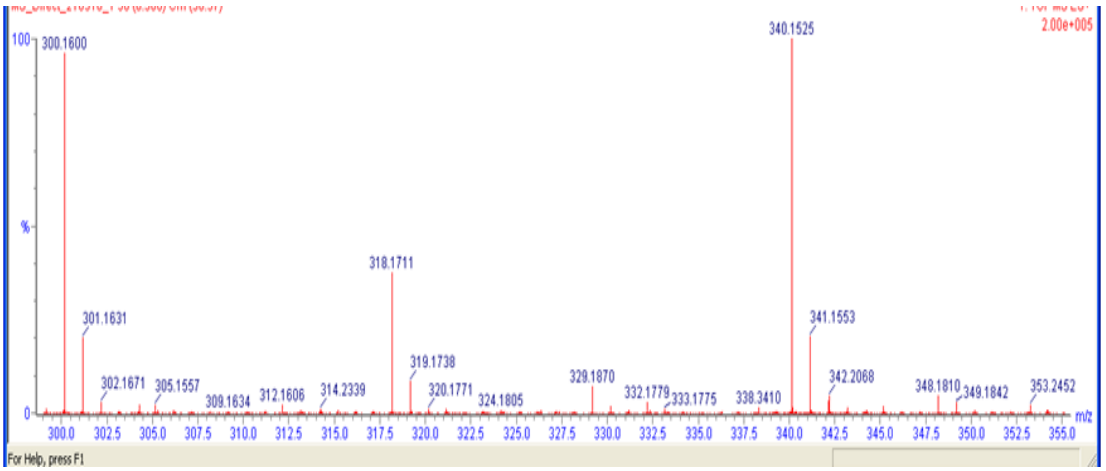

Figure 56: HRMS spectrum of 3C.

We repeated this procedure starting with a five-membered β-keto ester, **A3-2** to yield a nine-membered macrocycle, **3D** (**3D1** and **3D2**) (**Figure 57**). For this procedure, we did not isolate

the intermediate, **A3-3**. The yield over the two steps was 60% and the spectrum was comparable to literature.[47]

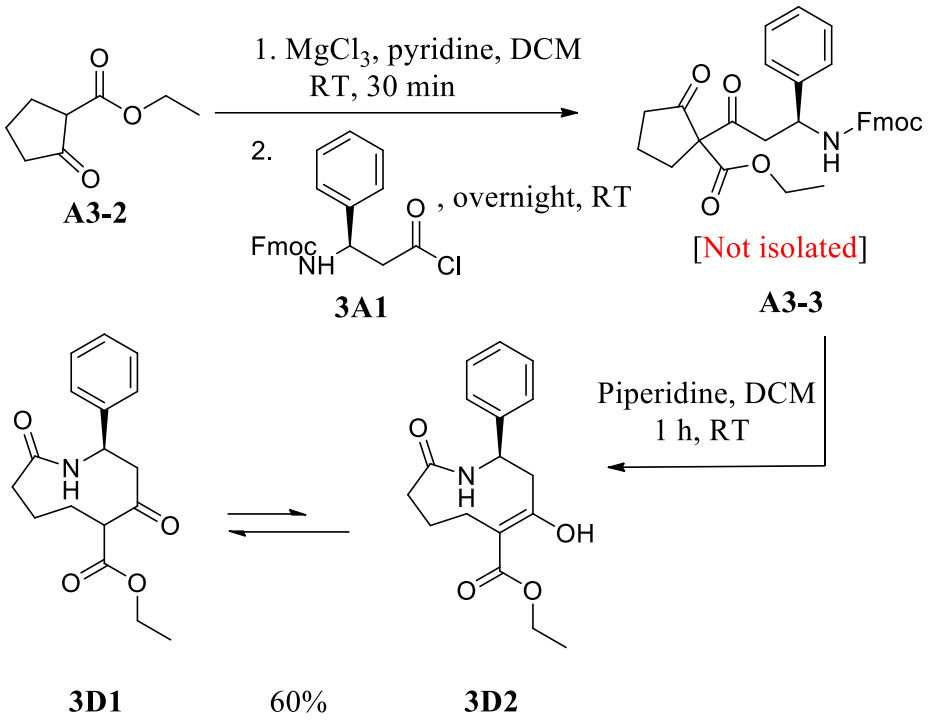

Figure 57: SuRE synthesis of 3D.

Once satisfied with our ability to prove the cyclization using NMR spectroscopy, we moved on to trying the SuRE methodology on a simple lactam — a more related precursor to our envisaged DHQ. To this end, macrocycle **3E** was synthesized (Please see chapter 5, section 3.2 for further details) as shown in **Figure 58**, without isolating the intermediate **3P**, and obtained in 12% yield.

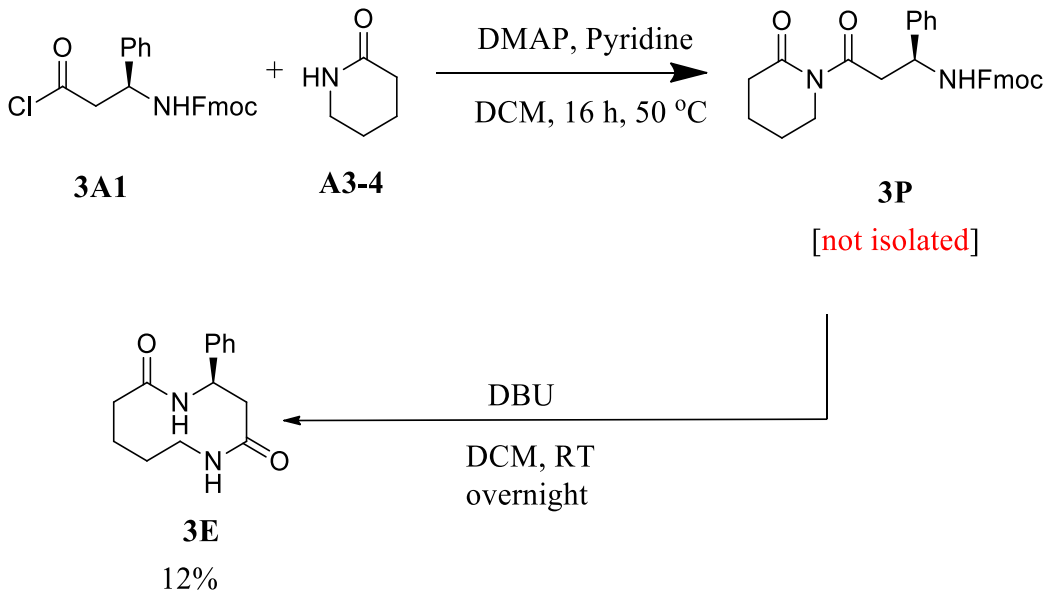

Figure 58: SuRE synthesis of 3E.

The structure of **3E** and the ^{1}H-NMR spectrum is given in **Figure 59** below. The structure was comparable to literature, although the yield was poor.[63]

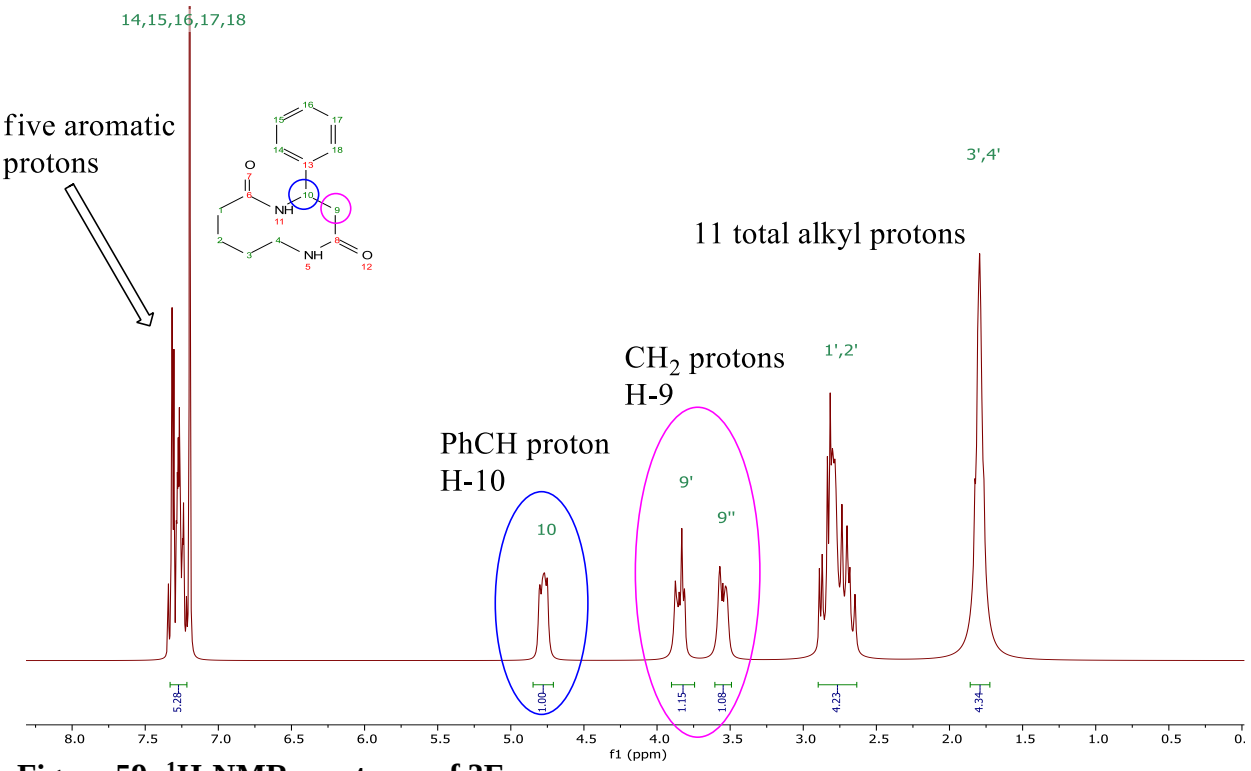

Figure 59: ^{1}H-NMR spectrum of 3E

As we had become accustomed to the SuRE conditions, we moved to applying this process to our DHQs precursor and selected the simple *N*-unsubstituted DHQ, **A3-5** as a model substrate (**Figure 60**).

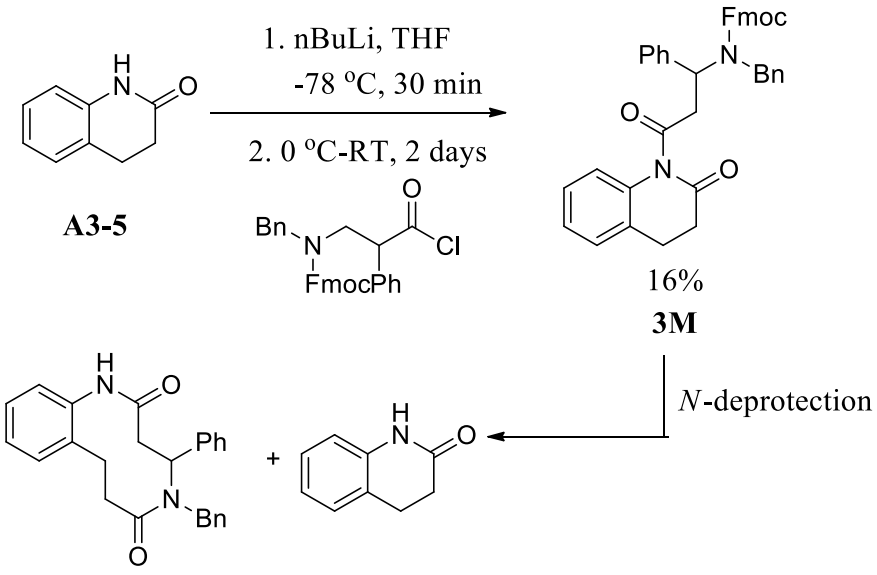

Figure 60: Attempted SuRE synthesis of 3O.

Unfortunately, only the DHQ-amino acid adduct, **3M** was obtained in 16% yield. Despite the low yield, we wanted to obtain proof of concept of the SuRE protocol, so we went on to do the deprotection step. Unfortunately, instead of obtaining the cyclized product, **3O**, the starting *N*-unsubstituted DHQ **A3-5** was recovered. We thus sought to find a different way to initiate the cyclization.

Unsworth and co-workers had been working on improving their methodology and had discovered a more efficient way of doing these macrocyclizations. They developed a **C**onjugate **A**ddition or **R**ing **E**xpansion (CARE) methodology which involves *N*-acylation of a lactam with acryloyl chloride, followed by a Michael addition (conjugate addition to the imide Michael acceptor) on treatment with an amine and subsequently ring expansion (**Figure 61**).[6] We therefore decided to move on from the SuRE methodology and try this instead. As before, we first tried the methodology on a simple lactam, **A3-4**, as shown in **Figure 61**, with n=1 and benzyl aniline as the amine.

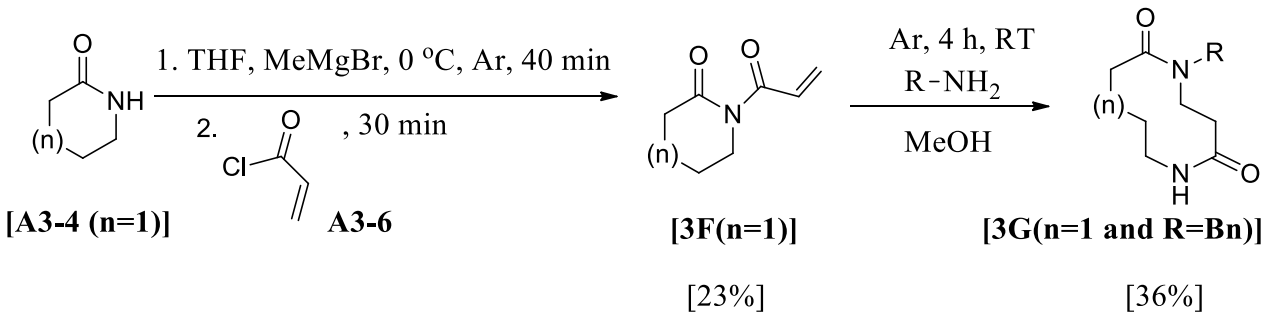

Figure 61: CARE synthesis of 3G.

The intermediate product (**3F**) was obtained in 23% yield and the final product (**3G**) in 36% yield. Although these yields were low, they showed improvement from the previous methodology. However, when we tried this methodology on our DHQ, the reaction failed to yield the desired product (**3H**) at the acylation step (**Figure 62A**). We suspected that these challenges were associated with the our attempts to generate the acryloyl chloride (**A3-6**) *in situ* from the acrylic acid **A3-7** (**Figure 62B**).[64]

We noted that the Unsworth group had used commercially available acryloyl chloride starting material (not available in South Africa at the time); however, we were reluctant to prepare the acryloyl chloride again as the process involved distillation and therefore possible exposure to this toxic chemical. We therefore decided to find other ways of achieving our desired goal.

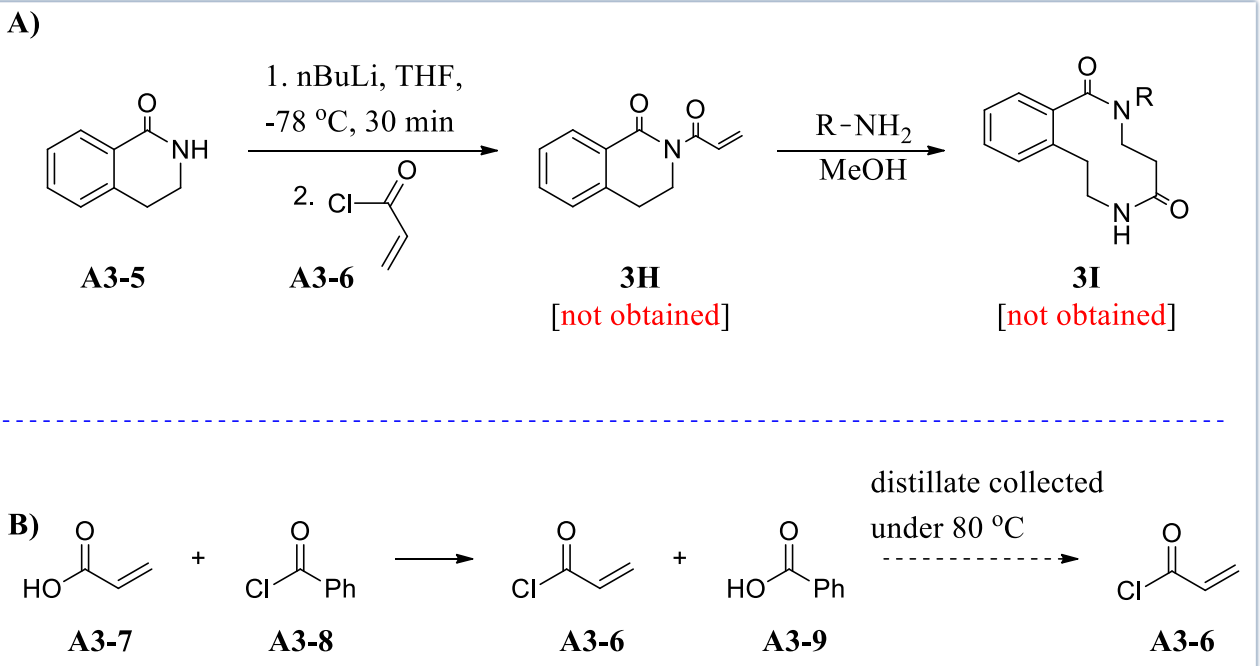

Figure 62: A) Attempted CARE synthesis of 3I. B) Synthesis of A3-6.

To ascertain if the problematic step was indeed related to the acylation of the *N*-unsubstituted DHQ (**A3-5**) we performed a trial reaction by subjecting **A3-5** to benzoyl chloride. In the event, we obtained the desired product in 61% yield (**Figure 63A**). With this promising result, we considered a route that involved acylation using 3-chloropropionyl chloride, with a view to ultimately access the desired amine following substitution of the alkyl chloride (**Figure 63B**). Disappointingly, the reaction once again failed at the acylation step.

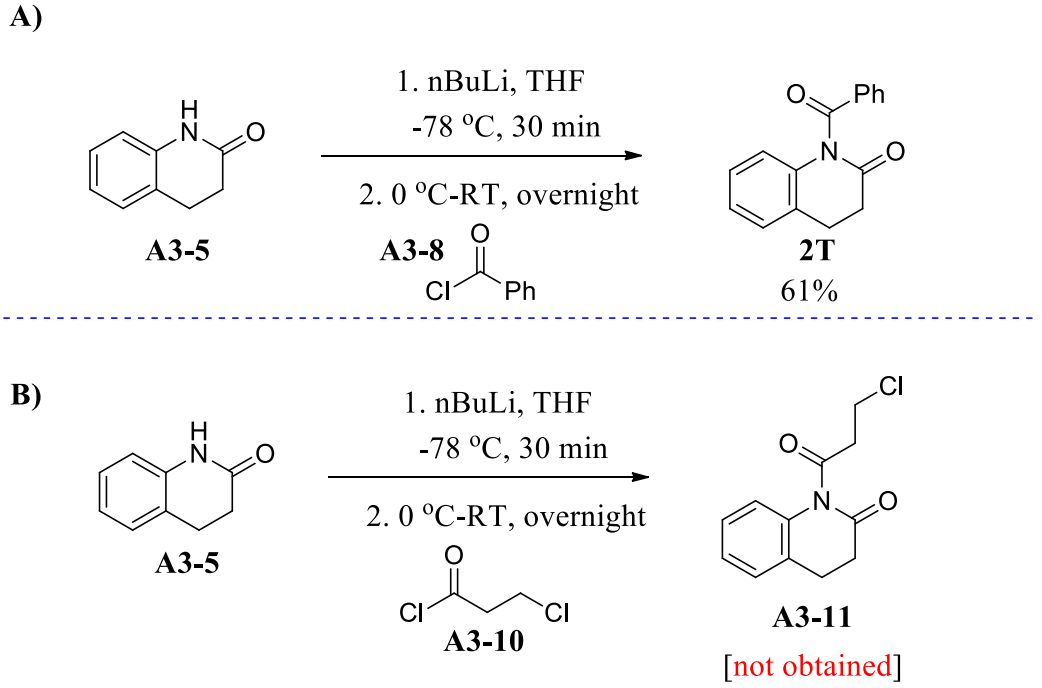

Figure 63: Acylation of A3-5 with A) benzoyl chloride B) 3-chloropropionyl chloride.

In light of these challenges, we considered that we did not necessarily need the cyclising fragment to be attached via an amide bond. Thus, we envisaged installing the cyclising tether via an alkylation instead (**Figure 64**). Somewhat gratifyingly, reaction with 1,3-dibromopropane yielded the alkylated product **3J** (confirmed by ^{1}H-NMR, **Figure 65**); however, as a 1:1 mixture with *N*-allyl substituted DHQ, **2V**, obtained via subsequent elimination.

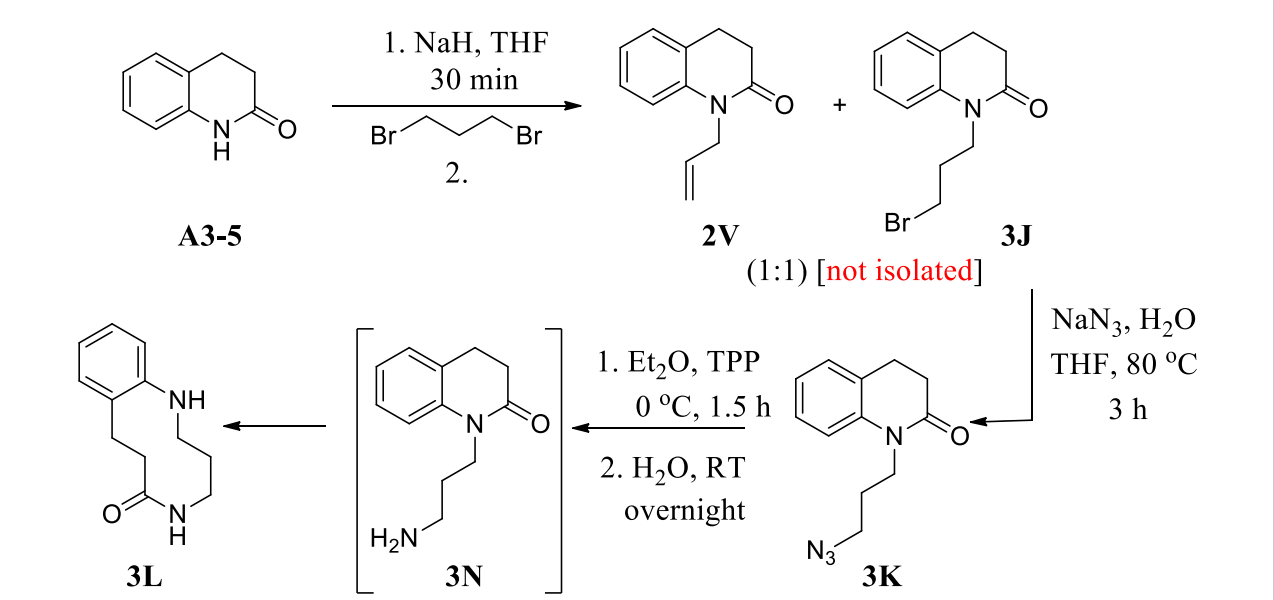

Figure 64: Alternative SuRE synthesis of 3L.

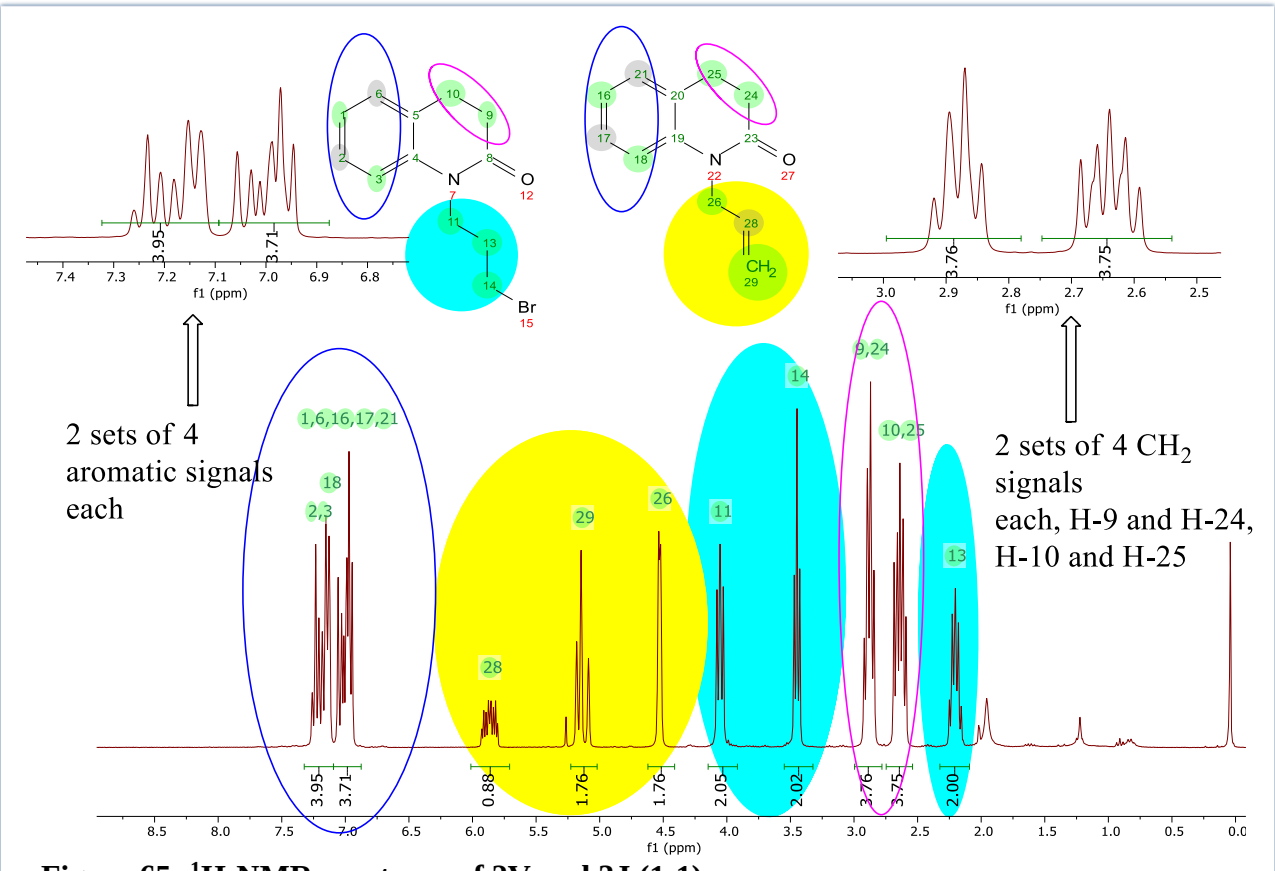

Figure 65: ^{1}H-NMR spectrum of 2V and 3J (1:1).

Successful formation of **3J** can be proved by the signals highlighted in blue in **Figure 65** above, showing two triplet signals integrating for two protons each from H-11 and H-14 at 4.05 and 3.45 ppm, respectively, and a multiplet also integrating for two protons at 2.21 ppm corresponding to H-13. The 4 aromatic signals are found in the two sets of 4 within the aromatic region and the H-9 and H-10 signals are contained within the two sets of 4 alkyl signals. The presence of these two sets, in addition to the signals highlighted in yellow points to the presence of *N*-allyl substituted DHQ, **2V**. Two sets of signals are also seen in the ^{13}C-NMR spectrum shown in **Figure 66** below.

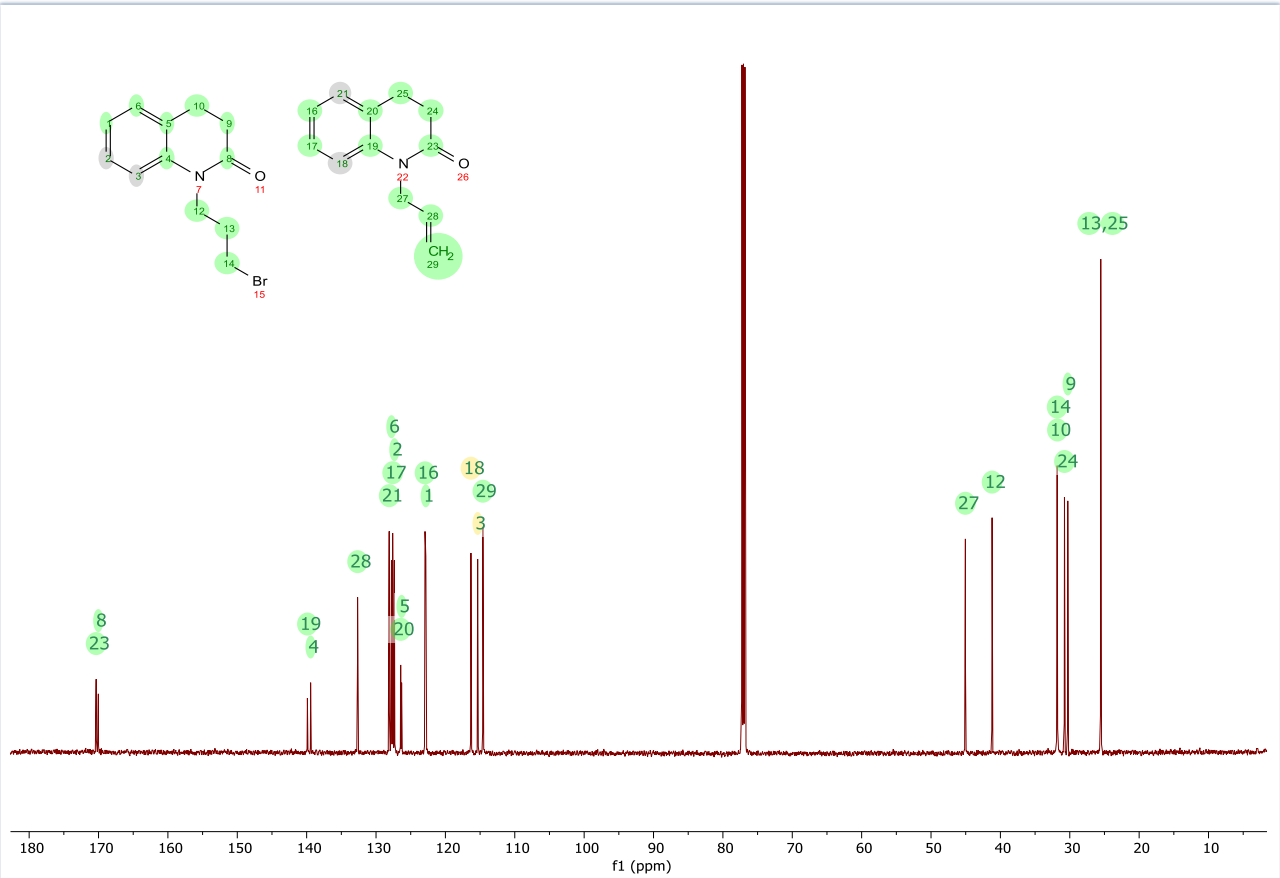

Figure 66: ^{13}C-NMR spectrum of 2V and 3J.

Due to the difficulty of separation, the mixture was carried forward to the next step where the bromine was substituted with an azide. The azide was confirmed by performing Staudinger reaction on the TLC plate to allow visualization using ninhydrin as a stain reagent.[65] The crude azide was then subjected to the Staudinger deprotection conditions with triphenyl phosphine (TPP). Analysis of the isolated product by ^{1}H-NMR spectroscopy revealed a product together with coeluted triphenyl phosphine oxide (TPO) from the column (**Figure 67**). While the non-TPO integrations (7.30 – 8.00 ppm) were consistent with our desired product **3L** (namely 4 aromatic protons and 11 aliphatic protons), we were aware that the uncyclized amine **3N**, would reveal a similar spectrum. We were

encouraged however by the downfield signal at 8.60 ppm, as this could be an indication of the N-H amide proton.

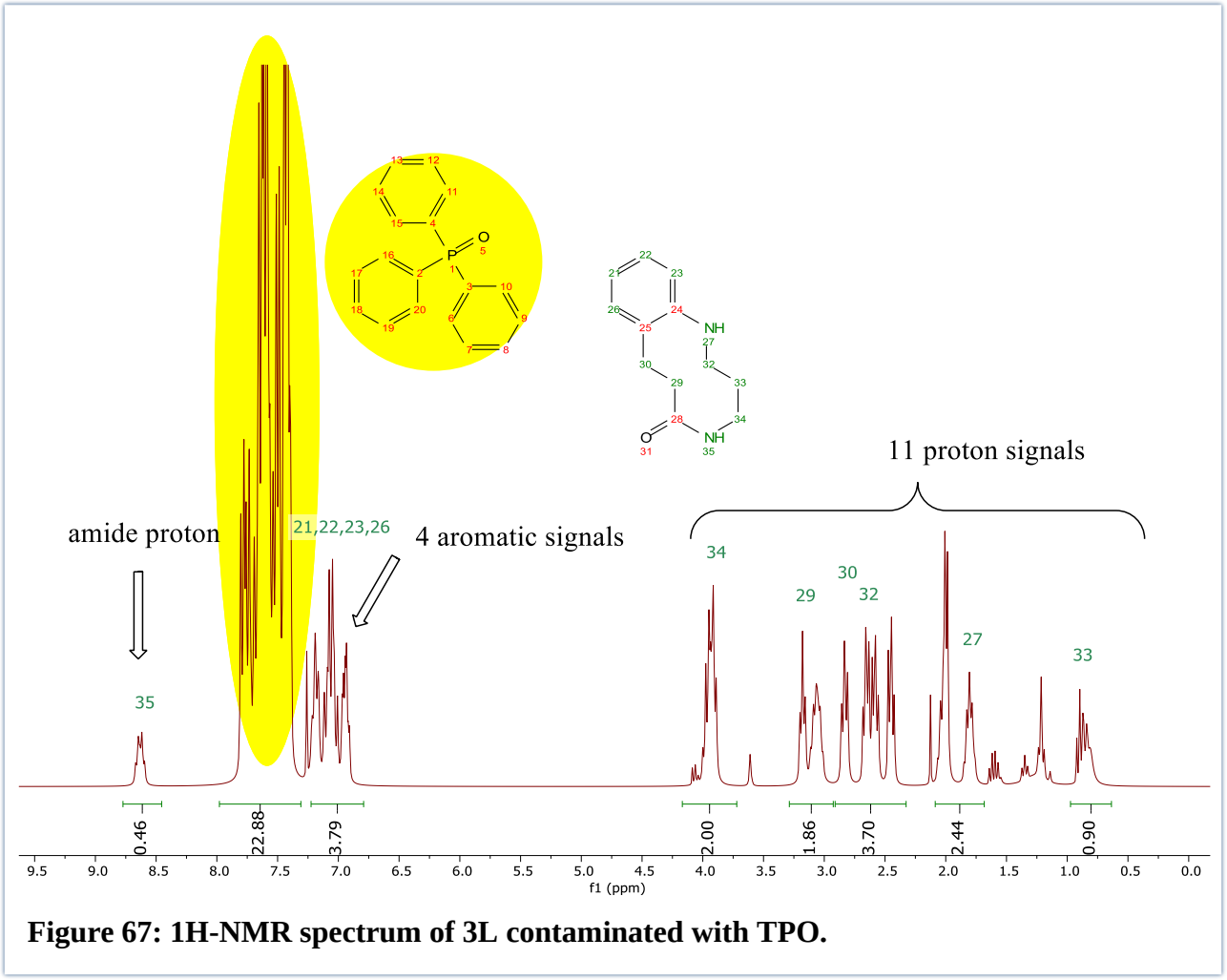

Figure 67: 1H-NMR spectrum of 3L contaminated with TPO.

3.2 Future Work and Considerations

We had attempted to remove the TPO in order to improve our spectroscopic data; however, this resulted in product degradation. To avoid these challenges, we considered using a nitrile group instead as these can be reduced via other methods (**Figure 68**).

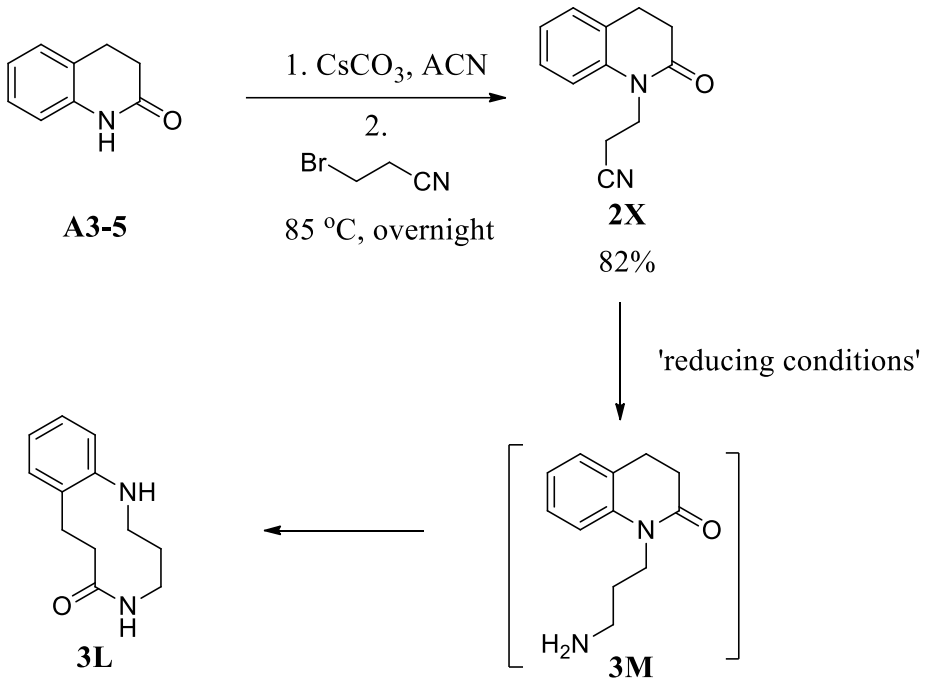

Figure 68: Different SuRE route envisaged.

In the event, the *N*-alkylated DHQ, **2X**, was indeed synthesised by substitution with 3-bromopropionitrile (confirmed by ^{1}H- and ^{13}C-NMR, **Figures 69** and **70**). This posed the challenge of finding a chemoselective method of reducing the nitrile without reducing the amide, as $LiAlH_4$ could possibly reduce both sites. We found that a similar transformation to what we were hoping to achieve used hydrogen and a PtO_2 catalyst.[66] Despite the fact that we did not have this catalyst on hand, time constraints prevented us from following up with both this route, as well as the azide method above. This however will be a point for future work.

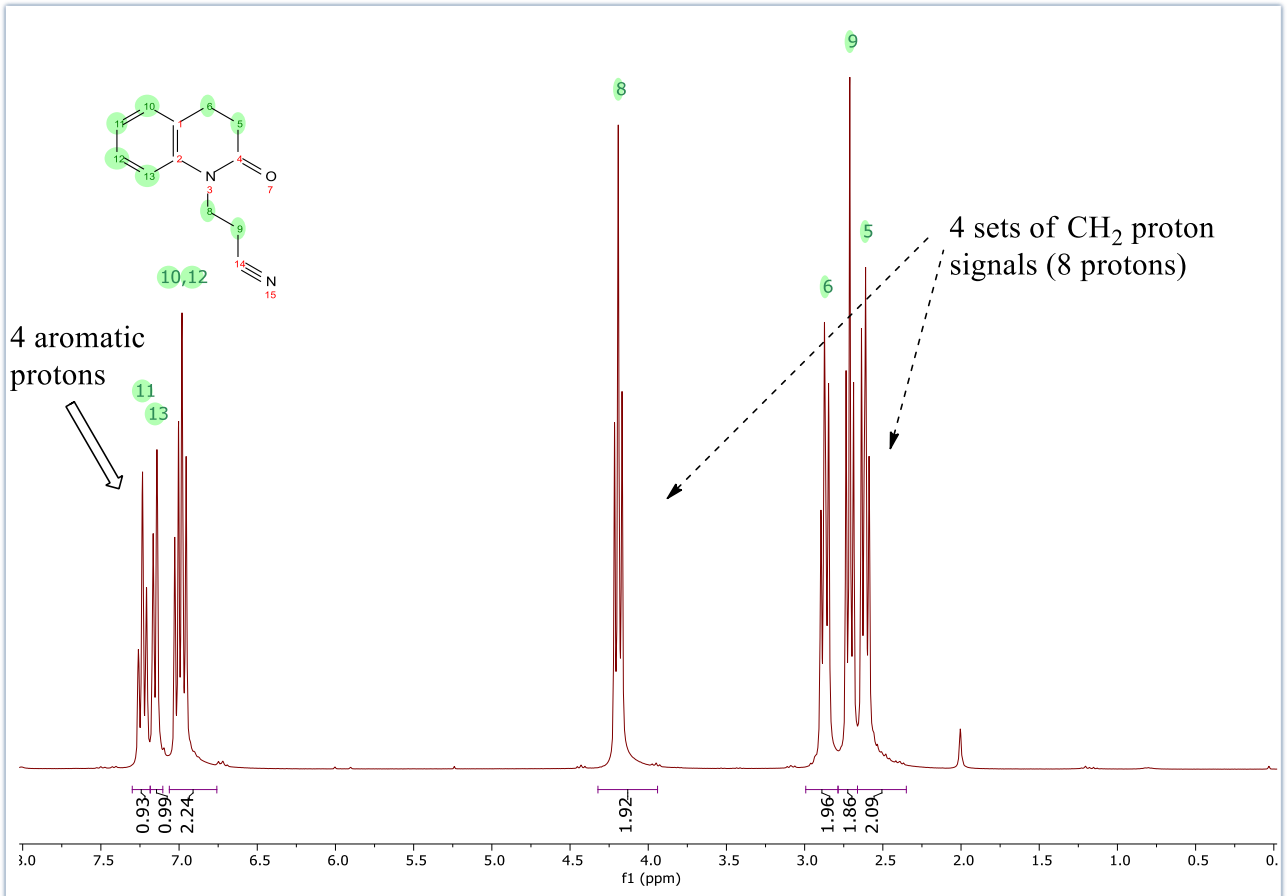

Figure 69: ^{1}H-NMR spectrum of 2X.

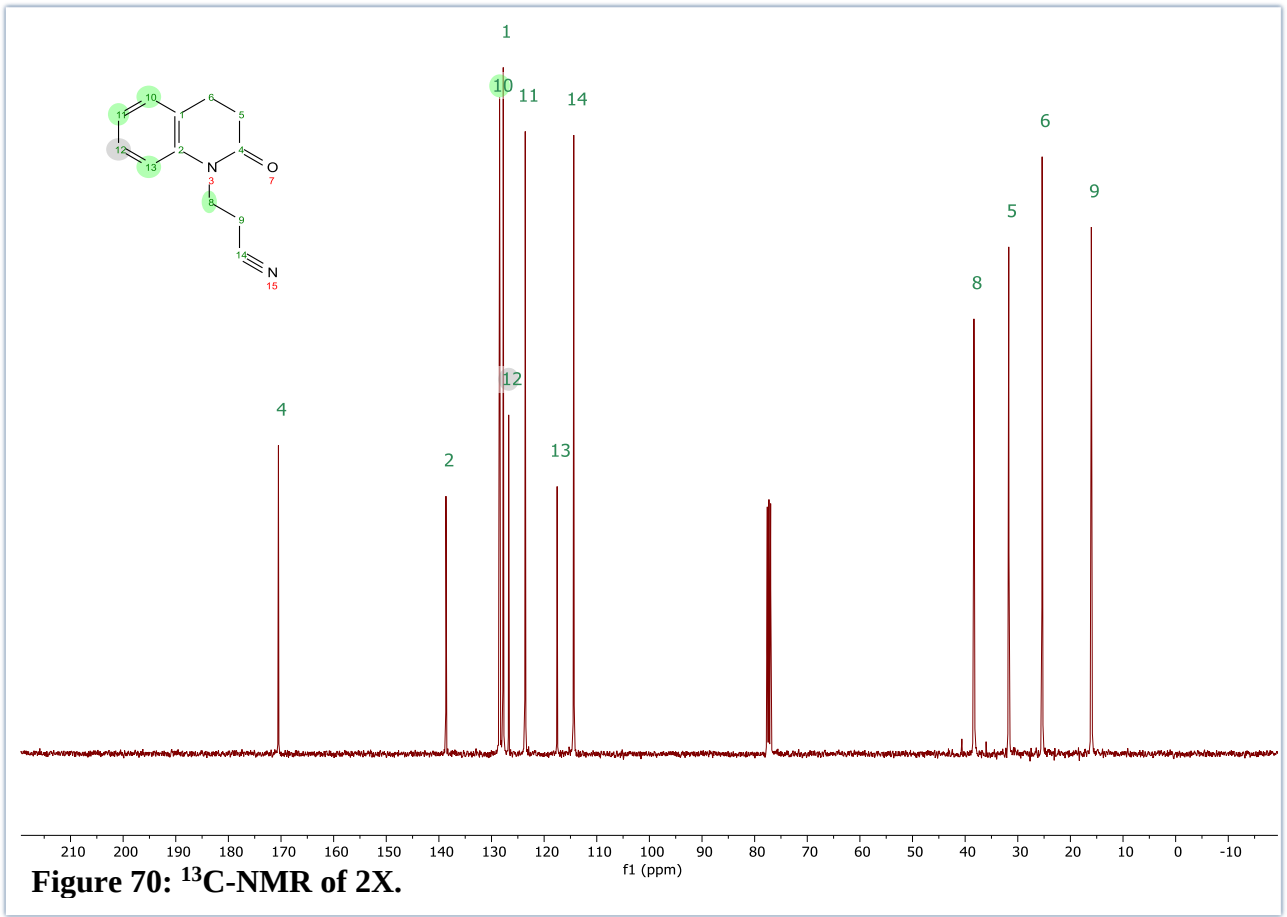

Figure 70: ^{13}C-NMR of 2X.

CHAPTER 4: QUINOLINONES

4.1 A Serendipitous Discovery

We considered a demethylation strategy for the synthesis of *N*-unsubstituted DHQs from *N*-methyl DHQs because the method we had developed (Chapter 2) makes use of an expensive catalyst, whereas synthesis of *N*-Me DHQs makes use of inexpensive 2-chlorothioxanthone (2-CTX). A literature search turned up a recent publication by Yi *et al* where demethylation was achieved using a Cu catalyst and NFSI as an oxidant (**Figure 71**).[7]

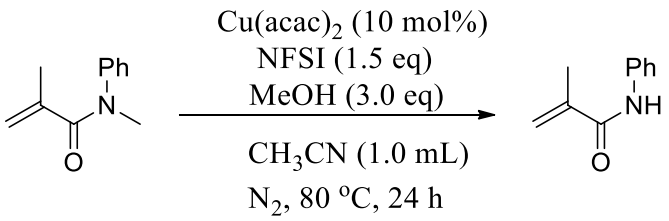

Figure 71: Demethylation strategy.

4.2 Results and Discussion

4.2.1 Preliminary Studies

We decided to attempt this method on our *N*-methyl DHQ (**A4-1**) as shown in **Figure 72** below. Interestingly however, rather than the expected product **4B**, we obtained the oxidation product, namely quinolinone **4A** in 51.7% yield.

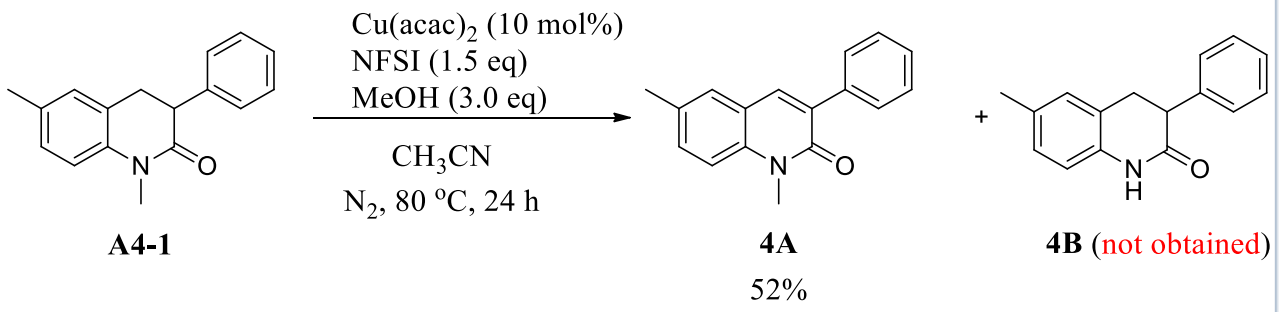

Figure 72: Attempted demethylation of A4-1.

The product was confirmed with ^{1}H-NMR spectroscopy and the spectrum is shown in **Figure 73**. The presence of the *N*-Me signal (H-12) at 3.78 ppm showed that our desired demethylation had failed. However, we could see that we had a new product as the alkyl signals from the starting material were no longer present and a new signal could be seen close to the aromatic region at 7.28 ppm, consistent with the alkenyl proton H-10 and in accordance with literature reports.[67]

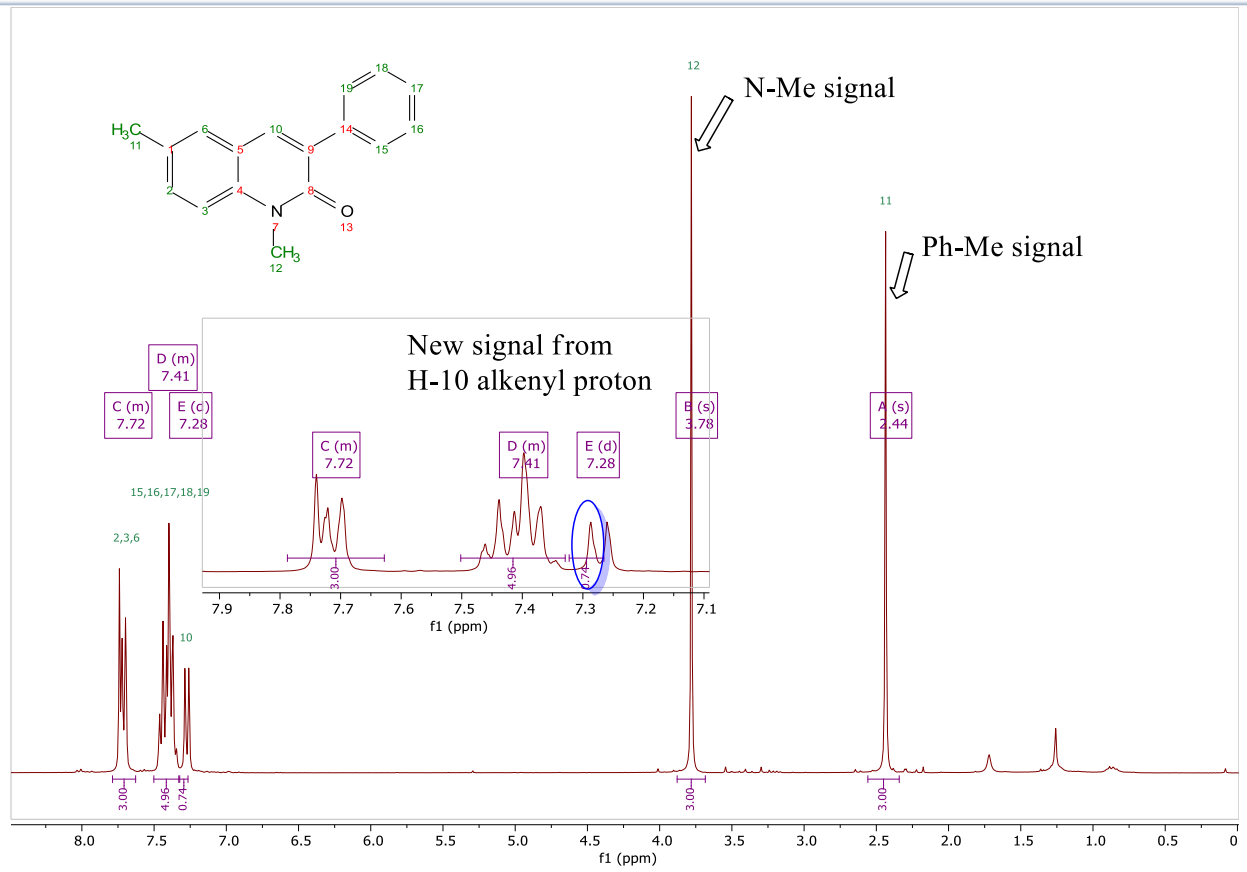

Figure 73: ^{1}H-NMR spectrum of 4A.

Our proposed view of this reaction is shown in **Figure 74**. Following the *in situ* formation of Cu(I), NFSI undergoes a single electron reduction to produce the NSI radical (**A**), with the concomitant regeneration of Cu(II). Hydrogen atom transfer (HAT from **A4-1**) by radical **A** produces the methine DHQ radical **A4-2** which is subsequently oxidised to its benzylic carbocation **A4-3** by Cu(II), after which elimination promoted by the fluoride anion affords quinolinone **4A**.

Although this was not what we set out to achieve, the result was exciting nonetheless as it meant that we had found a methodology to oxidize DHQs. Quinolinones are important biological molecules which have found use as antiviral, anticancer, antiulcer, and antihistaminic agents. Besides this, we saw this as an opportunity for late-stage functionalization of synthetic drug molecules, either by the simple oxidation or an oxidation followed by a substitution to introduce various R-groups.[8]

The utility of this methodology was exciting because existing methods for this transformation make use of expensive transition metals such as Pd[8–10] and Pt[11]and high temperatures.[12] To circumvent the use of high temperatures, we sought to make the method photochemical such that it can be run at room temperature. We surmised that we could instead use a Cu photocatalyst at room temperature, together with NFSI as the oxidant.

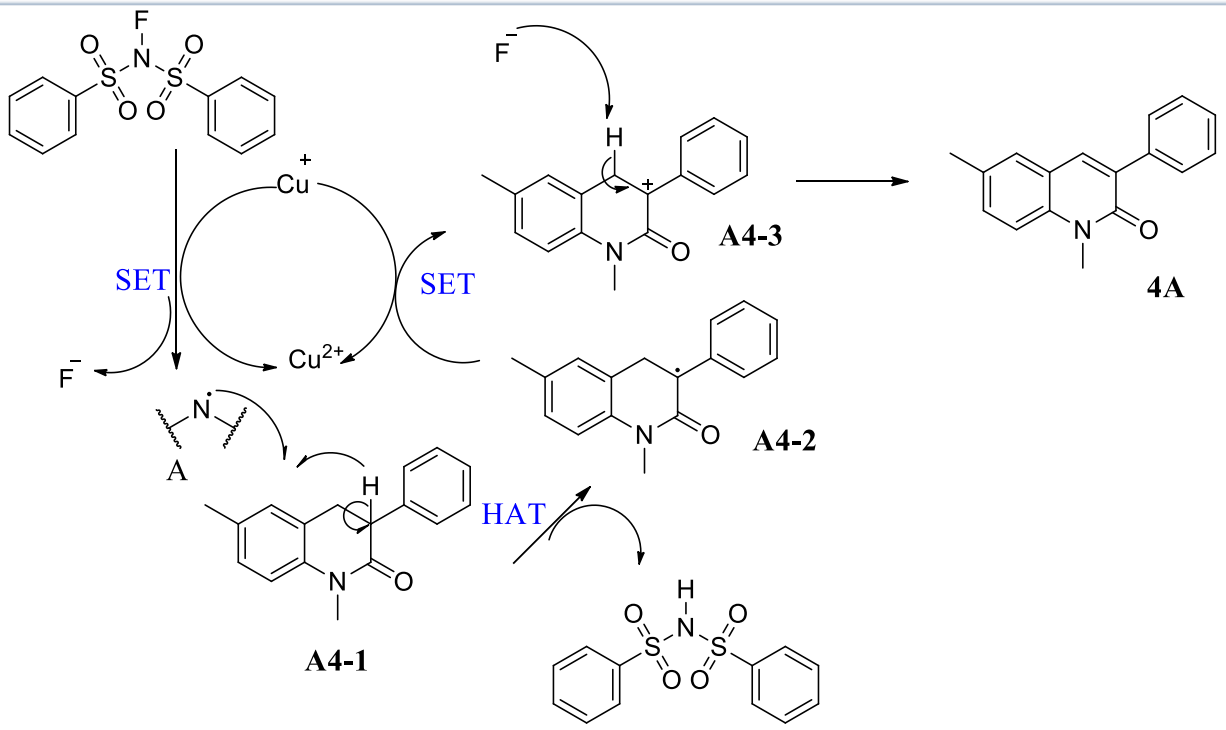

Figure 74: Proposed mechanism for the formation of 4A.

4.2.2 Catalyst Screen and Optimization

Our optimisation studies (**Table 2**) began with model DHQ **2W** using the copper catalyst [Cu(DMP)$_2$Cl]Cl (CuDMP) under blue light irradiation (450 nm) in accordance with its UV-Vis absorption spectra (see experimental section). Gratifyingly, **4B** was obtained in 69% yield (**entry 1**), while only trace product was observed in EtOH (**entry 2**). Control reactions in the absence of Cu and NFSI, confirmed the importance of these reagents (**entries 3–5**). Switching to a metal-free process, using 2-chlorothioxanthone (2-CTX) in ACN at 405 nm irradiation (see experimental section) gave a pleasing 72% yield (**entry 6**), while switching to greener solvents such as EtOAc and EtOH gave reduced yields of 65% and 58%, respectively (**entries 7–8**). Modification of the oxidant to either terminal oxygen, peroxide or persulfate, failed to produce any reaction (**entries 9–11**).

Table 2. Optimisation Studies.

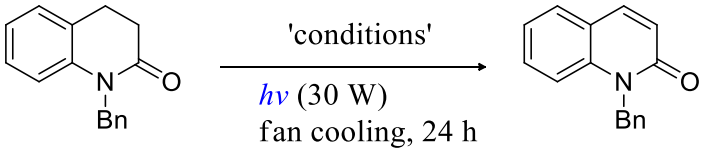

2W **4B**

Entry	Photocatalyst	Wavelength	Catalyst mol%	Oxidant	Solvent	Yield (%)
1	CuDMP	450	20	NFSI	ACN	69
2	CuDMP	450	20	NFSI	EtOH	trace
3	CuDMP	450	20	none	ACN	Not detected
4	none	405/450	-	none	ACN	Not detected
5	none	405/450	-	NFSI	ACN	Not detected
6	2-CTX	405	20	NFSI	ACN	72
7	2-CTX	405	20	NFSI	EtOAc	65
8	2-CTX	405	20	NFSI	EtOH	58
9	2-CTX	405	20	Air	ACN	Not detected
10	2-CTX	405	20	H_2O_2	ACN	trace
11	2-CTX	405	20	$Na_2S_2O_8$	ACN	trace

The oxidation of the model substrate, a *N*-Bn substituted DHQ (**2W**) to produce **4B** can be proven by a simple ^{1}H-NMR overlay of the two compounds (**Figure 75**). The alkyl signals at 2.82 ppm and 2.99 ppm in **2W** are absent in **4B**. Furthermore, the benzylic protons at 5.19 ppm in **2W** are further downfield at 5.53 ppm in **4B** and **4B** has new doublet signals at 6.79 ppm and 7.21 ppm corresponding to the two alkenyl protons (H-9 and H-10).

An overlay of the ^{13}C-NMR spectra of the two compounds also shows that **4B** does not have carbons in the alkyl region where they would be in **2W** (**Figure 76**). Rather, new signals for alkenyl carbons can be seen at 121.4 ppm and 140.1 ppm.

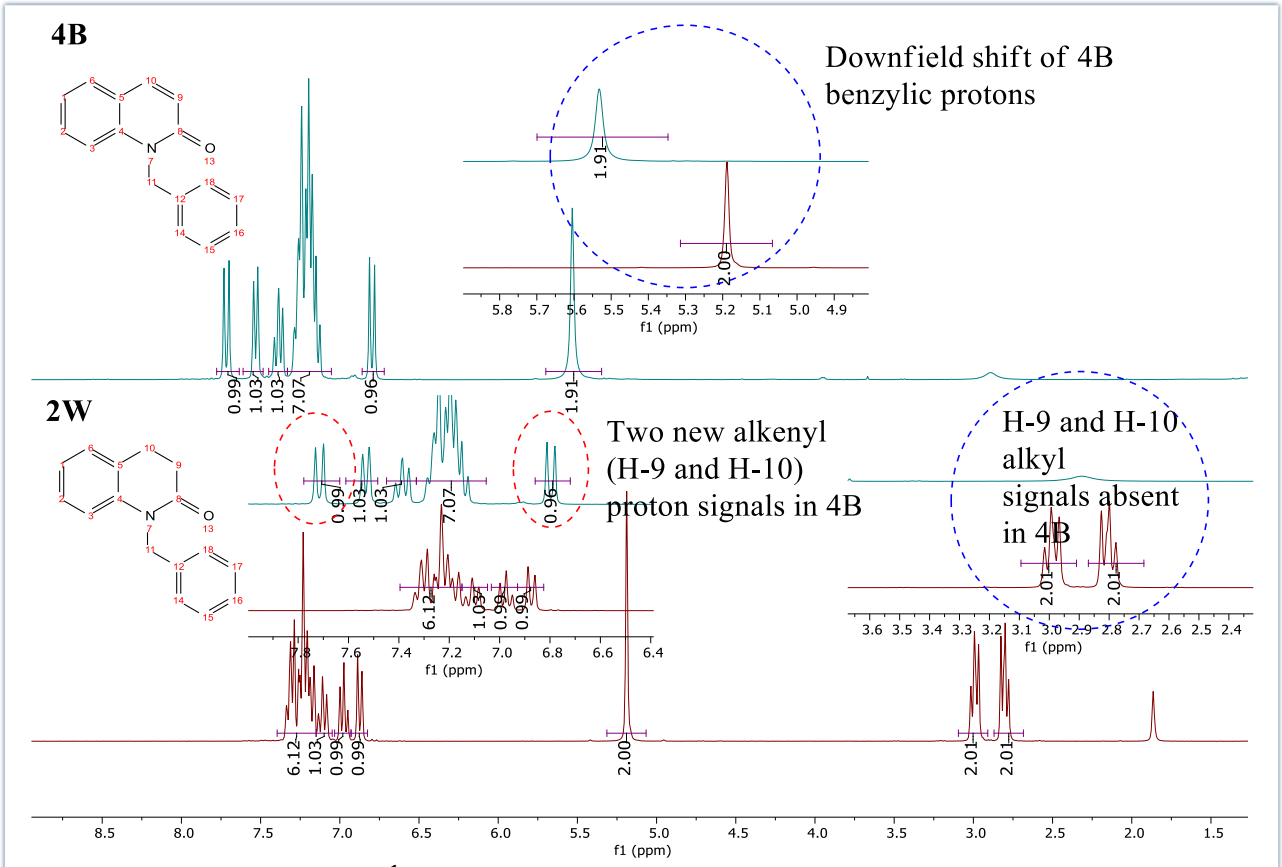

Figure 75: Overlayed ^{1}H-NMR spectra of 4B and 2W.

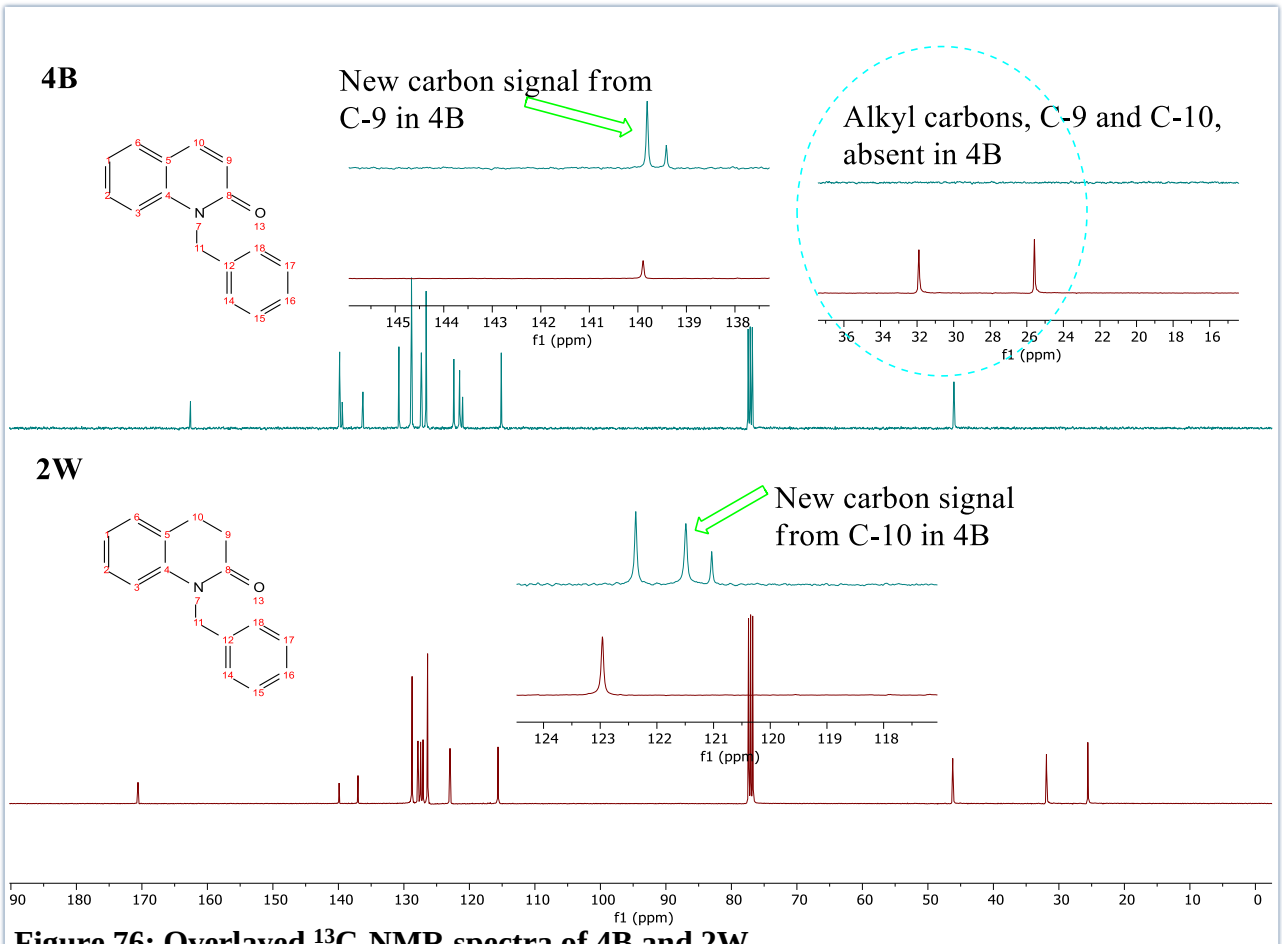

Figure 76: Overlayed ^{13}C-NMR spectra of 4B and 2W.

With the optimised reaction conditions in hand (**Table 2, entry 6**) we turned to exploring the substrate scope of the reaction (**Figure 77B**). Substrate **4A** is the initial quinolinone produced via the thermal method when demethylation was first tried; it would thus be worth investigating how the optimised reaction conditions affect the yield. Further investigations need to be carried out to determine if the same substrates produced using CuDMP (marked with superscript c in the substrate scope) could be produced with 2-CTX in comparable yields. This was done only in the case of compound **4B** (72% with 2-CTX versus 69% with CuDMP) and **4D** (75% with 2-CTX versus 62% with CuDMP) where 2-CTX showed improved yields, but time constraints limited further study.

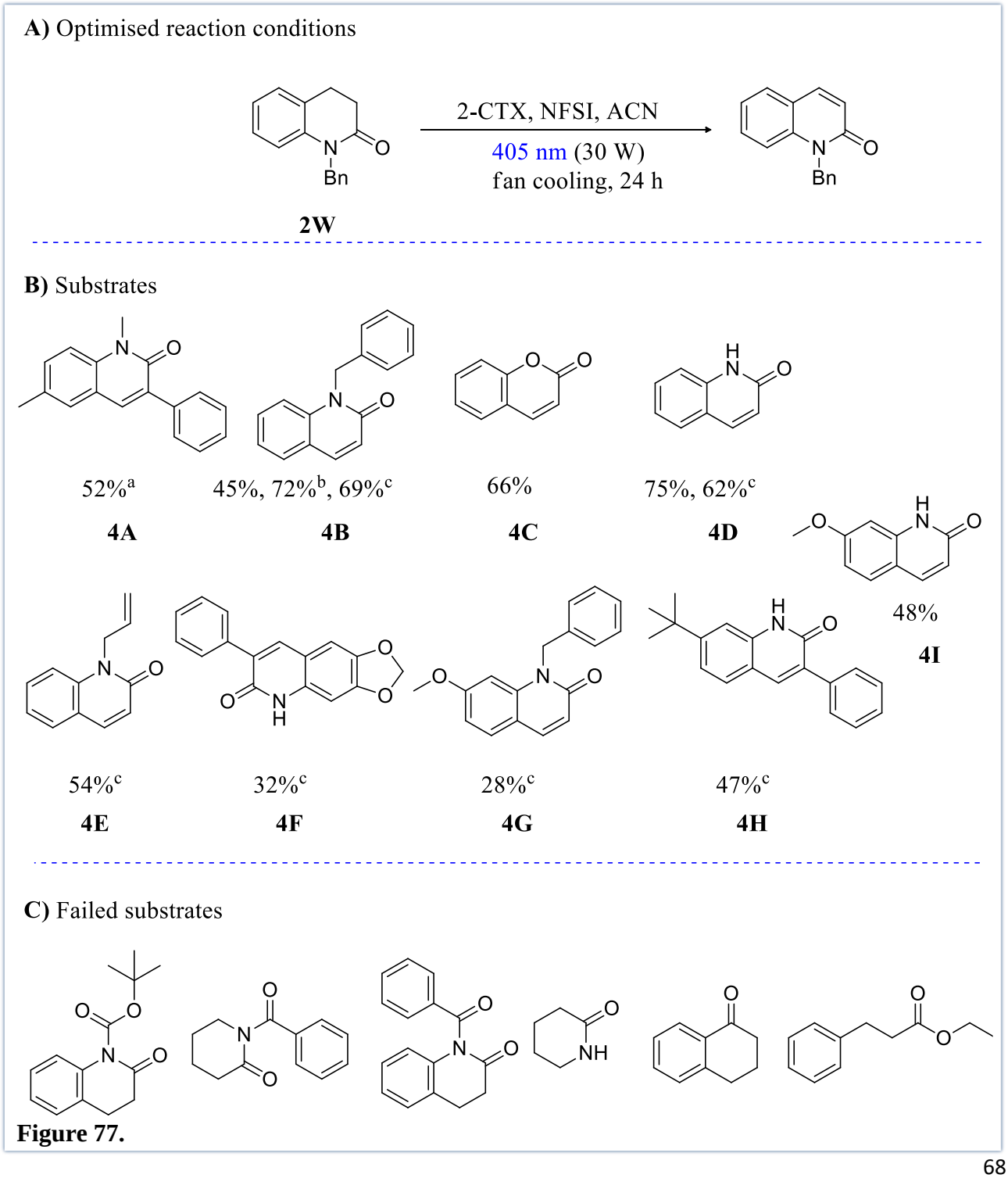

Figure 77.

It is interesting to note that the method works with a coumarin, as in **4C**, giving access to other chemical transformations. We considered the utility of this method with lactams, ketones, imides and acyclic substrates as this transformation typically makes use of metals such as Pd[68–70] and thus it would thus be advantageous to have a methodology that makes use of a cheap organic catalyst. Unfortunately, however, these did not work out with our conditions (**Figure 77C**). More work needs to be done in investigating a change in the conditions, such as using a base, which would allow for the oxidation process.

The proposed mechanism of the photocatalyzed reaction is shown in **Figure 78**. For the copper catalysed process (**Figure 78A**), the Cu^{II} catalyst is photoexcited to its triplet excited state following irradiation with visible light. Single electron transfer (SET) to NFSI produces NSI radical **A1**, together with a highly oxidising Cu^{III} species. A subsequent HAT from DHQ **A2** produces radical **A3**, which is subsequently oxidised to the tertiary carbocation **A4**, with the concurrent return of the photocatalyst to its ground state. Deprotonation by the fluoride anion finally produces the quinolinone product **A5**.

For the **2-CTX (Figure 78B)**, following the generation of the diradical triplet state **B2**, HAT from the DHQ **B4** produces DHQ methine radical **B6** together with the persistent ketyl radical **B3**. SET oxidation of **B6** by NFSI forms NSI radical **B5** as well as the carbocation **B7**, which is converted to DHQ product **B8** following deprotonation with fluoride anion. which performs a SET to NFSI. The DHQ cation (**B7**) is oxidised by the fluoride anion to produce the quinolinone. Catalyst turnover (back to **B1**) is then achieved by HAT of NSI radical **B5** and ketyl radical **B3**.

Since our optimised reaction conditions involved the organic 2-CTX and our prior work in the group used this same photosensitizer for the cyclisation step to produce the 3,4-dihydroquinolinone, we considered the possibility of making the DHQ and subsequently oxidising it to the quinolinone in one pot—formally achieving a Fujiwara-Moritani/Heck type transformation (**Figure 79**).[71] However, during development of this one-pot method using 2-CTX as photocatalyst, we encountered a challenge in the separation of our quinolinone product from the NHSI by-product.

We then turned to investigate some post-purification process chemistry that could help assist remove the residual NHSI, using compound **4D** as a model since the phenomenon seemed more prevalent in *N*-unprotected systems. While a simple base wash with K_2CO_3 (aq) and NaOH (aq) did not remove this by-product, literature reports revealed that overnight stirring with NaOH showed that sodium salts of NHSI could be recovered.[72] In the event, this did help us to remove all of the NHSI and we recovered the product **4D** in 44% yield.

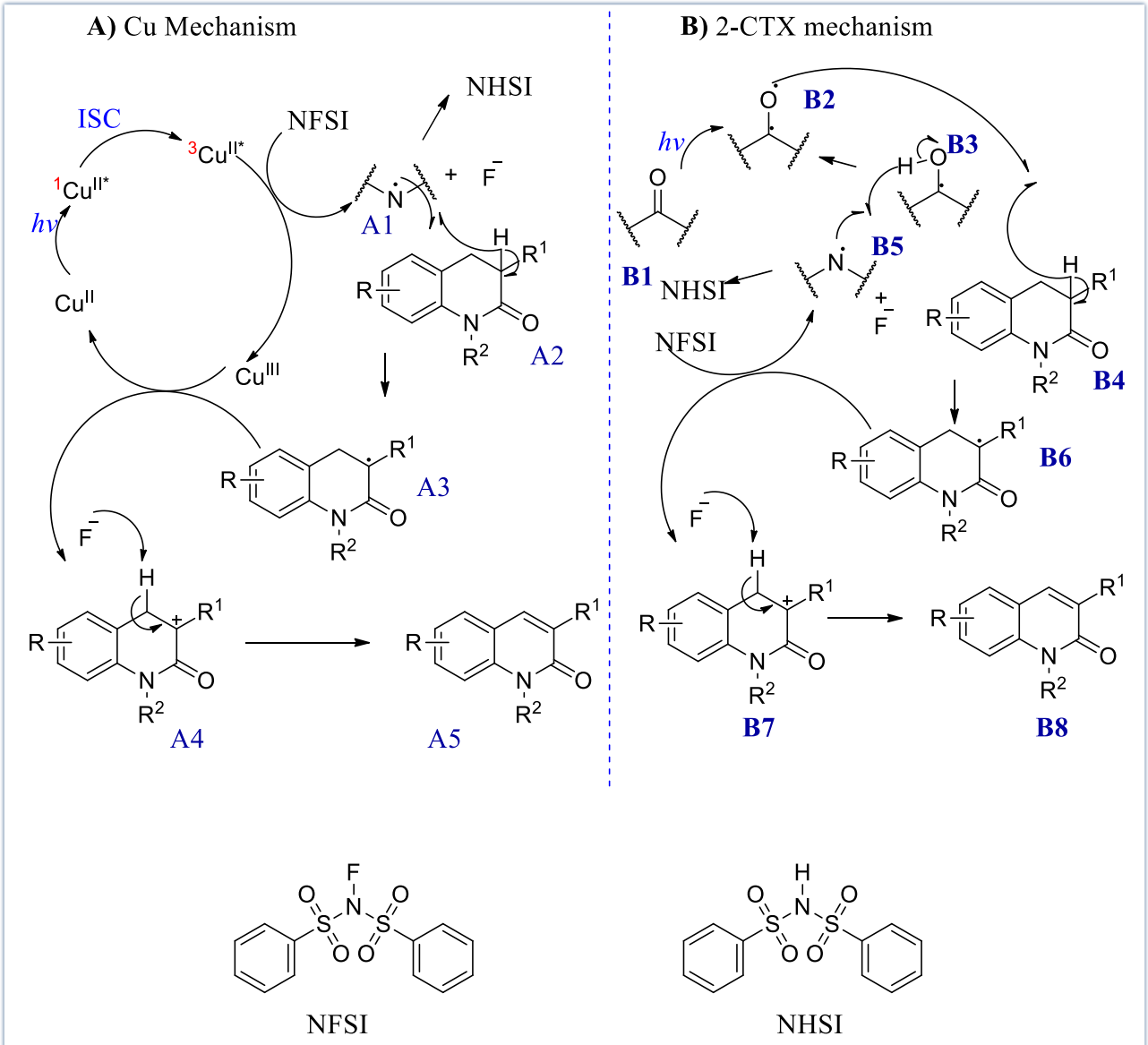

Figure 78: Proposed mechanisms for the photochemical formation of quinolinones via A) Cu and B) 2-CTX catalysis.

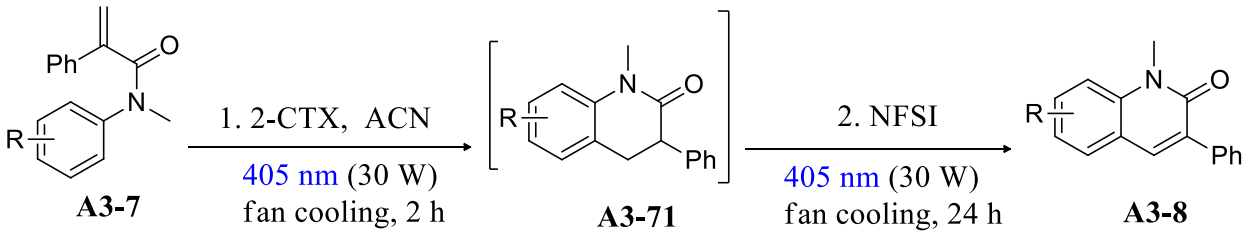

Figure 79: Overall Fujiwara-Moritani transformation.

The ^{1}H-NMR spectrum of **4D** obtained by this method is shown in **Figure 80**. The amide proton signal typically shows between 12 and 13 ppm as shown in the product ^{1}H-NMR spectrum displayed in **Figure 81**; however, in this case, this signal was missing (**Figure 80**). It is possible that the yield was lowered by deprotonation of the amide thereby making it a salt resulting in some of it being retained within the water layer. This showed that NaOH was effective in removing NHSI overnight, but was not effective for our process as it affected product recovery.

We recalled that our Cu photocatalyzed reactions did not share the same process chemistry complications, and indeed came across literature that showed that NHSI could be complexed to Cu.[73] This was interesting as it helped provide an explanation for the high catalyst loadings required for the CuDMP, together with its low to moderate yields (CuDMP is typically only required in 1–2 mol% in photochemical reactions). It was therefore possible that the by-product was poisoning our copper photocatalyst. With this in mind, we tried washing our 2-CTX catalysed reactions with $CuSO_4$ and were very pleased to find that our quinolinone products could be completely separated from the NHSI side product (**Figure 81**). Gratifyingly, the product yield was much higher at 75% yield as compared to the NaOH-treated reaction which yielded 44%. More studies would be needed to establish that this process chemistry was working the way we thought.

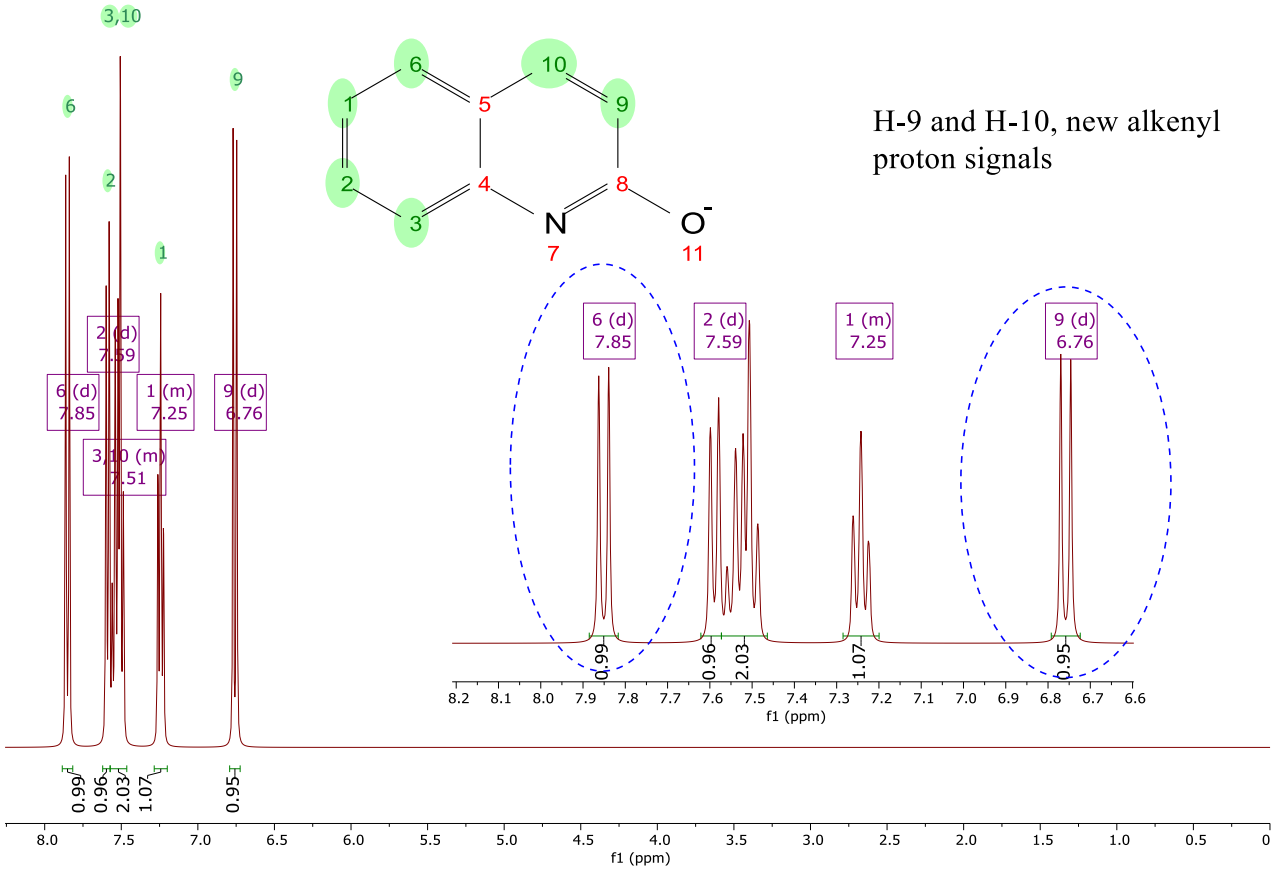

Figure 80: ^{1}H-NMR spectrum of 4D after treatment with NaOH overnight.

The quinolinone, **4D**, has been reported to exist as the keto (lactam) and/or enol (lactim) tautomeric forms. Although these are close in energy, in gas phase, the enol form has been found to be more stable.[74] However, the keto form has been found to be more stable in solution. The ^{1}H-NMR and ^{13}C-NMR we obtained in $CDCl_3$ at RT suggest that only one form was isolated. As shown in **Figure 81**, the H-7 signal is much more downfield at 12.46 ppm, whereas the amide proton signals are typically around 8 ppm from which our initial deduction was that **4D** exists exclusively as the enol tautomer when in solution in $CDCl_3$ at RT. However, literature suggests that the keto form is predominant in most cases, and a study has been conducted that shows that despite the H-7 signal being more downfield than what is typical for an amide, **4D** actually exists predominantly in the keto form.[75]

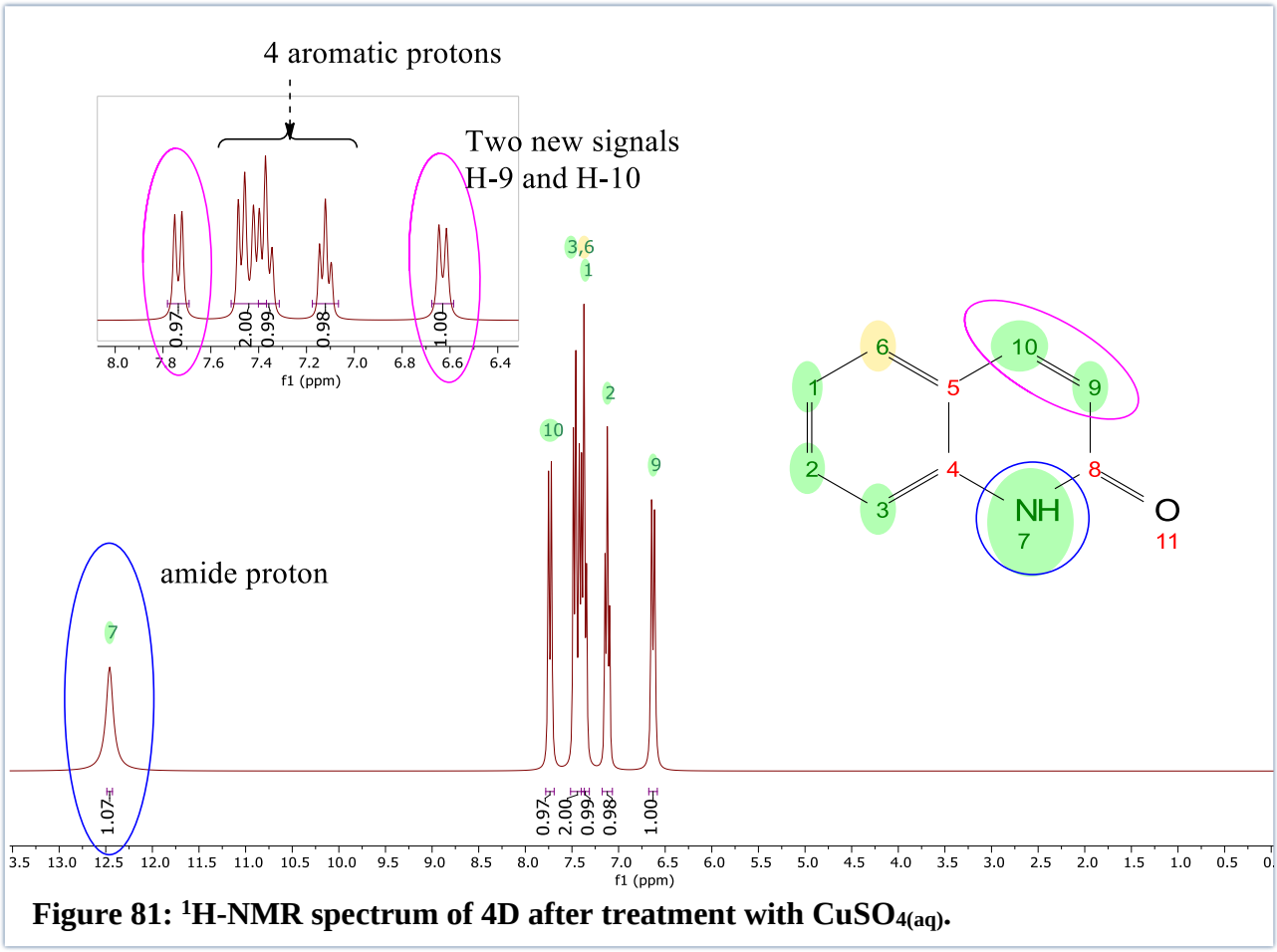

Figure 81: ^{1}H-NMR spectrum of 4D after treatment with $CuSO_{4(aq)}$.

The ^{13}C-NMR spectrum shown in **Figure 82** had the expected nine signals and agreed well with literature, with a characteristic resonance at 165 ppm consistent for an amide C=O.[76] Thus, we can conclude that our isolated product exists as the keto tautomer in $CDCl_3$ at RT.

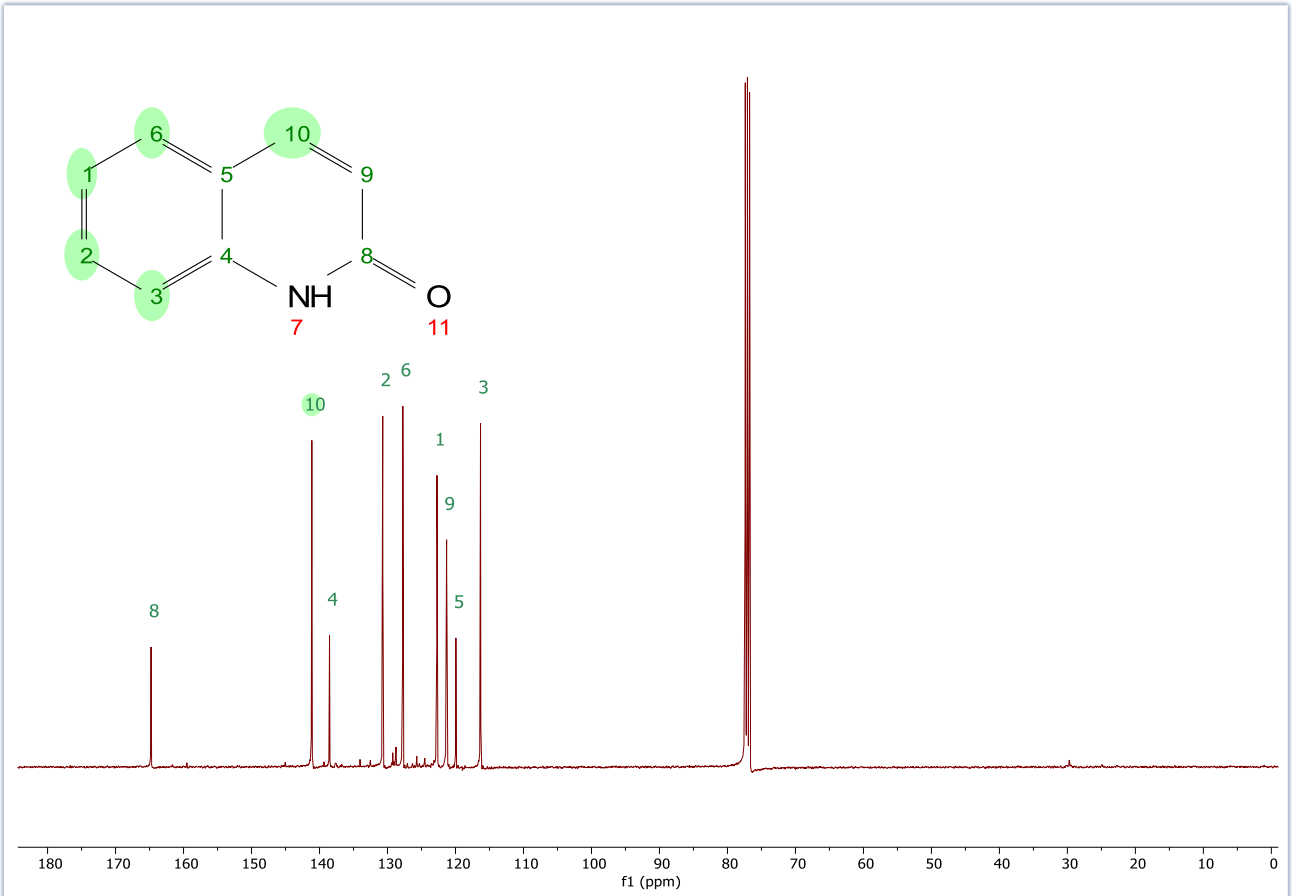

Figure 82: ^{13}C-NMR spectrum of 4D.

4.3 Conclusions and Recommendations

The serendipitous discovery of quinolinone formation as we sought out to demethylate a *N*-Me substituted DHQ to produce a *N*-unsubstituted DHQ led to the development and optimisation of an efficient photochemical method for the synthesis of quinolinones. Future work will focus on extending the methodology to acyclic substrates, i.e, investigating suitable reaction conditions that will allow usage of the same organic photocatalyst. Furthermore, since we have established that we can remove the NHSI by-product using $CuSO_4$, the one pot sequence to achieve a Fujiwara-Moritani/Heck type transformation can now be optimised. However, the initial goal of this investigation was to demethylate a *N*-Me substituted DHQ to produce a *N*-unsubstituted DHQ, hence future investigation should focus on developing methodology to achieve this.

CHAPTER 5: EXPERIMENTAL

GENERAL PROCEDURES

All reactions were carried out in oven-dried glassware under an inert nitrogen atmosphere, unless otherwise stated. Reagents were obtained from commercial sources (Sigma-Aldrich, Merck) and used as received unless otherwise stated. Solvents were evaporated under reduced pressure at 40 °C using a Buchi Rotavapor, unless otherwise stated. Reaction temperatures were achieved with heat (for > 25 °C) and dry ice/ice/liquid nitrogen (for 0 and -78 °C). Aqueous solutions were prepared using distilled water. Photochemical reactions were carried out using an EvoluChem™ PhotoRedOx Box under irradiation at an appropriate wavelength using an EvoluChem™ LED (30W). Standard borosilicate glass vessels were used. Where required, reactions were heated using a standard stirrer/metal heating block combination fitted with a temperature probe.

All reactions were monitored by TLC using aluminium-backed Merck silica-gel 60 F_{254} plates and aluminium oxide F_{254} plates, and compounds were visualised on TLC under a UV-lamp and/or were sprayed with a 2.5% solution of *p*-anisaldehyde in a mixture of sulfuric acid and ethanol (1:10 v/v), ninhydrin or potassium permanganate and then heated using a 1600 W heat gun. Normal phase column chromatography was carried out using silica-gel 60 or aluminium oxide and compounds eluted with the appropriate solvent mixtures. Preparative TLC was used with an appropriate solvent system where necessary.

All compounds were dried under vacuum before yields were determined and spectroscopic analyses performed. Nuclear Magnetic Resonance (NMR) spectra (^{1}H and ^{13}C) were recorded on either a Bruker XR400 MHz spectrometer (^{1}H at 400.0 MHz and ^{13}C at 100.6 MHz), a Bruker XR300 MHz spectrometer (^{1}H at 300.1 MHz) or a Bruker unity spectrometer (^{1}H at 600 MHz and ^{13}C at 151 MHz) and were carried out in $CDCl_3$, DMSO-d_6 and/or D_2O MeOD as the solvents, unless otherwise stated. Chemical shifts (δ) and J coupling values were reported in units of ppm and Hz, respectively. Chemical shifts for ^{1}H and ^{13}C were recorded using tetramethyl silane (TMS) as the internal standard. Assignments were confirmed by COSY, HSQC-DEPT and HMBC analysis when required. High-resolution mass spectra were obtained from the University of Stellenbosch Mass Spectrometry Service and recorded in electrospray positive mode with a time-of-flight analyser system on a Waters Synapt G2 machine.

2. Synthesis of DHQs

2.0 Synthesis of Acrylanilides and β-lactams

General Method [77]

To a mixture of aniline (1 eq.), carboxylic acid (1.2 eq.) and 2-chloro-1-methylpyridinium iodide (1.4 eq.) in DCM (5 mL/mmol of aniline) at 0 °C, was added DIPEA (3 eq.) dropwise and the reaction vessel allowed to warm up to room temperature. After 4 hours an equal amount of deionised water was added, and the mixture extracted with DCM (×3). The combined organic extracts were then dried over $MgSO_4$ and reduced *in vacuo*. The resultant residue was purified by flash column chromatography (PET/EtOAc) to give the products as listed below.

1,3-Diphenylazetidin-2-one (Compound 2A)[59]

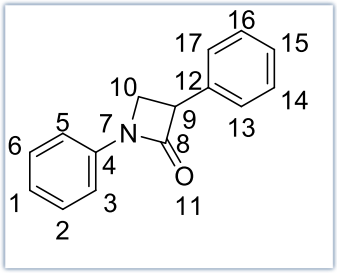

Obtained according to the general method in 14% yield, 201 mg. **R_f** 0.44 in EtOAc:PET (3:7).**^{1}H NMR** (300 MHz, DMSO-d_6) δ 7.54–6.98 (m, 10H, H-Ar), 4.64 (dd, J = 6.0, 2.9 Hz, 1H, H-9), 4.11 (t, J = 6.1 Hz, 1H, H-10), 3.76 (dd, J = 6.2, 2.9 Hz, 1H, H-10).**^{13}C NMR** (101 MHz, $CDCl_3$) δ 165.4 (C-8), 138.3 (C-Ar), 135.3 (C-Ar), 129.3 (C-Ar), 129.0 (C-Ar), 127.8 (C-Ar), 127.4 (C-Ar), 124.1 (C-Ar), 116.5 (C-Ar), 53.6 (C-9), 46.7 (C-10).

***N*,2-Diphenylacrylamide (Compound 2B)**[58]

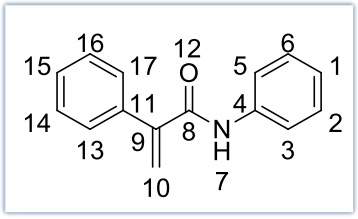

Obtained according to the general method in 27% yield, 405 mg. **R_f** 0.42 in 3:7 EtOAc:PET. **^{1}H NMR** (300 MHz, DMSO-d_6) δ 10.39–10.21 (s, 1H, H-7), 7.82–7.65 (m, 2H, H-Ar), 7.56–7.22 (m, 6H, H-Ar), 7.22–7.03 (m, 2H, H-Ar), 5.96 (s, 1H, H-10), 5.74 (s, 1H, H-10)

_N_-(3-(_Tert_-butyl) phenyl)-2-phenylacrylamide (Compound 2C)[78]

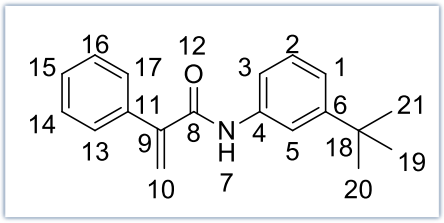

Obtained according to the general method in 32% yield, 358 mg. **R_f** 0.4 in 2:8 EtOAc:PET. **^{1}H NMR** (300 MHz, $CDCl_3$) δ 7.52-7.43 (m, 1H, H-7), 7.43–7.31 (m, 6H, H-Ar), 7.31-7.24 (m, 1H, H-Ar), 7.23-7.12 (m, 1H, H-Ar), 7.12-7.00 (m, *J* = 7.7, 1H, H-Ar), 6.20 (d, *J* = 1.2 Hz, 1H, H-10), 5.65 (d, *J* = 1.2 Hz, 1H, H-10), 1.23 (s, 9H, H-19/H-20/H-21)

_N_-(2-Fluoro-4-methylphenyl)-2-phenylacrylamide (Compound 2D)

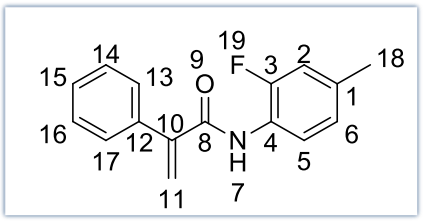

Obtained according to the general method in 14% yield, 289 mg. **R_f** 0.36 in 2:8 EtOAc:PET. **^{1}H NMR** (300 MHz, $CDCl_3$) δ 8.27-8.09 (m, 1H, H-Ar), 7.62–7.45 (s, 1H, H-7), 7.43–7.32 (m, 5H, H-Ar), 6.96–6.71 (m, 2H, H-Ar), 6.24 (s, 1H, H-11), 5.68 (s, 1H, H-11), 2.24 (s, 3H, H-18). **^{13}C NMR** (151 MHz, $CDCl_3$) δ 164.9 (C-8), 153.4 (C-Ar), 151.8 (C-10), 144.9 (C-Ar), 136.5 (C-Ar), 135.2 (C-Ar), 128.9 (C-Ar), 128.9 (C-Ar), 128.9 (C-Ar), 128.3 (C-11), 128.2 (C-Ar), 125.0 (C-Ar), 123.5 (C-Ar), 121.7 (C-Ar), 115.4 (C-Ar), 115.2 (C-Ar), 20.9 (C-18).

1-(Benzo[*d*] [1,3] dioxol-5-yl)-3-phenylazetidin-2-one (Compound 2E)

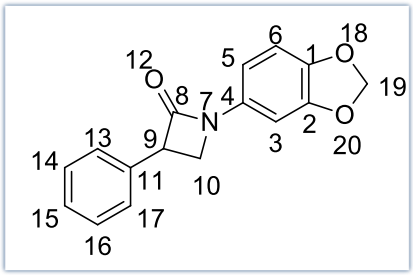

Obtained according to the general method in 16% yield, 416 mg. **R_f** 0.39 in 2:8 EtOAc:PET. **^{1}H NMR** (300 MHz, $CDCl_3$) δ 7.42–7.27 (m, 5H, H-Ar), 7.17 (d, *J* = 2.0 Hz, 1H, H-Ar), 6.86–6.67 (m, 2H, H-Ar), 6.96 (s, 2H, H-19), 4.50 (dd, *J* = 5.9, 2.8 Hz, 1H, H-9), 4.11-3.96 (m, 1H, H-10), 3.63 (dd, *J* = 5.8, 2.8 Hz, 1H, H-10).

_N_-(Benzo[_d_][1,3]dioxol-5-yl)-2-phenylacrylamide (Compound 2F)

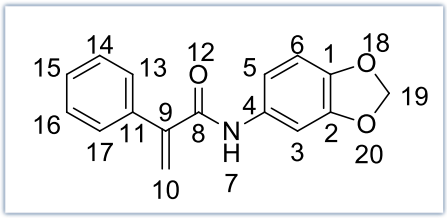

Obtained according to the general method in 24% yield, 630.8 mg. **R_f** 0.26 in 2:8 EtOAc:PET. **^{1}H NMR** (300 MHz, $CDCl_3$) δ 7.49–7.37 (m, 5H, H-Ar), 7.29 (d, *J* = 1.8 Hz, 2H, H-Ar), 6.81–6.64 (m, 2H, H-Ar), 6.29 (s, 1H, H-10), 5.95 (s, 2H, H-19), 5.71 (s, 1H, H-10). **^{13}C NMR** (151 MHz, $CDCl_3$) δ 172.0 (C-8), 146.9 (C-Ar), 143.4 (C-Ar), 138.3 (C-9), 131.1 (C-Ar), 128.6 (C-Ar), 128.1 (C-Ar), 128.0 (C-Ar), 127.3 (C-Ar), 115.5 (C-10), 108.2 (C-Ar), 107.2 (C-Ar), 106.7 (C-Ar), 101.4 (C-Ar), 101.2 (C-Ar), 97.7 (C-19).

3-Phenyl-1-(3,4,5-trimethoxyphenyl) azetidin-2-one (Compound 2G)

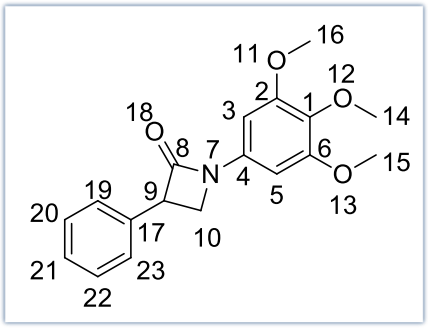

Obtained according to the general method in 8% yield, 99.5 mg. **R_f** 0.16 in 2:8 EtOAc:PET. **^{1}H NMR** (300 MHz, $CDCl_3$) δ 7.46–7.27 (m, 5H, H-Ar), 6.68 (s, 2H, H-Ar), 4.52 (dd, *J* = 5.9, 2.8 Hz, 1H, H-9), 4.15-4.01 (m, 1H, H-10), 3.88 (s, 6H, H-15/H-16), 3.82 (s, 3H, H-14), 3.67 (dd, *J* = 5.7, 2.9 Hz, 1H, H-10).

1-(3,4-Dichloro-2-methylphenyl)-3-phenylazetidin-2-one (Compound 2H)

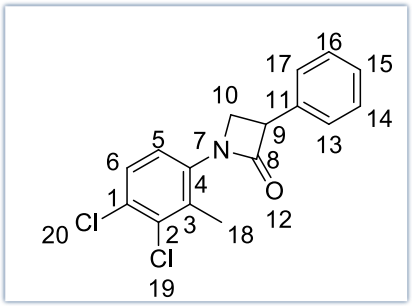

Obtained according to the general method in 10% yield, 161 mg. **R_f** 0.53 in 3:7 EtOAc:PET. **^{1}H NMR** (300 MHz, $CDCl_3$) δ 7.43–7.30 (m, 6H, H-Ar), 7.19 (d, *J* = 8.7 Hz, 1H, H-Ar), 4.36-4.19 (m, 1H, H-9), 4.04-3.88 (m, 1H, H-10), 3.87-3.66 (m, 1H, H-10), 2.06 (s, 3H, H-18)

1-(4-(2-Methoxyethoxy) phenyl)-3-phenylazetidin-2-one (Compound 2I)

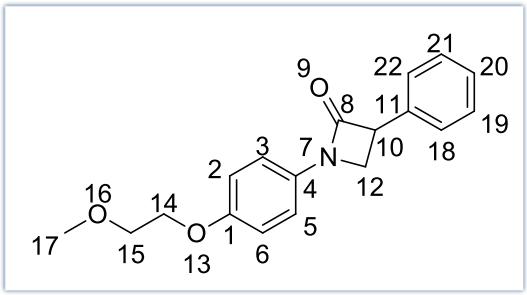

Obtained according to the general method in 13% yield, 118 mg. **R_f** 0.23 in 3:7 EtOAc:PET. **^{1}H NMR** (300 MHz, $CDCl_3$) δ 7.41–7.32 (m, 7H, H-Ar), 6.94 (d, *J* = 8.5 Hz, 2H, H-Ar), 4.50 (dd, *J* = 5.9, 2.7 Hz, 1H, H-10), 4.11 (t, *J* = 4.6 Hz, 2H, H-14), 4.07-3.99 (m, 1H, H-12), 3.75 (t, *J* = 4.6 Hz, 2H, H-15), 3.64 (dd, *J* = 5.7, 2.8 Hz, 1H, H-12), 3.46 (s, 3H, H-17).

***N*-(4-(2-Methoxyethoxy) phenyl)-2-phenylacrylamide (Compound 2J)**

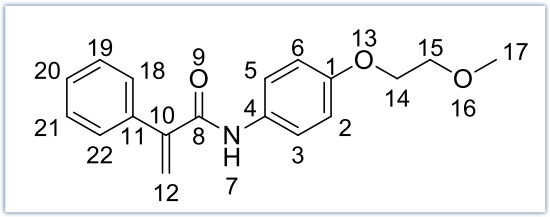

Obtained according to the general method in 4% yield, 35.7 mg. **R_f** 0.13 in 3:7 EtOAc:PET. **^{1}H NMR** (300 MHz, $CDCl_3$) δ 7.61–7.29 (m, 8H, H-Ar), 6.87 (d, *J* = 8.6 Hz, 2H, H-Ar), 6.26 (s, 1H, H-12), 5.69 (s, 1H, H-12), 4.08 (dd, *J* = 5.6, 3.8 Hz, 2H, H-14), 3.73 (dd, *J* = 5.5, 3.8 Hz, 2H, H-15), 3.44 (s, 3H, H-17). **^{13}C NMR** (151 MHz, $CDCl_3$) δ 165.0 (C-8), 155.8 (C-Ar), 145.1 (C-10), 136.8 (C-Ar), 131.0 (C-Ar), 128.9 (C-Ar), 128.8 (C-Ar), 128.3 (C-Ar), 123.1 (C-12), 121.6 (C-Ar), 115.0 (C-Ar), 71.0 (C-15), 67.6 (C-14), 59.2 (C-17).

1-(3,5-Dibromophenyl)-3-phenylazetidin-2-one (Compound 2K)

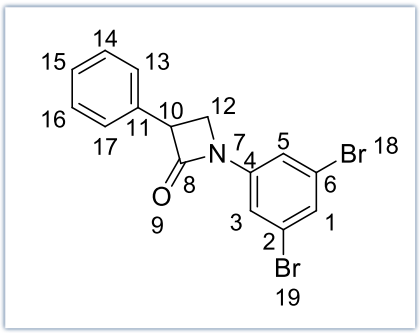

Obtained according to the general method in 8% yield, 128.7 mg. **R_f** 0.50 in 3:7 EtOAc:PET. **^{1}H NMR** (300MHz, $CDCl_3$) δ 7.56–7.49 (m, 2H, H-Ar), 7.43–7.30 (m, 6H, H-Ar), 4.57 (dd, *J* = 6.1, 3.0 Hz, 1H, H-10), 4.15-3.99 (m, 1H, H-12), 3.69 (dd, *J* = 5.9, 3.0 Hz, 1H, H-12). **^{13}C NMR** (151 MHz, $CDCl_3$) δ 206.9 (C-6), 165.5 (C-Ar), 140.0 (C-Ar), 134.5 (C-Ar), 129.5 (C-Ar), 129.0 (C-Ar), 128.0 (C-Ar), 127.3 (C-Ar), 123.4 (C-Ar), 118.2 (C-Ar), 54.0 (C-Ar), 47.0 (C-Ar), 30.9 (C-10), 30.9 (C-12).

***N*-(3,5-Dibromophenyl)-2-phenylacrylamide (Compound 2L)**[79]

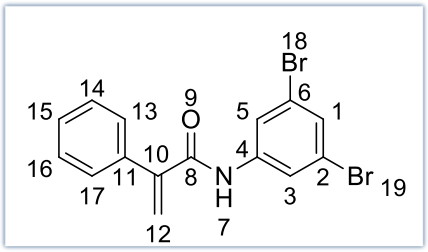

Prepared as per general method A and obtained in 13% yield, 202.4 mg. **R_f** 0.39 in 3:7 EtOAc:PET. **^{1}H NMR** (300 MHz, $CDCl_3$) δ 7.77–7.64 (m, 2H, H-Ar), 7.57–7.36 (m, 7H, H-Ar), 6.32 (s, 1H, H-12), 5.78 (s, 1H, H-12). **^{13}C NMR** (151 MHz, $CDCl_3$) δ 165.2 (C-8), 144.4 (C-Ar), 139.7 (C-Ar), 136.1 (C-Ar), 130.0 (C-10), 129.1 (C-Ar), 128.2 (C-Ar), 124.4 (C-Ar), 123.0 (C-Ar), 121.4 (C-Ar).

***N*-(4-Bromo-3,5-difluorophenyl)-2-phenylacrylamide (Compound 2M)**

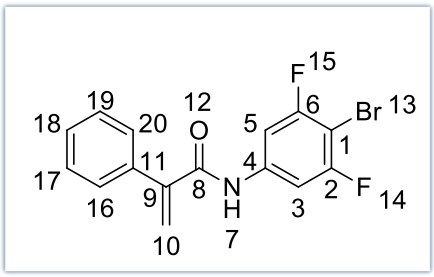

To a solution of 749 mg aniline (1.0 eq.) and 1.4 mL of triethylamine (1.2 eq.) in DCM (3 mL/mmol of aniline) at 0 °C, was added acid chloride (1.2 eq.) dropwise and the solution allowed to warm up to room temperature. After 1.5 h an equal amount of deionised water was added, and the mixture extracted with DCM (×3). The combined organic extracts were then washed with $NaHCO_3$ (×2), dried over $MgSO_4$ and reduced *in vacuo* to give the product which was purified by flash chromatography (PET/EtOAc) to obtain the product in 8% yield, 101 mg. **R_f** 0.51 in 3:7 EtOAc:PET. **^{1}H NMR** (300 MHz, $CDCl_3$) δ 7.58–7.35 (m, 6H, H-Ar), 7.31–7.21 (m, 2H, H7/H18), 6.34 (d, *J* = 1.1 Hz, 1H, H-10), 5.77 (d, *J* = 1.1 Hz, 1H, H-10).

2.1 Synthesis of DHQs

General Method

A mixture of acrylanilide and (Ir[dF(CF_3)ppy_2])dtbpy)PF_6 (2 mol%) in TFE and $CHCl_3$ (4:1) were degassed and exposed to 450 nm light over a period of 24 h. Reaction completion was monitored using TLC. The solvent was removed *in vacuo*. The residue was then purified by flash chromatography (Petroleum ether/EtOAc) to give the product.

3-Phenyl-3,4-dihydroquinolin-2(1*H*)-one (Compound 2N)[62]

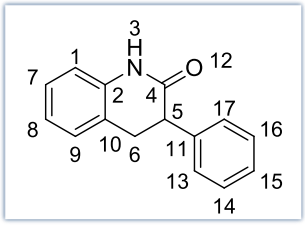

Obtained according to the general method in 93% yield, 104 mg. **R_f** 0.40 in 3:7 EtOAc:PET. **^{1}H NMR** (300 MHz, $CDCl_3$) δ 9.14 (s, 1H, H-3) 7.35-7.20 (m, 5H, H-Ar), 7.18–7.07 (m, 2H, H-Ar), 6.96 (dd, *J* = 8.2, 6.7 Hz, 1H, H-15), 6.83–6.75 (m, 1H, H-Ar), 3.86 (dd, *J* = 8.8, 6.9 Hz, 1H, H-5), 3.33–3.09 (m, 2H, H-6)

7-(*Tert*-butyl)-3-phenyl-3,4-dihydroquinolin-2(1*H*)-one (Compound 2O)[80]

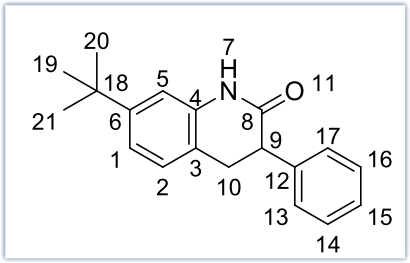

Obtained according to the general method in 41% yield, 99 mg. **R_f** 0.35 in 3:7 EtOAc:PET. **^{1}H NMR** (300 MHz, $CDCl_3$) δ 8.22 (s, 1H, H-7), 7.36–7.26 (m, 2H, H-Ar), 7.26–7.19 (m, 2H, H-Ar), 7.12–6.95 (m, 2H, H-Ar), 6.74 (d, *J* = 1.8 Hz, 1H, H-Ar), 3.83 (t, *J* = 8.3 Hz, 1H, H-9), 3.19 (d, *J* = 8.3 Hz, 2H, H-10), 1.27 (s, 9H, H-19/H-20/H-21). **^{13}C NMR** (151 MHz, $CDCl_3$) δ 172.1 (C-8), 151.2 (C-Ar), 138.5 (C-Ar), 136.7 (C-Ar), 128.6 (C-Ar), 128.2 (C-Ar), 127.6 (C-Ar), 127.2 (C-Ar), 120.4 (C-Ar), 120.2 (C-Ar), 112.4 (C-Ar), 46.7 (C-9), 34.6 (C-18), 33.1 (C-10), 31.3 (C-19/ C-20/ C-21).

5-(*Tert*-butyl)-3-phenyl-3,4-dihydroquinolin-2(1*H*)-one (Compound 2P)

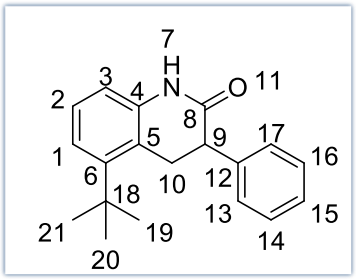

Obtained according to the general method in 22% yield, 53 mg. **R_f** 0.27 in 3:7 EtOAc:PET. **^{1}H NMR** (300MHz, $CDCl_3$) δ 8.27 (s, 1H, H-7), 7.39–7.33 (m, 1H, H-Ar), 7.33–7.31 (m, 1H, H-Ar), 7.31–7.26 (m, 2H, H-Ar), 7.25-7.22 (m, 1H, H-Ar), 7.18–7.06 (m, 2H, H-Ar), 6.70 (dd, *J* = 7.1, 1.9 Hz, 1H, H-Ar), 3.78 (dd, *J* = 10.8, 5.3 Hz, 1H, H-9), 3.55 (dd, *J* = 15.6, 5.3 Hz, 1H, H-10), 3.34 (dd, *J* = 15.6, 10.8 Hz, 1H, H-10), 1.33 (s, 9H, H-19/H-20/H-21). **^{13}C NMR** (151 MHz, $CDCl_3$) δ 172.1 (C-8), 148.3 (C-Ar), 138.3 (C-Ar), 128.7 (C-Ar), 128.3 (C-Ar), 127.3 (C-Ar), 127.1 (C-Ar), 122.4 (C-Ar), 121.2 (C-Ar), 114.2 (C-Ar), 46.6 (C-Ar), 35.6 (C-Ar), 33.5 (C-Ar), 31.3 (C-9), 30.9 (C-18), 29.7 (C-10), 22.7 (C-19/ C-20/ C-21).

6-Bromo-5,7-difluoro-3-phenyl-3,4-dihydroquinolin-2(1*H*)-one (Compound 2Q)

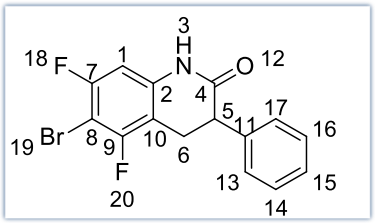

Obtained according to the general method in 100% yield, 52 mg. **R_f** 0.23 in 2:8 EtOAc:PET. **^{1}H NMR** (300 MHz, $CDCl_3$) δ 9.22 (s, 1H, H-3), 7.72–7.22 (m, 4H, H-Ar), 7.16 (s, 1H, H-Ar), 6.43 (dd, *J* = 8.6, 1.9 Hz, 1H, H-Ar), 3.81 (dd, *J* = 8.9, 6.6 Hz, 1H, H-5), 3.33-3.08 (m, 2H, H-6).

8-Fluoro-6-methyl-3-phenyl-3,4-dihydroquinolin-2(1*H*)-one (Compound 2R)

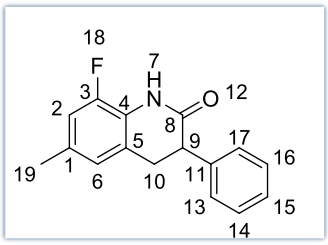

Obtained according to the general method in 22% yield, 28 mg. **R_f** 0.12 in 3:7 EtOAc:PET. **^{1}H NMR** (300 MHz, $CDCl_3$) δ 7.90-7.71 (broad s, 1H, H-7), 7.44–7.27 (m, 3H, H-Ar), 7.26–7.17 (m, 2H, H-Ar), 6.85–6.71 (m, 2H, H-Ar), 3.86 (t, *J* = 7.9 Hz, 1H, H-9), 3.23 (d, *J* = 7.9 Hz, 2H, H-10), 2.28 (s, 3H, H-19)

7-Phenyl-7,8-dihydro-[1,3]dioxolo[4,5-*g*]quinolin-6(5*H*)-one (Compound 2S)

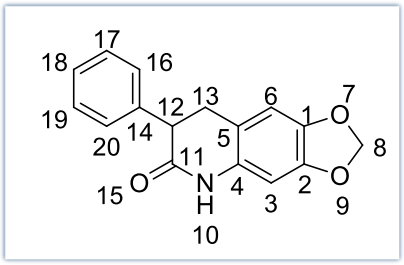

Obtained according to the general method in 55% yield, 276.9 mg. **R_f** 0.21 in 3:7 EtOAc:PET. **^{1}H NMR** (300 MHz, $CDCl_3$) δ 9.28 (s, 1H, H-10), 7.25–7.13 (m, 5H, H-Ar), 6.53 (s, 1H, H-Ar), 6.31 (s, 1H, H-Ar), 5.82 (s, 2H, H-8), 3.74 (dd, *J* = 8.7, 6.5 Hz, 1H, H-12), 3.21–2.90 (m, 2H, H-13). **^{13}C NMR** (101 MHz, $CDCl_3$) δ 172.0 (C-11), 146.9 (C-Ar), 143.4 (C-Ar), 138.2 (C-Ar), 131.0 (C-Ar), 128.7 (C-Ar), 128.1 (C-Ar), 128.0 (C-Ar), 127.4 (C-Ar), 115.6 (C-Ar), 108.2 (C-Ar), 101.2 (C-8), 97.7 (C-Ar), 46.5 (C-12), 33.4 (C-13).

Preparation of *N*-substituted DHQs

1-Benzoyl-3,4-dihydroquinolin-2(1*H*)-one (Compound 2T)[81]

To 500 mg of dihydroquinoline (1 eq.) in THF at -78 ℃ was added 1.5 mL of nBuLi (1.1 eq.) dropwise. The mixture was left to stir for 30 min, after which 0.4 mL of benzoyl chloride (1.1 eq.) was added. The temperature of the reaction mixture was allowed to gradually rise to room temperature and allowed to stir for 3 h. The reaction mixture was quenched with water and washed with acid and base. The organic extracts were reduced *in vacuo* and the residue was purified using flash chromatography to afford the product in 61% yield, 524 mg. **R_f** 0.37 in 3:7 EtOAc:PET. **^{1}H NMR** (300 MHz, Chloroform-*d*) δ 7.90 (d, *J* = 7.7 Hz, 2H, H-Ar), 7.68-7.55 (m, 1H, H-Ar), 7.54-7.37 (m, 2H, H-Ar), 7.27 (d, *J* = 7.2 Hz, 1H, H-Ar), 7.21–6.97 (m,2H, H-Ar), 6.81 (d, *J* = 7.8 Hz, 1H, H-Ar), 3.11 (dd, *J* = 8.7, 5.8 Hz, 2H, H-5), 2.81 (dd, *J* = 8.5, 6.0 Hz, 2H, H-6).**^{13}C NMR** (101 MHz, $CDCl_3$) δ 173.6 (C-4), 170.8 (C-12), 138.1 (C-Ar), 134.3 (C-Ar), 133.5 (C-Ar), 130.1 (C-Ar), 129.0 (C-Ar), 128.3 (C-Ar), 127.6 (C-Ar), 125.9 (C-Ar), 124.4 (C-Ar), 117.5 (C-Ar), 32.4 (C-5), 25.8 (C-6).

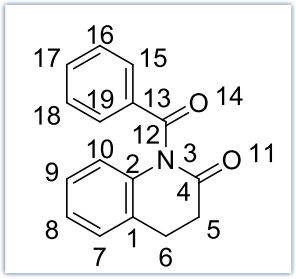

1-Benzoylpiperidin-2-one (Compound 2U)[70]

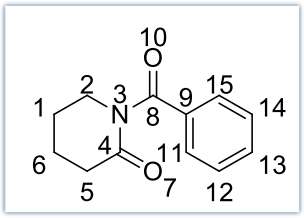

To 1.0 g of 2-piperidinone (1 eq.) in THF at -78 ℃ was added 7 mL of *n*-BuLi (1.1 eq.) dropwise. The mixture was left to stir for 30 min, after which the 1.3 mL of benzoyl chloride (1.1 eq.) was added. The temperature of the reaction mixture was allowed to gradually rise to room temperature and allowed to stir for 3 h. The reaction mixture was quenched with water and washed with acid and base. The organic extracts were reduced *in vacuo* and the residue was purified using flash chromatography to afford the product in 89% yield, 1.65 g. **R_f** 0.27 in 3:7 EtOAc:PET. **^{1}H NMR** (300 MHz, Chloroform-*d*) δ 7.45 (d, *J* = 7.5 Hz, 2H, H-Ar), 7.41–7.33 (m, 1H, H-Ar), 7.33–7.23 (m, 2H, H-Ar), 3.69 (t, *J* = 5.6 Hz, 2H, H-2), 2.45 (t, *J* = 6.3 Hz, 2H, H-5), 1.98–1.71 (m, 4H, H-1/H-6).**^{13}C NMR** (101 MHz, $CDCl_3$) δ 174.7 (C-4), 173.6 (C-8), 136.2 (C-Ar), 131.5 (C-Ar), 128.2 (C-Ar), 127.9 (C-Ar), 48.5 (C-Ar), 46.2 (C-Ar), 43.9 (C-2), 34.7 (C-5), 22.8 (C-1), 21.5 (C-6).

1-Allyl-3,4-dihydroquinolin-2(1*H*)-one (Compound 2V)[82]

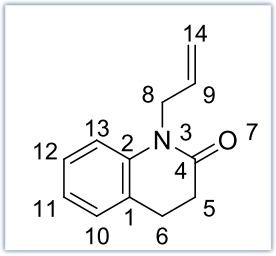

A mixture of 294.4 mg of DHQ (1 eq.) and 160 mg of NaH (3 eq.) in THF was left to stir for 30 min, after which 1 mL of allylbromide (6 eq.) was added. The reaction mixture was left to stir at room temperature overnight. The reaction mixture was quenched with water and extracted with EtOAc. The organic extracts were reduced *in vacuo* and the residue was purified using flash chromatography to afford the product in 67% yield, 252.3 mg. **R_f** 0.29 in 3:7 EtOAc:PET. **^{1}H NMR** (300 MHz, Chloroform-*d*) δ 7.25–7.12 (m, 2H, H-Ar), 7.06-6.92 (m, 2H, H-Ar), 5.89 (ddt, *J* = 15.6, 9.9, 4.7 Hz, 1H, H-9), 5.28–5.02 (m, 2H, H-14), 4.55 (dd, *J* = 5.3, 2.3 Hz, 2H, H-8), 2.92 (dd, *J* = 8.8, 5.9 Hz, 2H, H-5), 2.69 (dd, *J* = 8.8, 6.0 Hz, 2H, H-6).**^{13}C NMR** (101 MHz, $CDCl_3$) δ 170.1 (C-4), 139.9 (C-2), 132.6 (C-9), 127.8 (C-Ar), 127.4 (C-Ar), 126.3 (C-Ar), 122.9 (C-Ar), 116.3 (C-Ar), 115.4 (C-14), 45.1 (C-8), 31.8 (C-5), 25.6 (C-6).

1-Benzyl-3,4-dihydroquinolin-2(1*H*)-one (Compound 2W)[83]

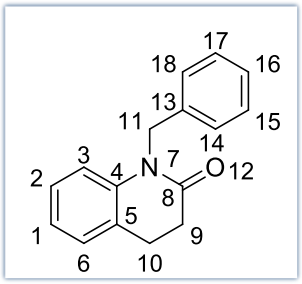

A mixture of 1.5 g of dihydroquinolinone (1 eq.), 6.5 g of cesium carbonate (2 eq.) and 2.4 mL of benzyl bromide (2 eq.) in ACN was refluxed at 85 ℃ overnight. The reaction mixture was washed with water and extracted with EtOAc. The organic extracts were reduced under pressure and the residue was purified using flash chromatography to afford the product in 90% yield, 2.14 g. **R_f** 0.39 in 3:7 EtOAc:PET. **^{1}H NMR** (300 MHz, $CDCl_3$) δ 7.40–7.15 (m, 6H, H-Ar), 7.15-7.05 (m, 1H, H-Ar), 7.03-6.93 (m, 1H, H-Ar), 6.87 (d, *J* = 8.1 Hz, 1H, H-Ar), 5.19 (s, 2H, H-11), 2.99 (dd, *J* = 8.8, 5.8 Hz, 2H, H-9), 2.80 (dd, *J* = 8.7, 5.8 Hz, 2H, H-10).**^{13}C NMR** (101 MHz, $CDCl_3$) δ 170.6 (C-8), 139.9 (C-Ar), 137.0 (C-Ar), 128.8 (C-Ar), 127.9 (C-Ar), 127.5 (C-Ar), 127.1 (C-Ar), 126.4 (C-Ar), 123.0 (C-Ar), 115.6 (C-Ar), 77.4 (C-Ar), 77.1 (C-Ar), 76.8 (C-Ar), 46.2 (C-11), 31.9 (C-9), 25.6 (C-10).

3-(2-Oxo-3,4-dihydroquinolin-1(2*H*)-yl)propanenitrile (Compound 2X)

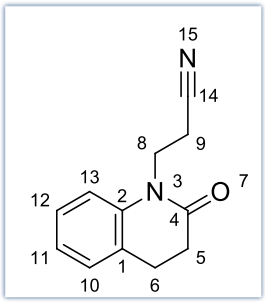

A mixture of 1.47 g of DHQ (1 eq.), 6.52 g of cesium carbonate (2 eq.) and 1 mL of bromopropionitrile (2 eq.) in ACN was refluxed at 85 ℃ overnight. The reaction mixture was washed with water and extracted with EtOAc. The organic extracts were reduced under pressure and the residue was purified using flash chromatography to afford the product in 82% yield, 1.64 g. **R_f** 0.26 in 3:7 EtOAc:PET. **^{1}H NMR** (300 MHz, Chloroform-*d*) δ 7.30–7.18 (m, 1H, H-Ar), 7.15 (d, *J* = 7.4 Hz, 1H, H-Ar), 7.06–6.76 (m, 2H, H-Ar), 4.19 (t, *J* = 7.2 Hz, 2H, H-8), 2.87 (dd, *J* = 8.7, 6.0 Hz, 2H, H-9), 2.71 (t, *J* = 7.2 Hz, 2H, H-5), 2.66-2.35 (m, 2H, H-6).**^{13}C NMR** (101 MHz, $CDCl_3$) δ 170.5 (C-4), 138.7 (C-Ar), 128.5 (C-Ar), 127.8 (C-Ar), 126.7 (C-Ar), 123.6 (C-Ar), 117.5 (C-Ar), 114.4(C-14), 38.3 (C-8), 31.7 (C-5), 25.4 (C-6), 16.0 (C-9).

1-Benzyl-7-methoxy-3,4-dihydroquinolin-2(1*H*)-one (Compound 2Y)

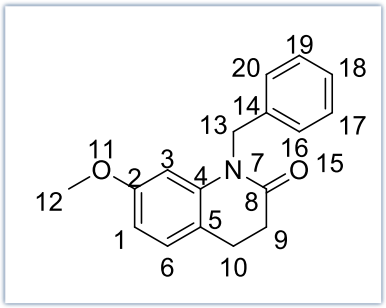

A mixture of 354 mg of DHQ (1 eq.), 1.3 g of cesium carbonate (2 eq.) and 0.5 mL of benzyl bromide (2 eq.) in ACN was refluxed at 85 ^{0}C overnight. The reaction mixture was washed with water and extracted with EtOAc. The organic extracts were reduced under pressure and the residue was purified using flash chromatography to afford the product in 96% yield, 511.5 mg. **R_f** 0.27 in 3:7 EtOAc:PET. **^{1}H NMR** (300 MHz, Chloroform-*d*) δ 7.47 – 7.16 (m, 5H, H-Ar), 7.11 (d, *J* = 8.1 Hz, 1H, H-Ar), 6.63 – 6.32 (m, 2H, H-Ar), 5.21 (s, 2H, H-13), 3.71 (s, 3H, H-12), 2.96 (dd, *J* = 8.8, 5.6 Hz, 2H, H-9), 2.82 (dd, *J* = 8.7, 5.6 Hz, 2H, H-10).**^{13}C NMR** (101 MHz, $CDCl_3$) δ 170.8 (C-8), 159.0 (C-Ar), 140.9 (C-Ar), 137.0 (C-Ar), 128.8 (C-Ar), 128.3 (C-Ar), 127.1 (C-Ar), 126.5 (C-Ar), 118.5 (C-Ar), 107.0 (C-Ar), 103.2 (C-Ar), 55.3 (C-13), 46.3 (C-12), 32.3 (C-9), 24.8 (C-10).

***Tert*-butyl 2-oxo-3,4-dihydroquinoline-1(2*H*)-carboxylate (Compound 2Z)**[84]

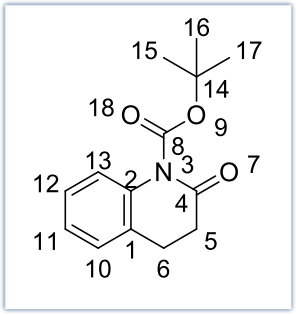

441.6 mg of DHQ (1 eq.) and 0.5 mL of TEA (1.1 eq.) were dissolved in 6 mL of DCM and the reaction vessel was placed in an ice-bath. 785.7 mg of $(Boc)_2O$ (1.2 eq.) and 18.3 mg DMAP (cat) were added to the mixture and the resultant solution was allowed to warm to RT and stirred for 6 h. The reaction mixture was quenched with saturated $NH_4Cl_{(aq)}$. The organic layer was extracted with DCM and dried over anhydrous $MgSO_4$. The organic extracts were reduced under pressure and the residue was purified using flash chromatography to afford the product in 84% yield, 625.5 mg. **R_f** 0.42 in 3:7 EtOAc:PET. **^{1}H NMR** (300 MHz, Chloroform-*d*) δ 7.30 – 7.12 (m, 2H, H-Ar), 7.12-6.99 (m, 1H, H-Ar), 6.94 (d, *J* = 8.0 Hz, 1H, H-Ar), 2.95 (dd, *J* = 8.6, 5.9 Hz, 2H, H-5), 2.66 (dd, *J* = 8.6, 5.8 Hz, 2H, H-6), 1.60 (s, 9H, H-15/H-16/H-17). **^{13}C NMR** (101 MHz, $CDCl_3$) δ 169.4 (C-4), 151.8 (C-8), 137.1 (C-Ar), 128.0 (C-Ar), 127.3 (C-Ar), 125.9 (C-Ar), 124.1 (C-Ar), 117.0 (C-Ar), 85.0 (C-14), 32.3 (C-5), 27.7 (C-15/C-16/C-17), 25.5 (C-6).

3.0 Synthesis of Medium-Sized Rings

3.1 Synthesis Starting from β-keto Esters

3-({[(9*H*-fluoren-9-yl) methoxy] carbonyl} amino)-3-phenylpropanoic acid (Compound 3A)[85]

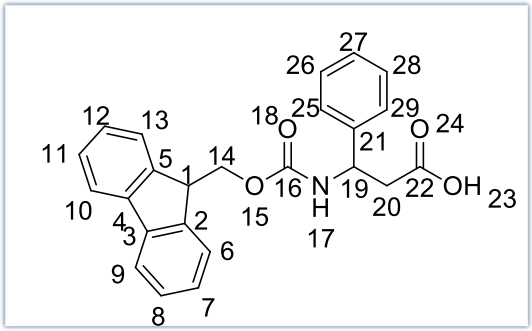

7.4 g (44.9 mmol) of *β*-phenylalanine was dissolved in 96 mL of boiling 10% aqueous sodium carbonate solution. 12.8 g (49.4 mmol) of 9-fluorenylmethyl chloroformate (Fmoc-Cl) was dissolved in 80 mL of dioxane and added dropwise to the solution of *β*-phenylalanine in aqueous potassium carbonate. The reaction was left at room temperature (RT) overnight. The reaction mixture was diluted with water and stripped three times with diethyl ether. The aqueous layer was acidified with 6 N HCl to a pH of 2 and extracted with ethyl acetate × 3. The organic extracts were dried over $MgSO_4$ and concentrated *in vacuo* to obtain the crude product. The product was recrystallized by dissolving in hot diethyl ether and adding petroleum ether. The product was filtered under reduced pressure and dried under vacuum. The product was obtained as a white solid in 81 % yield, 14 g. **R_f** 0.20 in 100% EtOAc. **^{1}H NMR** (300 MHz, $CDCl_3$) δ 12.70-11.70 (broad s, 1H, H-23), 7.93 (d, *J* = 8.6 Hz, 1H, H-17), 7.85 (d, *J* = 7.7 Hz, 2H, H-Ar), 7.65 (d, *J* = 7.6 Hz, 2H, H-Ar), 7.47–7.34 (m, 2H, H-Ar), 7.34–7.25 (m, 5H, H-Ar), 7.25–7.11 (m, 2H, H-Ar), 4.93 (td, *J* = 8.5, 6.0 Hz, 1H, H-1), 4.32–4.19 (m, 2H, H-14), 4.19–4.09 (m, 1H, H-19), 2.75–2.50 (m, 2H, H-20)

Ethyl 1-(3-{[(9*H*-fluoren-9-yl) methoxy] carbonyl} amino-3-phenylpropanoyl)-2-oxocyclohexanecarboxylate (Compound 3B)[47]

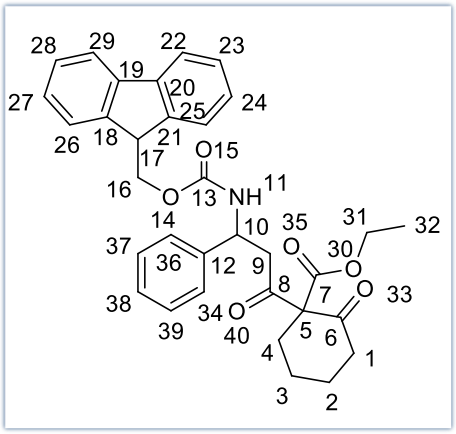

A mixture of 0.16 mL (1 mmol) of ethyl-2-oxocyclohexane carboxylate, 190.4 mg (2 mmol) of magnesium chloride and 0.5 mL (6 mmol) of pyridine in 7 mL of DCM was stirred at RT for 30 min. Freshly prepared acid chloride (3 mmol) was dissolved in 3 mL of DCM and added to the mixture. The reaction mixture was left to stir overnight at RT. The reaction mixture was diluted with 63 mL of DCM and washed with 63 mL of 10% HCl (aq). The aqueous layer was extracted with three times with DCM. The combined organic extracts were dried over magnesium sulphate. The product was purified using silica gel chromatography with ethyl acetate and petroleum ether, 5% ethyl acetate to 15% ethyl acetate. The product was an off-white solid isolated in 23% yield, 101 mg. **R_f** 0.21 in 3:7 EtOAc:Hexane. **^{1}H NMR** (400 MHz, DMSO-d_6) δ 7.83 (d, *J* = 7.7 Hz, 2H, H-Ar), 7.71 (dd, *J* = 16.1, 8.5 Hz, 1H, H-11), 7.65-7.57 (m, 2H, H-Ar), 7.39–7.32 (m, 2H, H-Ar), 7.31–7.21 (m, 6H, H-Ar), 7.21–7.15 (m, 1H, H-Ar), 5.09-4.88 (m, 1H, H-10), 4.32-4.18 (m, 2H, H-31), 4.19–3.91 (m, 3H, H-16/H-17), 3.10-2.96 (m, 1H, H-9), 2.94-2.79 (m, 1H, H-9), 2.42–2.34 (m, 1H, H-4), 2.34–2.30 (m, 1H, H-4), 2.30–2.22 (m, 1H, H-1), 2.22–2.07 (m, 1H, H-1), 1.81–1.60 (m, 2H, H-3), 1.57–1.37 (m, 2H, H-2), 1.16 – 1.01 (m, 3H, H-32). **^{13}C NMR** (101 MHz, DMSO) δ 204.9 (C-6), 201.5 (C-8), 167.6 (C-7), 155.1 (C-13), 143.8 (C-Ar), 143.7 (C-Ar), 142.7 (C-Ar), 142.7 (C-Ar), 140.6 (C-Ar), 130.0 (C-Ar), 128.8 (C-Ar), 128.2 (C-Ar), 128.0 (C-Ar), 127.5 (C-Ar), 127.0 (C-Ar), 126.9 (C-Ar), 126.4 (C-Ar), 126.2 (C-Ar), 125.0 (C-Ar), 120.0 (C-Ar), 74.6 (C-5), 65.2 (C-31), 61.7 (C-16), 50.0 (C-10), 46.6 (C-17), 45.9 (C-9), 40.6 (C-4), 31.6 (C-1), 25.9 (C-3), 20.8 (C-2), 13.7 (C-32).

Ethyl 4,10-dioxo-2-phenylazecane-5-carboxylate/(*Z*)-ethyl 4-hydroxy-10-oxo-2-phenyl-1,2,3,6,7,8,9,10-octahydroazecine-5-carboxylate (Compound 3C)[47]

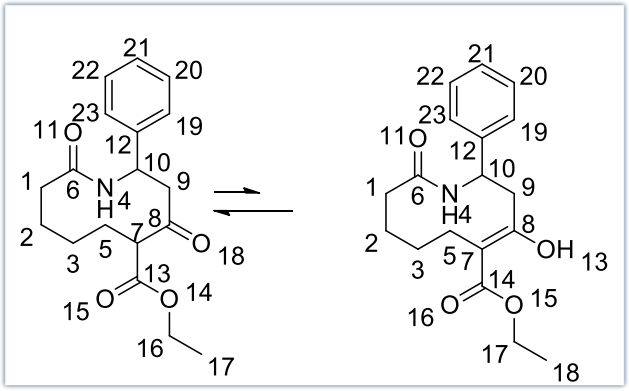

A mixture of 101 mg (0.2 mmol) of **3B** and 0.2 mL (2 mmol) of piperidine in 2 mL of DCM was stirred for 1 h at RT. The reaction mixture was washed with 1 M HCl. The aqueous layer was extracted three times with DCM. The combined organic extracts were dried over $MgSO_4$ and concentrated under vacuum. The product was purified using silica gel chromatography and isolated in 40% yield, 58.7 mg. **R_f** 0.20 in 5:5 EtOAc:Hexane. **^{1}H NMR** (300 MHz, $CDCl_3$) δ 12.72-12.57 (broad s, 1H, enol H-13), 8.76-8.32 (m, 1H, H-5), 7.37–7.27 (m, 4H, H-Ar), 7.27–7.18 (m, 1H, H-Ar), 5.30–5.13 (m, 1H, H-10), 4.43–4.27 (m, 1H, keto H-7), 4.13–3.98 (m, 2H, H-16), 3.26–3.13 (m, 1H, H-9), 2.65–2.50 (m, 1H, H-9), 2.41–2.31 (m, 1H, H-4), 1.90–1.79 (m, 1H, H-4), 1.78–1.32 (m, 5H, H-1/H-2/H-3), 1.17–1.06 (m, 3H, H-17), 1.06–0.93, (m, 1H, H-2). **^{13}C NMR** (101 MHz, DMSO) δ 205.7 (C-8), 171.7 (C-7), 168.9 (C-6), 141.8 (C-Ar), 141.4 (C-Ar), 128.3 (C-Ar), 127.1 (C-Ar), 126.1 (C-Ar), 126.1 (C-Ar), 60.9 (C-16), 55.6 (C-7), 50.7 (C-10), 49.2 (C-9), 36.3 (C-4), 25.7 (C-1), 22.3 (C-3), 21.2 (C-2), 13.9 (C-17).

Ethyl 4,9-dioxo-2-phenylazonane-5-carboxylate/(*Z*)-ethyl 4-hydroxy-9-oxo-2-phenyl-2,3,6,7,8,9-hexahydro-1*H*-azonine-5-carboxylate (Compoun d 3D)[47]

A mixture of 0.12 mL (0.8 mmol) of ethyl-2-oxocyclopentane carboxylate, 152.3 mg (1.6 mmol) of magnesium chloride and 0.5 mL (6 mmol) of pyridine in 7 mL of DCM was stirred at RT for 30 min. Freshly prepared acid chloride (2.4 mmol) was dissolved in 3 mL of DCM and added to the mixture. The reaction mixture was left to stir overnight at RT. The reaction mixture was diluted with 63 mL of DCM and washed with 63 mL of 10% HCl (aq). The aqueous layer was extracted with three times with DCM. The combined organic extracts were dried over magnesium sulphate. The crude product was redissolved in 8 mL of DCM and 0.8 mL of piperidine were added. The mixture was stirred for 1 h at RT. The reaction mixture was washed with 1 M HCl. The aqueous layer was extracted three

times with DCM. The combined organic extracts were dried over $MgSO_4$ and concentrated under vacuum. The product was purified using silica gel chromatography and isolated in 60% yield over the 2 steps, 30.5 mg. **R_f** 0.20 in 3:7 EtOAc:Hexane. **^{1}H NMR** (300 MHz, $CDCl_3$) δ 12.94–12.75 (broad s, 1H, enol H-11), 8.81–7.92 (m, 1H, H-5), 7.55–7.04 (m, 5H, H-Ar), 5.06 (t, *J* = 10.8 Hz, 1H, H-9), 4.36–3.89 (m, 2H, H-15), 3.36-3.04 (m, 2H, keto H-6), 3.02-2.85 (m, 1H, H-8), 2.85–2.55 (m, 1H, H-8), 2.46–2.19 (m, 2H, H-4), 2.12–1.44 (m, 4H, H-2/H-3), 1.26 (t, *J* = 7.1 Hz, 2H, H-16), 1.20-1.09 (m, 1H, H-16).

3.2 Synthesis Starting from Lactams

4-Phenyl-1,5-diazecane-2,6-dione (Compound 3E)[63]

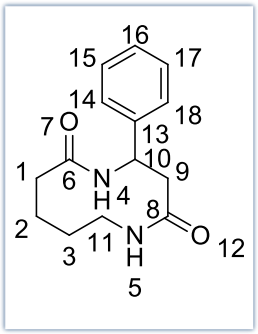

A mixture of δ-valerolactam (198.3 mg, 2 mmol), DMAP (24.4 mg, 0.2 mmol) and pyridine (1 mL, 12 mmol) in DCM (15 mL) under an argon atmosphere was stirred at RT for 30 mins. Next, a solution of acid chloride (3 mmol, 1.50 eq. freshly prepared) in DCM (3 mL) was added and the resulting mixture was refluxed at 50 ^oC for 16 h. The mixture was then diluted with DCM (30 mL) and washed with 10% aq. HCl (30 mL). The aqueous layer was then extracted with DCM (3 × 30 mL) and the combined organic extracts dried over $MgSO_4$ and concentrated *in vacuo*. The crude material was then re-dissolved in DCM (2 mL) and DBU (0.2 mL, 1.7 mmol) was added, followed by stirring at RT overnight, before the solvent was removed *in vacuo*. The compound was purified by flash column chromatography and obtained as a solid in 12% yield, 5.2 mg. **R_f** 0.01 in 6:3 EtOAc:Hexane. **^{1}H NMR** (300 MHz, $CDCl_3$) δ 7.59–7.38 (broad s, 1H, H-11), 7.33–7.22 (m, 5H, H-Ar), 4.85–4.71 (m, 1H, H-10), 3.90–3.74 (m, 1H, H-9), 3.60–3.49 (m, 1H, H-9), 2.90–2.63 (m, 4H, H-1/H-4), 1.86–1.72 (m, 4H, H-2/H-3).

1-Acryloylpiperidin-2-one (Compound 3F)[86]

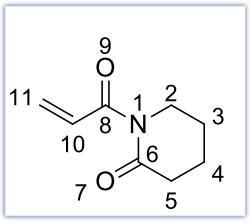

A mixture of acrylic acid (1 eq.), benzoyl chloride (2 eq.) and a very small amount (0.0015 eq.) of hydroquinone were allowed to heat up under vacuum with a distillation setup. The fractions were collected at 75 °C. The freshly distilled acid chloride was immediately used for the next reaction. To 2-piperidinone (1 eq.) in dry THF under argon at 0 °C, MeMgBr (1.1 eq.) was added over 30 min. The reaction was allowed to stir for 10 min after this. The freshly prepared acryloyl chloride (1.5 eq.) was then added and the reaction was allowed to stir for 30 min. The reaction was washed with 10 mL saturated ammonium chloride solution and extracted with 10 mL × 3 diethyl ether. The organic extracts were washed with 10 mL sodium hydrogen carbonate and dried over magnesium sulphate. The organic extracts were dried *in vacuo* and the product was purified using silica gel chromatography. The product was obtained as a clear yellow oil in 23% yield, 356.9 mg. **R_f** 0.38 in 100% EtOAc. **^{1}H NMR** (300 MHz, $CDCl_3$) δ 6.91 (dd, *J* = 16.9, 10.3 Hz, 1H, H-10), 6.26 (d, *J* = 17.2 Hz, 1H, H-11), 5.63 (d, *J* = 9.8 Hz, 1H, H-11), 3.71–3.61 (m, 2H, H-2), 2.57–2.43 (m, 2H, H-5), 1.86-1.68 (m, 4H, H-3/H-4). **^{13}C NMR** (101 MHz, $CDCl_3$) δ 173.75 (C-6), 169.59 (C-8), 131.90 (C-10), 127.86 (C-11), 44.15 (C-2), 34.77 (C-5), 22.45 (C-4), 20.65 (C-3).

5-Benzyl-1,5-diazecane-2,6-dione (Compound 3G)[86]

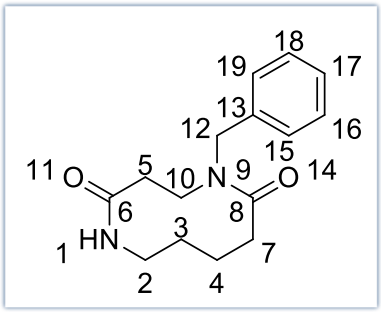

A mixture of 1-acryloylpiperidin-2-one (1 eq.) and benzylamine (1 eq.) in methanol was allowed to stir under argon for 4 h at RT. The reaction mixture was washed with base and extracted with EtOAc and the solvent was dried over $MgSO_4$ and reduced *in vacuo*. The product was purified using silica gel chromatography (EtOAc, PET and MeOH) to obtain a white solid in 36 % yield, 204.9 mg. **R_f** 0.01 in 100% EtOAc. **^{1}H NMR** (300 MHz, $CDCl_3$) δ 7.40–7.27 (m, 5H, H-Ar), 5.24–4.98 (m, 1H, H-1), 4.85 (d, *J* = 14.0 Hz, 1H, H-12), 4.48 (d, *J* = 14.5 Hz, 1H, H-12), 4.06-3.90 (m, 1H, H-10), 3.90-3.71 (m, 1H, H-10), 3.4-3.21 (m, 1H, H-2), 3.02–2.80 (m, 1H, H-2), 2.79–2.58 (m, 1H, H-7), 2.28–2.10 (m, 3H, H-5/H-7), 2.08-1.90 (m, 1H, H-3), 1.72–1.67 (m, 1H, H-3), 1.67–1.59 (m, 1H, H-4), 1.59–1.49 (m, 1H, H-4). **^{13}C NMR** (101 MHz, $CDCl_3$) δ 174.0 (C-8), 171.0 (C-6), 138.2 (C-Ar), 129.0 (C-Ar), 128.9 (C-Ar), 128.3 (C-Ar), 127.9 (C-Ar), 126.7 (C-Ar), 49.6 (C-12), 45.5 (C-10), 39.3 (C-2), 37.8 (C-5), 28.3 (C-7), 25.9 (C-4), 23.9 (C-3).

1-(3-Bromopropyl)-3,4-dihydroquinolin-2(1*H*)-one (Compound 3J)

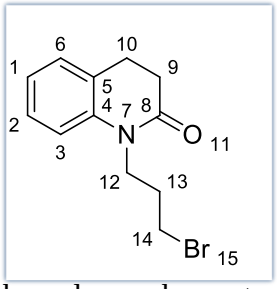

To a solution of 601 mg 3,4-dihydro-2(1*H*)-quinolinone in THF, 607.9 mg of NaH was added and the mixture was left to stir for 30 min at RT. 8 mL of 1,3-dibromopropane were added and the reaction was left to stir overnight at RT. The reaction was quenched with water and the extracted with EtOAc. The solvent was dried over $MgSO_4$ and reduced *in vacuo* and the product purified by column chromatography to obtain the product in 23% yield. **^{1}H NMR** (300 MHz, Chloroform-*d*) δ 7.09–6.90 (m, 4H, H-Ar), 4.12–3.94 (m, 2H, H-12), 3.45 (t, *J* = 6.5 Hz, 2H, H-14), 2.88–2.80 (m, 2H, H-9), 2.64–2.56 (m, 2H, H-10), 2.30–2.11 (m, 2H, H-13). **^{13}C NMR** (151 MHz, Chloroform-*d*) δ 170.0 (C-8), 139.4 (C-Ar), 127.8 (C-Ar), 127.4 (C-Ar), 126.3 (C-Ar), 122.8 (C-Ar), 115.4 (C-Ar), 41.2 (C-12), 31.8 (C-14), 31.8 (C-10), 30.3 (C-9), 25.5 (C-13).

2,3,4,5,7,8-Hexahydrobenzo[f][1,5]diazecin-6(1*H*)-one (Compound 3L)

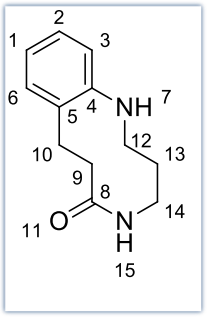

A mixture of 1 eq. compound **3J**, 2 eq. NaN_3, H_2O and THF were refluxed at 80 °C to obtain and azide which was carried forward crude. A mixture of the azide, Et_2O and PPh_3 was stirred at 0 °C for 1.5 h. H_2O was added to the reaction mixture and it was left to stir at RT overnight. The product was extracted with EtOAc and the solvent was dried over $MgSO_4$ and reduced *in vacuo*. The product was purified using silica gel chromatography (PET/EtOAc/MeOH) and obtained as a mixture with TPO. **^{1}H NMR** (300 MHz) δ 8.69–8.55 (m, 1H) 7.22–6.79 (m, 4H), 4.17–3.72 (m, 2H), 3.29–2.93 (m, 2H), 2.91–2.33 (m, 4H), 2.09–1.68 (m, 2H), 0.97–0.64 (m, 1H).

(9*H*-Fluoren-9-yl)methylbenzyl(3-oxo-3-(2-oxo-3,4-dihydroquinolin-1(2*H*)-yl)-1-phenylpropyl)carbamate (Compound 3M)

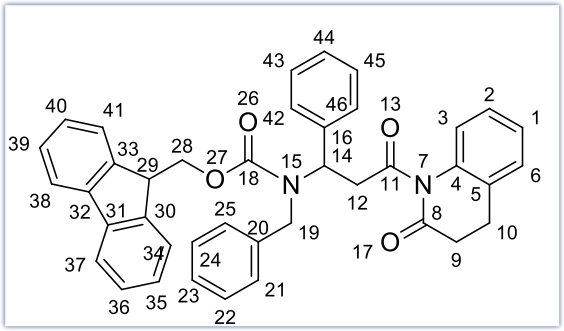

To a solution of 824 mg 3,4-dihydro-2(1*H*)-quinolinone in 10 mL THF at -78 °C, 2.5 mL of *n*-BuLi (2.5 M in hexanes) was added and the mixture was left to stir for 30 min. Freshly prepared acid chloride was added at 0 °C and the reaction was left to stir at RT overnight. The reaction was quenched with 1 M $HCl_{(aq)}$ and the extracted with EtOAc. The solvent was dried over $MgSO_4$ and reduced *in vacuo* and the product purified by silica gel chromatography (PET/EtOAc) to obtain the product in 16% yield. **^{1}H NMR** (300 MHz, Chloroform-*d*) δ 7.77 (d, *J* = 7.7 Hz, 2H, H-Ar), 7.71–7.39 (m, 4H, H-Ar), 7.34 (d, *J* = 10.0 Hz, 9H, H-Ar), 7.22-6.58 (m, 7H, H-Ar), 5.52–5.09 (m, 1H, H-14), 4.80–4.42 (m, 3H, H-28/H-29), 4.39-4.06 (m, 2H, H-19), 4.05-3.31 (m, 2H, H-12), 2.91–2.39 (m, 4H, H-9/H-10).

4.0 SYNTHESIS OF QUINOLINONES

1,6-Dimethyl-3-phenylquinolin-2(1*H*)-one (Compound 4A)[67]

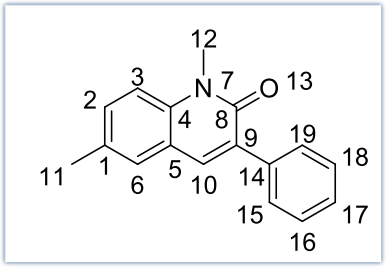

A mixture of 41 mg of *N*-methyl dihydroquinolinone (1 eq.), 4.2 mg of $Cu(acac)_2$ (10 mol%), 75.7 mg of NFSI (1.5 eq.) and 15.4 mg of MeOH (3.0 eq.) in ACN was refluxed at 80 ^{0}C under argon for 24 h. The reaction mixture was concentrated under reduced pressure and purified by column chromatography (Hexanes/EtOAc) to afford the product in 52% yield, 21.2 mg. **R_f** 0.44 in 1:1 EtOAc:PET. **^{1}H NMR** (300MHz, $CDCl_3$) δ 7.79-7.63 (m, 3H, H-Ar), 7.50-7.33 (m, 5H, H-Ar), 7.32-7.27 (m, 1H, H-10), 3.78 (s, 3H, H-12), 2.44 (s, 3H, H-11).

1-Benzylquinolin-2(1*H*)-one (Compound 4B)[87]

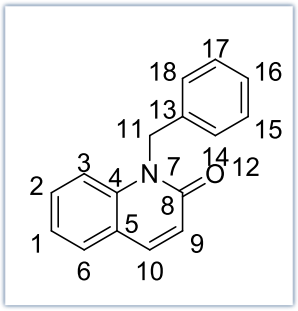

A mixture of 118.7 mg of *N*-benzyl dihydroquinolinone (1 eq.), 236.5 mg of NFSI (1.5 eq.) and 24.7 mg of CTX (20 mol%) in ACN was degassed and exposed to 405 nm light for 2 h. The reaction mixture was concentrated under reduced pressure and purified by flash chromatography (PET/EtOAc) to afford the product in 45% yield, 52.6 mg. **R_f** 0.25 in 3:7 EtOAc:PET. **^{1}H NMR** (300 MHz, $CDCl_3$) δ 7.72 (d, *J* = 9.4 Hz, 1H, H-9), 7.53 (d, *J* = 7.7 Hz, 1H, H-Ar), 7.45-7.33 (m, 1H, H-Ar), 7.33–7.05 (m, 7H, H-Ar), 6.80 (d, *J* = 9.4 Hz, 1H, H-10), 5.53 (s, 2H, H-11). **^{13}C NMR** (101 MHz, $CDCl_3$) δ 162.6 (C-8), 139.8 (C-10), 139.4 (C-Ar), 136.3 (C-Ar), 130.8 (C-Ar), 128.9 (C-Ar), 128.8 (C-Ar), 127.3 (C-Ar), 126.6 (C-Ar), 122.4 (C-Ar), 121.5 (C-Ar), 121.0 (C-9), 115.1 (C-Ar), 46.0 (C-11).

2*H*-Chromen-2-one (Compound 4C)[75]

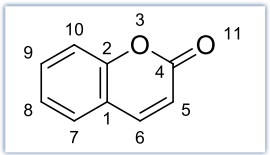

A mixture of dihydroquinolinone (1 eq.), NFSI (1.5 eq.) and CTX (20 mol%) in ACN was degassed and exposed to 405 nm light for 2 h. The reaction mixture was concentrated under reduced pressure and purified by flash chromatography (PET/EtOAc) to afford the product in 66% yield, 192.2 mg. **R_f** 0.29 in 3:7 EtOAc:PET. **^{1}H NMR** (300 MHz, Chloroform-*d*) δ 8.00 (d, *J* = 8.0 Hz, 2H, H-Ar), 7.82-7.67 (m, 1H, H-5), 7.65-7.55 (m, 2H, H-Ar), 7.55-7.21 (m, 1H, H-6).

Quinolin-2(1*H*)-one (Compound 4D)[76]

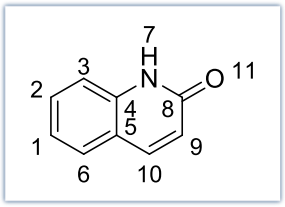

A mixture of 50 mg of dihydroquinolinone, 160.8 mg of NFSI and 37.5 mg of $[Cu(dmp)_2Cl]Cl$ in acetonitrile was degassed and left subjected to 450 nm with stirring overnight. The solvent was removed *in-vacuo* and the reaction mixture was purified by flash chromatography (PET/EtOAc) to obtain the product as an off-white solid in 62% yield, 30.5 mg. (75 % yield with CTX as catalyst). **R_f** 0.14 in 3:2 EtOAc:PET. **^{1}H NMR** (300 MHz, $CDCl_3$) δ 12.87 (s, 1H, H-7), 7.82 (d, *J* = 9.5 Hz, 1H, H-9), 7.62–7.35 (m, 3H, H-Ar), 7.25-7.08 (m, 1H, H-Ar), 6.73 (d, *J* = 9.5 Hz, 1H, H-10). **^{13}C NMR** (101 MHz, $CDCl_3$) δ 164.8 (C-8), 141.1 (C-10), 138.5 (C-Ar), 130.7 (C-Ar), 127.8 (C-Ar), 122.7 (C-Ar), 121.3 (C-9), 119.9 (C-Ar), 116.3 (C-Ar).

1-Allylquinolin-2(1*H*)-one (Compound 4E)[9]

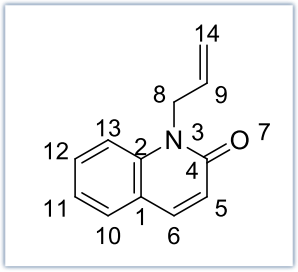

A mixture of 100 mg of *N*-allyl dihydroquinolinone, 236.5 mg of NFSI and 55 mg of $[Cu(dmp)_2Cl]Cl$ in acetonitrile was degassed and subjected to 450 nm light with stirring overnight. The solvent was removed *in-vacuo* and the reaction mixture was purified by flash chromatography (PET/EtOAc) to obtain the product in 54% yield, 50.1 mg. **R_f** 0.26 in 3:7 EtOAc:PET. **^{1}H NMR** (300 MHz, Chloroform-*d*) δ 7.68 (d, *J* = 9.5 Hz, 1H, H-5), 7.62–7.41 (m, 2H, H-Ar), 7.30 (d, *J* = 8.5 Hz, 1H, H-Ar), 7.24-7.06 (m, 1H, H-Ar), 6.71 (d, *J* = 9.4 Hz, 1H, H-6), 5.94 (ddt, *J* = 16.0, 10.1, 4.8 Hz, 1H, H-14), 5.19 (d, *J* = 10.5 Hz, 1H, H-14), 5.06 (d, *J* = 17.3 Hz, 1H, H-9), 4.99-4.80 (m, 2H, H-8). **^{13}C NMR** (101 MHz, $CDCl_3$) δ 162.0 (C-4), 139.5 (C-6), 139.3 (C-Ar), 131.7 (C-9), 130.6 (C-Ar), 129.1 (C-Ar), 128.8 (C-Ar), 122.2 (C-Ar), 121.6 (C-5), 120.8 (C-14), 117.0 (C-Ar), 44.6 (C-8).

7-Phenyl-[1,3]dioxolo[4,5-g]quinolin-6(5*H*)-one (Compound 4F)[10]

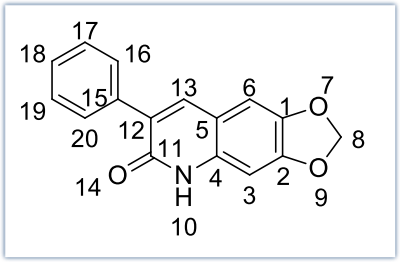

A mixture of 30 mg of dihydroquinolinone, 47.3 mg of NFSI and 11 mg of $[Cu(dmp)_2Cl]Cl$ in acetonitrile was degassed and subjected to 450 nm light with stirring overnight. The solvent was removed in-vacuo and the reaction mixture was purified by flash chromatography (PET/EtOAc) to obtain the product in 32 % yield, 8.4 mg. **R_f** 0.10 in 3:7 EtOAc:PET. **^{1}H NMR** (300 MHz, DMSO-d_6) δ 11.88 (s, 1H, H-10), 7.98 (s, 1H, H-13), 7.73 (d, *J* = 7.5 Hz, 2H, H-Ar), 7.54–7.26 (m, 4H, H-Ar), 6.84 (s, 1H, H-Ar), 6.10 (s, 2H, H-8).**^{13}C NMR** (101 MHz, DMSO) δ 160.7 (C-11), 150.0 (C-Ar), 143.2 (C-Ar), 137.4 (C-13), 136.5 (C-12), 135.4 (C-Ar), 128.4 (C-Ar), 128.4 (C-Ar), 127.9 (C-Ar), 127.4 (C-Ar), 113.9 (C-Ar), 105.3 (C-Ar), 101.7 (C-Ar), 94.7 (C-8).

1-Benzyl-7-methoxyquinolin-2(1*H*)-one (Compound 4G)

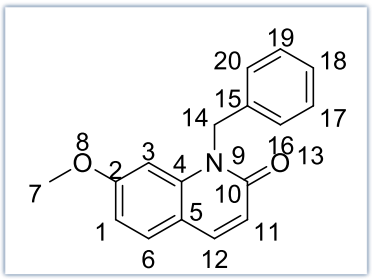

A mixture of 100 mg of dihydroquinolinone, 189 mg of NFSI and 44 mg of $[Cu(dmp)_2Cl]Cl$ in acetonitrile was degassed and subjected to 450 nm light with stirring overnight. The solvent was removed in-vacuo and the reaction mixture was purified by flash chromatography (PET/EtOAc) to obtain the product in 28% yield, 27.1 mg. **R_f** 0.18 in 3:7 EtOAc:PET. **^{1}H NMR** (300 MHz, Chloroform-*d*) δ 7.56 (d, *J* = 9.4 Hz, 1H, H-11), 7.35 (d, *J* = 8.6 Hz, 1H, H-Ar), 7.25–7.04 (m, 5H, H-Ar), 6.73–6.48 (m, 3H, H-Ar//H-12), 5.42 (s, 2H, H-14), 3.63 (s, 3H, H-7).**^{13}C NMR** (101 MHz, $CDCl_3$) δ 163.0 (C-Ar), 161.7 (C-10), 141.1 (C-Ar), 139.4 (C-Ar), 136.4 (C-12), 130.1 (C-Ar), 128.9 (C-Ar), 127.3 (C-Ar), 126.7 (C-Ar), 118.4 (C-Ar), 115.2 (C-11), 110.0 (C-Ar), 99.6 (C-Ar), 55.5 (C-7), 46.1 (C-14).

7-(*Tert-butyl*)-3-phenylquinolin-2(1*H*)-one (Compound 4H)

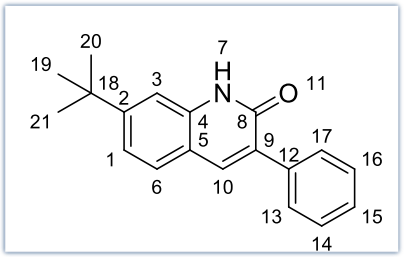

A mixture of 24.4 mg of dihydroquinolinone, 47.3 mg of NFSI and 11 mg of [Cu(dmp)$_2$Cl]Cl in acetonitrile was degassed and subjected to 450 nm light with stirring overnight. The solvent was removed in-vacuo and the reaction mixture was purified by flash chromatography (PET/EtOAc) to obtain the product in 47% yield, 11.3 mg.**^{1}H NMR** (300 MHz, Chloroform-*d*) δ 12.05 (s, 1H, H-7), 7.93 (s, 1H, H-10), 7.85 (d, *J* = 7.5 Hz, 2H, H-Ar), 7.56 (d, *J* = 8.3 Hz, 1H, H-Ar), 7.51–7.38 (m, 4H, H-Ar), 7.30 (d, *J* = 8.3 Hz, 1H, H-Ar), 1.39 (s, 9H, H-19/H-20/H-21).**^{13}C NMR** (101 MHz, $CDCl_3$) δ 163.4 (C-8), 154.4 (C-Ar), 138.1 (C-10), 138.1 (C-9), 136.3 (C-Ar), 131.3 (C-Ar), 129.0 (C-Ar), 128.2 (C-Ar), 128.0 (C-Ar), 127.5 (C-Ar), 120.9 (C-Ar), 118.2 (C-Ar), 112.0 (C-Ar), 35.2 (C-18), 31.1 (C-19/C-20/C-21).

7-Methoxyquinolin-2(1*H*)-one (Compound 4I)[88]

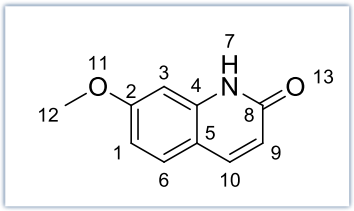

A mixture of 300 mg of dihydroquinolinone (1 eq.), 819.8 mg of NFSI (1.5 eq.) and 83.9 mg of CTX (20 mol%) in ACN was degassed and exposed to 405 nm light for 2 h. The reaction mixture was concentrated under reduced pressure and purified by flash chromatography (PET/EtOAc) to afford the product in 48% yield, 141.5 mg. **^{1}H NMR** (300 MHz, Chloroform-d) δ 12.61 (s, 1H, H-7), 7.73 (d, *J* = 9.4 Hz, 1H, H-9), 7.43 (d, *J* = 8.7 Hz, 1H, H-Ar), 7.00–6.72 (m, 2H, H-Ar), 6.56 (d, *J* = 9.3 Hz, 1H, H-10), 3.90 (s, 3H, H-12).

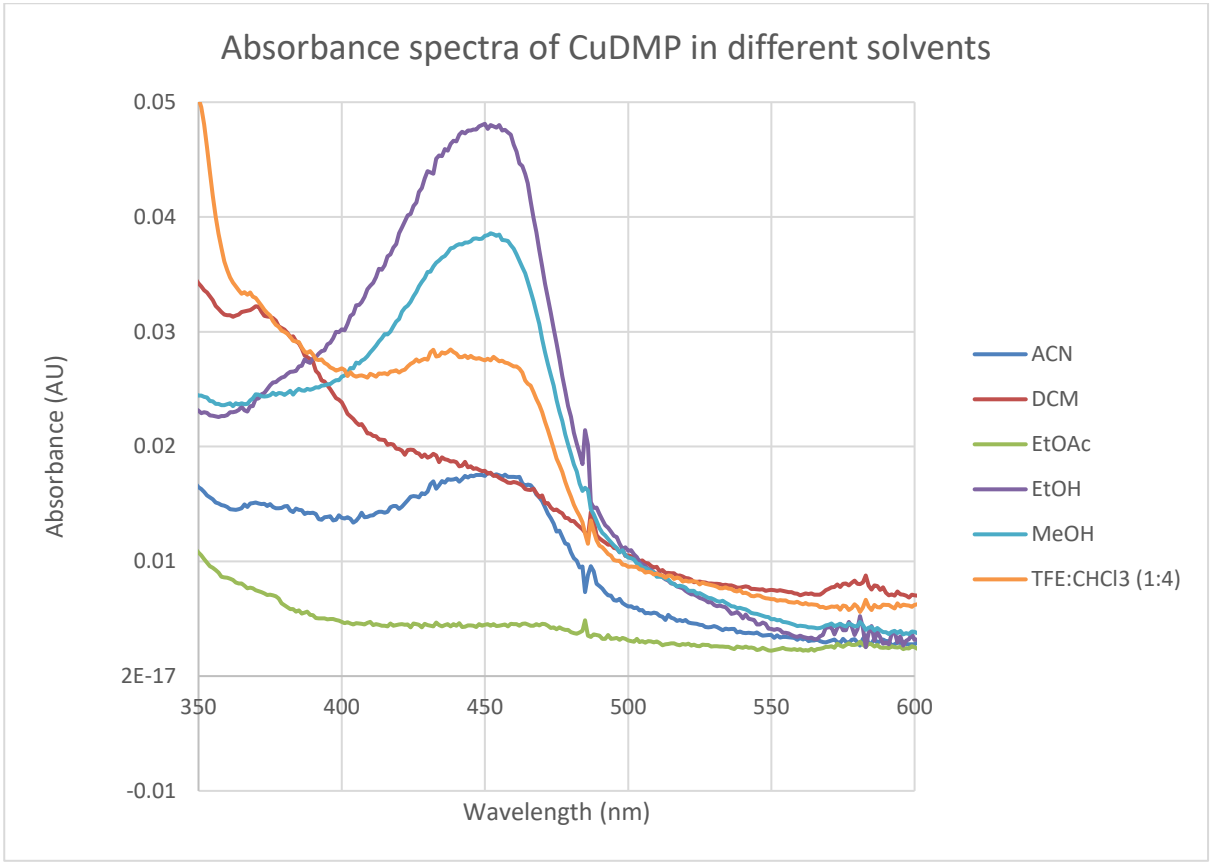
Absorbance spectra of CuDMP in different solvents
Absorbance (AU)
0.05
0.04
0.03
0.02
0.01
2E-17
-0.01
350
400
450
500
550
600
Wavelength (nm)
ACN
DCM
EtOAc
EtOH
MeOH
TFE:CHCl3 (1:4)

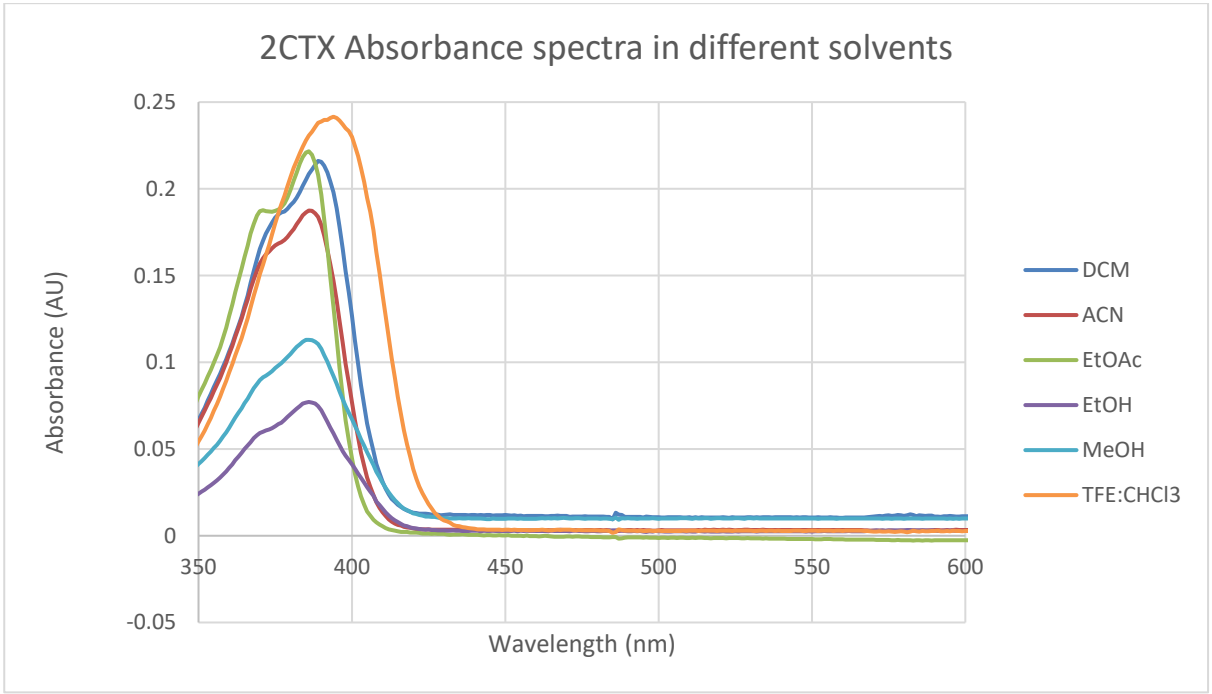
2CTX Absorbance spectra in different solvents
Absorbance (AU)
0.25
0.2
0.15
0.1
0.05
0
-0.05
350
400
450
500
550
600
Wavelength (nm)
DCM
ACN
EtOAc
EtOH
MeOH
TFE:CHCl3

6.0 References

1. Yu, X. & Sun, D. Macrocyclic drugs and synthetic methodologies toward macrocycles. *Molecules* **18**, 6230–6268 (2013).

2. Oddy, M. J., Kusza, D. A. & Petersen, W. F. Visible-light mediated metal-free 6π-photocyclization of *N*-acrylamides: thioxanthone triplet energy transfer enables the synthesis of 3,4-dihydroquinolin-2-ones. *Organic Letters* **23**, 8963–8967 (2021).

3. Liu, Z., Zhong, S., Ji, X., Deng, G. & Huang, H. Photoredox cyclization of *N* - arylacrylamides for synthesis of dihydroquinolinones. *Organic Letters* **24**,349–353 (2022).

4. Cheng, H., Lam, T., Liu, Y., Tang, Z. & Che, C. Photoinduced hydroarylation and cyclization of alkenes with luminescent platinum (II) complexes research articles. *Angewandte Chemie-International Edition* **60**, 1383–1389 (2021).

5. Liu, Z., Zhong, S., Ji, X., Deng, G. J. & Huang, H. Hydroarylation of activated alkenes enabled by proton-coupled electron transfer. *ACS Catalysis* **11**, 4422–4429 (2021).

6. Palate, K. Y., Yang, Z., Whitwood, A. C. & Unsworth, W. P. Synthesis of medium-ring lactams and macrocyclic peptide mimetics via conjugate addition/ring expansion cascade reactions. *RSC Chemical Biology* **3**, 334–340 (2022).

7. Yi, X. *et al.* Copper-catalyzed radical *N*-demethylation of amides using *N*-fluorobenzenesulfonimide as an oxidant. *Organic Letters* **22**, 4583–4587 (2020).

8. Silva, V. L. M. & Silva, A. M. S. Palladium-catalysed synthesis and transformation of quinolones. *Molecules* **24**, 228 (2019).

9. Tadd, A. C., Matsuno, A., Fielding, M. R. & Willis, M. C. Cascade palladium-catalyzed alkenyl aminocarbonylation/ Intramolecular aryl amidation: An annulative synthesis of 2-quinolones. *Organic Letters* **11**, 583–586 (2009).

10. Liu, J. L., Xu, R. R., Wang, W., Qi, X. & Wu, X. F. Palladium-catalyzed carbonylative cyclization of benzyl chlorides with anthranils for the synthesis of 3-arylquinolin-2(1: H)-ones. *Organic and Biomolecular Chemistry* **19**, 3584–3588 (2021).

11. Chen, M., Rago, A. J. & Dong, G. Platinum-catalyzed desaturation of lactams, ketones, and lactones. *Angewandte Chemie - International Edition* **57**, 16205–16209 (2018).

12. Zhang, X. *et al.* Iron-catalyzed α , β -dehydrogenation of carbonyl compounds. *Organic Letters* **23**, 1611-1615 (2021).

13. Driggers, E. M., Hale, S. P., Lee, J. & Terrett, N. K. The exploration of macrocycles for drug discovery - An underexploited structural class. *Nature Reviews Drug Discovery* **7**, 608–624 (2008).

14. Yudin, A. K. Macrocycles: Lessons from the distant past, recent developments, and future directions. *Chemical Science* **6**, 30–49 (2015).

15. Yu, X. & Sun, D. Macrocyclic drugs and synthetic methodologies toward macrocycles. *Molecules* **18**, 6230–6268 (2013).

16. Marsault, E. & Peterson, M. L. Macrocycles are great cycles: applications, opportunities, and challenges of synthetic macrocycles in drug discovery. *Journal of Medicinal Chemistry* **54**, 1961–2004 (2011).

17. Frank, A. T. *et al.* Natural macrocyclic molecules have a possible limited structural diversity. *Molecular Diversity* **11**, 115–118 (2007).

18. Mallinson, J. & Collins, I. Macrocycles in new drug discovery. *Future Medicinal Chemistry* **4**, 1409–1438 (2012).

19. Kitsiou, C. *et al.* The synthesis of structurally diverse macrocycles by successive ring expansion. *Angewandte Chemie-International Edition* **127**, 16020–16024 (2015).

20. Stephens, T. C., Lawer, A., French, T. & Unsworth, W. P. Iterative assembly of macrocyclic lactones using successive ring expansion reactions. *Chemistry - A European Journal* **24**, 13947–13953 (2018).

21. Stotani, S. & Giordanetto, F. Overview of macrocycles in clinical development and clinically used. *Practical Medicinal Chemistry with Macrocycles* (eds. Marsault E and Peterson M.L) 411–499 (John Wiley & Sons, Inc., 2017).

22. White, C. J. & Yudin, A. K. Contemporary strategies for peptide macrocyclization. *Nature Chemistry* **3**, 509–524 (2011).

23. William, A. D. *et al.* Discovery of kinase spectrum selective macrocycle (16*E*)-14-methyl-20-oxa-5, 7,14,26-tetraazatetracyclo[19.3.1.1(2,6).1(8,12)]heptacosa-1(25),2(26),3,5,8(27) ,9,11,16,21,23-decaene (SB1317/TG02), a potent inhibitor of cyclin dependent kinases (CDKs), Janus kinase 2 (JAK2), and FMS-like tyrosine kinase-3 (FLT3) for the treatment of cancer. *Journal of Medicinal Chemistry* **55**, 169–196 (2012).

24. William, A. D. *et al.* Discovery of the macrocycle (9 *E*)-15-(2-(Pyrrolidin-1-yl)ethoxy)-7,12,25- trioxa-19,21,24-triaza-tetracyclo[18.3.1.1(2,5).1(14,18)]hexacosa-1(24),2,4,9, 14(26),15,17,20,22-nonaene (SB1578), a potent inhibitor of Janus kinase 2/FMS-like tyrosine kinase-3 (JAK2/FLT3) for the treatment of rheumatoid arthritis. *Journal of Medicinal Chemistry* **55**, 2623–2640 (2012).

25. Hoffmann, H. *et al.* Discovery, structure elucidation, and biological characterization of nannocystin A, a macrocyclic myxobacterial metabolite with potent antiproliferative properties. *Angewandte Chemie-International Edition* **127**, 10283–10286 (2015).

26. United Nation. *The millenium development goals report*. (2015)

27. de-Graft Aikins, A. *et al. Open access commentary biomed central tackling Africa's chronic disease burden: from the local to the global*. *Globalization and Health* vol. 6 http://www.globalizationandhealth.com/content/6/1/5 (2010).

28. World Health Organization. *Global tuberculosis report 2020.* (2020).

29. Shah, N. S. *et al.* Transmission of extensively drug-resistant tuberculosis in South Africa. *New England Journal of Medicine* **376**, 243–253 (2017).

30. Conrad, M. D. & Rosenthal, P. J. Antimalarial drug resistance in Africa: the calm before the storm? *The Lancet Infectious Diseases* **19**, e338–e351(2019).

31. World Health Organization. *World malaria report 2020: 20 years of global progress and challenges*.(2020).

32. Maharaj, R., Kissoon, S., Lakan, V. & Kheswa, N. Rolling back malaria in Africa - challenges and opportunities to winning the elimination battle. *South African Medical Journal* **109**, 53–56 (2019).

33. Alihodžić, S. *et al.* Current trends in macrocyclic drug discovery and beyond-Ro5. *Progress in Medicinal Chemistry* **57**, 113–233 (Elsevier B.V, 2018).

34. Gradillas, A. & Pérez-Castells, J. Macrocyclization by ring-closing metathesis in the total synthesis of natural products: reaction conditions and limitations. *Angewandte Chemie - International Edition* **45**, 6086–6101 (2006).

35. Shen, X. *et al.* Kinetically *E*-selective macrocyclic ring-closing metathesis. *Nature* **541**, 380–385 (2017).

36. Grisi, F. *et al.* Synthesis of unsaturated macrocycles by Ru-catalyzed ring-closing metathesis: A comparative study. *European Journal of Organic Chemistry* 5928–5934 doi:10.1002/ejoc.201200960 (2012).

37. Biju, P. *et al.* Synthesis of novel anti-inflammatory steroidal macrocycles using ring closing metathesis reaction. *Tetrahedron Letters* **56**, 636–638 (2015).

38. Barrett, A. G. M. *et al.* Synthesis of diverse macrocyclic peptidomimetics utilizing ring-closing metathesis and solid-phase synthesis. *Journal of Organic Chemistry* **69**, 1028–1037 (2004).

39. Cohrt, A. E. & Nielsen, T. E. Solid-phase synthesis of peptide thioureas and thiazole-containing macrocycles through Ru-catalyzed ring-closing metathesis. *ACS Combinatorial Science* **16**, 71–77 (2014).

40. Alexander, V. Design and synthesis of macrocyclic ligands and their complexes of lanthanides and actinides. *Chemical Reviews* **95**, 273-342 (1995).

41. Sresutharsan, A., Tieu, W., Richardson-Sanchez, T., Soe, C. Z. & Codd, R. Dimeric and trimeric homo- and heteroleptic hydroxamic acid macrocycles formed using mixed-ligand Fe(III)-based metal-templated synthesis. *Journal of Inorganic Biochemistry* **177**, 344–351 (2017).

42. Nicolaou, K. C. & Mathison, C. J. N. Synthesis of imides,*N*-acyl vinylogous carbamates and ureas, and nitriles by oxidation of amides and amines with Dess-Martin periodinane. *Angewandte Chemie-International Edition* **117**, 6146–6151 (2005).

43. Poddar, R., Jain, A. & Kidwai, M. Bis[(L)prolinate-N,O]Zn: A water-soluble and recycle catalyst for various organic transformations. *Journal of Advanced Research* **8**, 245–270 (2017).

44. Janvier, P., Bois-Choussy, M., Bienaymø, H. & Zhu, J. A One-pot four-component (ABC_2) synthesis of macrocycles. *Angewandte Chemie-International Edition* **42**, 811-814 (2003).

45. Braverman, S. C. M. *Comprehensive Organic Synthesis*. 910-911 (Elsevier, 2014).

46. Donald, J. R. & Unsworth, W. P. Ring-expansion reactions in the synthesis of macrocycles and medium-sized rings. *Chemistry - A European Journal* **23**, 8780–8799 (2017).

47. Baud, L. G., Manning, M. A., Arkless, H. L., Stephens, T. C. & Unsworth, W. P. Ring-expansion approach to medium-sized lactams and analysis of their medicinal lead-like properties. *Chemistry - A European Journal* **23**, 2225–2230 (2017).

48. Engl, O. D., Fritz, S. P., Käslin, A. & Wennemers, H. Organocatalytic route to dihydrocoumarins and dihydroquinolinones in all stereochemical configurations. *Organic Letters* **16**, 5454–5457 (2014).

49. Mieriņa, I., Jure, M. & Stikute, A. Synthetic approaches to 4-(het) aryl-3,4-dihydroquinolin-2(1*H*)-ones. *Chemistry of Heterocyclic Compounds* **52**, 509–523 (2016).

50. Beeler, A. B. Introduction: Photochemistry in organic synthesis. *Chemical Reviews* **116**, 9629–9630 (2016).

51. Hammond, G. S. & Turro, N. J. Organic photochemistry, *Biochemical Journal* **235**, 1541-1553 (1963).

52. Gensch, T., Teders, M. & Glorius, F. Approach to comparing the functional group tolerance of reactions. *Journal of Organic Chemistry* **82**, 9154–9159 (2017).

53. Yoon, T. P., Ischay, M. A. & Du, J. Visible light photocatalysis as a greener approach to photochemical synthesis. *Nature Chemistry* **2**, 527–532 (2010).

54. Romero, N. A. & Nicewicz, D. A. Organic photoredox catalysis. *Chemical Reviews* **116**, 10075–10166 (2016).

55. Prier, C. K., Rankic, D. A. & MacMillan, D. W. C. Visible light photoredox catalysis with transition metal complexes: applications in organic synthesis. *Chemical Reviews* **113**, 5322–5363 (2013).

56. Turro, Nicholas, J., Ramamurthy, V. & Scaiano, J, C. Photochemistry of enones and dienones. *Modern Molecular Photochemistry of Organic Molecules* 801–846 (2010).

57. Strieth-Kalthoff, F., James, M. J., Teders, M., Pitzer, L. & Glorius, F. Energy transfer catalysis mediated by visible light: principles, applications, directions. *Chemical Society Reviews* **47**, 7190–7202 (2018).

58. Sai, K. K. S., Esteves, P. M., Da Penha, E. T. & Klumpp, D. A. Superacid-promoted reactions of α-ketoamides and related systems. *Journal of Organic Chemistry* **73**, 6506–6512 (2008).

59. Lange, J., Bissember, A. C., Banwell, M. G. & Cade, I. A. Synthesis of 2,3-dihydro-4(1*H*)-quinolones and the corresponding 4(1*H*)-quinolones via low-temperature Fries rearrangement of *N*-arylazetidin-2-ones. *Australian Journal of Chemistry* **64**, 454-470 (2011).

60. Huang, H., Iwasawa, N. & Mukaiyama, T. A convenient method for the construction of β-lactam compounds from β-amino acids using 2-chloro-1-methylpyridinium iodide as condensing reagent. *Chemistry letters* 1465-1466 (1984).

61. Venkatraman, R. K. & Orr-Ewing, A. J. Solvent effects on ultrafast photochemical pathways. *Accounts of Chemical Research* **54**, 4383–4394 (2021).

62. Felpin, F. X., Coste, J., Zakri, C. & Fouquet, E. Preparation of 2-quinolones by sequential heck reduction-cyclization (HRC) reactions by using a multitask palladium catalyst. *Chemistry - A European Journal* **15**, 7238–7245 (2009).

63. Stephens, T. C. *et al.* Synthesis of cyclic peptide mimetics by the successive ring expansion of lactams. *Chemistry - A European Journal* **23**, 13314–13318 (2017).

64. Herbert, G. & Brown, H. C. A Convenient preparation of volatile acid chlorides. *Journal of the American Chemical Society* **60**, 1325–1328 (1938).

65. Poulou, E. & Hackenberger, C. P. R. Staudinger ligation and reactions – from bioorthogonal labeling to next-generation biopharmaceuticals. *Israel Journal of Chemistry* **63**, Preprint at https://doi.org/10.1002/ijch.202200057 (2023).

66. Nishimura, S. *Handbook of heterogeneous catalytic hydrogenation for organic synthesis*. (J. Wiley, 2001).

67. Liu, L. *et al.* PhI(OCOCF3)2-mediated C-C bond formation concomitant with a 1,2-aryl shift in a metal-free synthesis of 3-arylquinolin-2-ones. *Organic Letters* **15**, 2906–2909 (2013).

68. Ceylan, S., Coutable, L., Wegner, J. & Kirschning, A. Inductive heating with magnetic materials inside flow reactors. *Chemistry - A European Journal* **17**, 1884–1893 (2011).

69. Diao, T. & Stahl, S. S. Synthesis of cyclic enones via direct palladium-catalyzed aerobic dehydrogenation of ketones. *Journal of the American Chemical Society* **133**, 14566–14569 (2011).

70. Chen, M. & Dong, G. Direct catalytic desaturation of lactams enabled by soft enolization. *Journal of the American Chemical Society* **139**, 7757–7760 (2017).

71. Mulligan, C. J., Parker, J. S. & Hii, K. K. (Mimi). Revisiting the mechanism of the Fujiwara-Moritani reaction. *Reaction Chemistry and Engineering* **5**, 1104–1111 (2020).

72. Cotton, F. A. & Stokely, P. F. Structural Basis for the Acidity of Sulfonamides. Crystal Structures of Dibenzenesulfonamide and Its Sodium Salt. *Journal of the American Chemical Society* **92**, 294-302 (1970).

73. Hangan, A. C. *et al.* New Cu^{+2} complexes with *N*-sulfonamide ligands: potential antitumor, antibacterial, and antioxidant agents. *Molecules* **27**, (2022).

74. Nimios, M. R., Kelley, D. F. & Bernstein, E. R. Spectroscopy and structure of 2-hydroxyqulnoline. *Journal of Physical Chemistry* **91**, 6610-6614 (1987).

75. Park, K. K. & Lee, J. J. Facile synthesis of 4-phenylquinolin-2(1*H*)-one derivatives from *N*-acyl-*O*-aminobenzophenones. *Tetrahedron* **60**, 2993–2999 (2004).

76. Igoe, N. *et al.* Design of a biased potent small molecule inhibitor of the bromodomain and PHD finger-containing (brpf) proteins suitable for cellular and *in vivo* studies. *Journal of Medicinal Chemistry* **60**, 668–680 (2017).

77. Liu, L. *et al.* Metal-Free Synthesis of 3-arylquinolin-2-ones from acrylic amides via a highly regioselective 1,2-aryl migration: an experimental and computational study. *Journal of Organic Chemistry* **81**, 4058–4065 (2016).

78. Zhao, X. *et al.* Divergent aminocarbonylations of alkynes enabled by photoredox/nickel dual catalysis. *Angewandte Chemie - International Edition* **60**, 26511–26517 (2021).

79. Wu, L., Wang, F., Chen, P. & Liu, G. Enantioselective construction of quaternary all-carbon centers via copper-catalyzed arylation of tertiary carbon-centered radicals. *Journal of American Chemical Society* **141**, 1887–1892 (2019).

80. Zhang, L., Qureshi, Z., Sonaglia, L. & Lautens, M. Sequential rhodium/palladium catalysis: enantioselective formation of dihydroquinolinones in the presence of achiral and chiral ligands. *Angewandte Chemie - International Edition* **53**, 13850–13853 (2014).

81. Trost, B. M. *et al.* Palladium-catalyzed decarboxylative asymmetric allylic alkylation of dihydroquinolinones. *Organic Letters* **21**, 1784–1788 (2019).

82. Xie, D. & Zhang, S. Selective reduction of quinolinones promoted by a SmI_2/H_2O/MeOH system. *Journal of Organic Chemistry* **87**, 8757–8763 (2022).

83. Chisholm, D. R., Zhou, G. L., Pohl, E., Valentine, R. & Whiting, A. Practical synthetic strategies towards lipophilic 6-iodotetrahydroquinolines and -dihydroquinolines. *Beilstein Journal of Organic Chemistry* **12**, 1851–1862 (2016).

84. Guarna, A. *et al.* Benzo[c]quinolizin-3-ones: a novel class of potent and selective nonsteroidal inhibitors of human steroid 5α-reductase 1. *Journal of Medicinal Chemistry* **43**, 3718–3735 (2000).

85. Le Foll Devaux, A. *et al.* A Meldrum's acid based multicomponent synthesis of *N*-Fmoc-isoxazolidin-5-ones: entry to *N*-Fmoc-β-amino acids. *European Journal of Organic Chemistry* 3265–3273 (2017).

86. Stephens, T. C. & Unsworth, W. P. Consecutive ring-expansion reactions for the iterative assembly of medium-sized rings and macrocycles. *Synlett* **31**, 133–146 (2020).

87. Feng, B. *et al.* Specific *N*-alkylation of hydroxypyridines achieved by a catalyst- and base-free reaction with organohalides. *Journal of Organic Chemistry* **83**, 6769–6775 (2018).

88. Surivet, J. P. *et al.* Synthesis and characterization of tetrahydropyran-based bacterial topoisomerase inhibitors with antibacterial activity against gram-negative bacteria. *Journal of Medicinal Chemistry* **60**, 3776–3794 (2017).

89. Antibiotic Resistance Outline Diagram, Illustrated Mechanism in Bacteria Cell Stock Vector - Illustration of mechanism, health: 231919386. https://www.dreamstime.com/mechanisms-antibiotic-resistance-outline-diagram-illustrated-example-alternation-drug-target-activation-drug-efflux-pumps-image231919386.

90. Tse, B. N., Snyder, T. M., Shen, Y. & Liu, D. R. Translation of DNA into a library of 13 000 synthetic small-molecule macrocycles suitable for *in vitro* selection. *Journal of the American Chemical Society* **130**, 15611–15626 (2008).

91. Clausena excavata. http://www.epharmacognosy.com/2021/10/clausena-excavata.html.

92. Fluorescence Spectroscopy | JASCO. https://jascoinc.com/learning-center/theory/spectroscopy/fluorescence-spectroscopy/.

APPENDICES

1,3-Diphenylazetidin-2-one (Compound 2A)

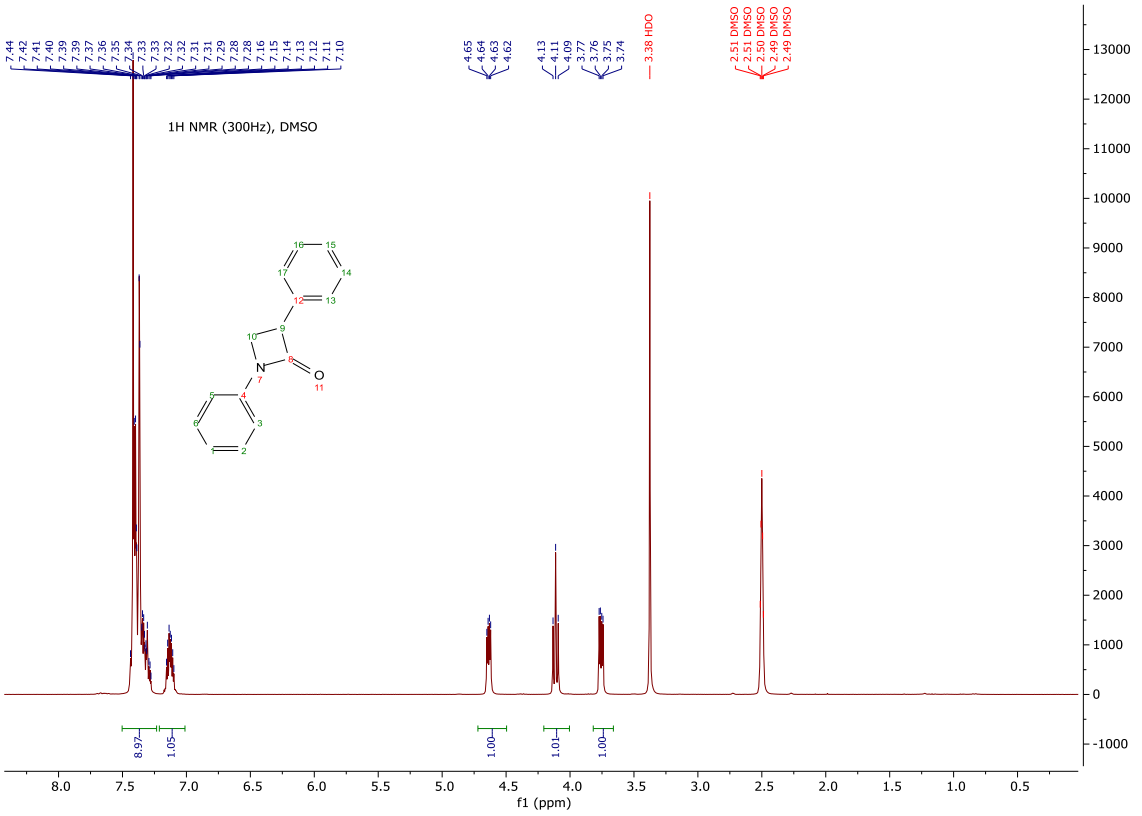

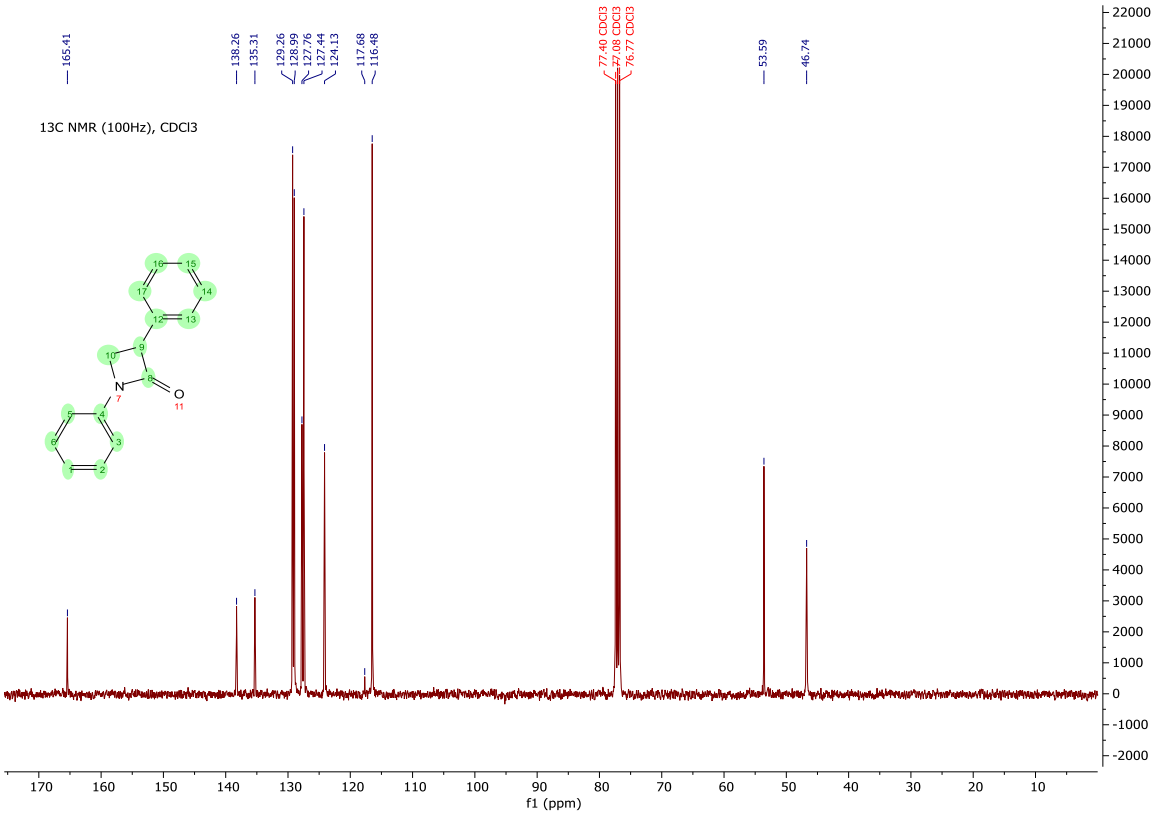

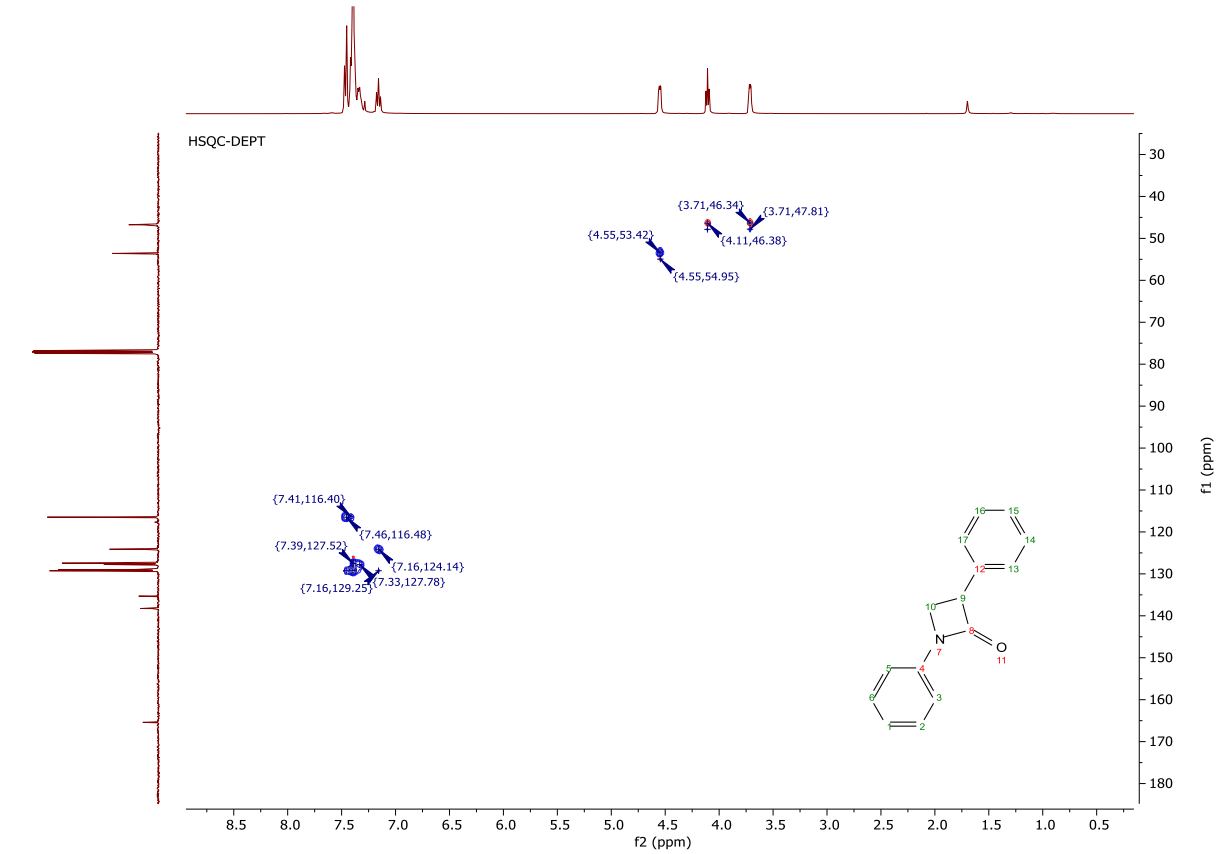
HSQC-DEPT
{3.71,46.34}
{3.71,47.81}
{4.11,46.38}
{4.55,53.42}
{4.55,54.95}
{7.41,116.40}
{7.46,116.48}
{7.39,127.52}
{7.16,124.14}
{7.33,127.78}
{7.16,129.25}
f1 (ppm)
f2 (ppm)

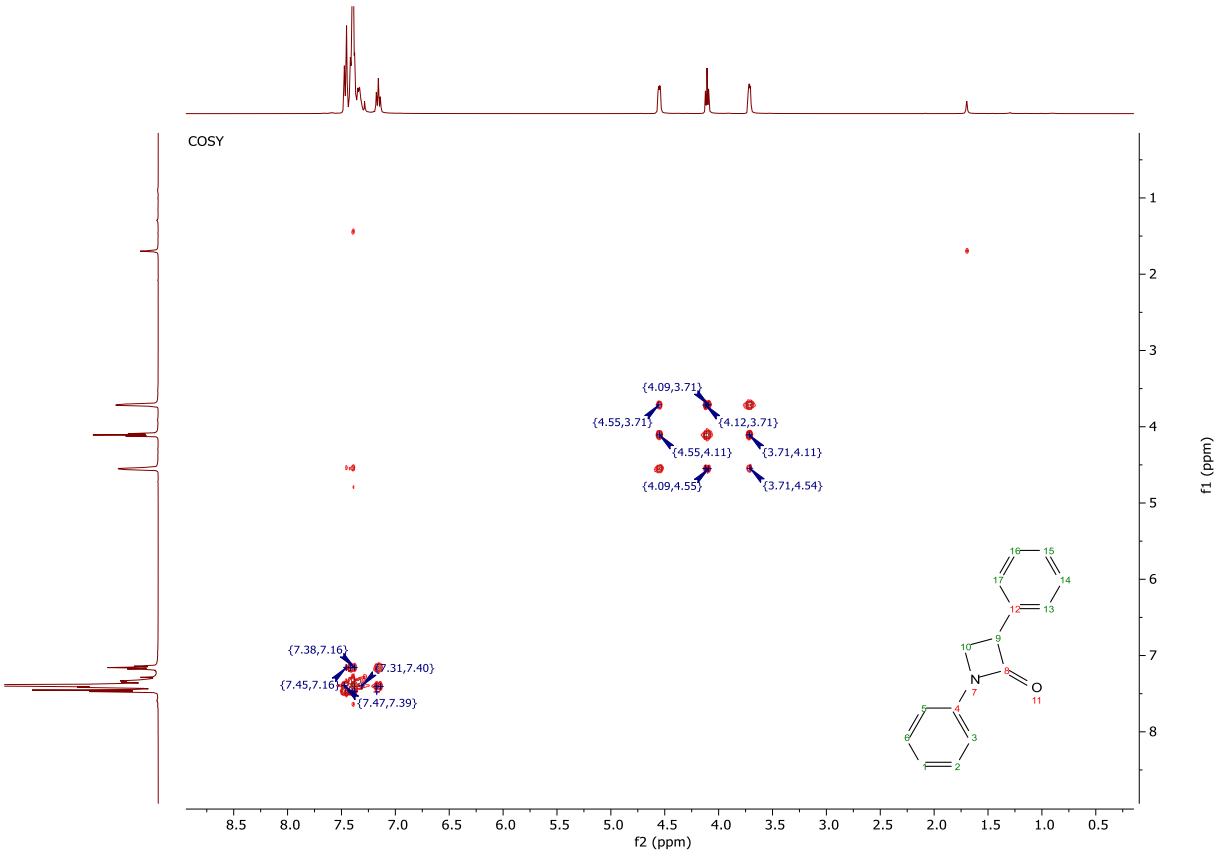
COSY
{4.09,3.71}
{4.55,3.71}
{4.12,3.71}
{4.55,4.11}
{3.71,4.11}
{4.09,4.55}
{3.71,4.54}
{7.38,7.16}
{7.31,7.40}
{7.45,7.16}
{7.47,7.39}
f1 (ppm)
f2 (ppm)

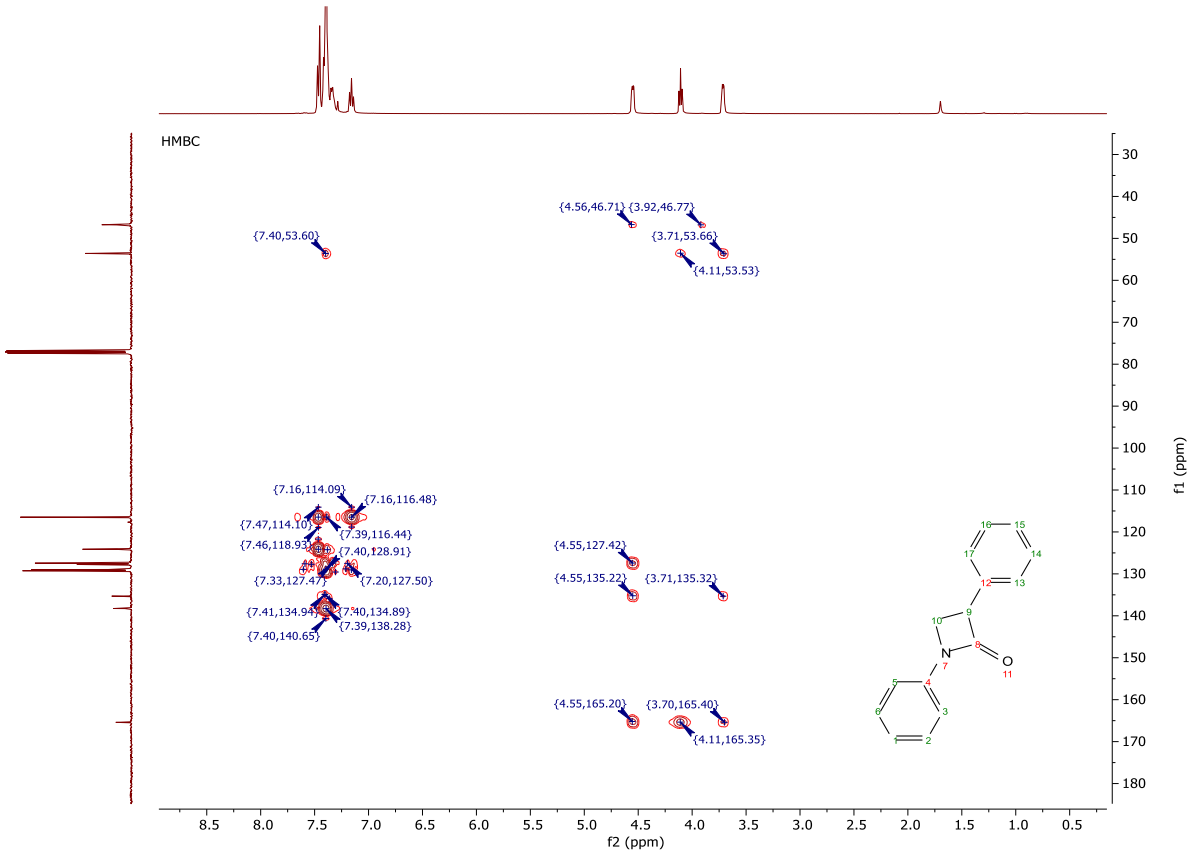

N,2-Diphenylacrylamide (Compound 2B)

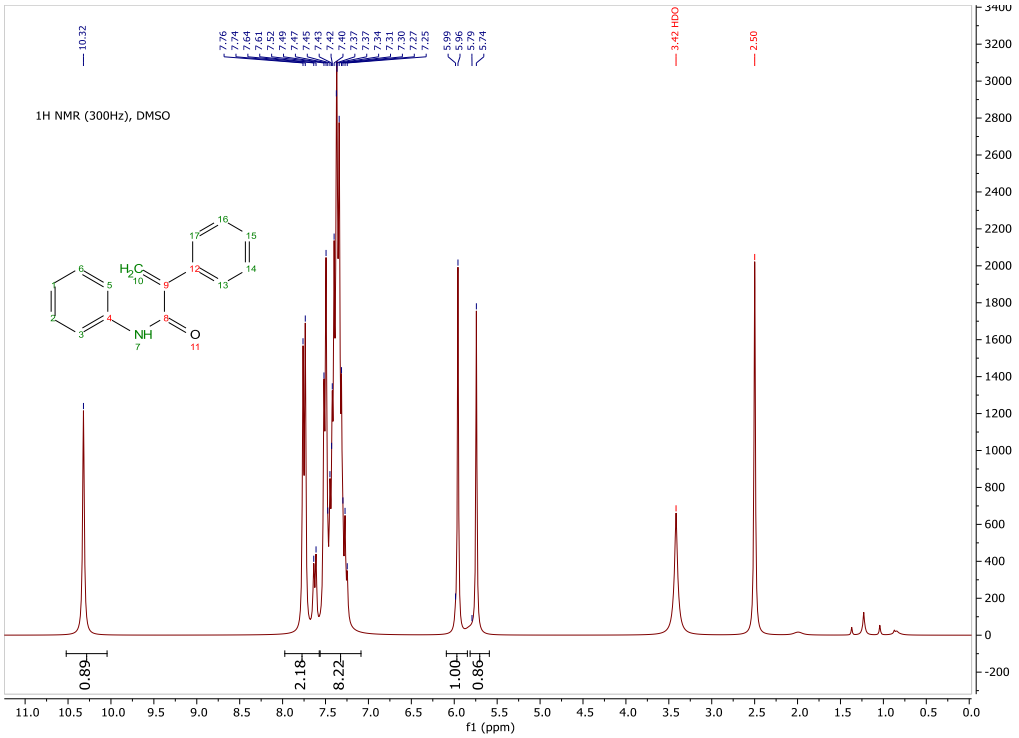

N-(3-(*Tert*-butyl) phenyl)-2-phenylacrylamide (Compound 2C)

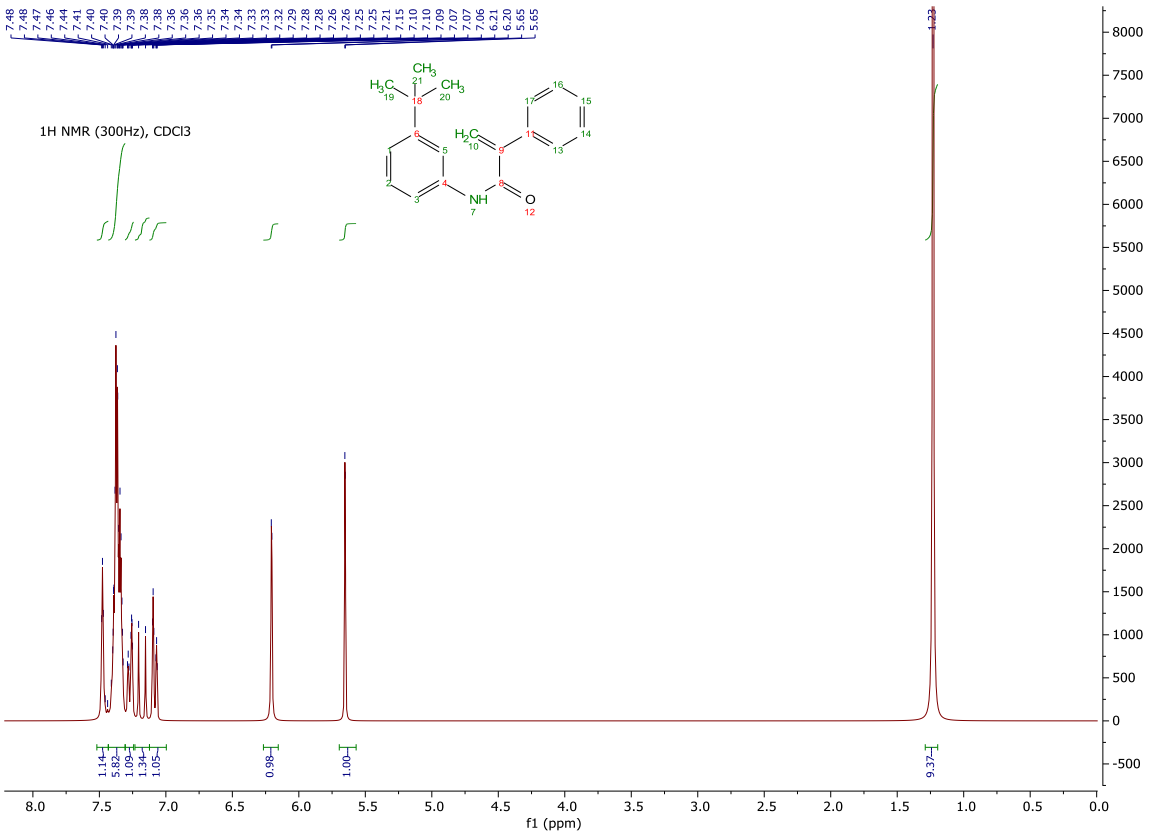

N-(2-Fluoro-4-methylphenyl)-2-phenylacrylamide (Compound 2D)

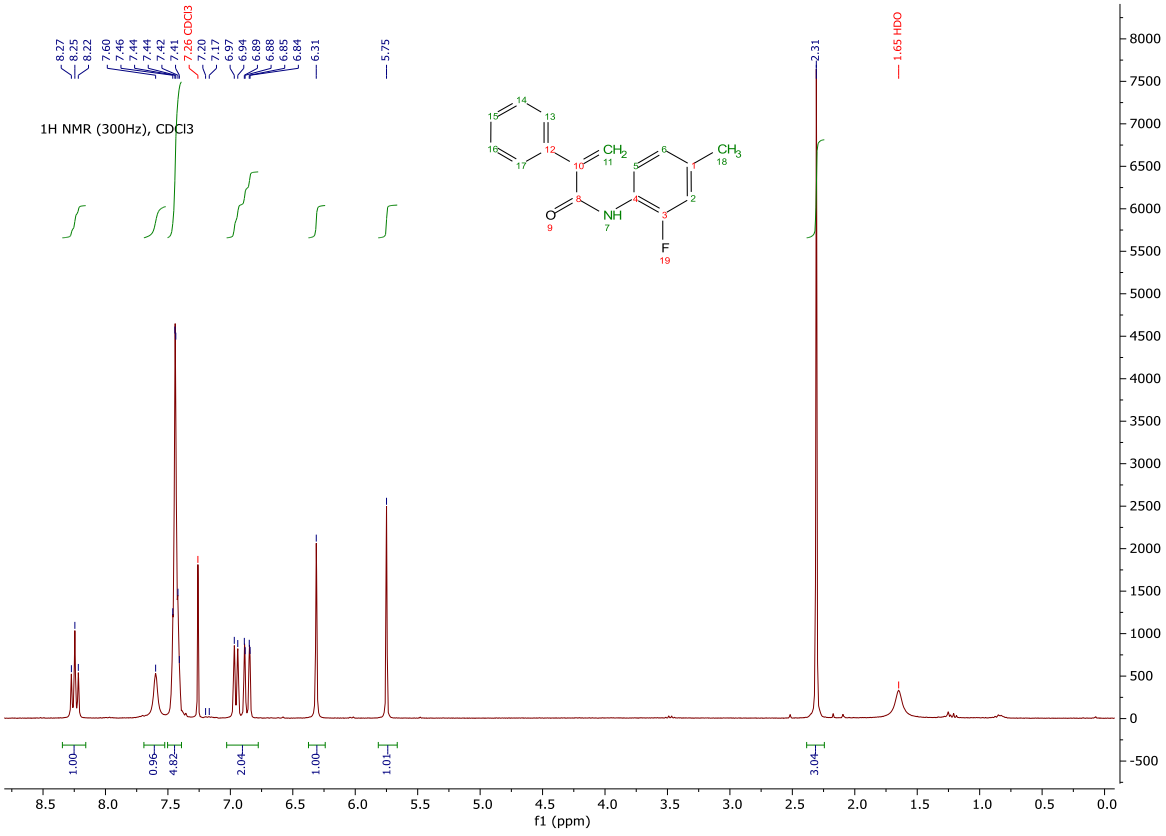

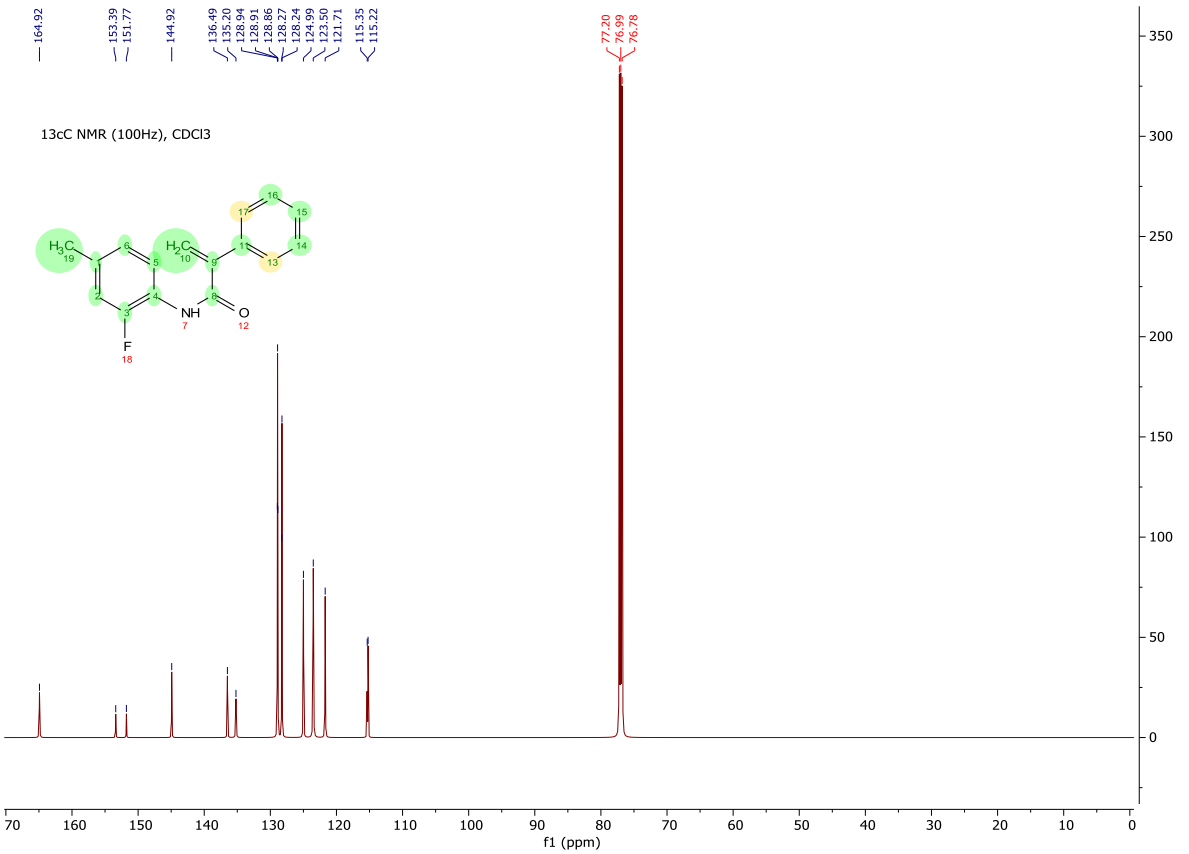

1-(Benzo[d] [1,3] dioxol-5-yl)-3-phenylazetidin-2-one (Compound 2E)

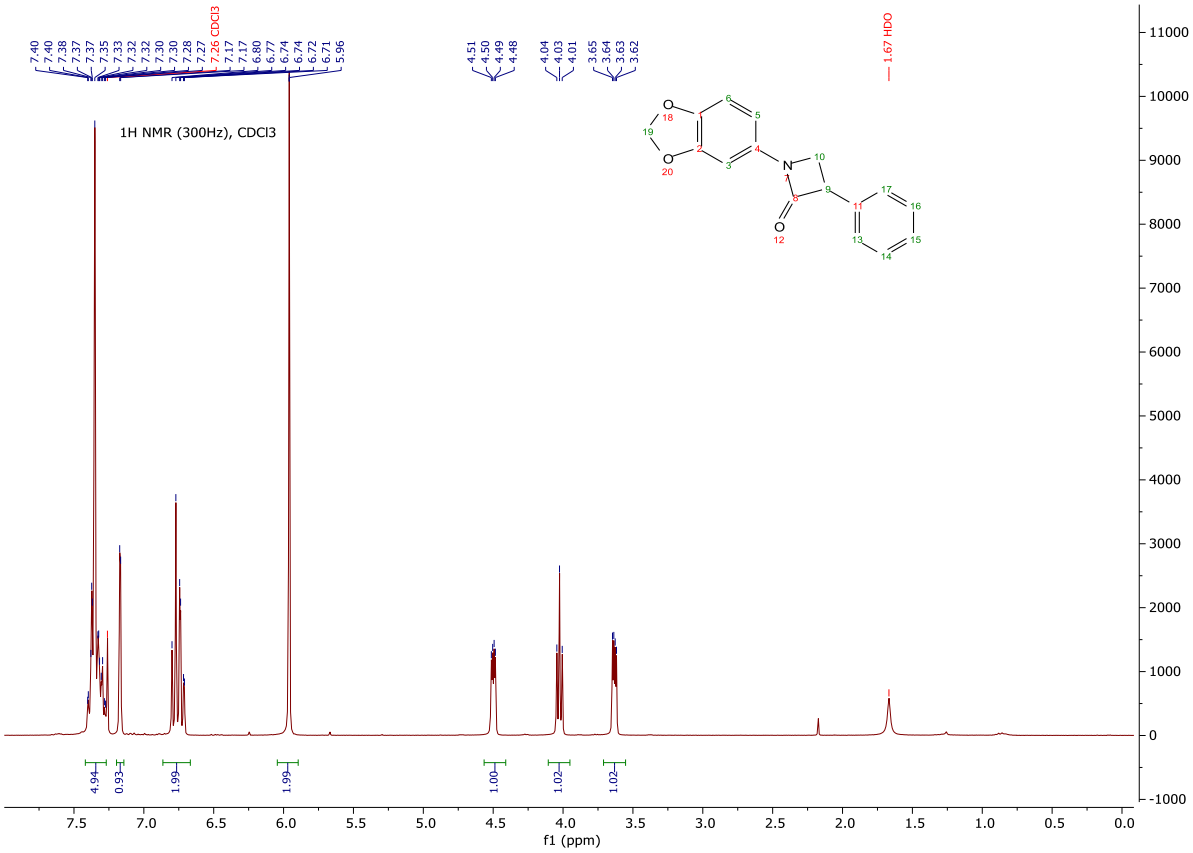

N-(Benzo[d][1,3]dioxol-5-yl)-2-phenylacrylamide (Compound 2F)

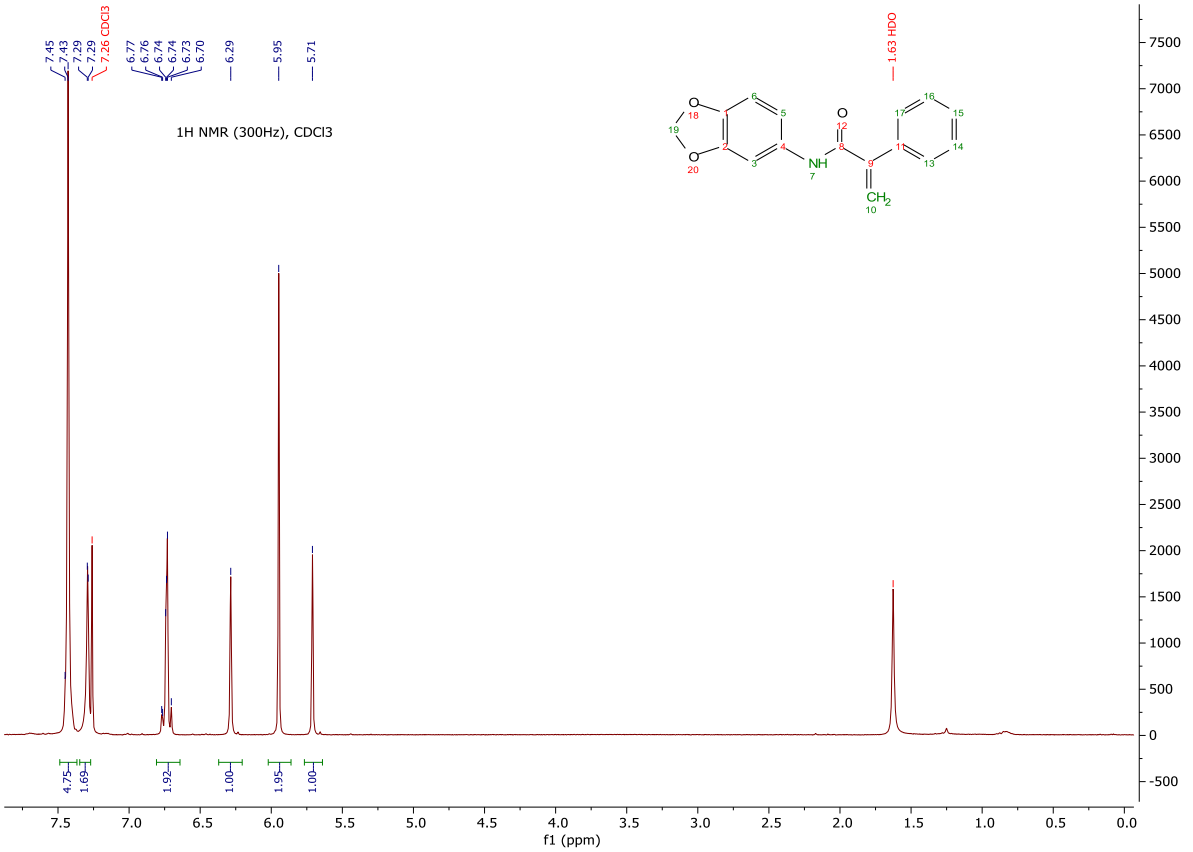

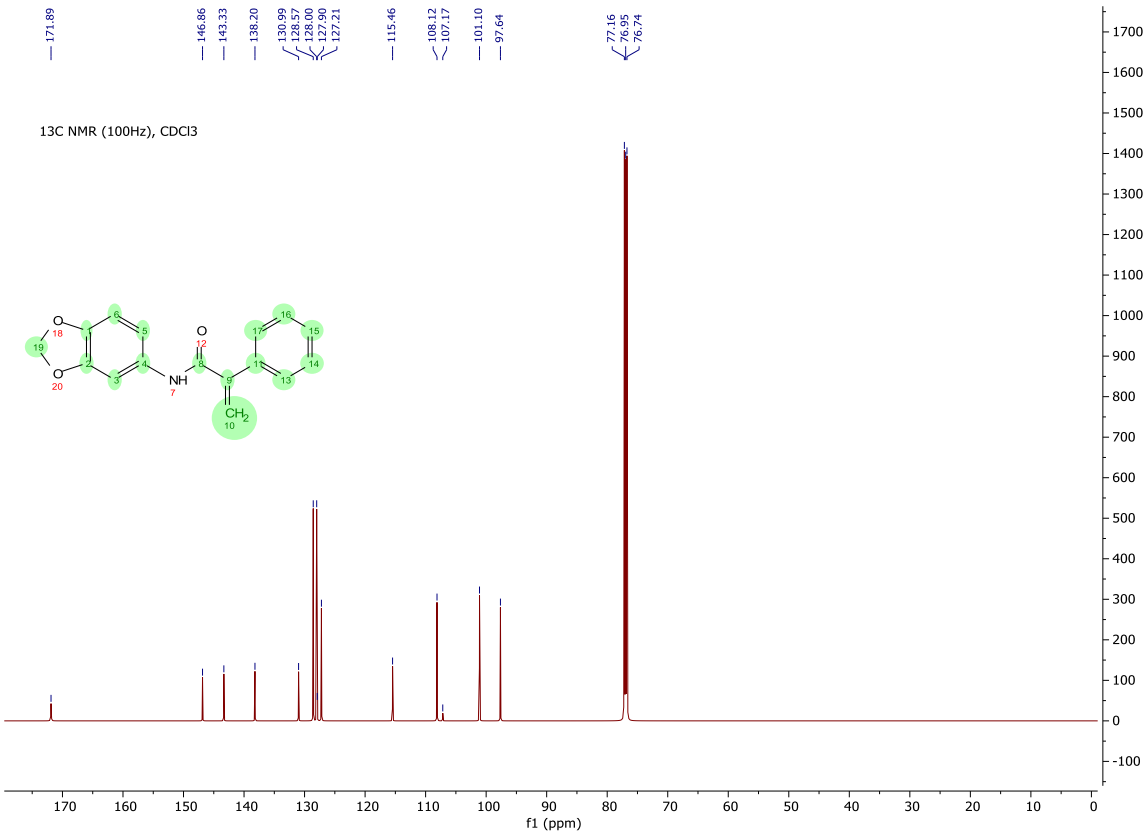

3-Phenyl-1-(3,4,5-trimethoxyphenyl) azetidin-2-one (Compound 2G)

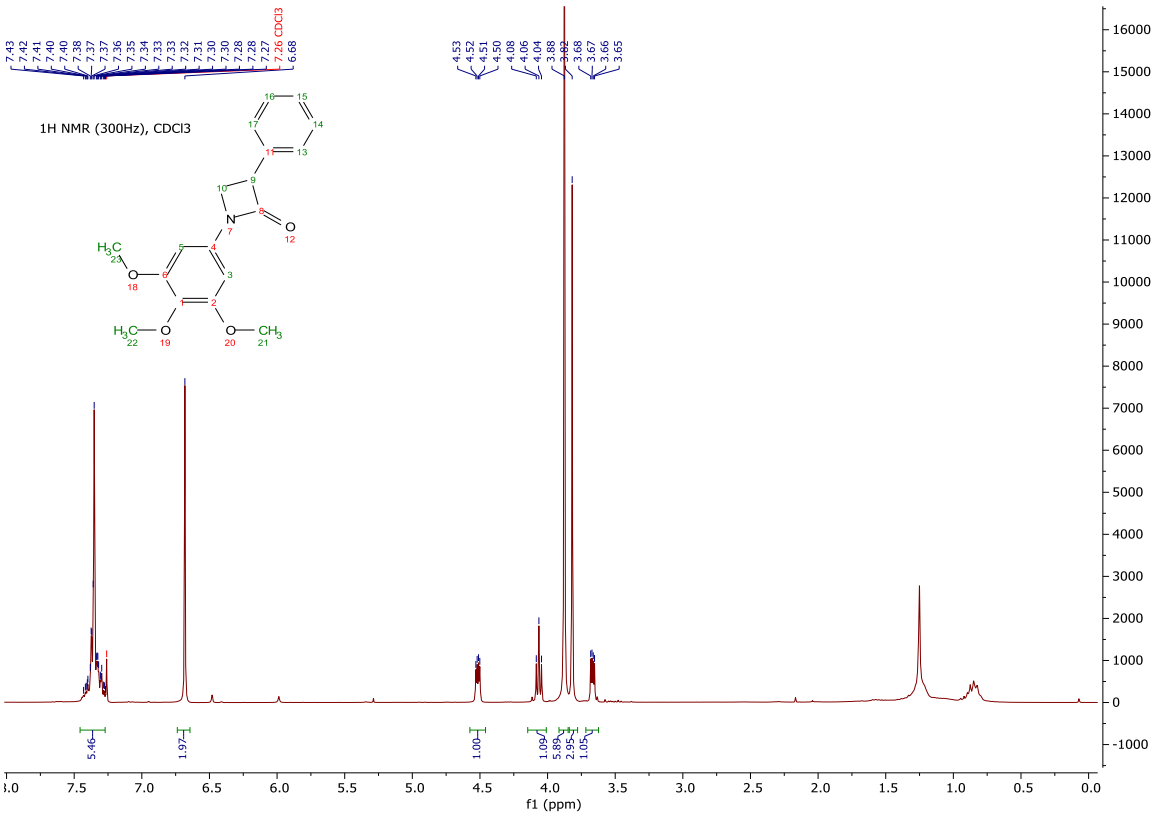

1-(3,4-Dichloro-2-methylphenyl)-3-phenylazetidin-2-one (Compound 2H)

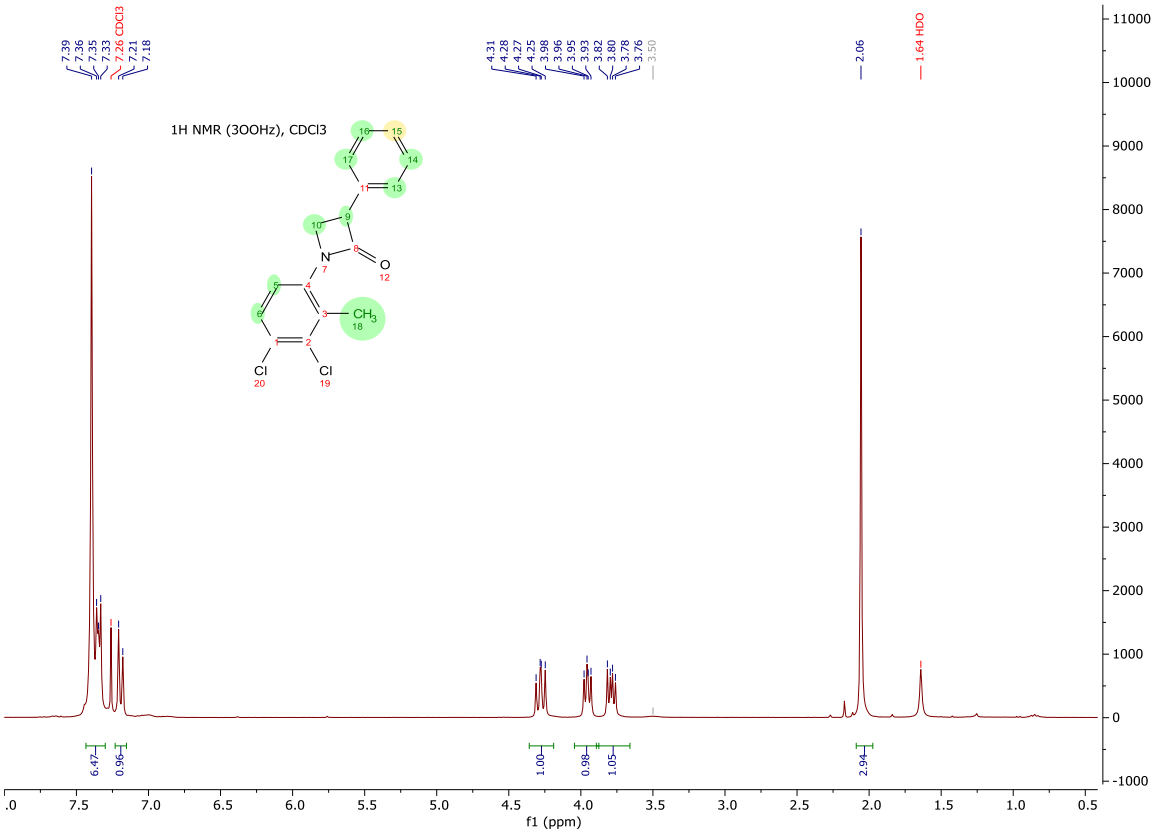

1-(4-(2-Methoxyethoxy) phenyl)-3-phenylazetidin-2-one (Compound 2I)

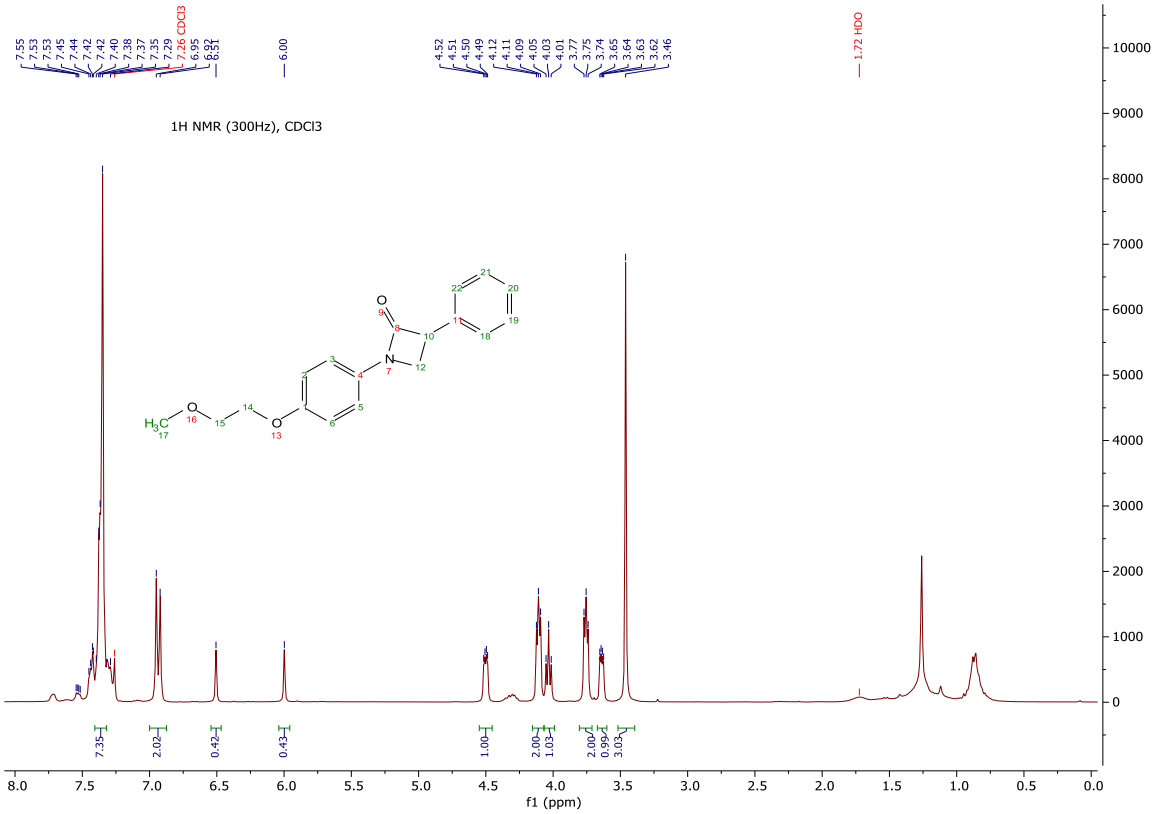

N-(4-(2-Methoxyethoxy) phenyl)-2-phenylacrylamide (Compound 2J)

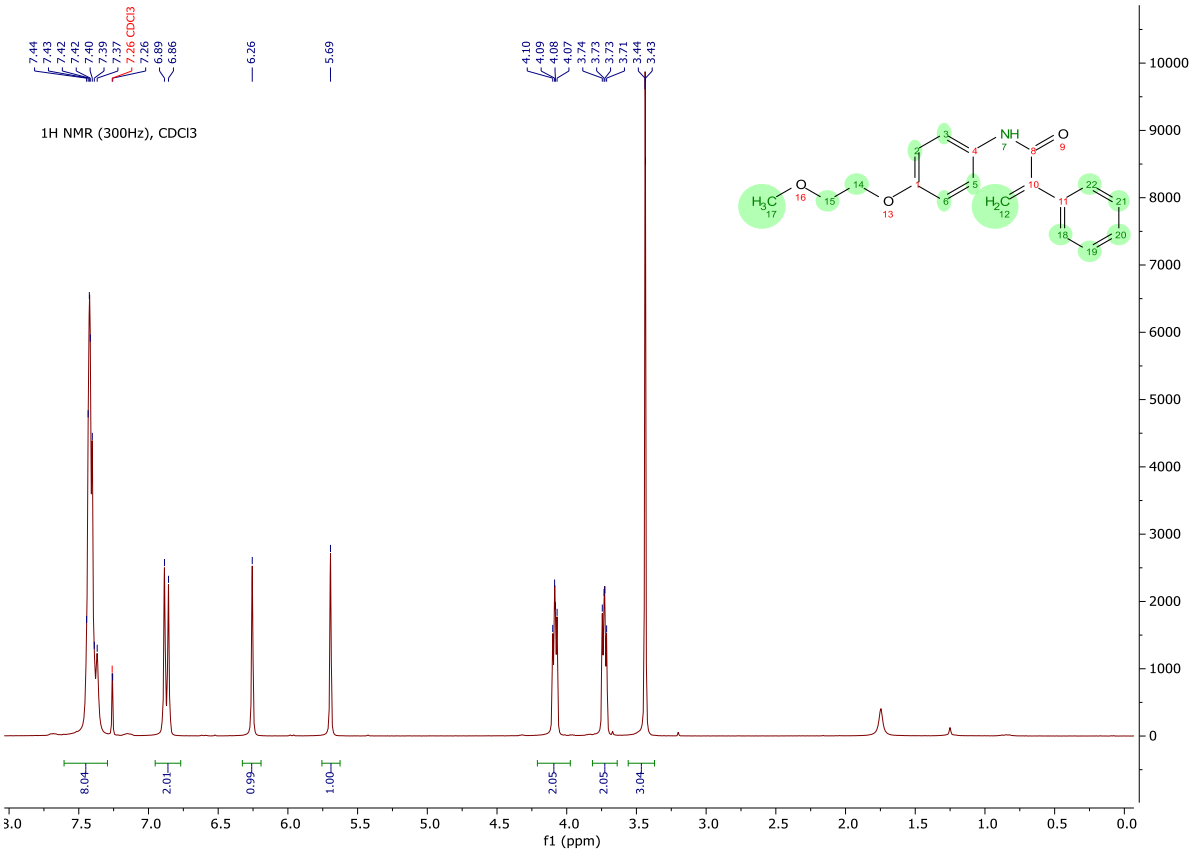

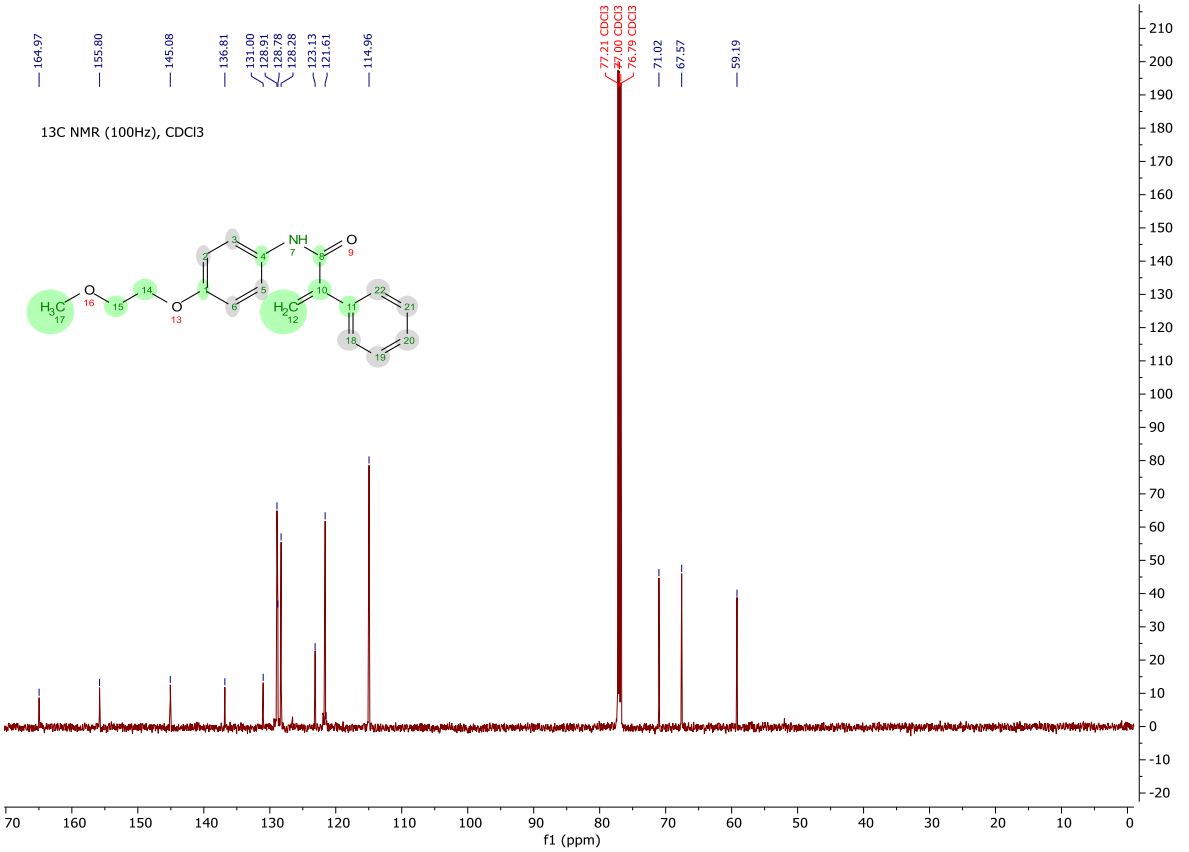

1-(3,5-Dibromophenyl)-3-phenylazetidin-2-one (Compound 2K)

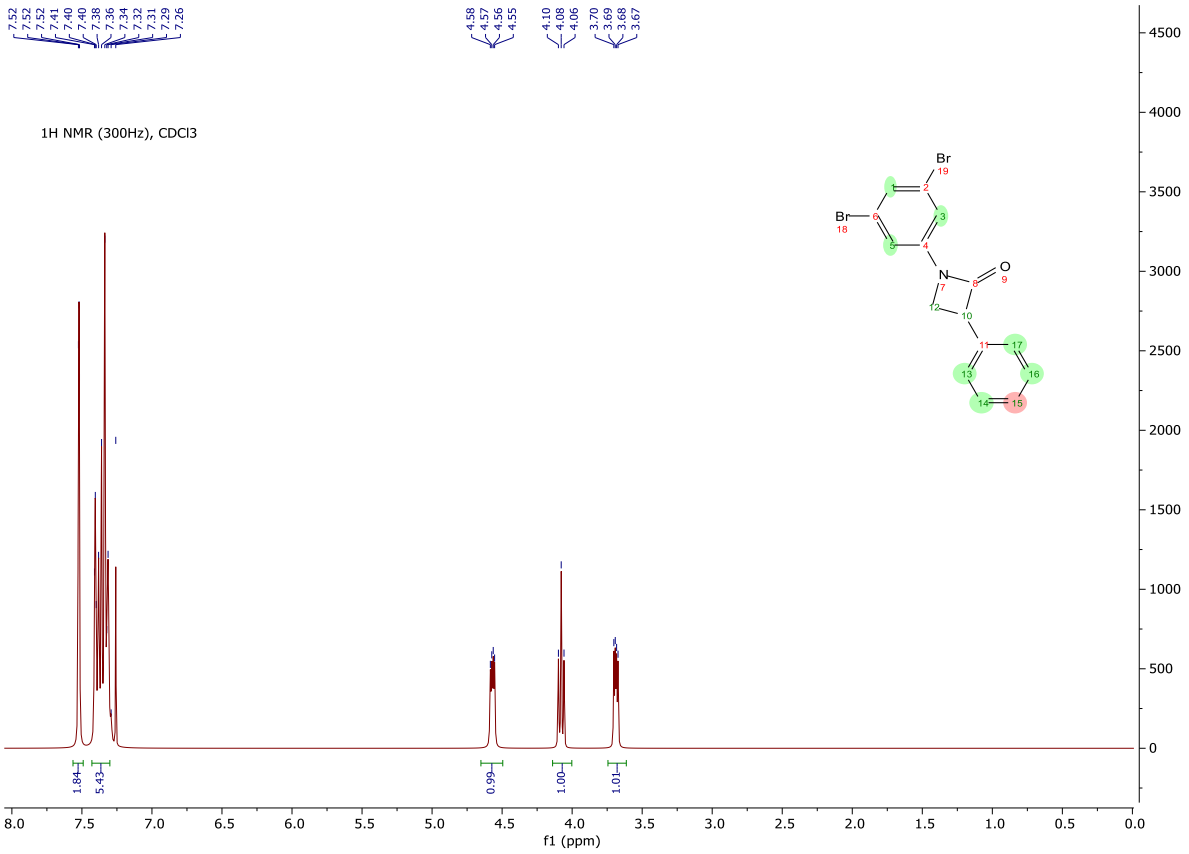

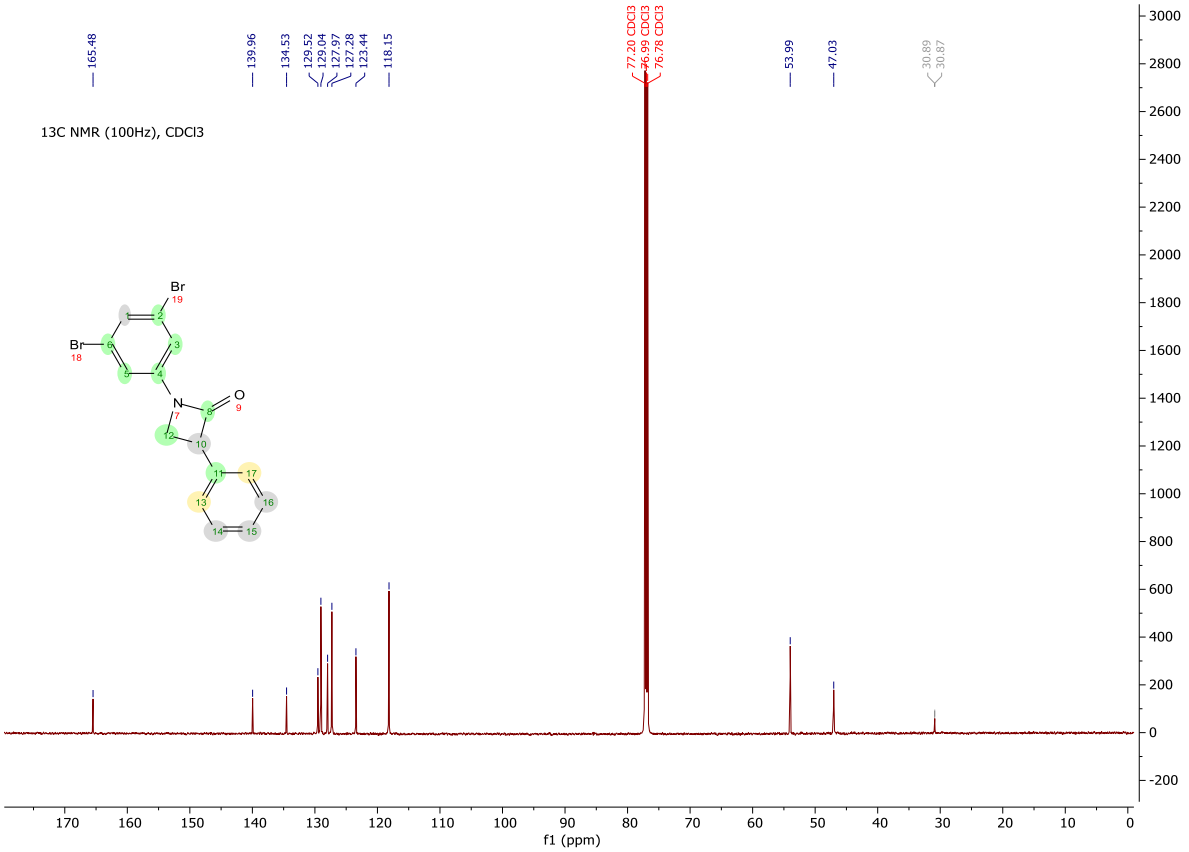

N-(3,5-Dibromophenyl)-2-phenylacrylamide (Compound 2L)

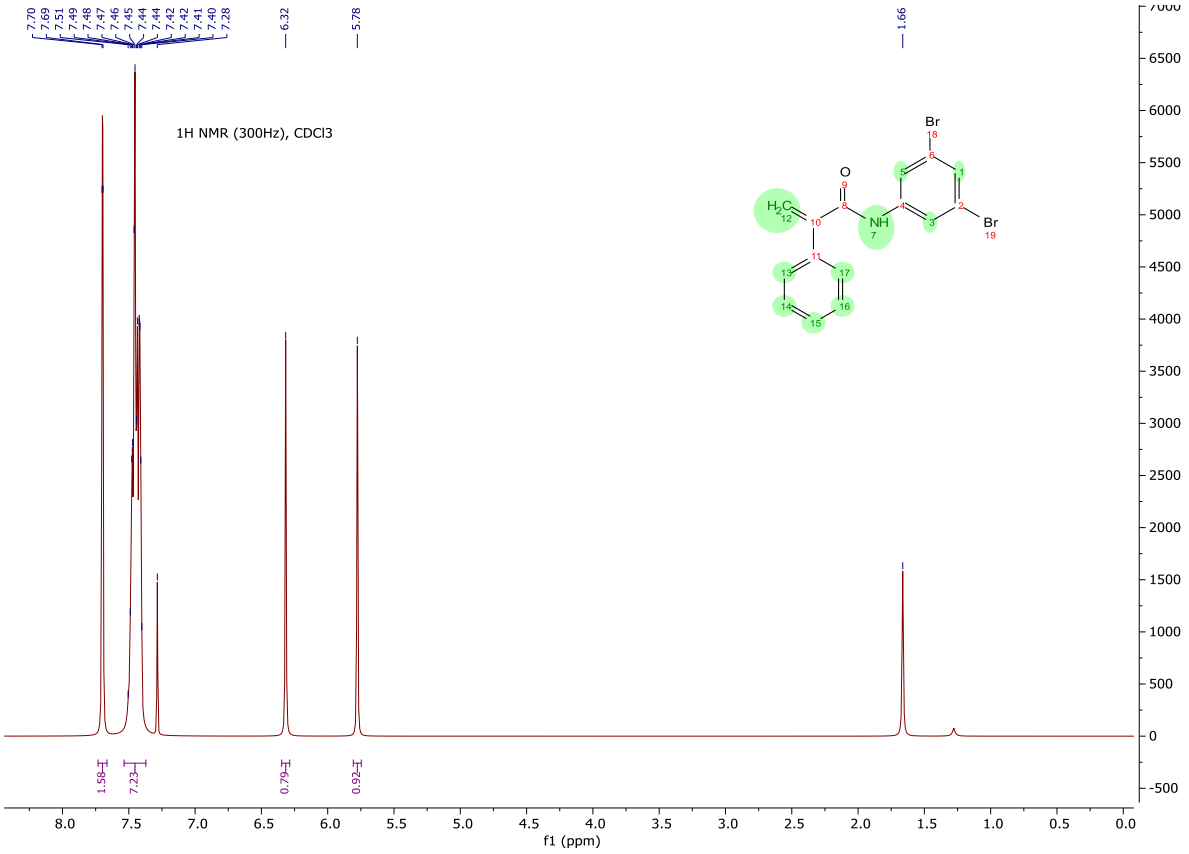

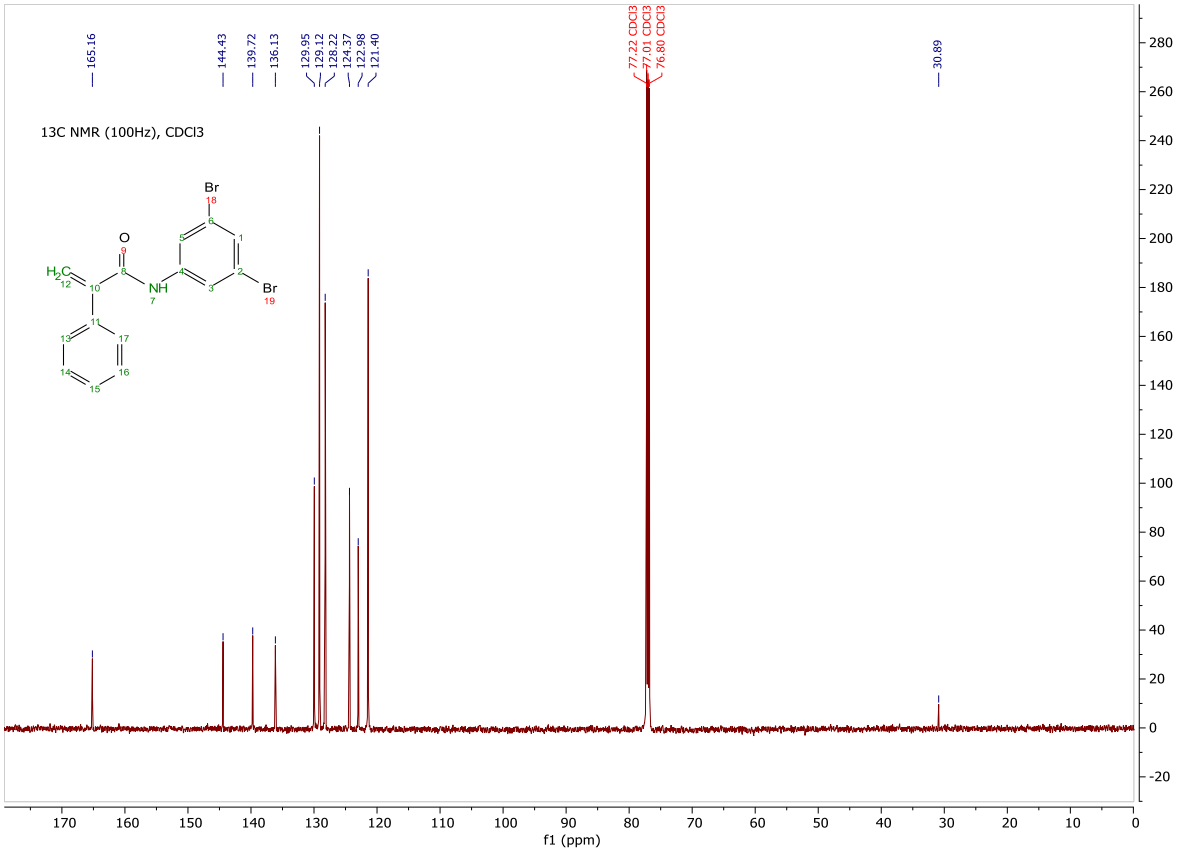

N-(4-Bromo-3,5-difluorophenyl)-2-phenylacrylamide (Compound 2M)

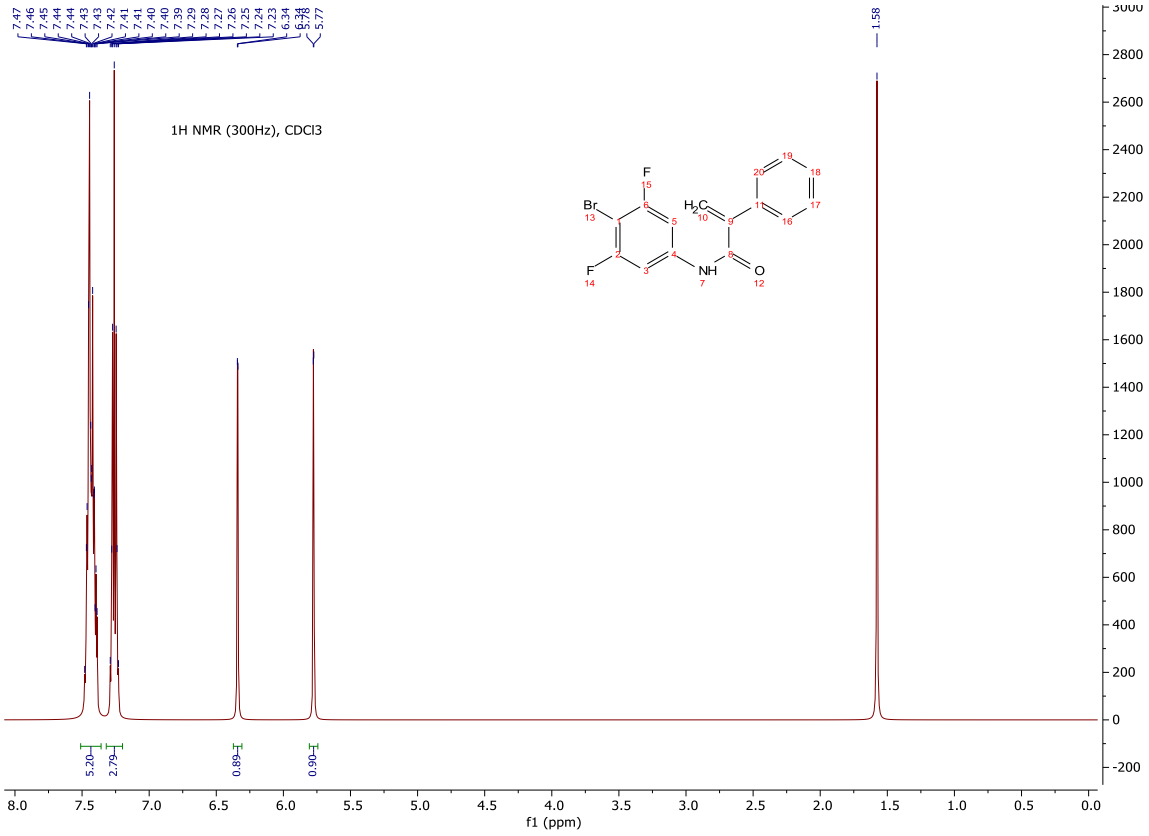

3-Phenyl-3,4-dihydroquinolin-2(1*H*)-one (Compound 2N)

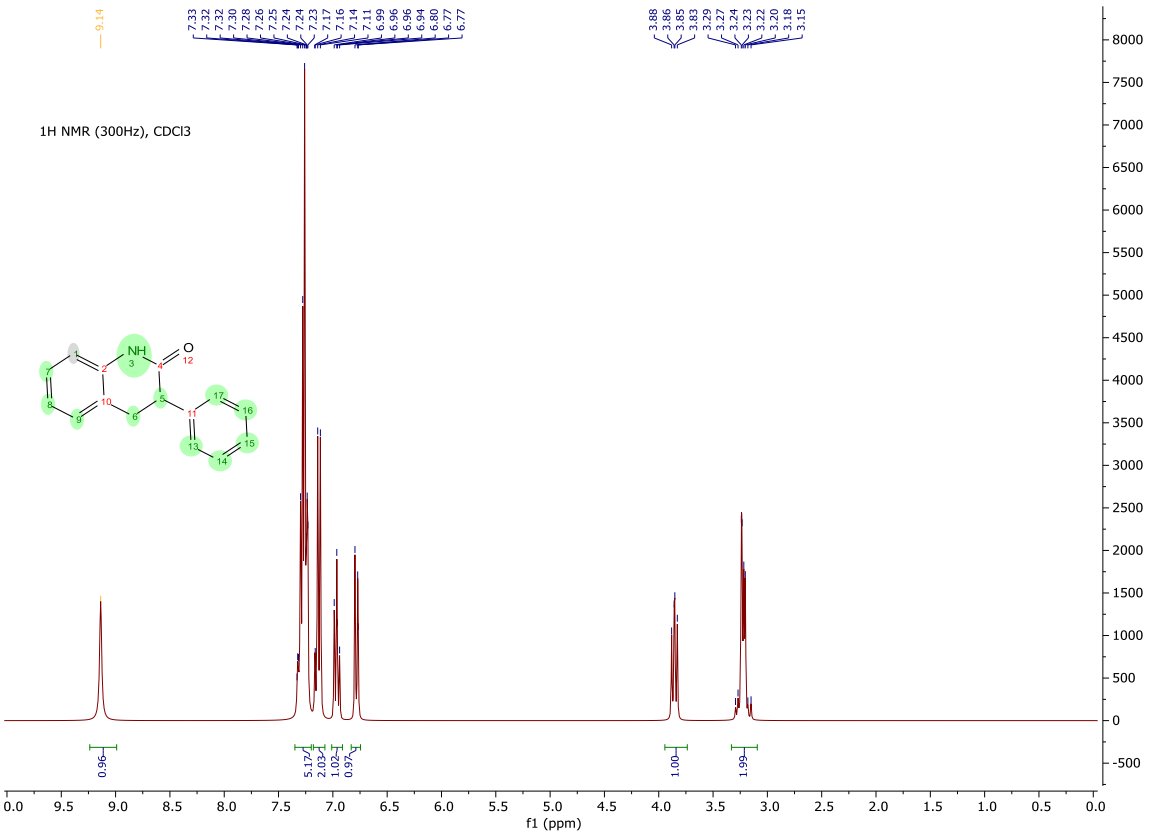

7-(*Tert*-butyl)-3-phenyl-3,4-dihydroquinolin-2(1*H*)-one (Compound 2O)

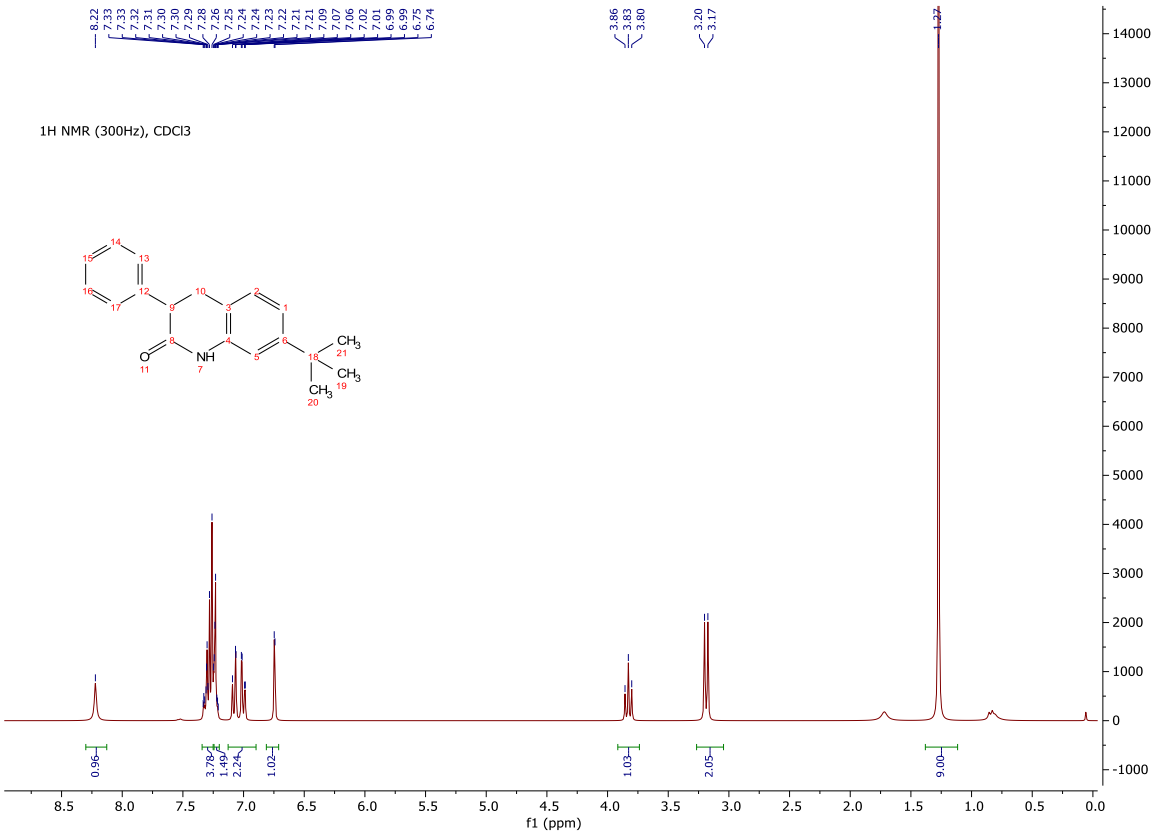

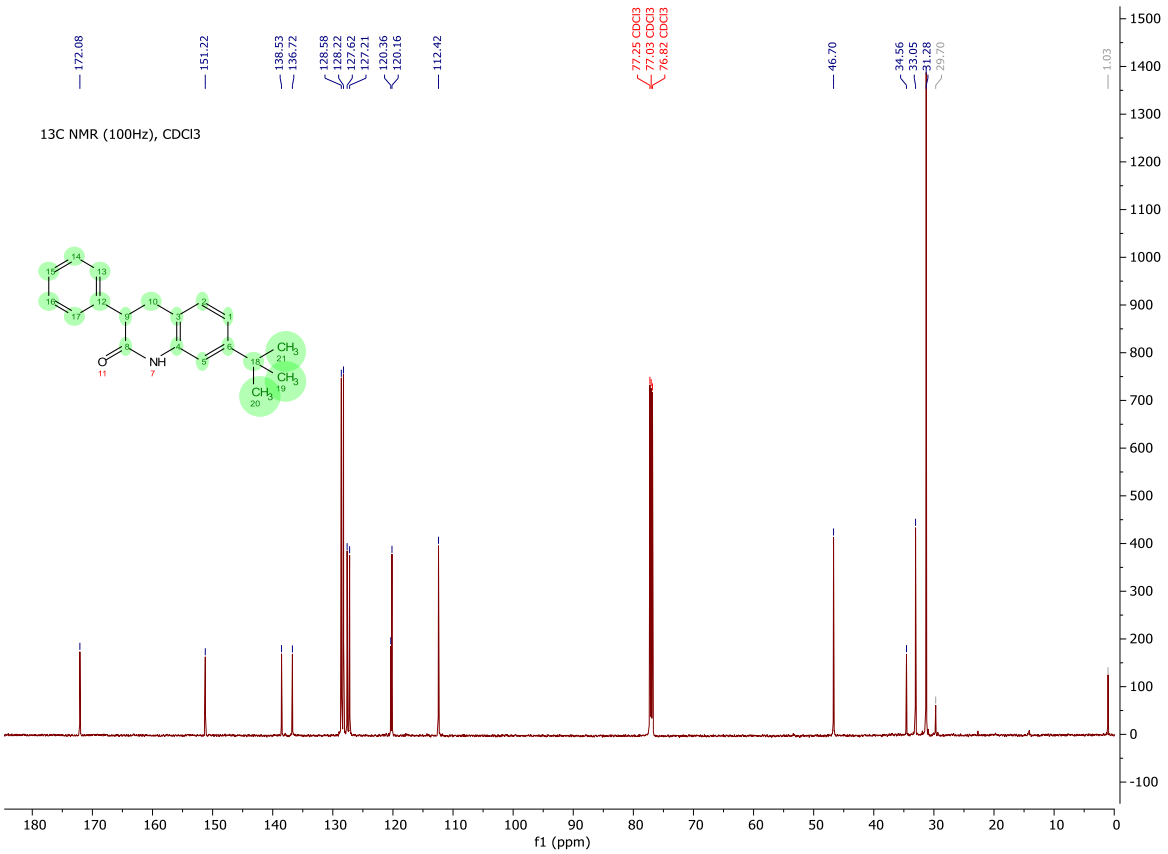

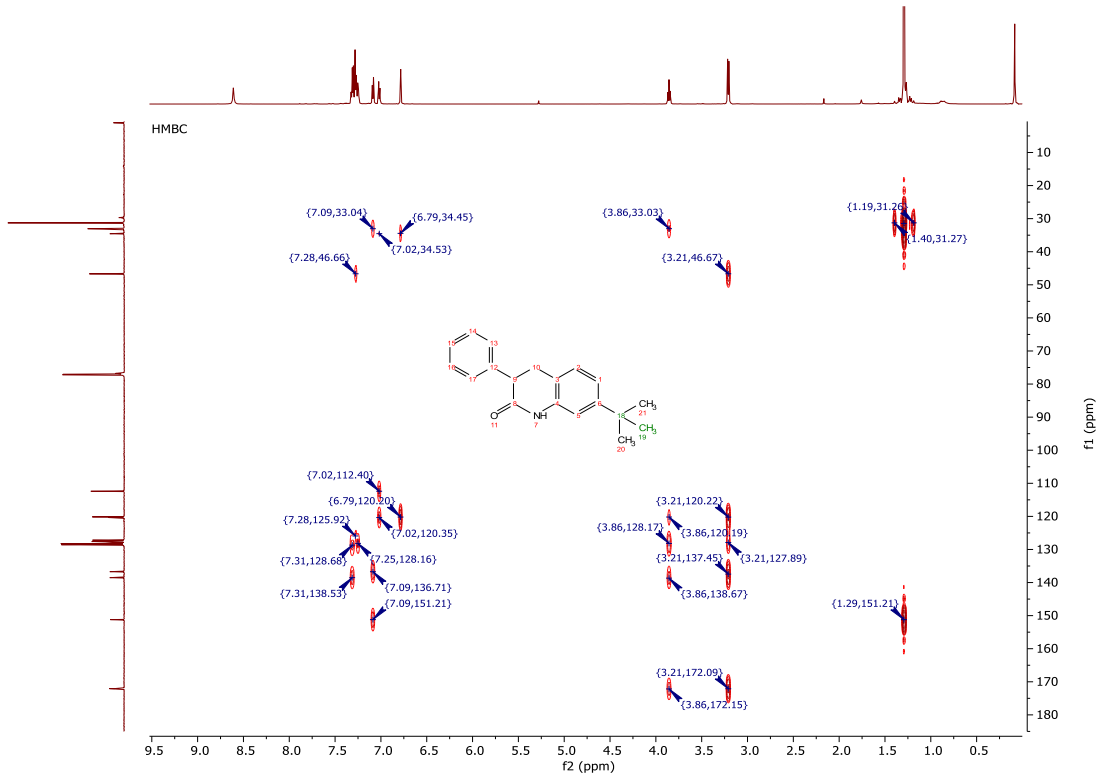

5-(*Tert*-butyl)-3-phenyl-3,4-dihydroquinolin-2(1*H*)-one (Compound 2P)

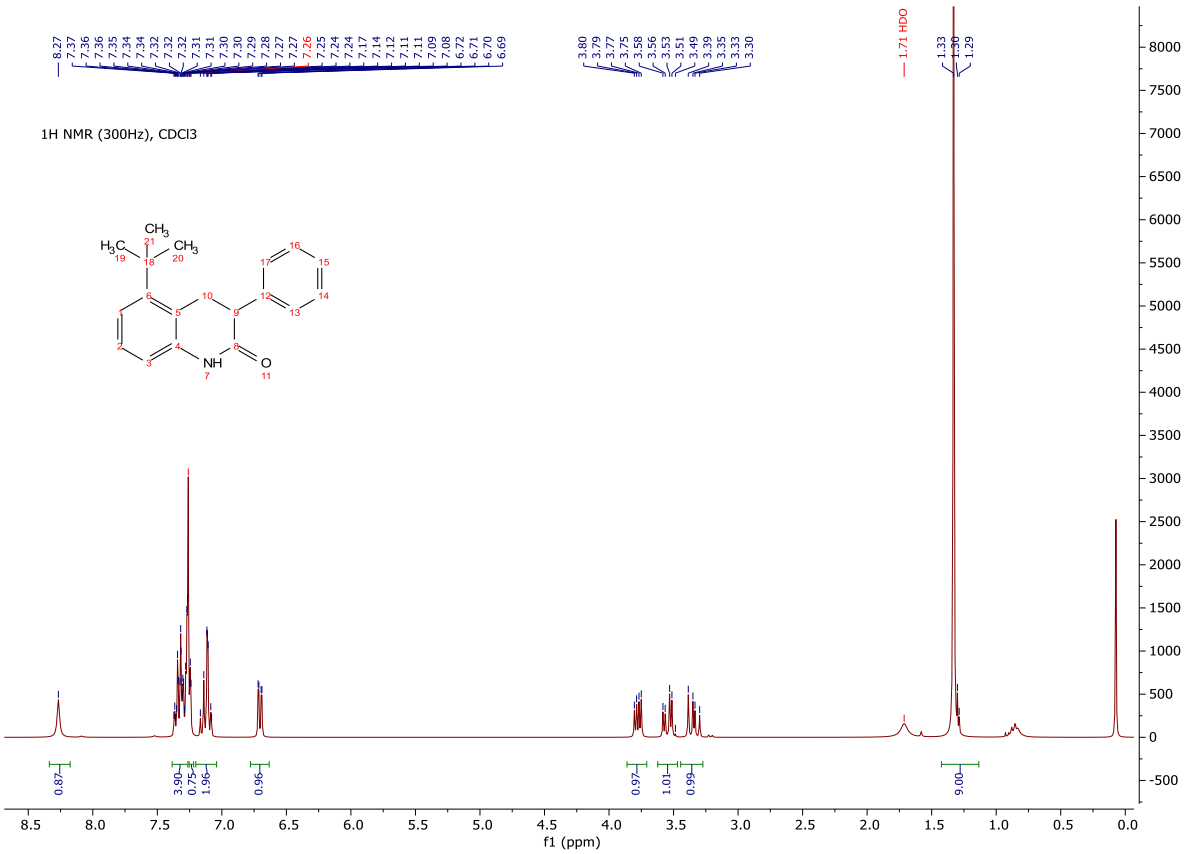
1H NMR (300Hz), CDCl3
f1 (ppm)

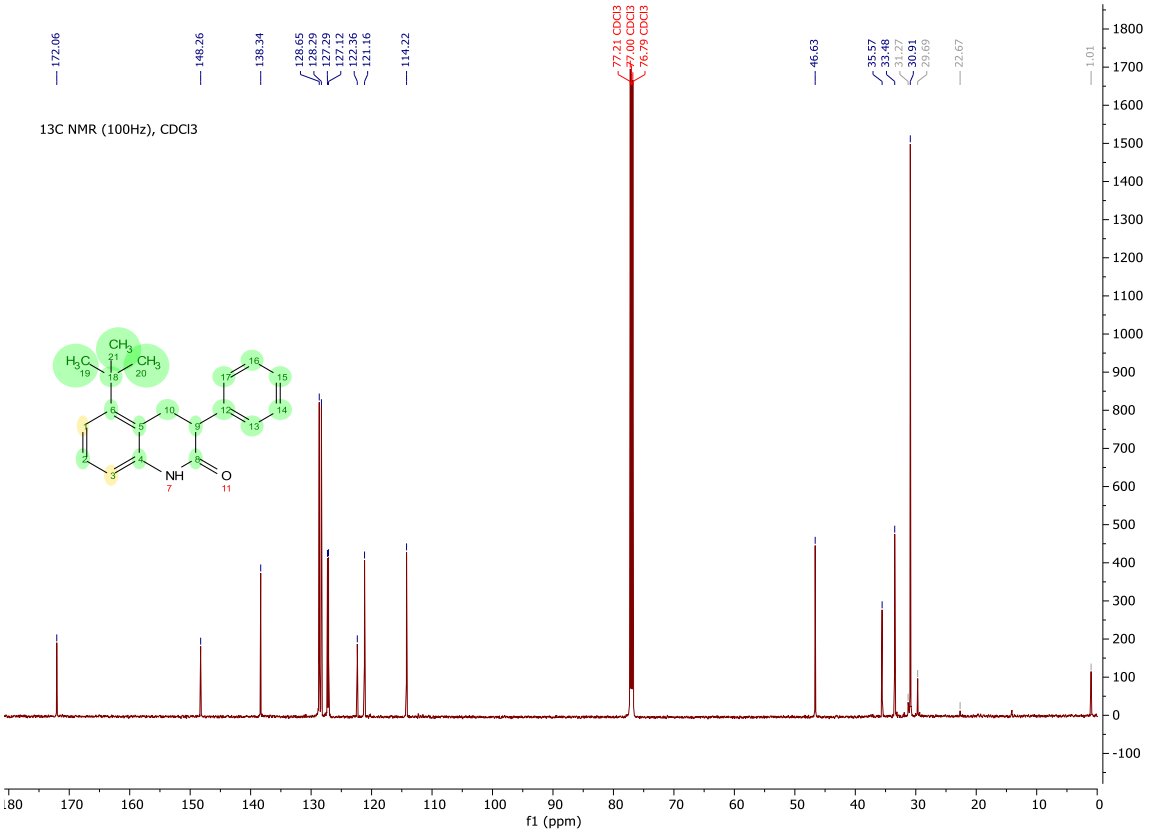
13C NMR (100Hz), CDCl3
f1 (ppm)

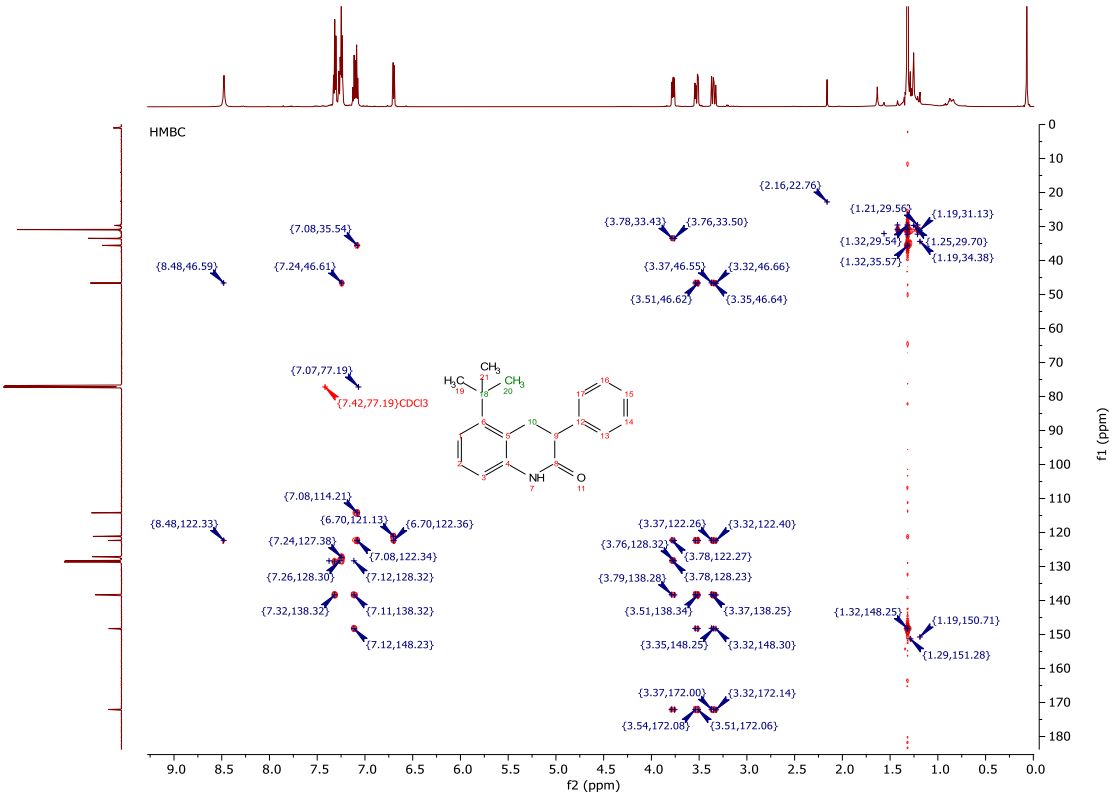

6-Bromo-5,7-difluoro-3-phenyl-3,4-dihydroquinolin-2(1*H*)-one (Compound 2Q)

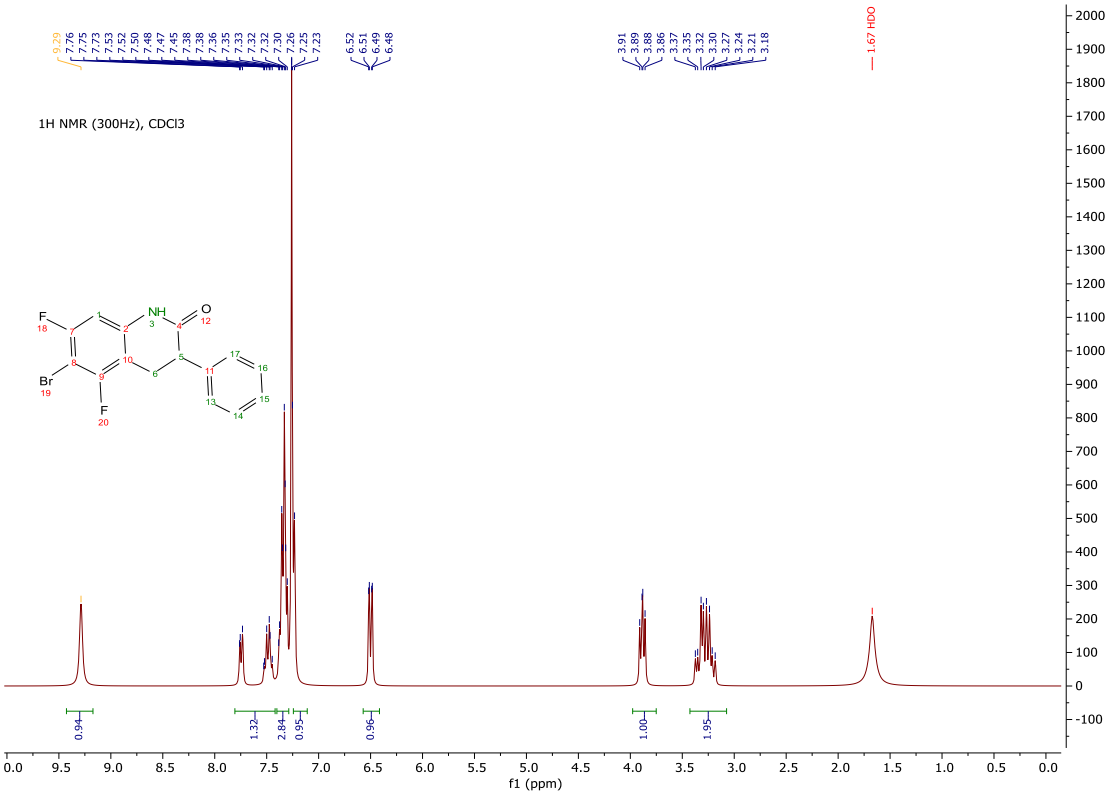

8-Fluoro-6-methyl-3-phenyl-3,4-dihydroquinolin-2(1*H*)-one (Compound 2R)

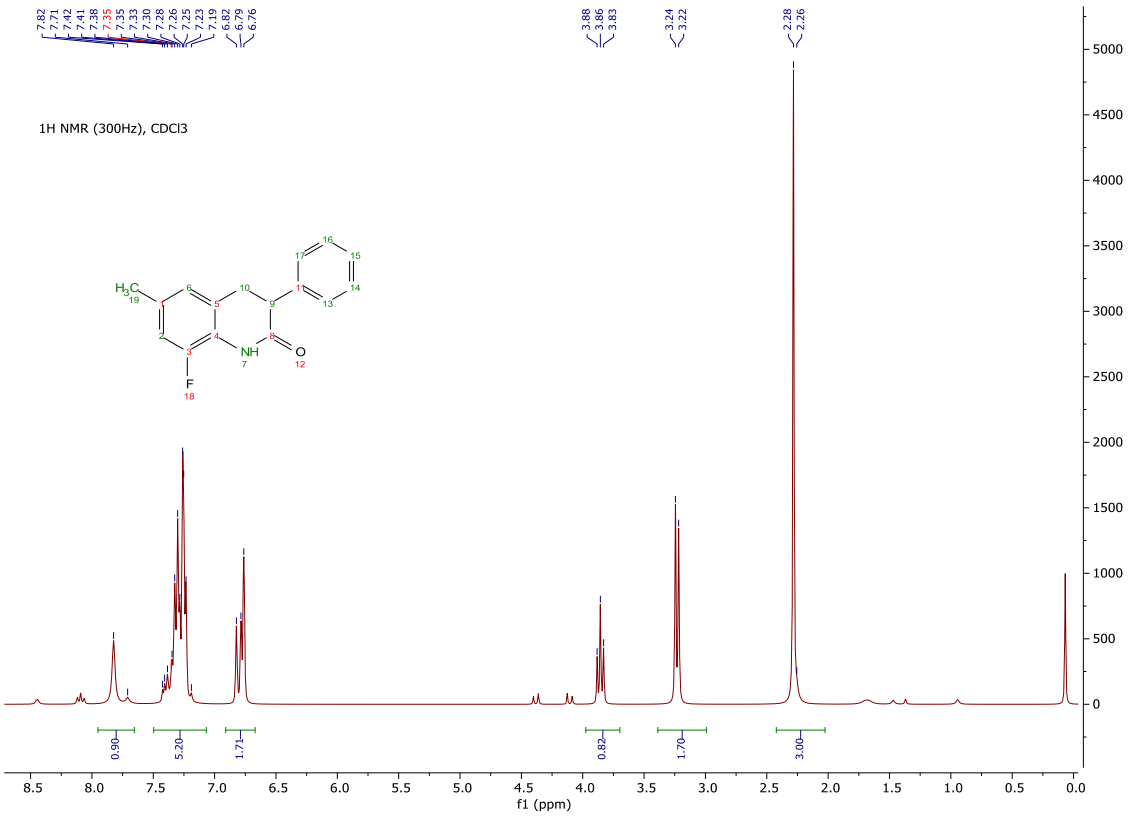

7-Phenyl-7,8-dihydro-[1,3]dioxolo[4,5-g]quinolin-6(5*H*)-one (Compound 2S)

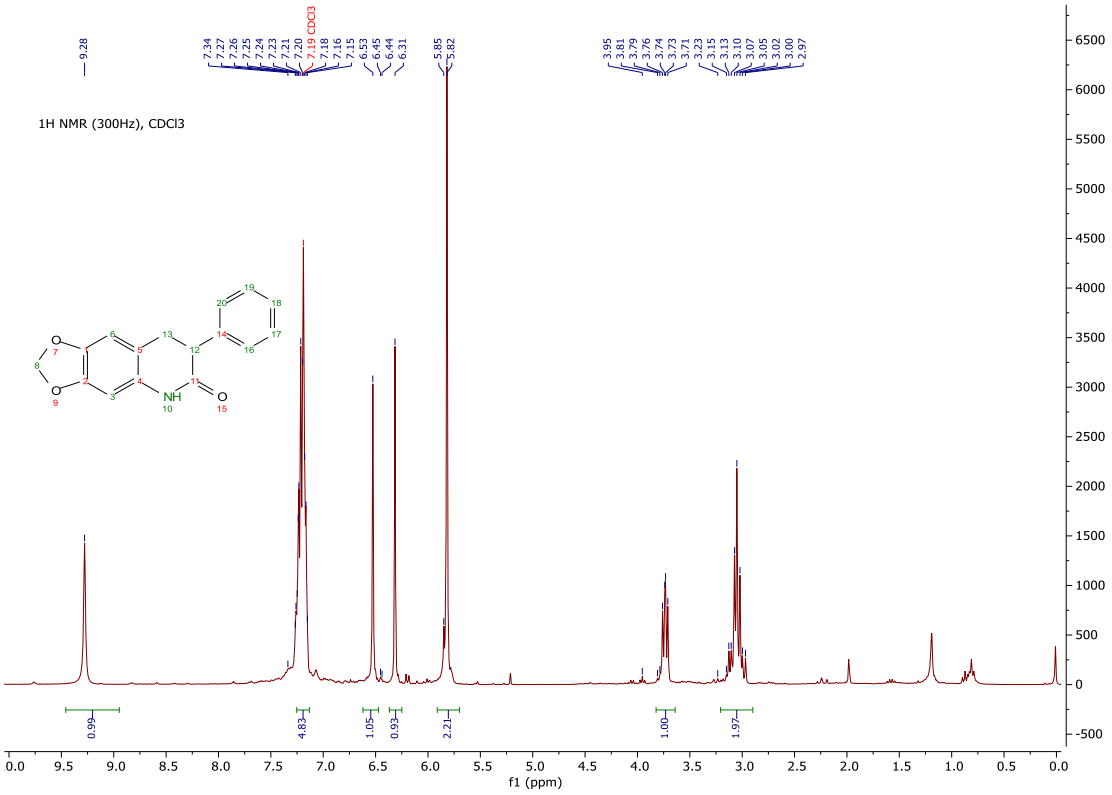

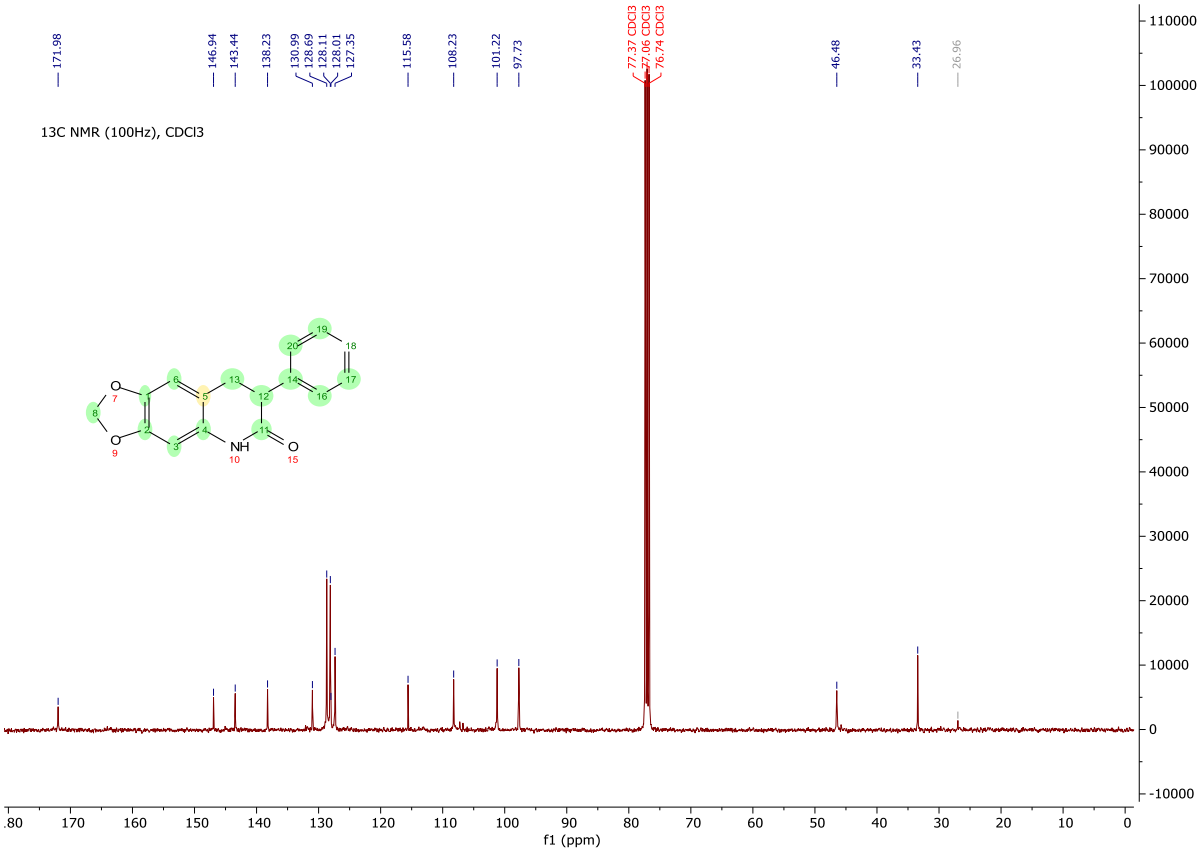

1-Benzoyl-3,4-dihydroquinolin-2(1*H*)-one (Compound 2T)

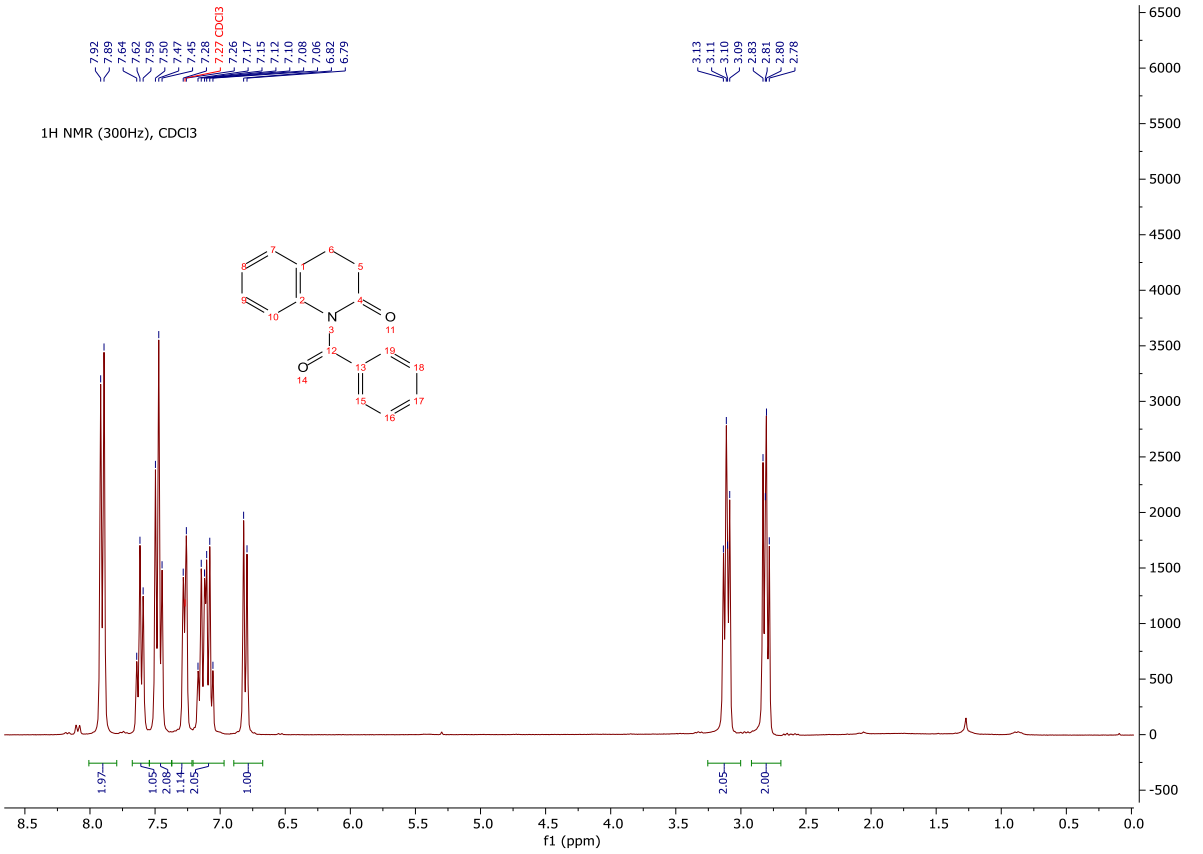

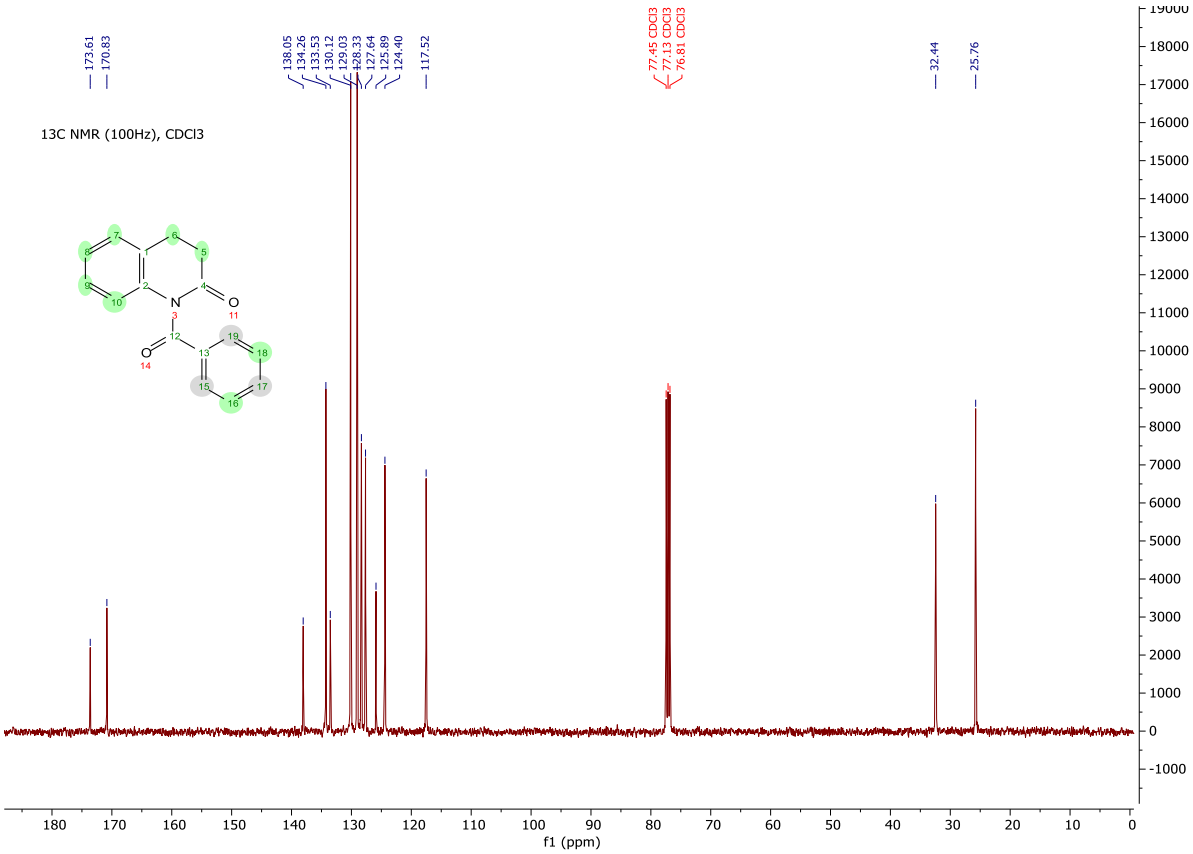

1-Benzoylpiperidin-2-one (Compound 2U)

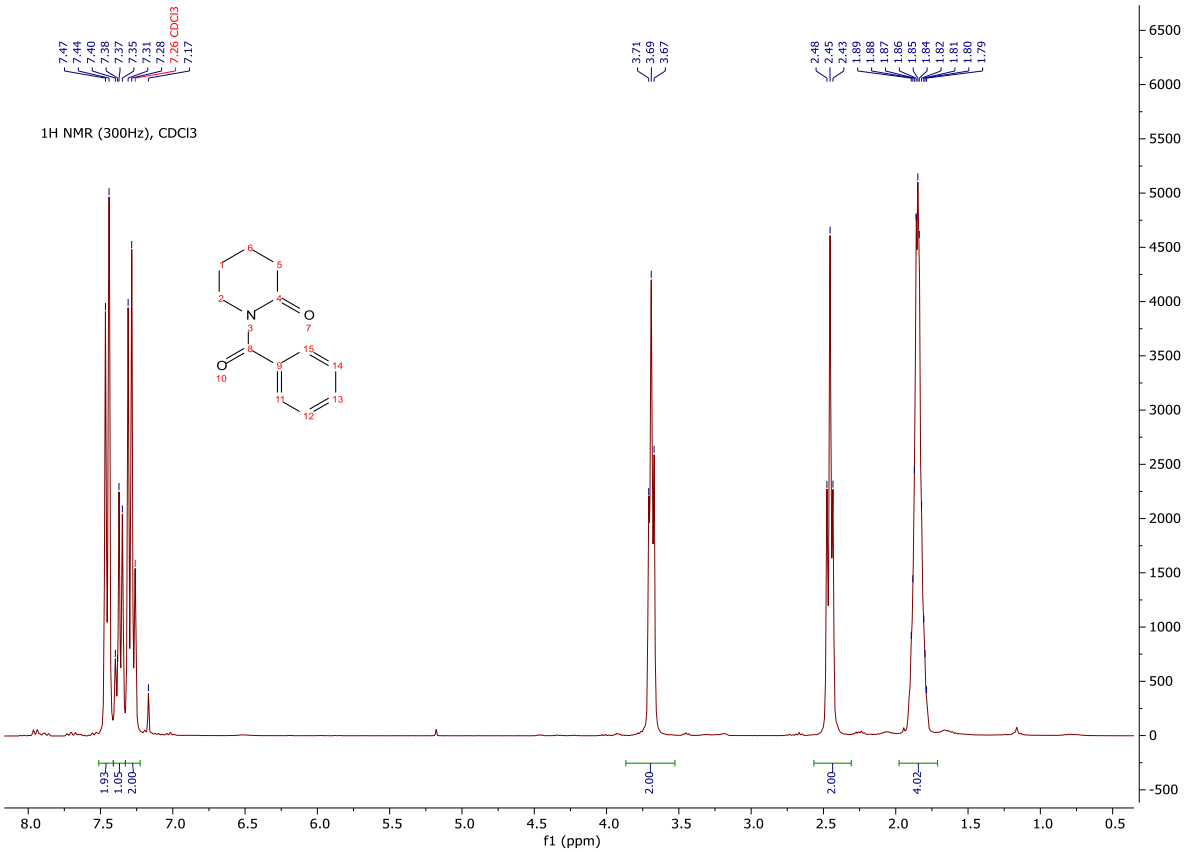

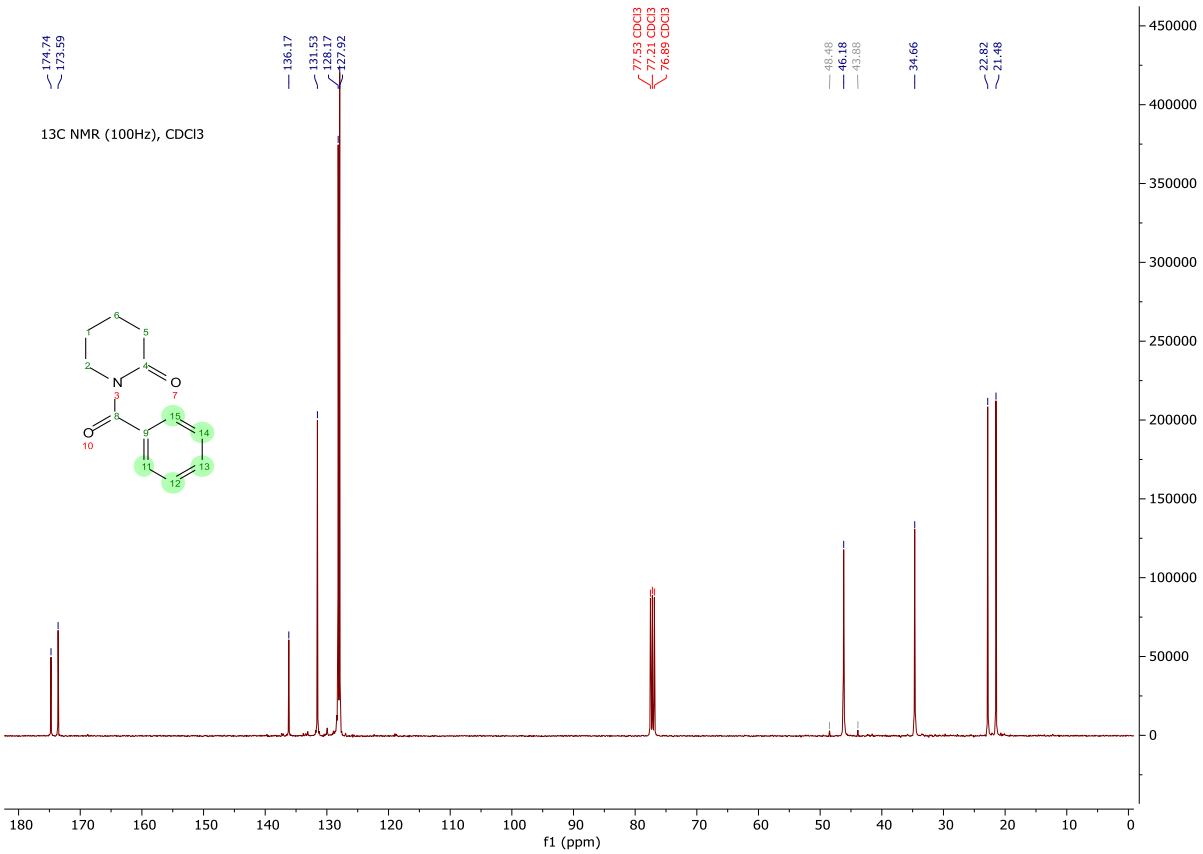

1-Allyl-3,4-dihydroquinolin-2(1*H*)-one (Compound 2V)

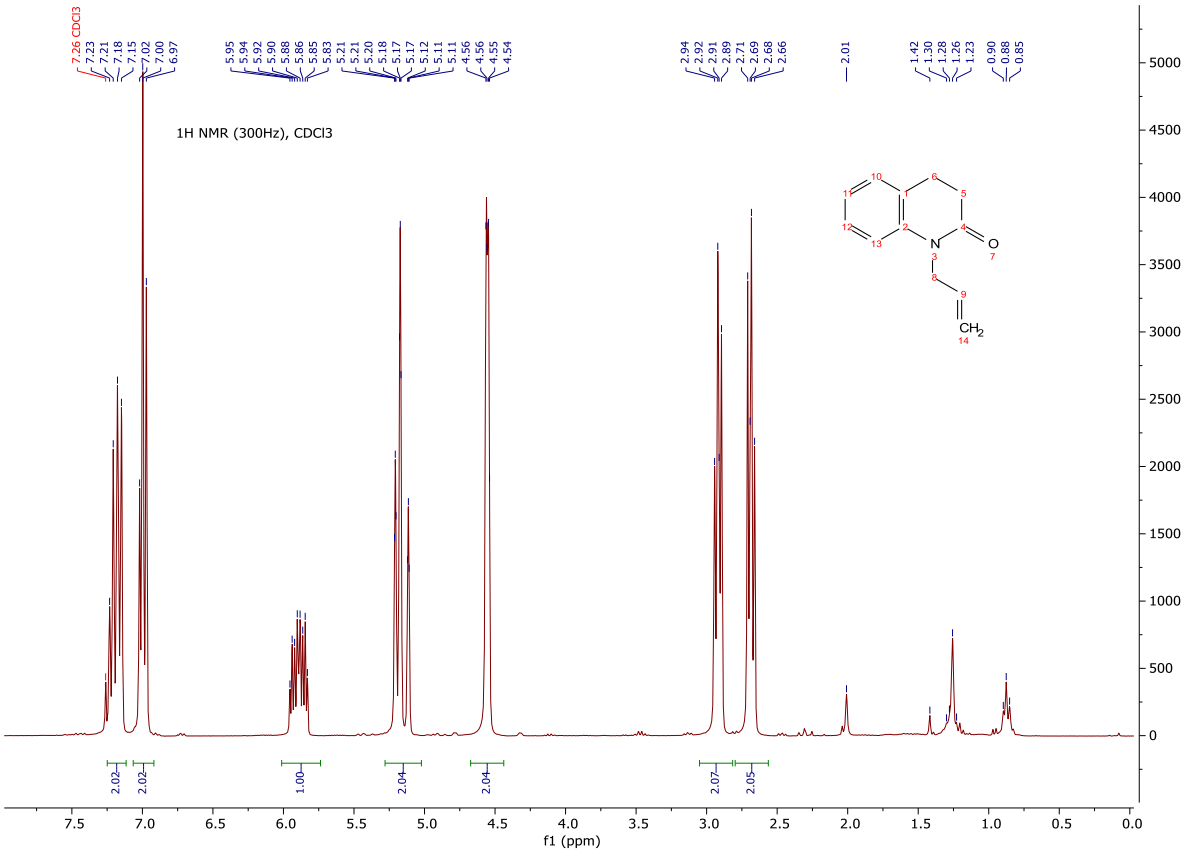

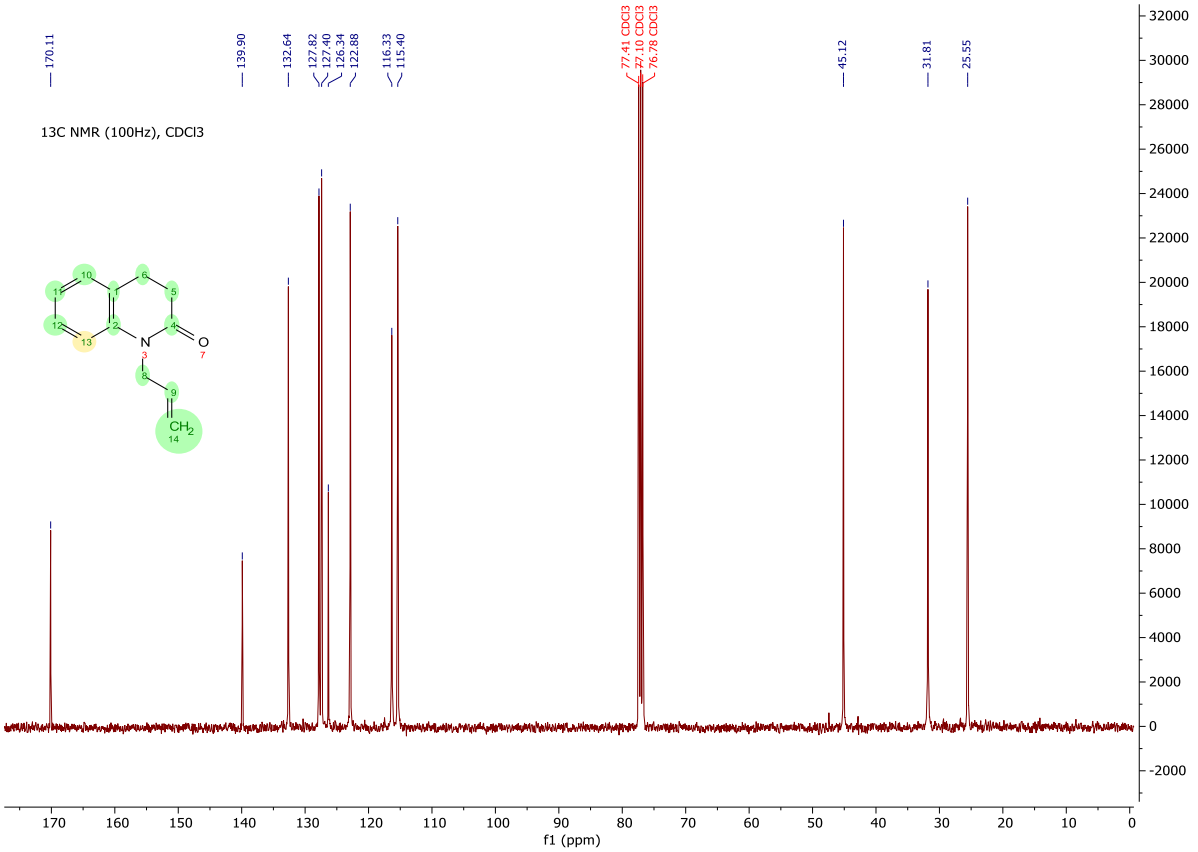

1-Benzyl-3,4-dihydroquinolin-2(1*H*)-one (Compound 2W)

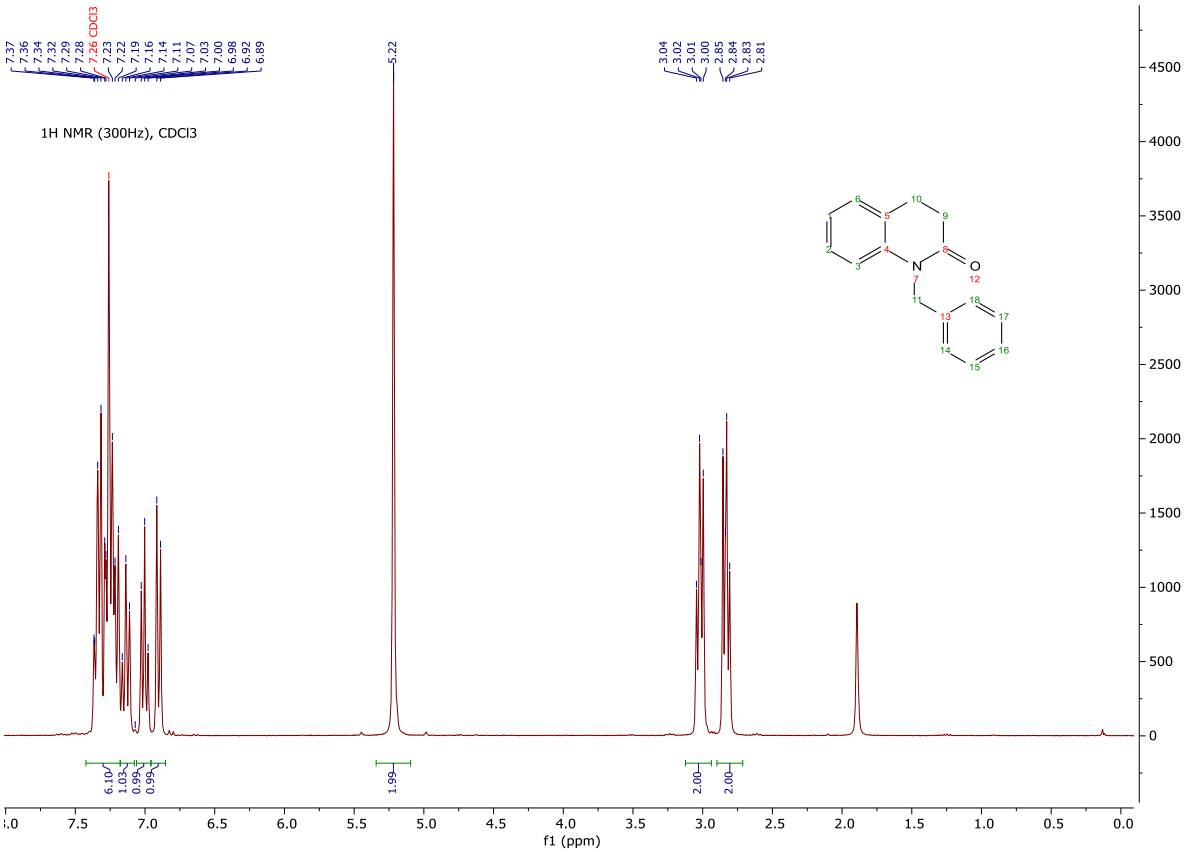

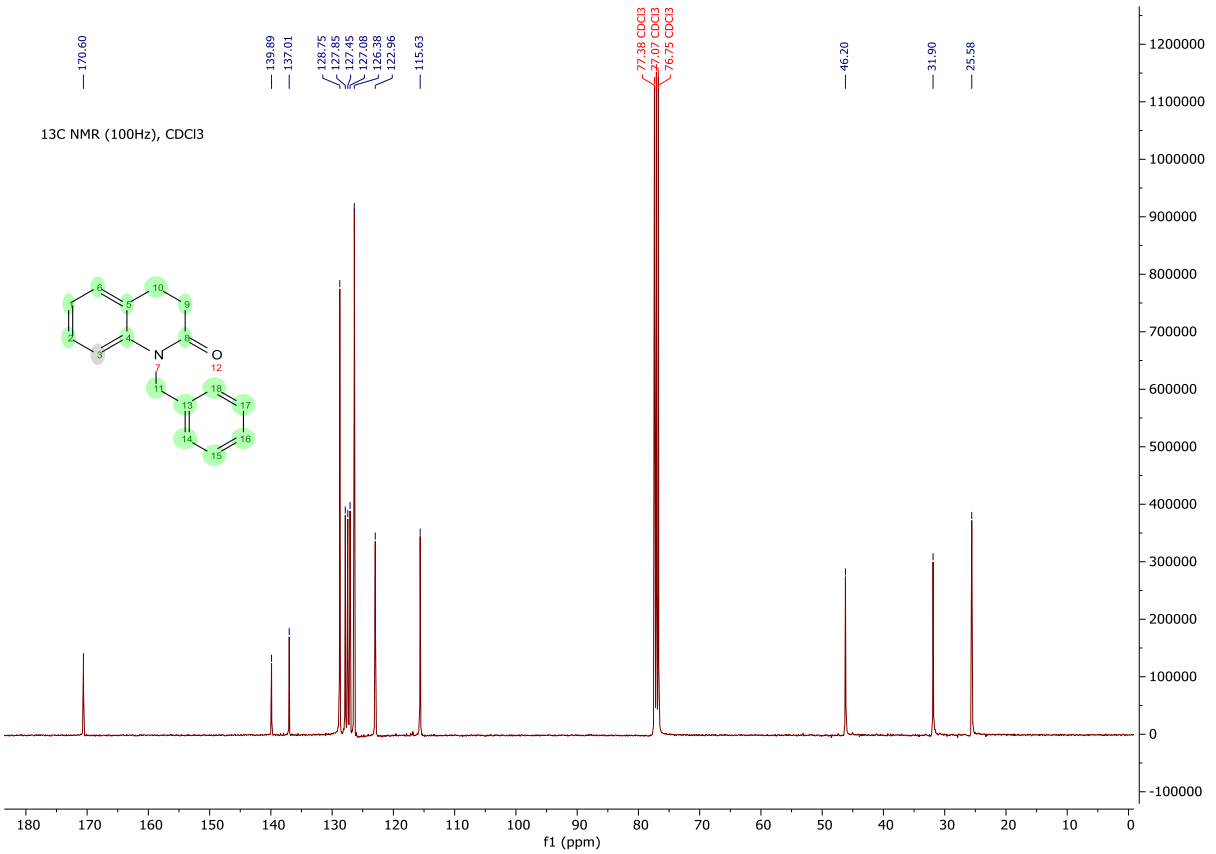

3-(2-Oxo-3,4-dihydroquinolin-1(2H)-yl)propanenitrile (Compound 2X)

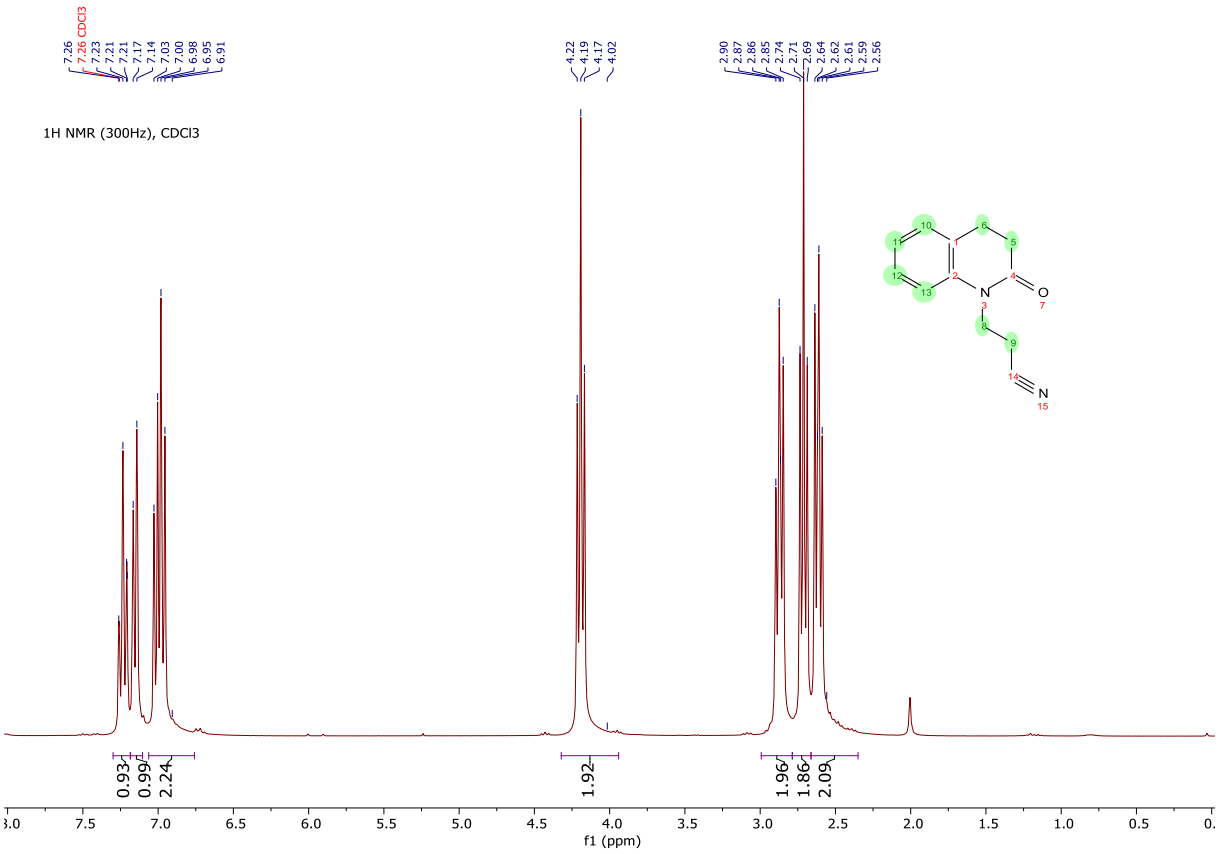

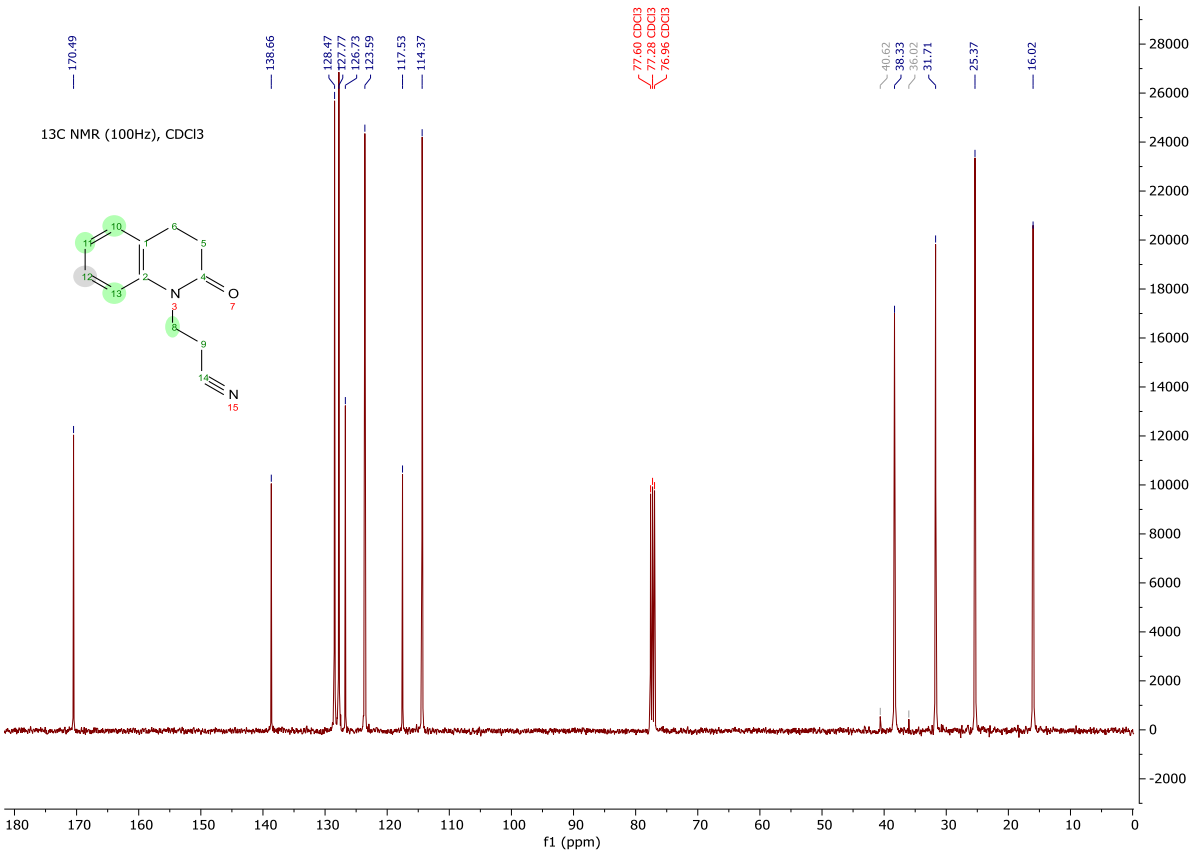

1-Benzyl-7-methoxy-3,4-dihydroquinolin-2(1*H*)-one (Compound 2Y)

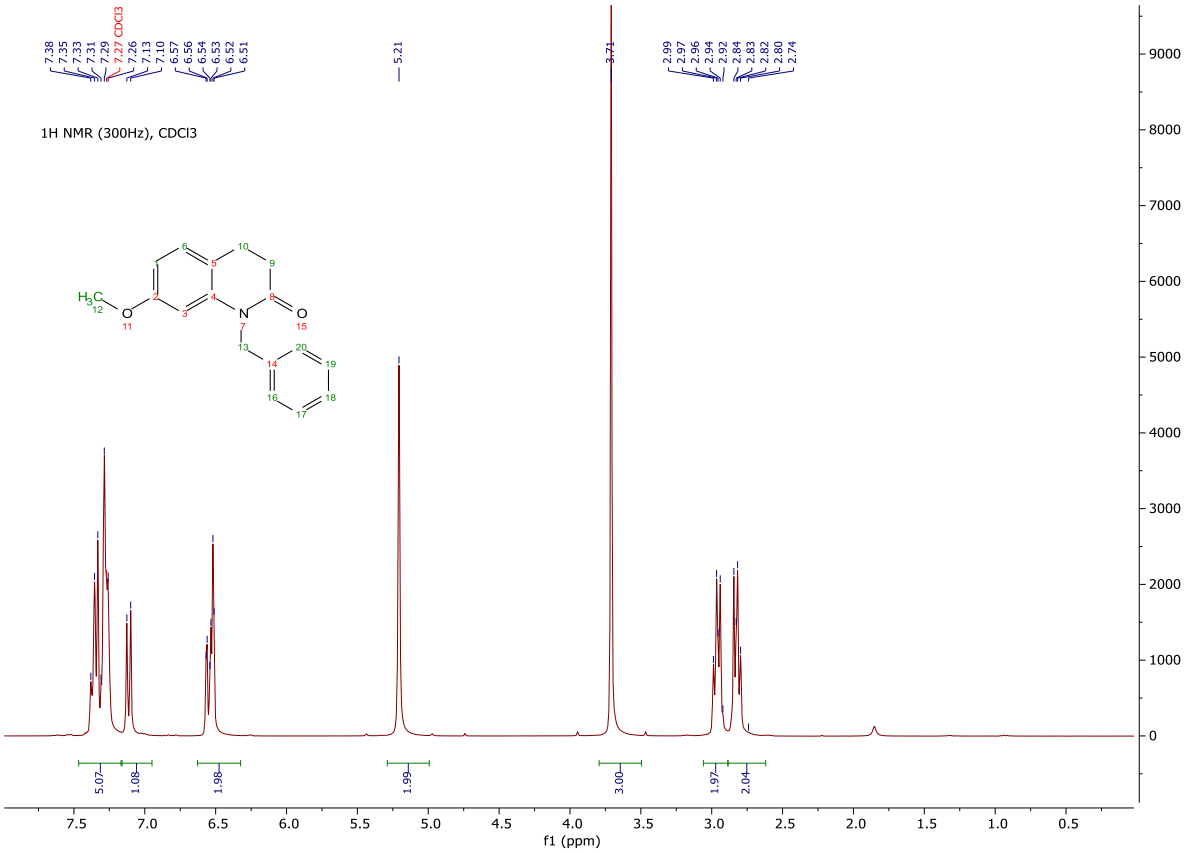

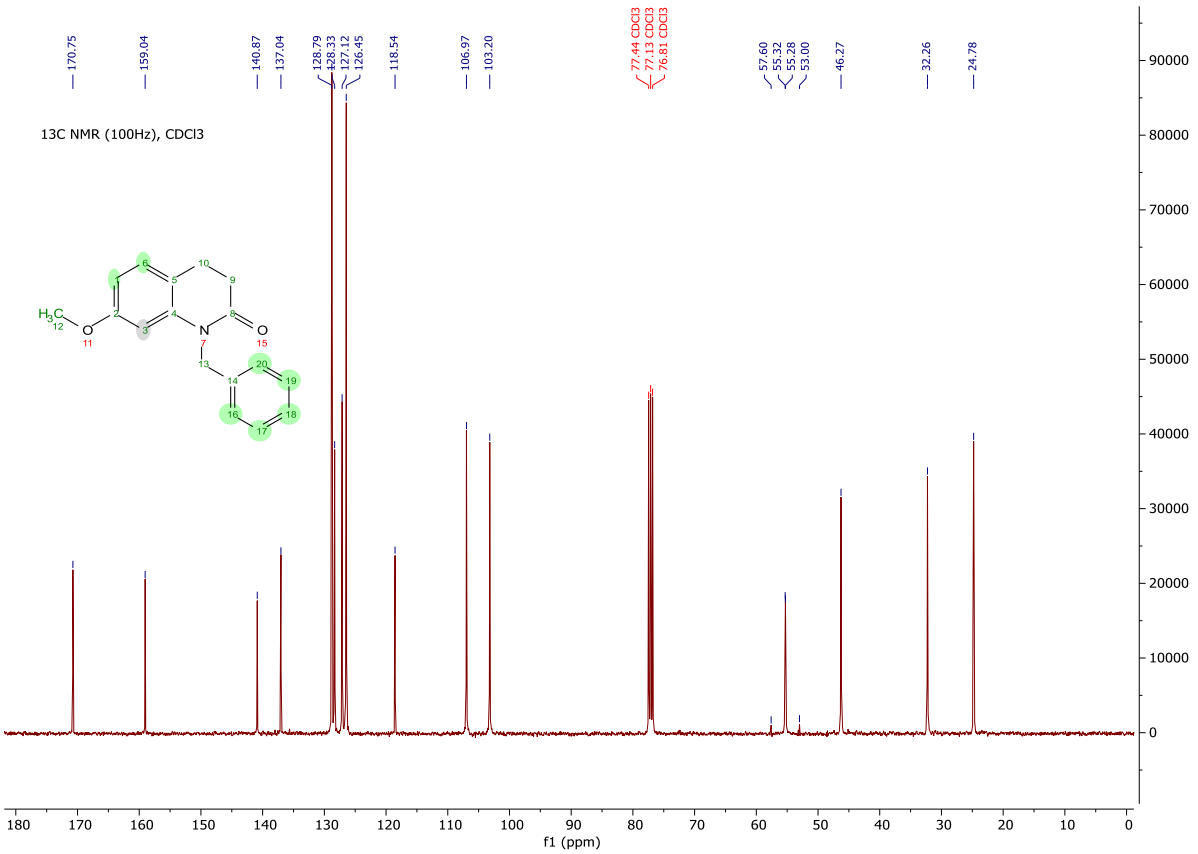

Tert-butyl 2-oxo-3,4-dihydroquinoline-1(2*H*)-carboxylate (Compound 2Z)

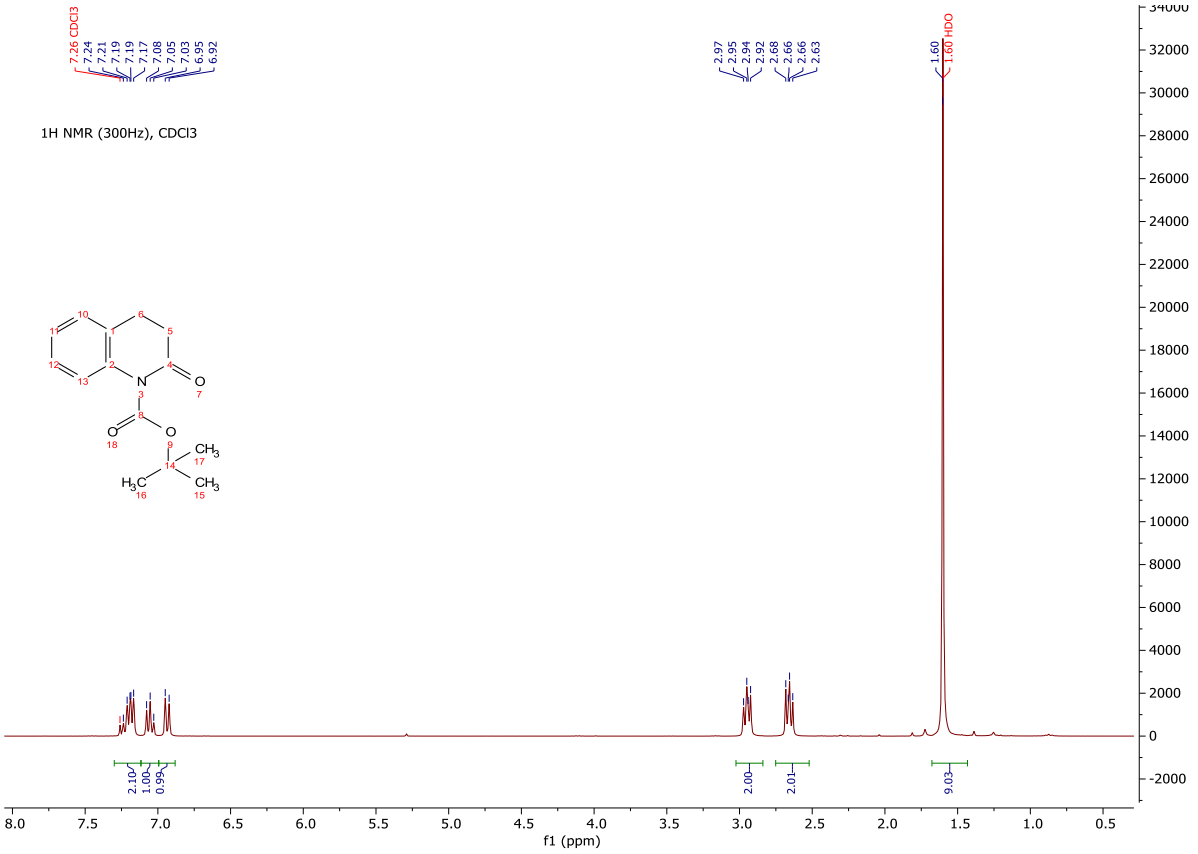

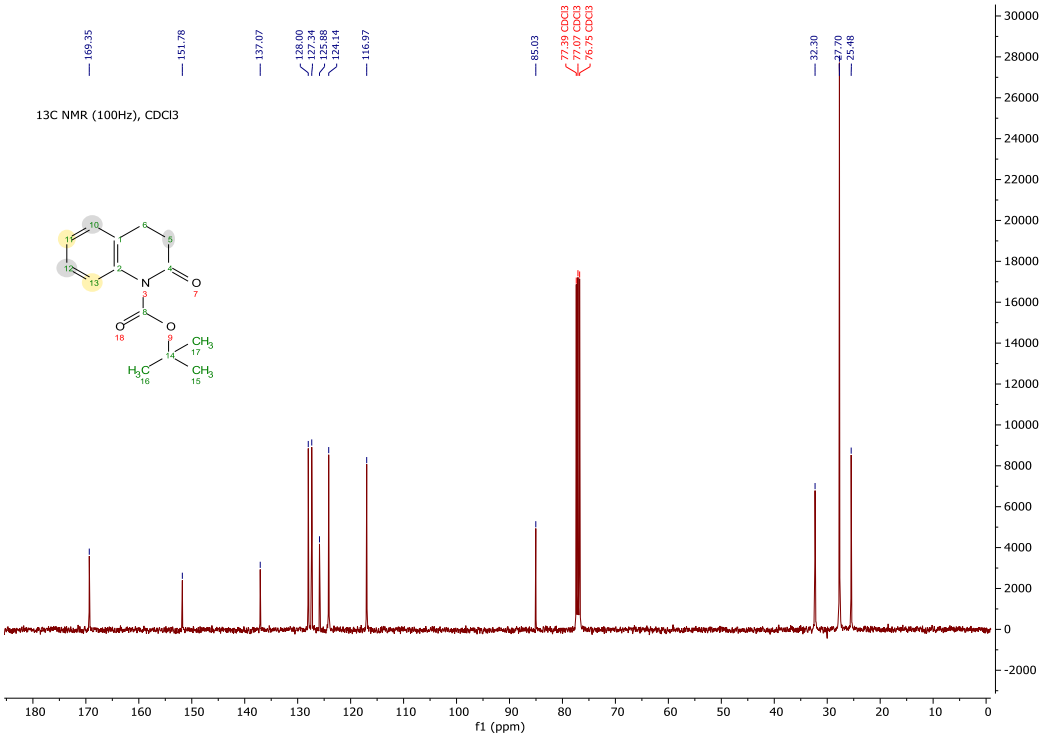

3-((((9H-fluoren-9-yl) methoxy) carbonyl) amino)-3-phenylpropanoic acid (Compound 3A)

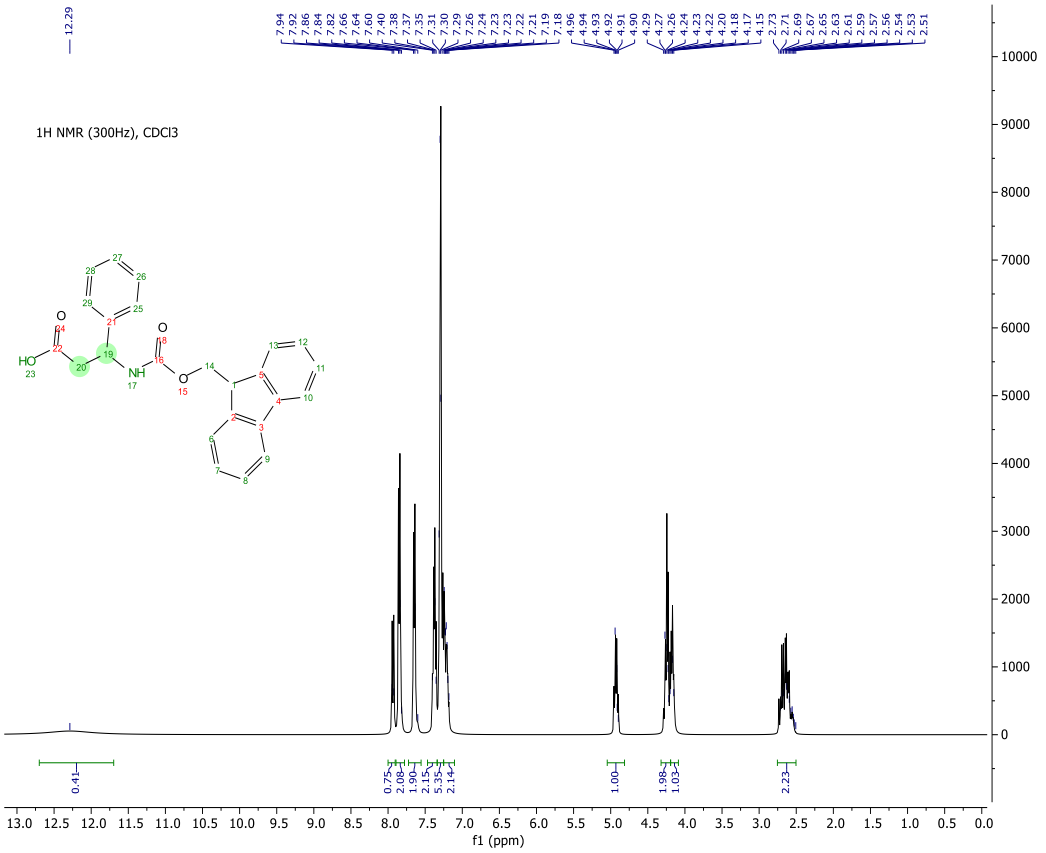

Ethyl 1-(3-((((9H-fluoren-9-yl) methoxy) carbonyl) amino)-3-phenylpropanoyl)-2-oxocyclohexanecarboxylate (Compound 3B)

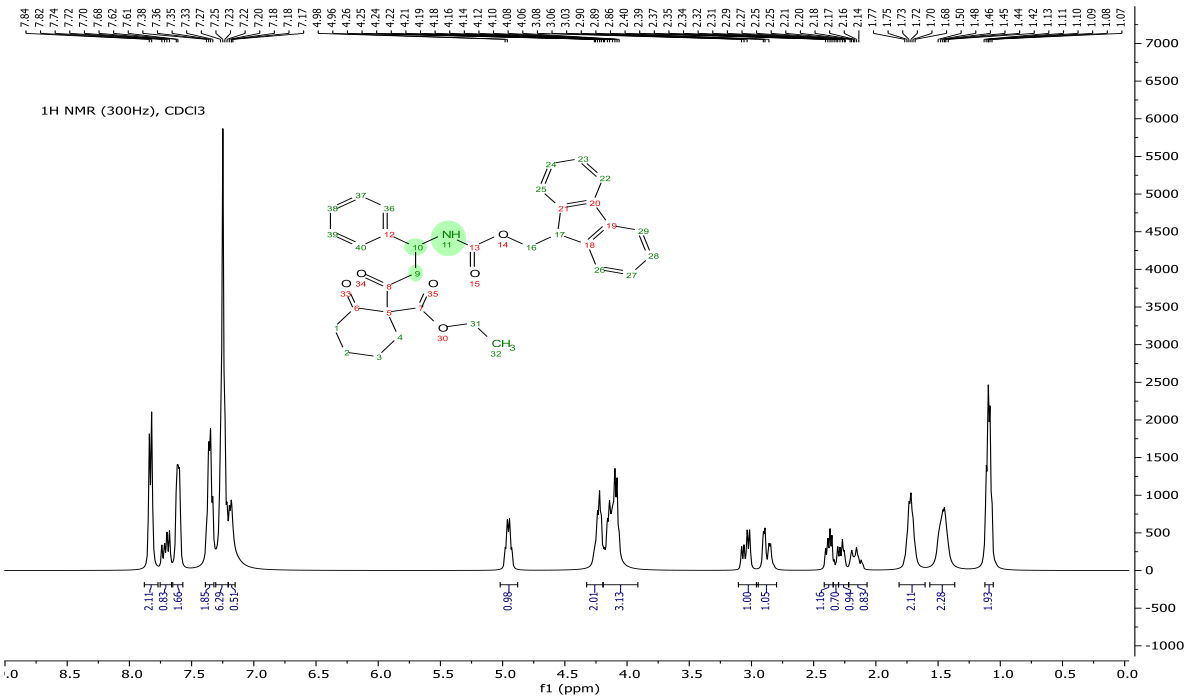
1H NMR (300Hz), CDCl3
f1 (ppm)

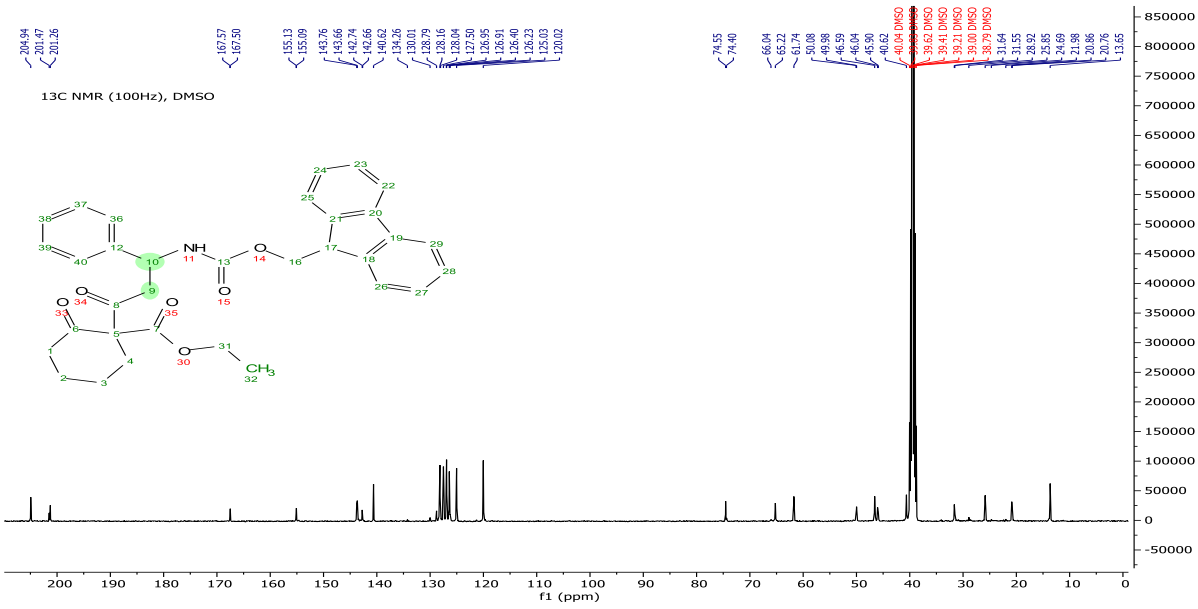
13C NMR (100Hz), DMSO
f1 (ppm)

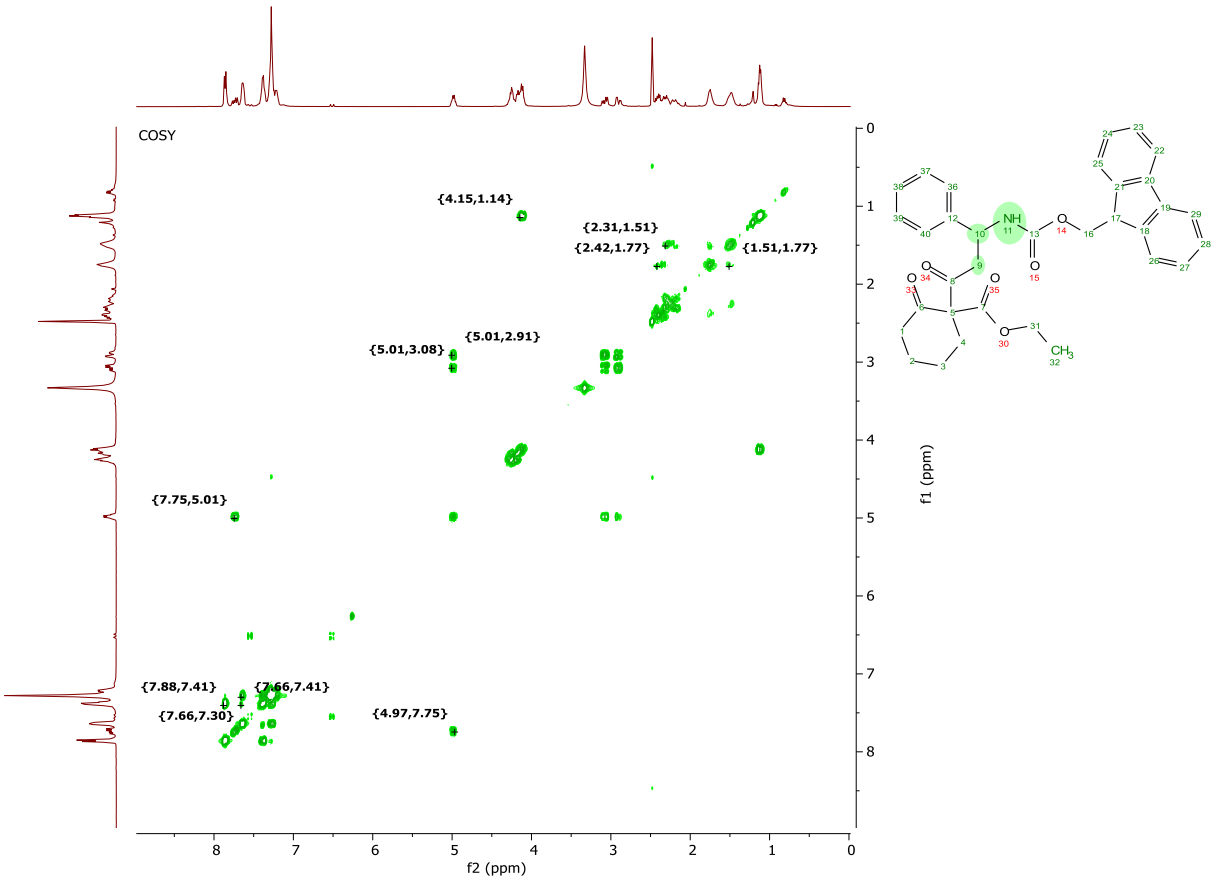
COSY
{4.15,1.14}
{2.31,1.51}
{2.42,1.77}
{1.51,1.77}
{5.01,3.08}
{5.01,2.91}
{7.75,5.01}
{7.88,7.41}
{7.66,7.41}
{7.66,7.30}
{4.97,7.75}
f2 (ppm)
f1 (ppm)

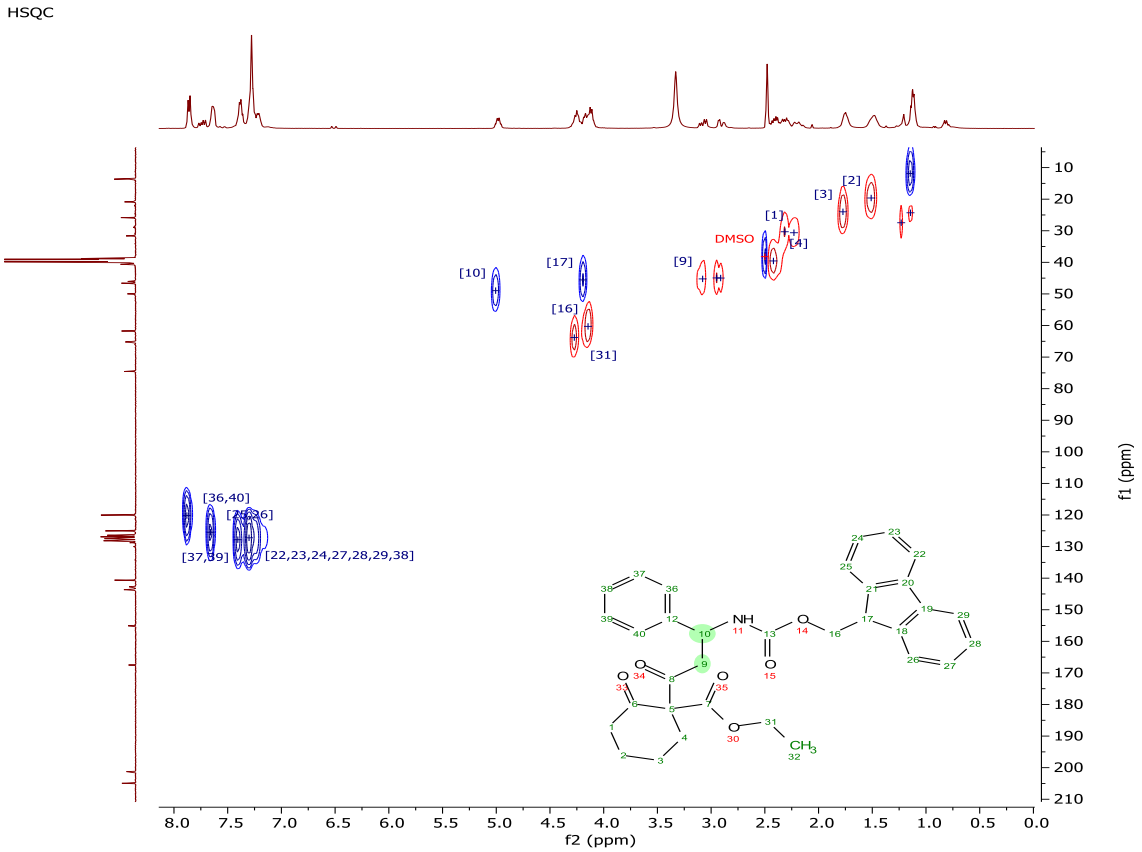
HSQC
DMSO
[1]
[2]
[3]
[4]
[9]
[10]
[16]
[17]
[31]
[36,40]
[37,39]
[22,23,24,27,28,29,38]
f2 (ppm)
f1 (ppm)

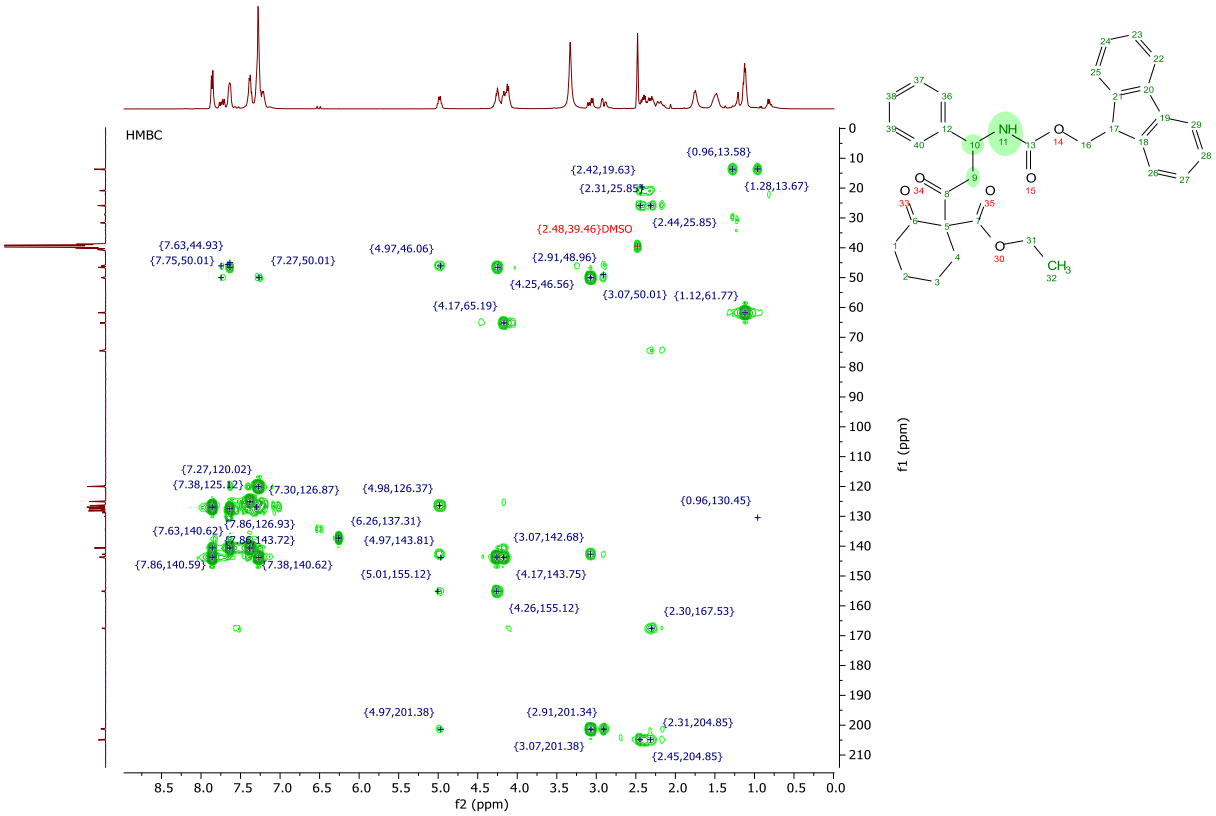

Ethyl 4,10-dioxo-2-phenylazecane-5-carboxylate/(Z)-ethyl 4-hydroxy-10-oxo-2-phenyl-1,2,3,6,7,8,9,10-octahydroazecine-5-carboxylate (Compound 3C)

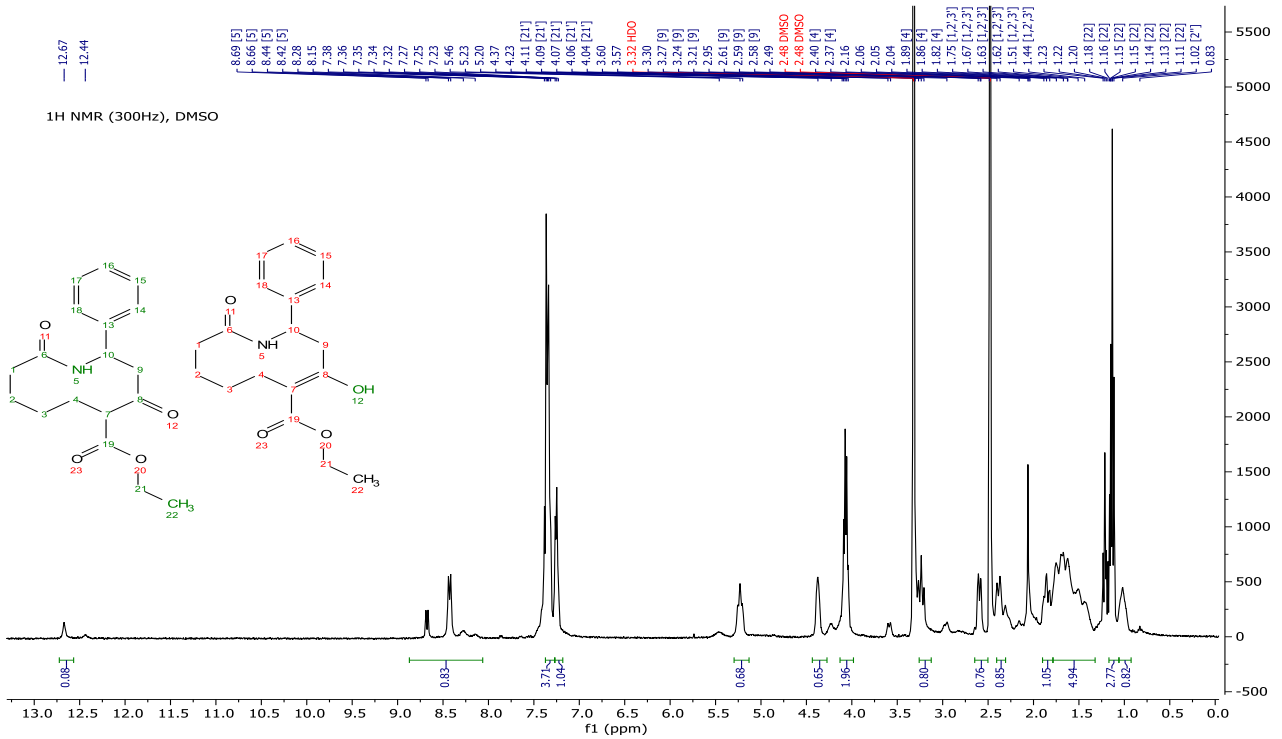

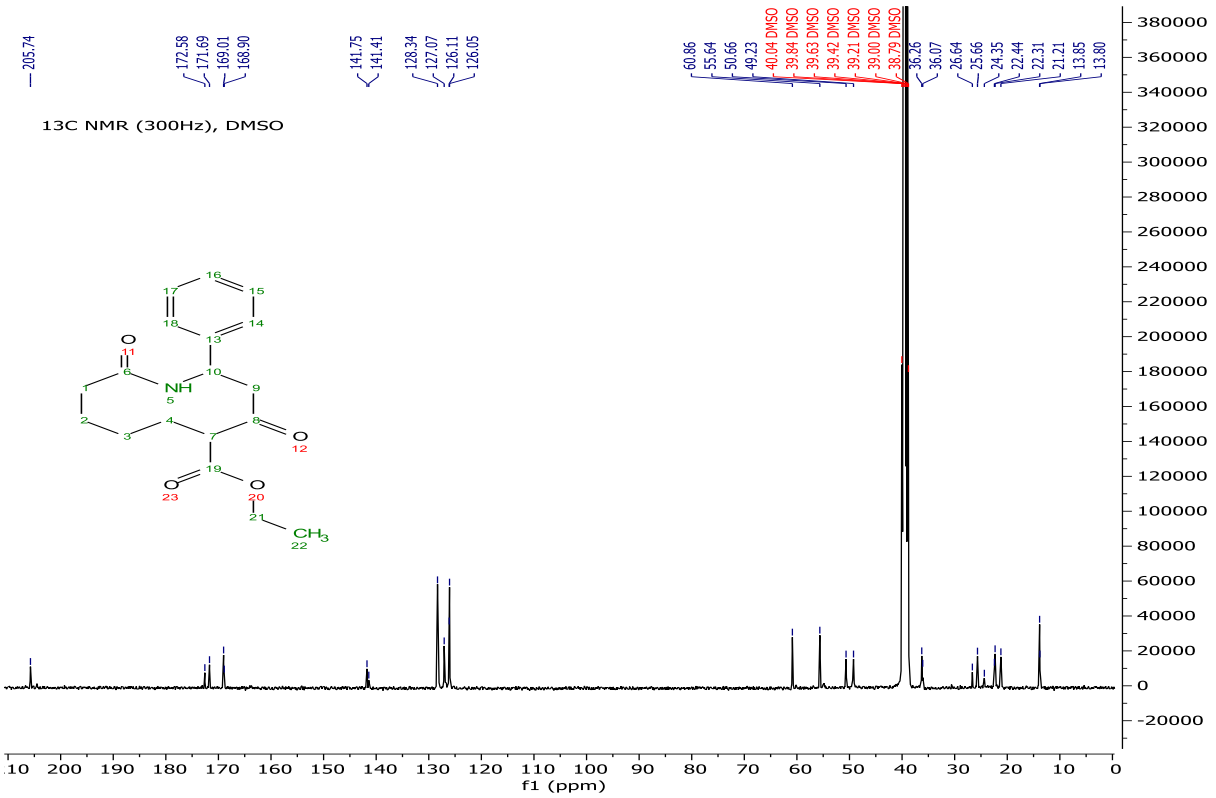
13C NMR (300Hz), DMSO
205.74
172.58
171.69
169.01
168.90
141.75
141.41
128.34
127.07
126.11
126.05
60.86
55.64
50.66
49.23
40.04 DMSO
39.84 DMSO
39.63 DMSO
39.42 DMSO
39.21 DMSO
39.00 DMSO
38.79 DMSO
36.26
36.07
26.64
25.66
24.35
22.44
22.31
21.21
13.85
13.80
f1 (ppm)

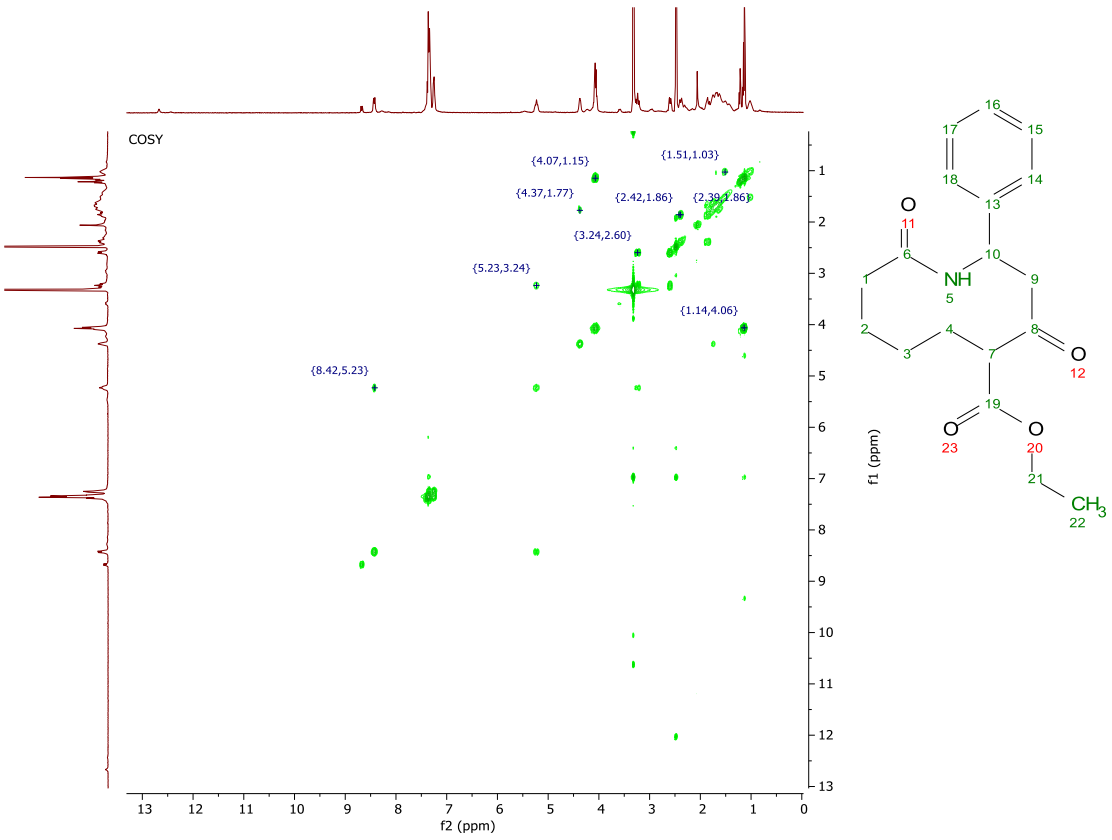
COSY
{4.07,1.15}
{1.51,1.03}
{4.37,1.77}
{2.42,1.86}
{2.39,2.86}
{3.24,2.60}
{5.23,3.24}
{1.14,4.06}
{8.42,5.23}
f2 (ppm)
f1 (ppm)

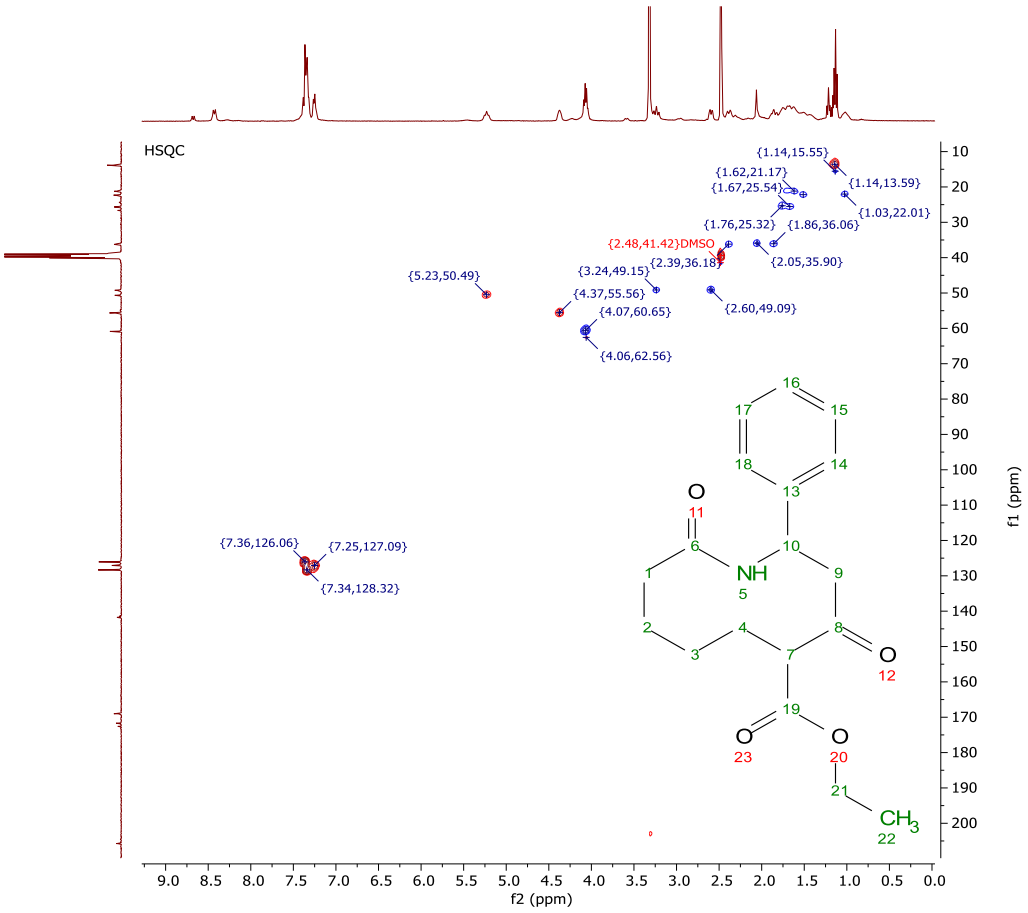

Ethyl 4,9-dioxo-2-phenylazonane-5-carboxylate/(Z)-ethyl 4-hydroxy-9-oxo-2-phenyl-2,3,6,7,8,9-hexahydro-1*H*-azonine-5-carboxylate (Compound 3D)

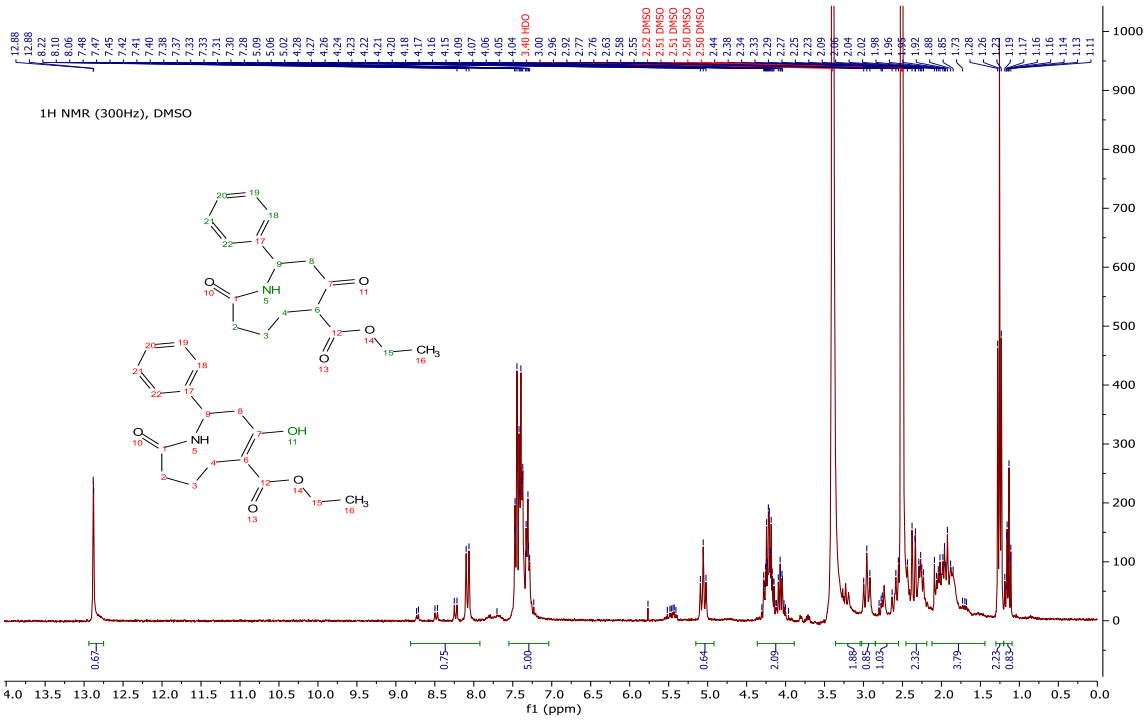

4-Phenyl-1,5-diazecane-2,6-dione (Compound 3E)

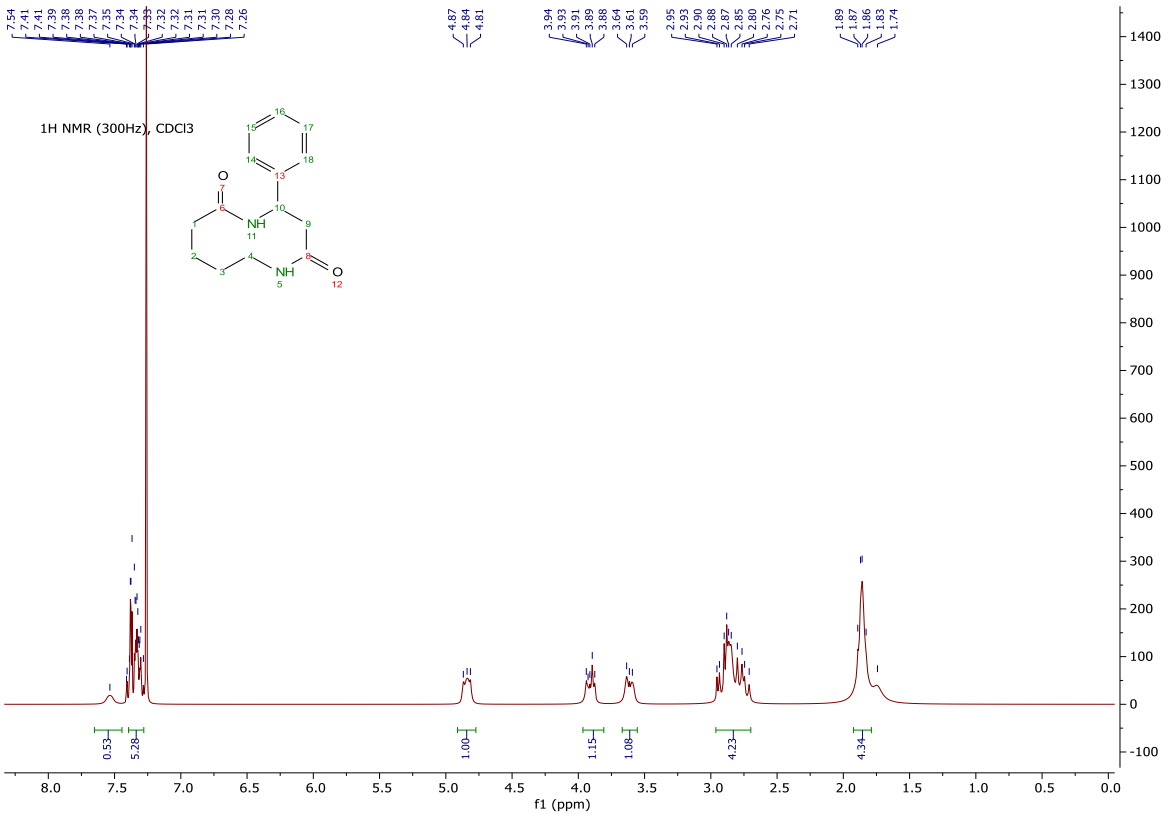

1-Acryloylpiperidin-2-one (Compound 3F)

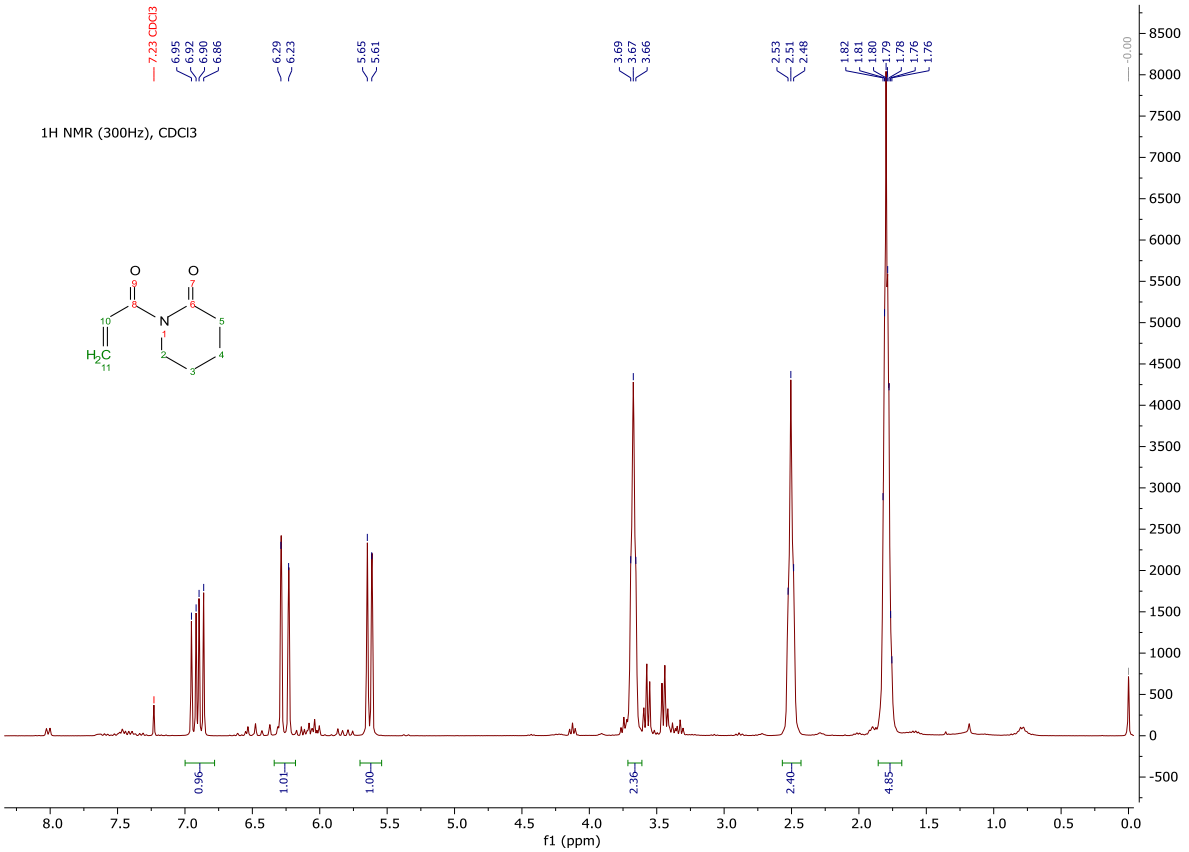

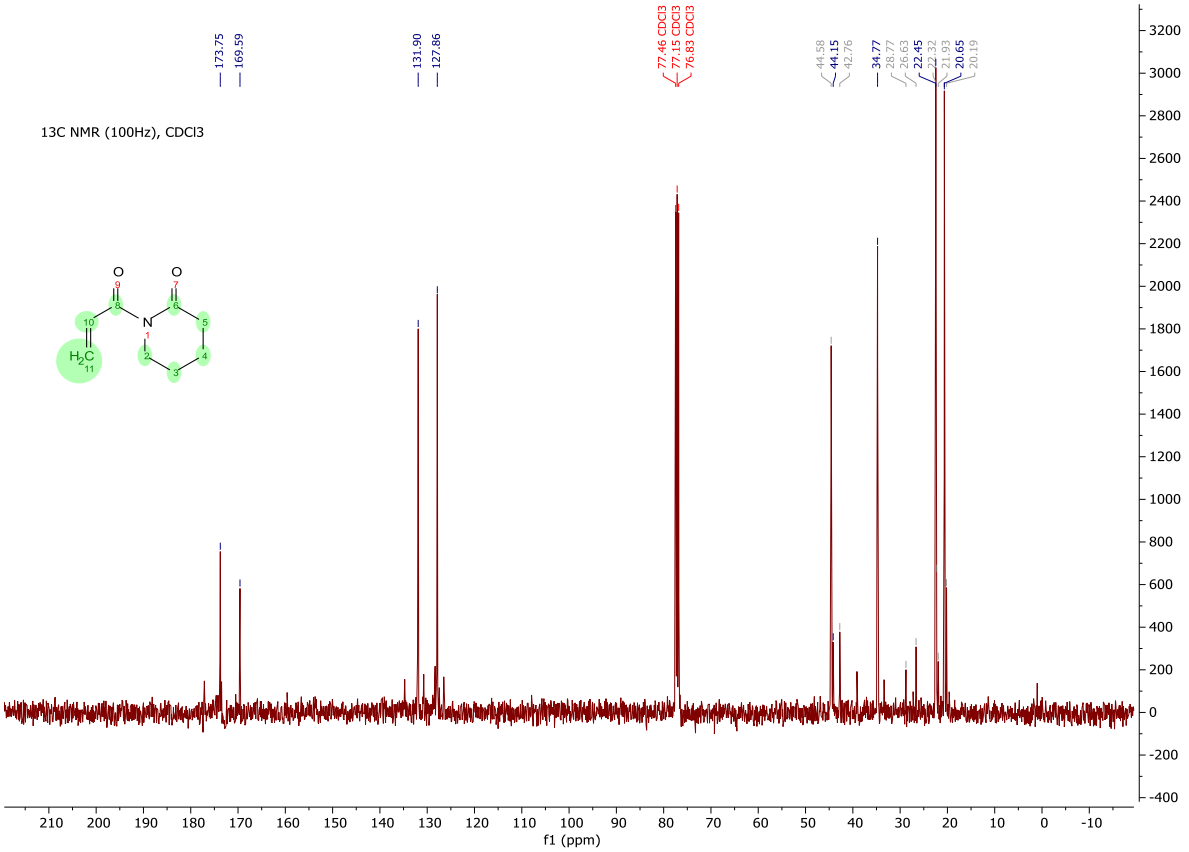

5-Benzyl-1,5-diazecane-2,6-dione (Compound 3G)

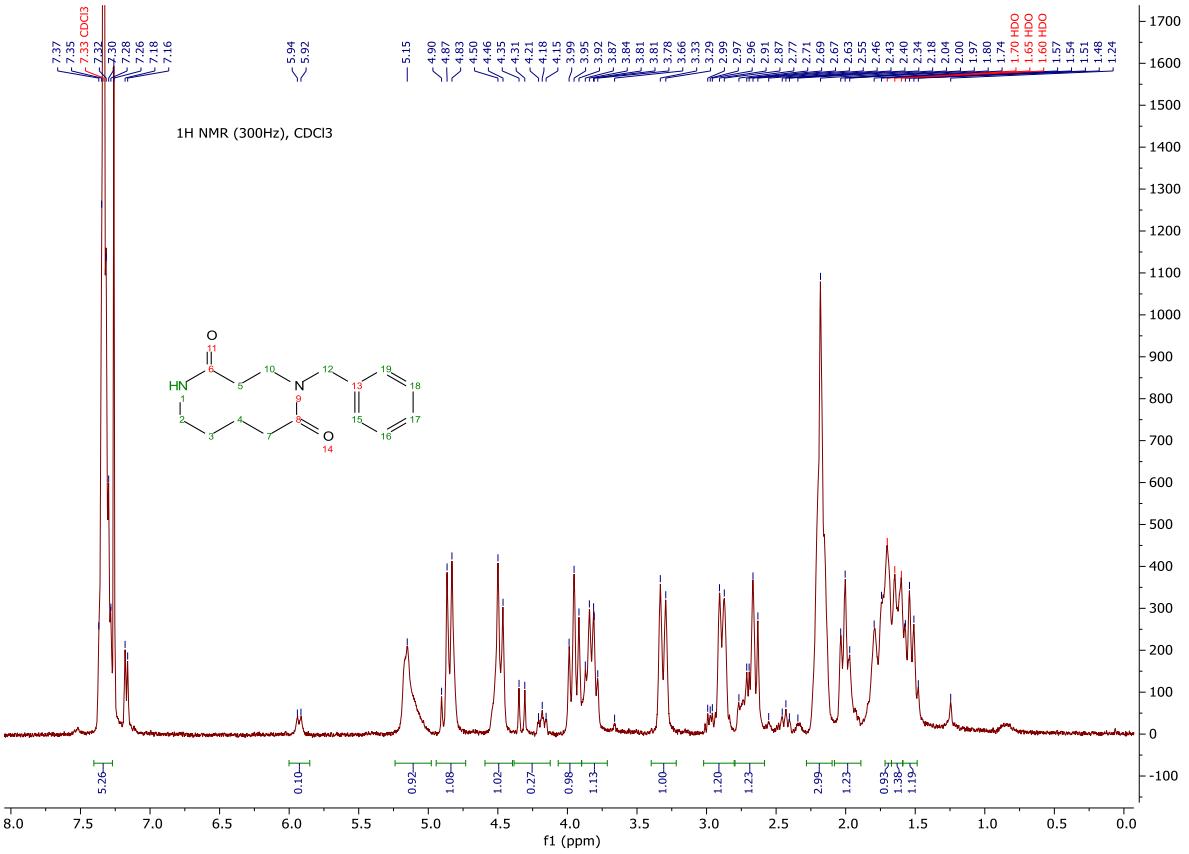

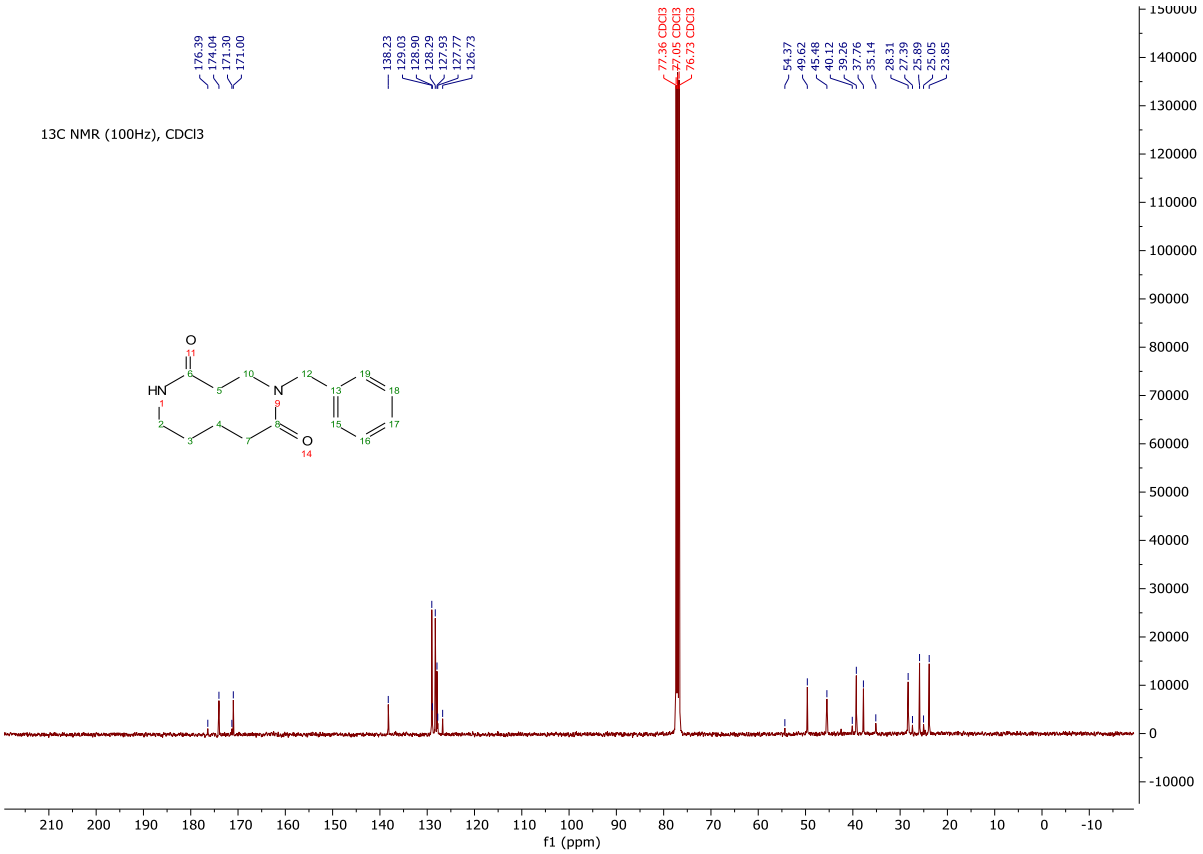
13C NMR (100Hz), CDCl3
176.39
174.04
171.30
171.00
138.23
129.03
128.90
128.29
127.93
127.77
126.73
77.36 CDCl3
77.05 CDCl3
76.73 CDCl3
54.37
49.62
45.48
40.12
39.26
37.76
35.14
28.31
27.39
25.89
25.05
23.85
f1 (ppm)

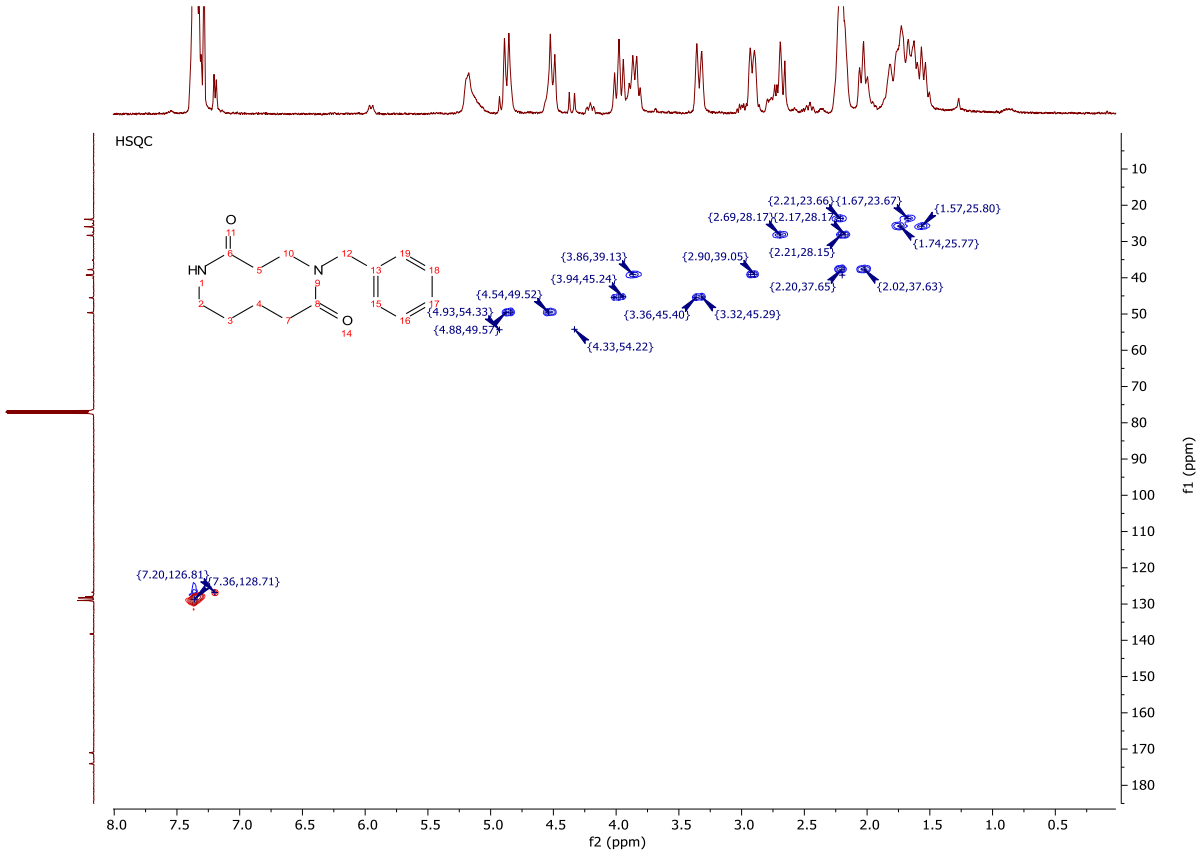
HSQC
{2.21,23.66}
{1.67,23.67}
{1.57,25.80}
{2.69,28.17}
{2.17,28.17}
{2.21,28.15}
{1.74,25.77}
{3.86,39.13}
{2.90,39.05}
{3.94,45.24}
{2.20,37.65}
{2.02,37.63}
{4.54,49.52}
{4.93,54.33}
{3.36,45.40}
{3.32,45.29}
{4.88,49.57}
{4.33,54.22}
{7.20,126.81}
{7.36,128.71}
f2 (ppm)
f1 (ppm)

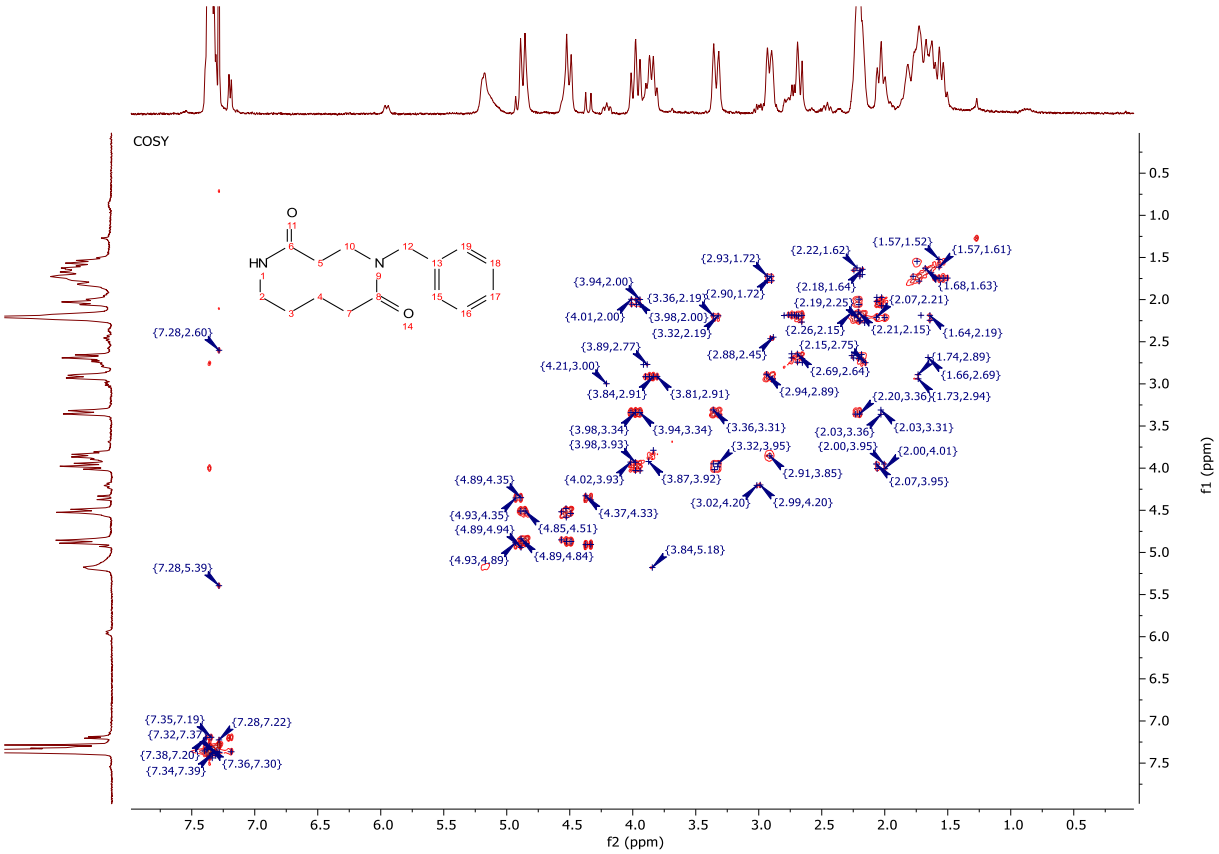

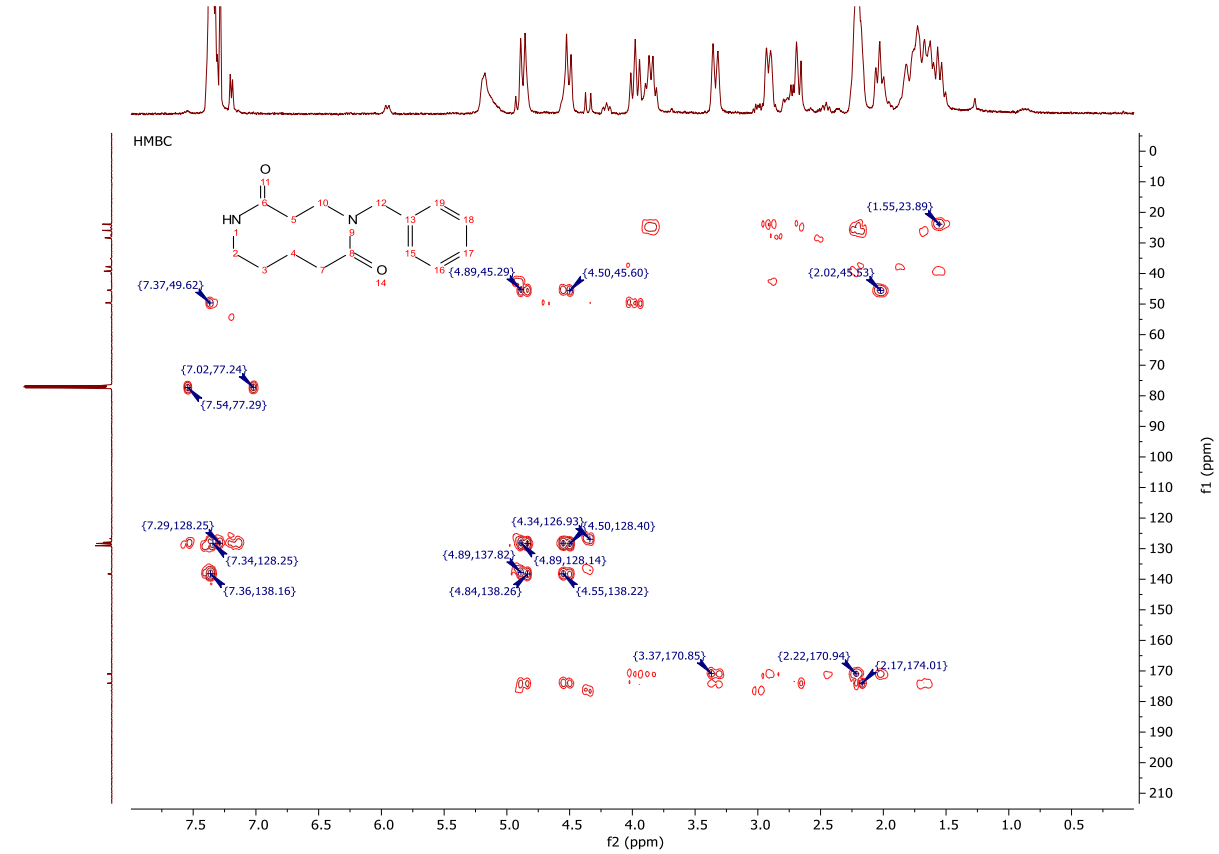

1-(3-Bromopropyl)-3,4-dihydroquinolin-2(1*H*)-one (Compound 3J)

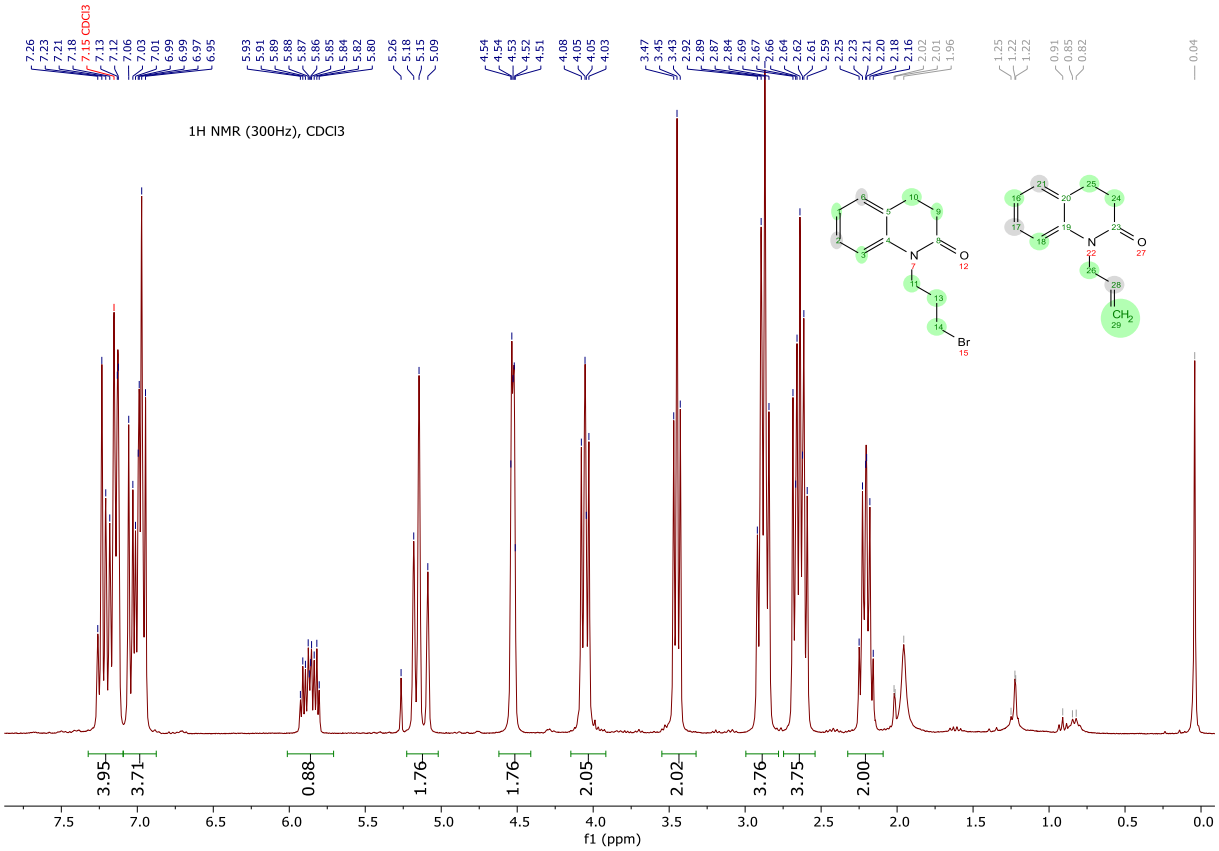

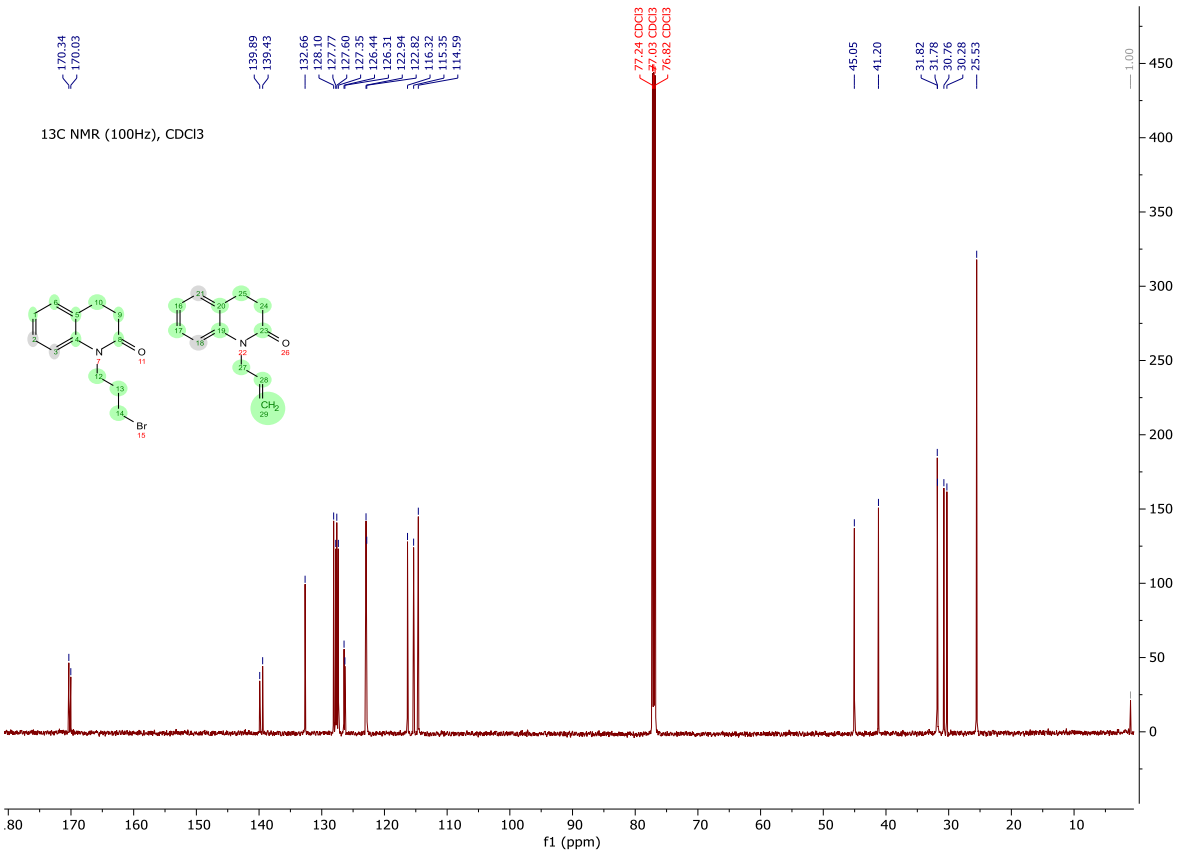

2,3,4,5,7,8-Hexahydrobenzo[f][1,5]diazecin-6(1*H*)-one (Compound 3L)

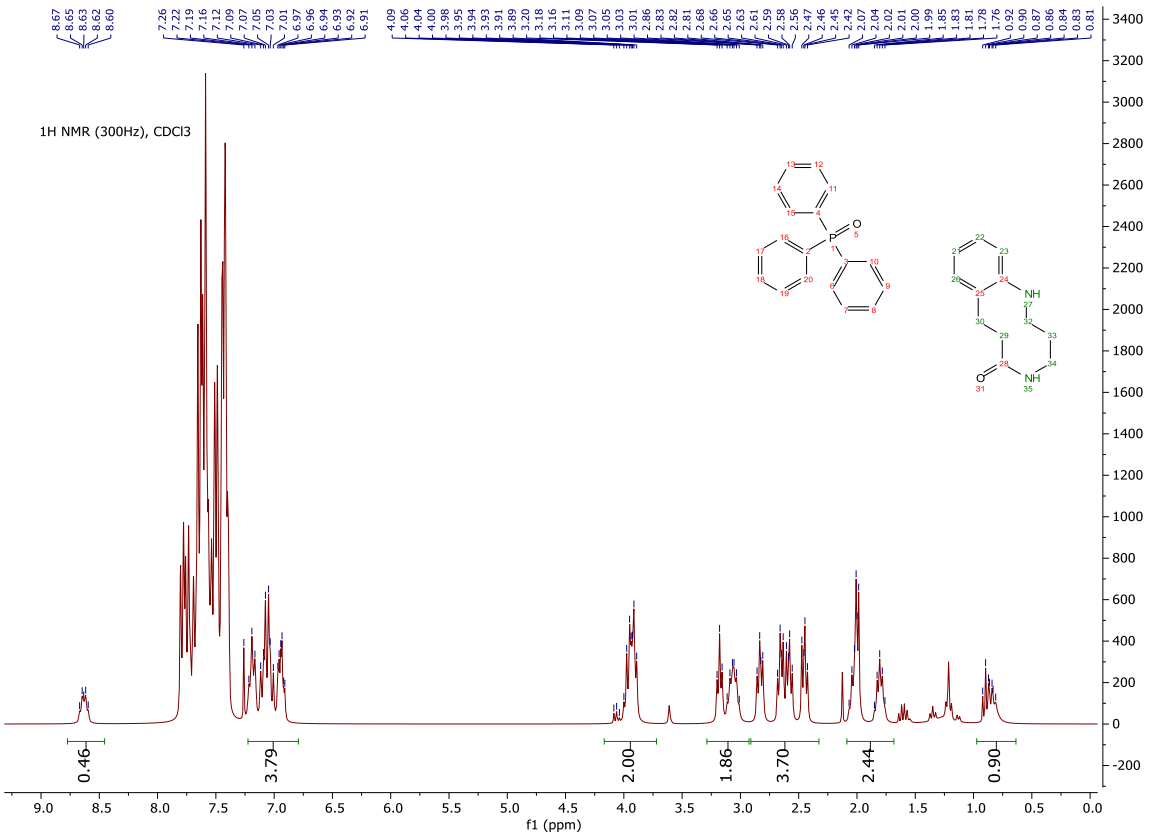

(9*H*-Fluoren-9-yl)methylbenzyl(3-oxo-3-(2-oxo-3,4-dihydroquinolin-1(2*H*)-yl)-1-phenylpropyl)carbamate (Compound 3M)

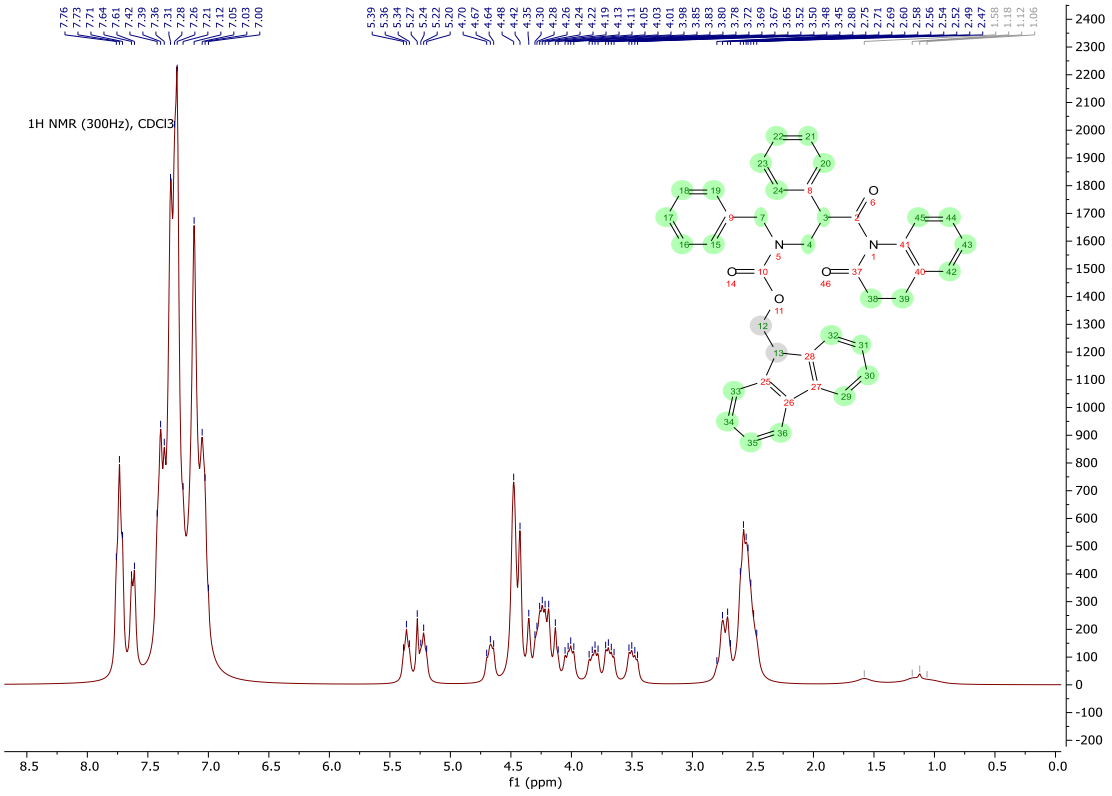

1,6-Dimethyl-3-phenylquinolin-2(1*H*)-one (Compound 4A)

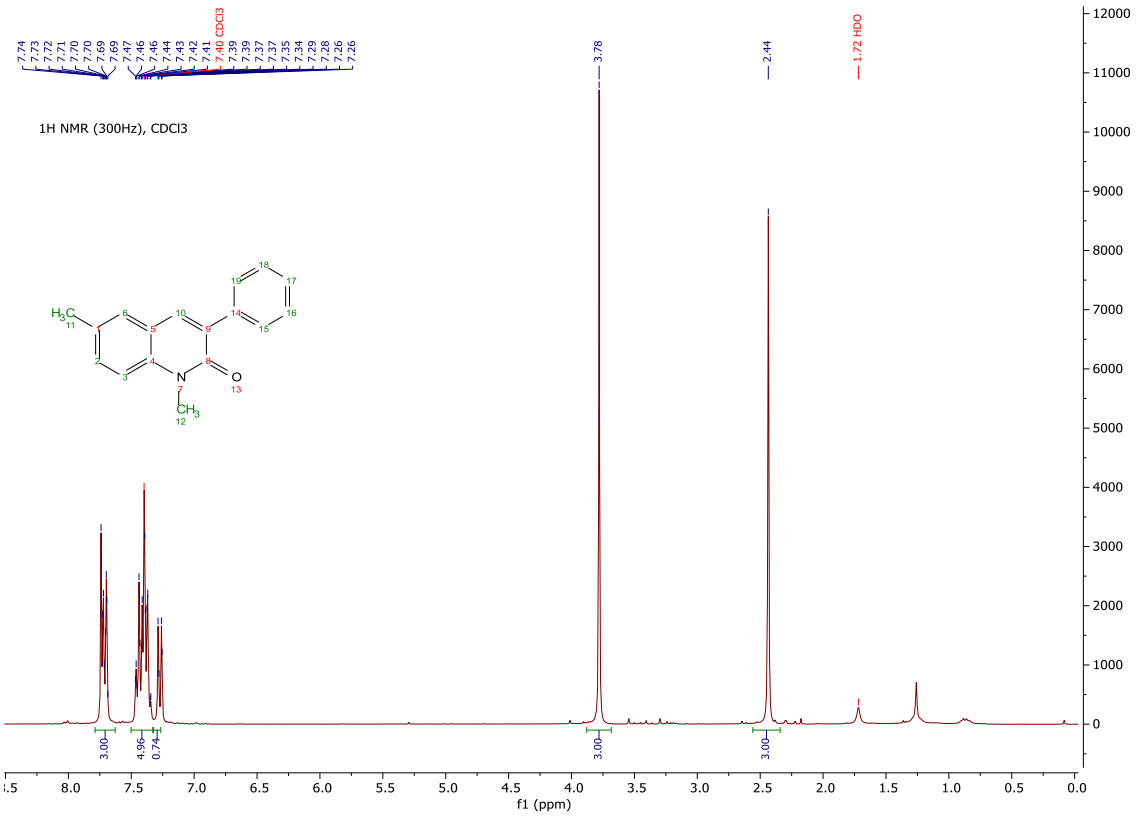

1-Benzylquinolin-2(1*H*)-one (Compound 4B)

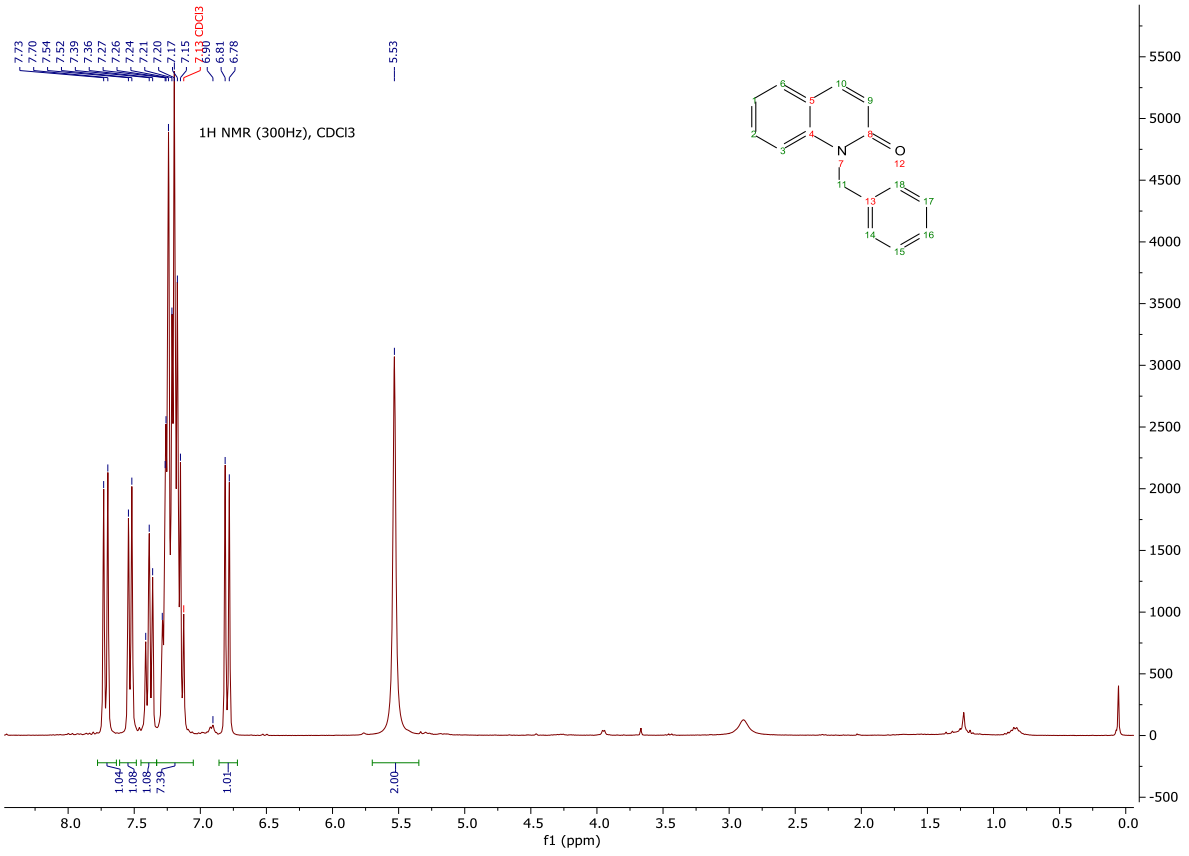

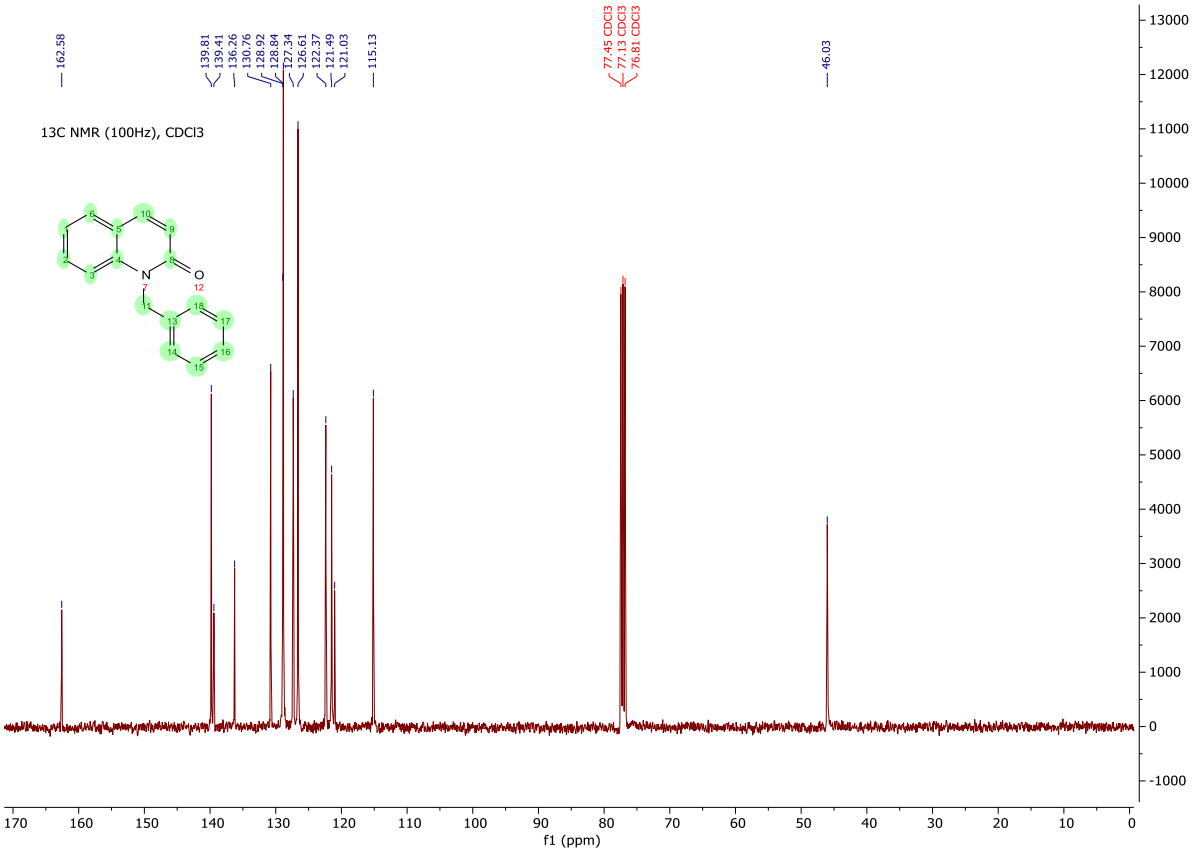

2H-Chromen-2-one (Compound 4C)

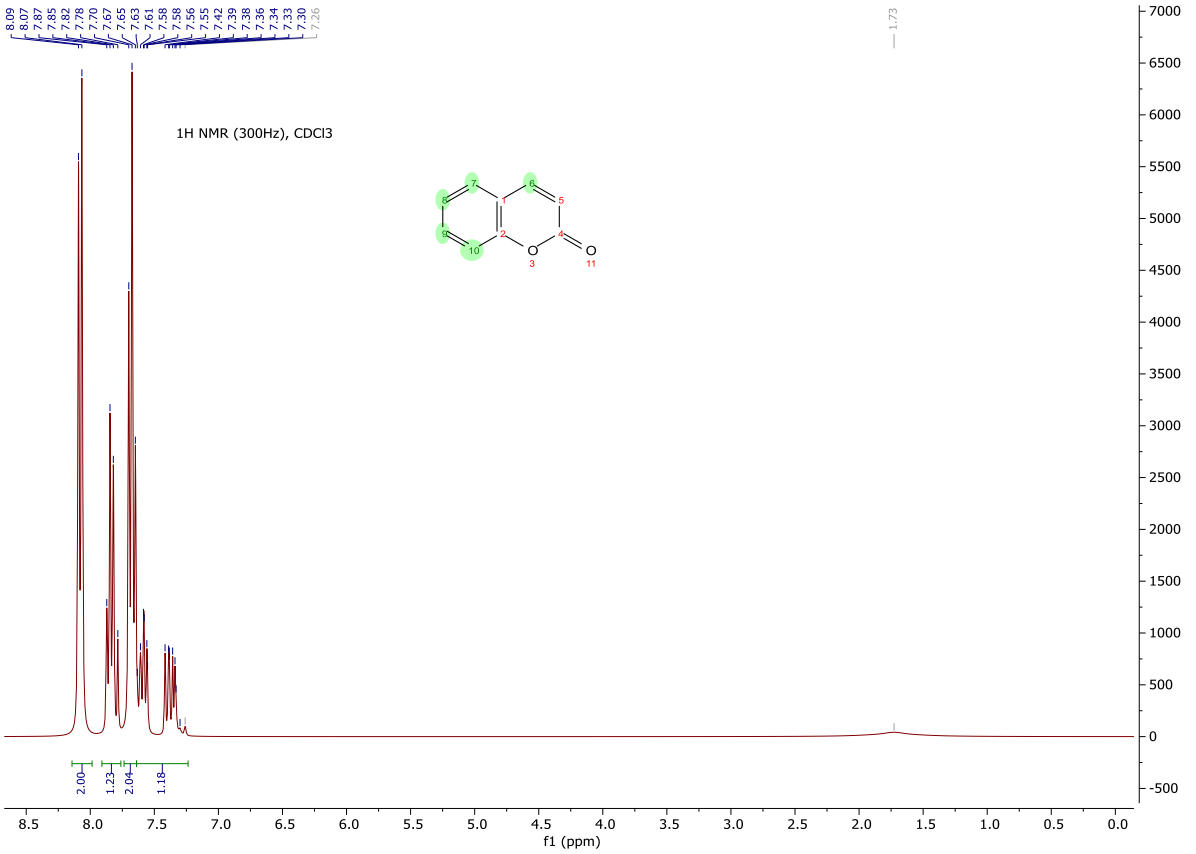

Quinolin-2(1*H*)-one (Compound 4D)

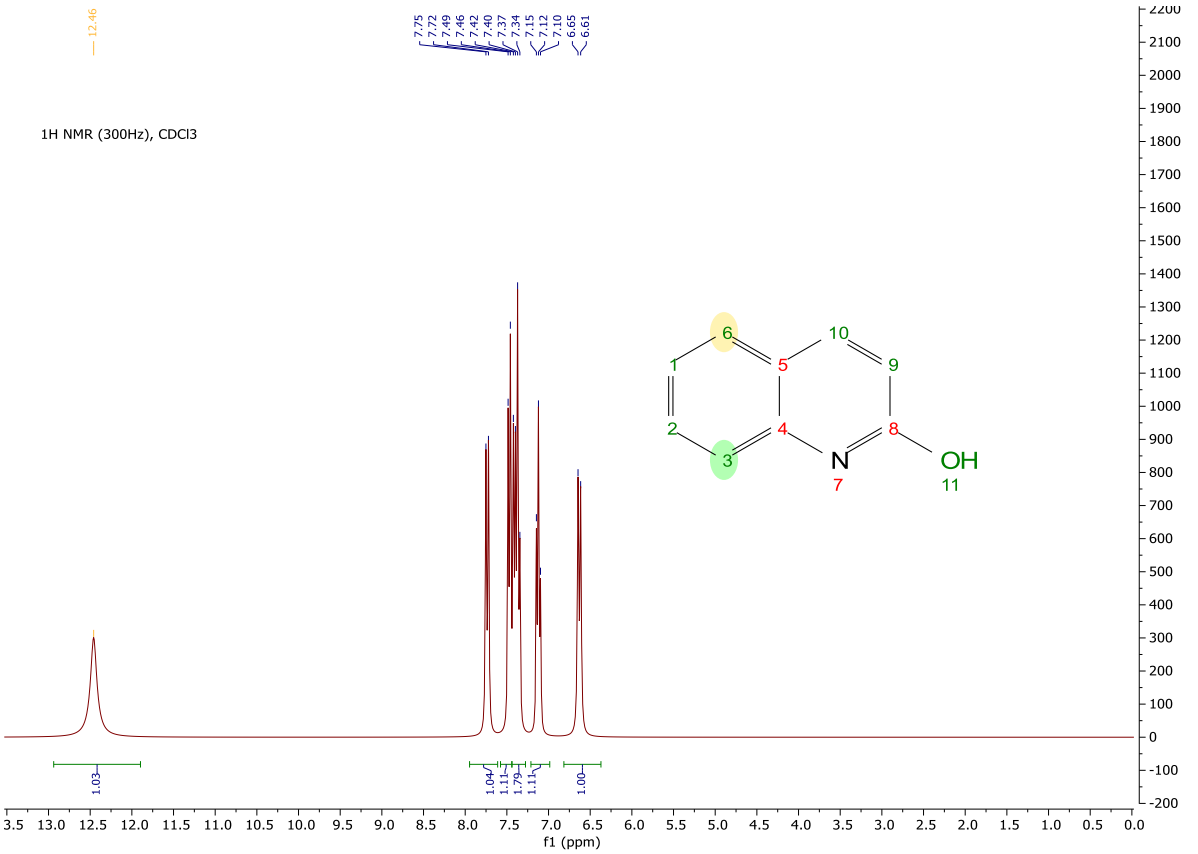

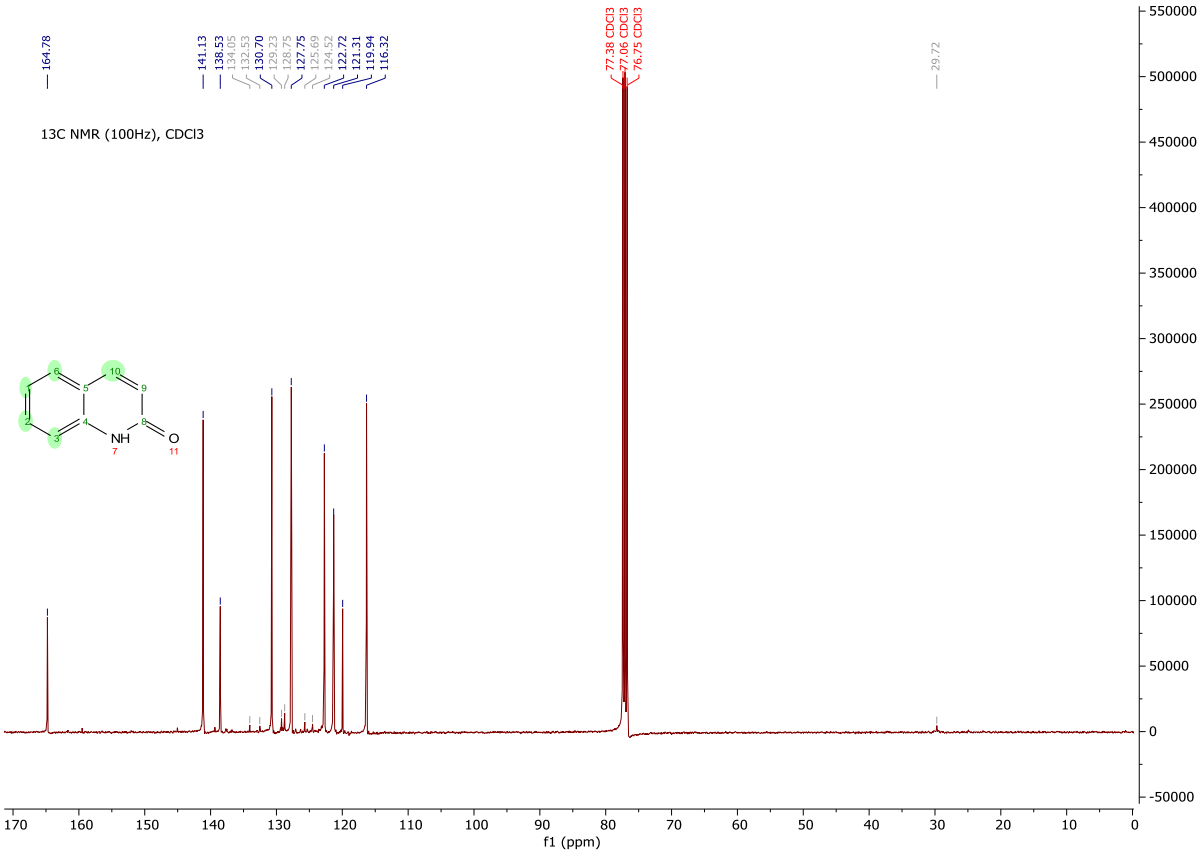

1-Allylquinolin-2(1*H*)-one (Compound 4E)

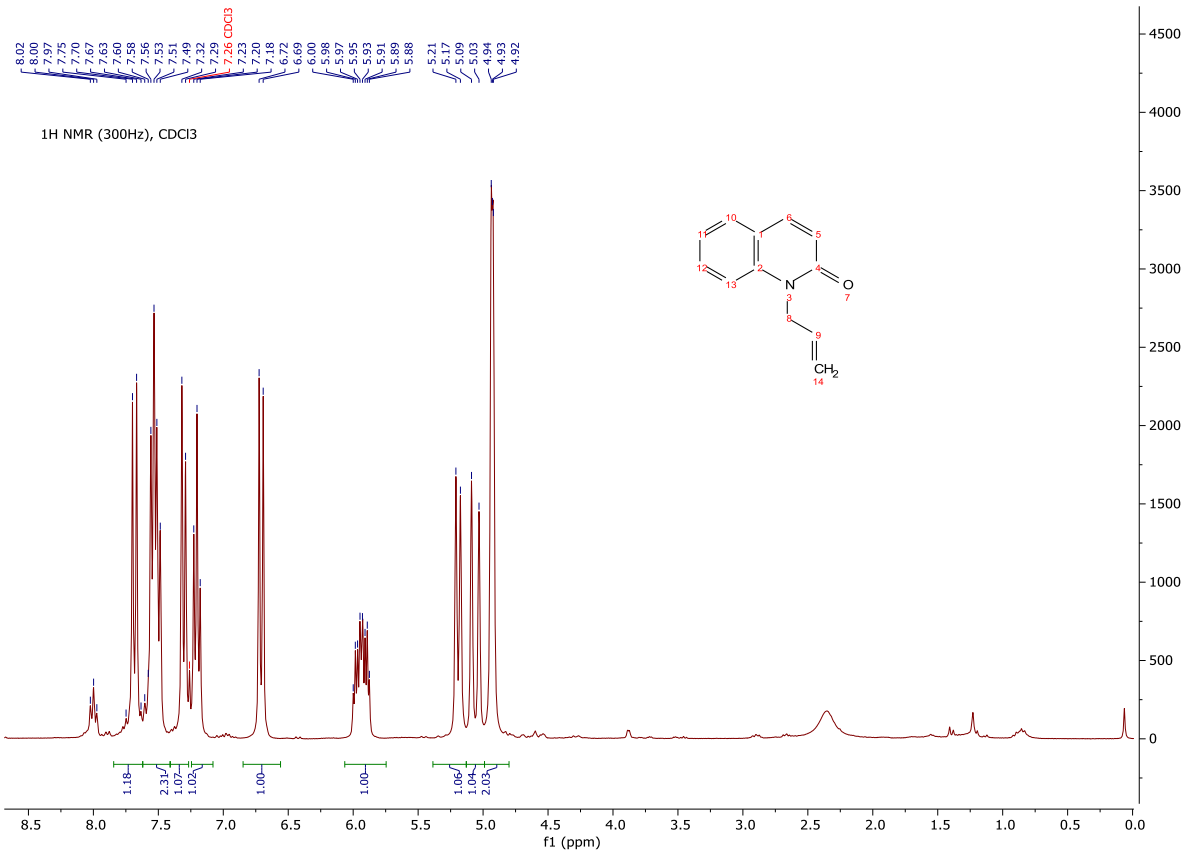

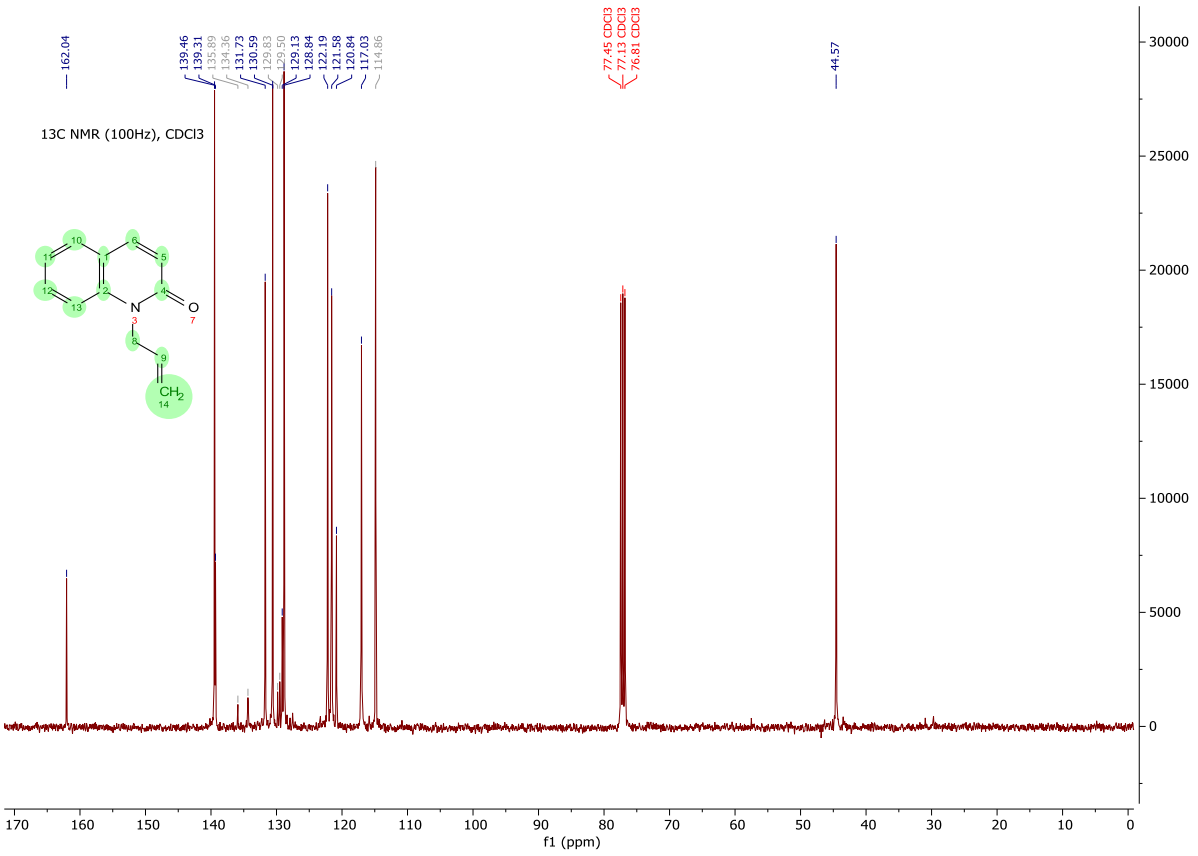

7-Phenyl-[1,3]dioxolo[4,5-g]quinolin-6(5*H*)-one (Compound 4F)

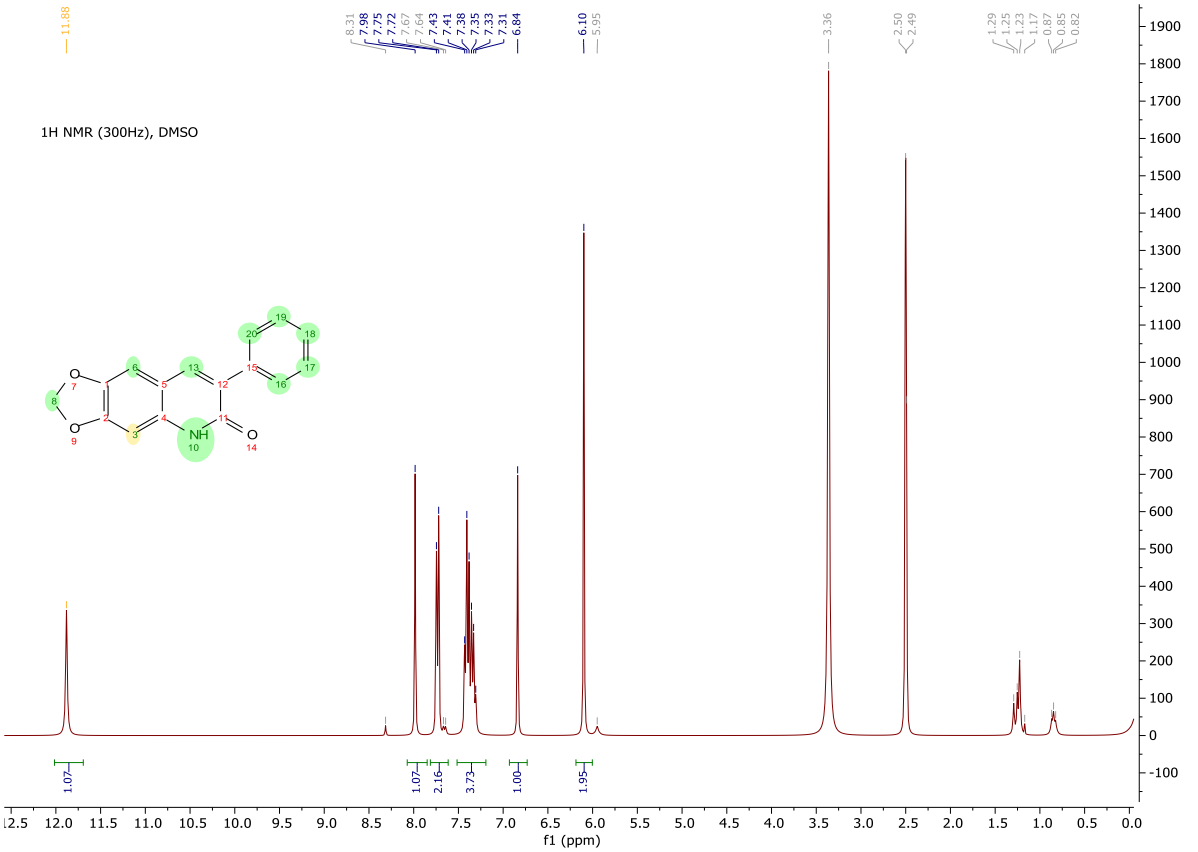

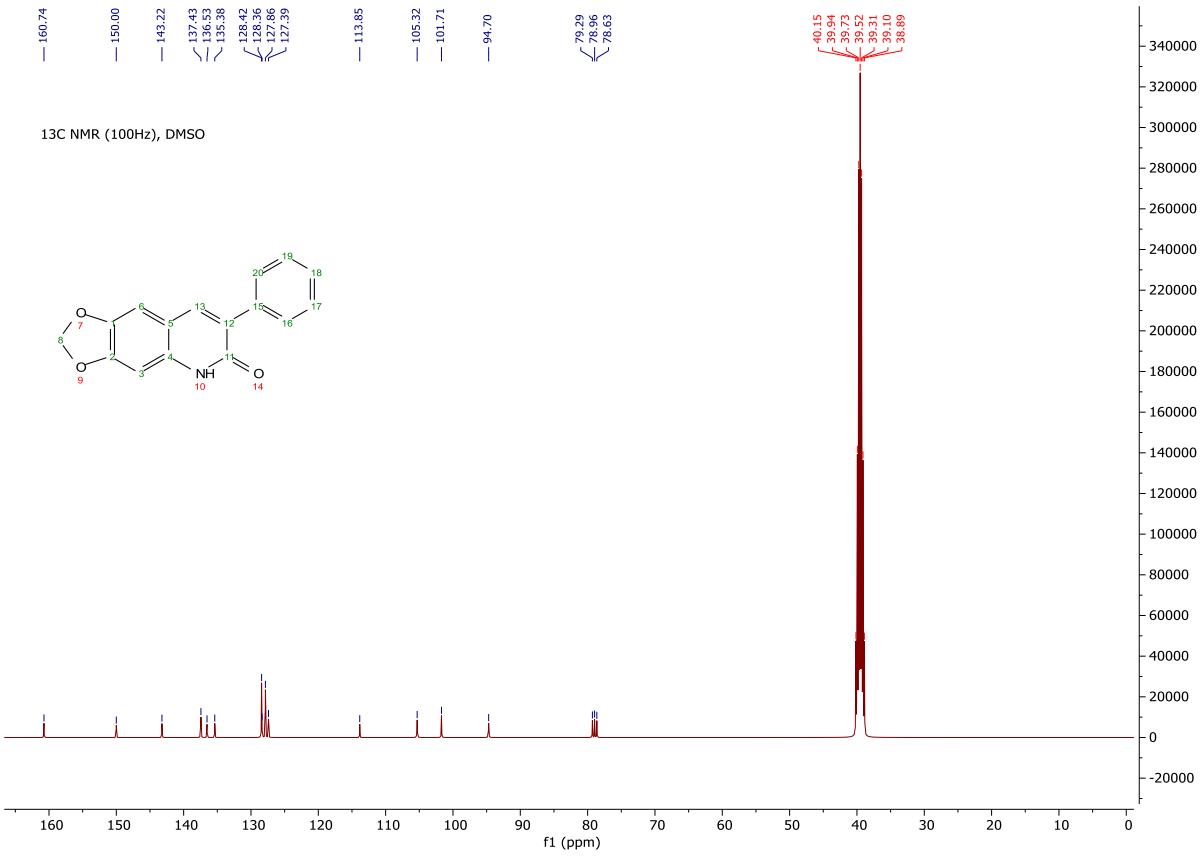

1-Benzyl-7-methoxyquinolin-2(1*H*)-one (Compound 4G)

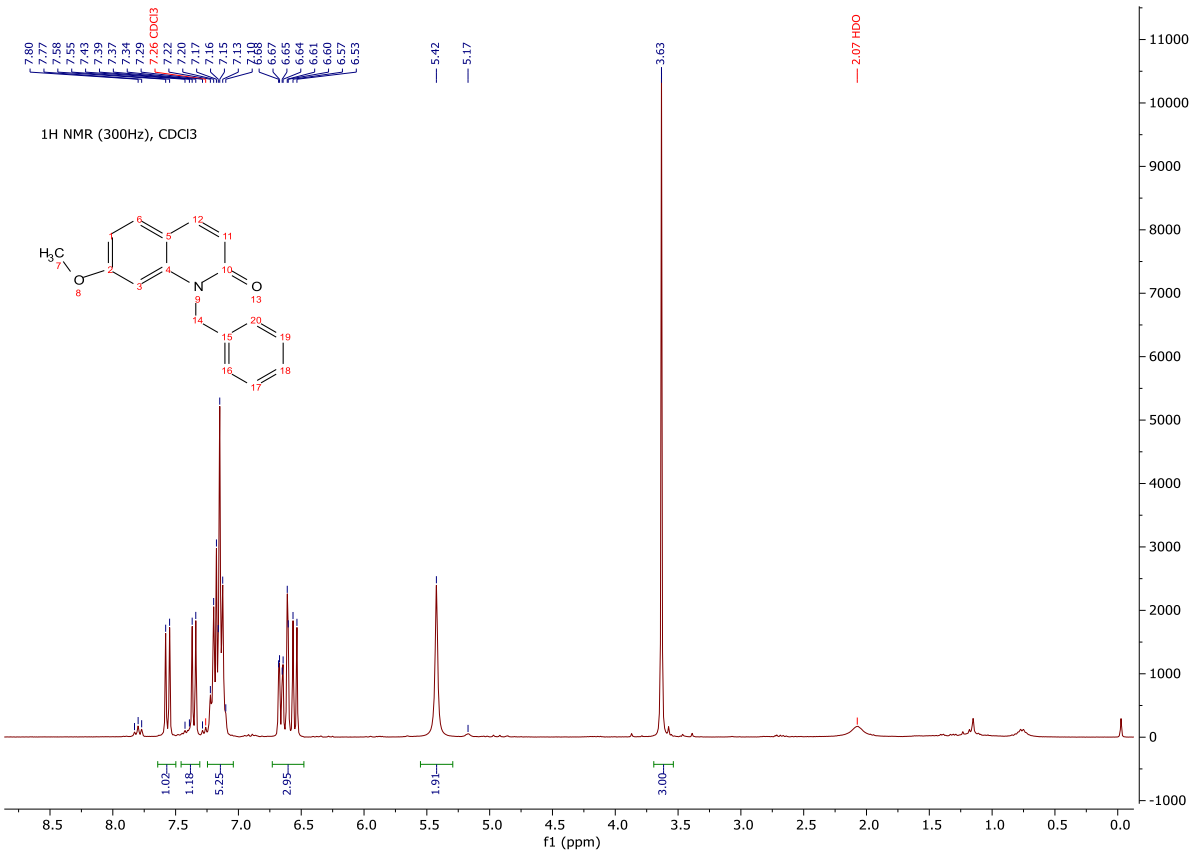

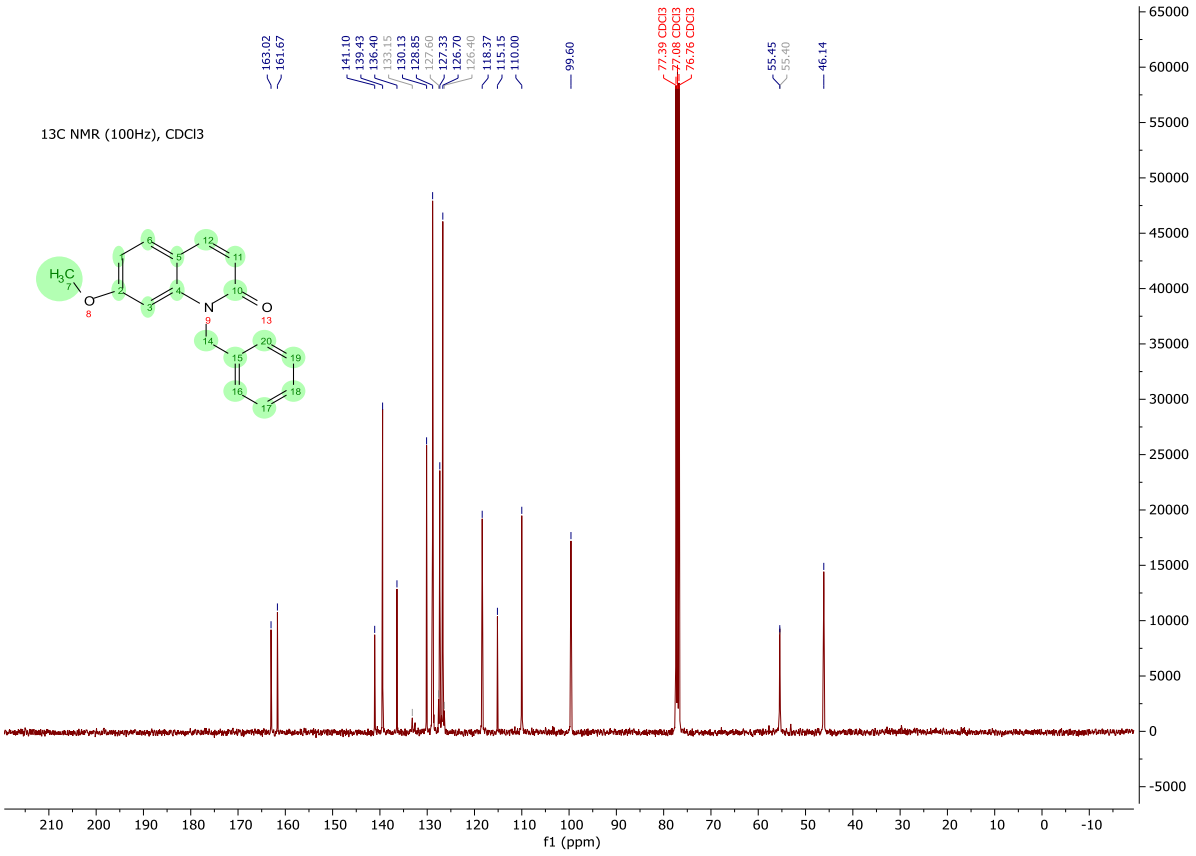

7-(*Tert*-butyl)-3-phenylquinolin-2(1*H*)-one (Compound 4H)

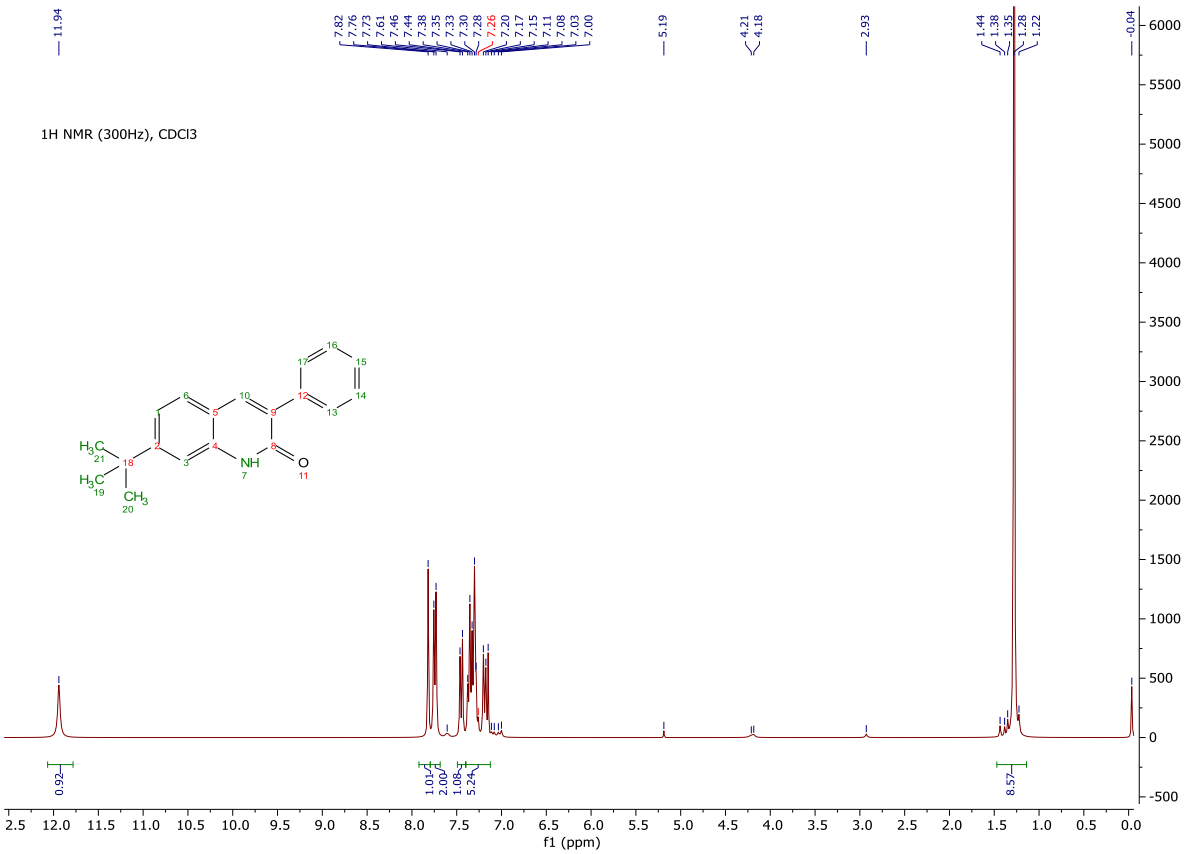

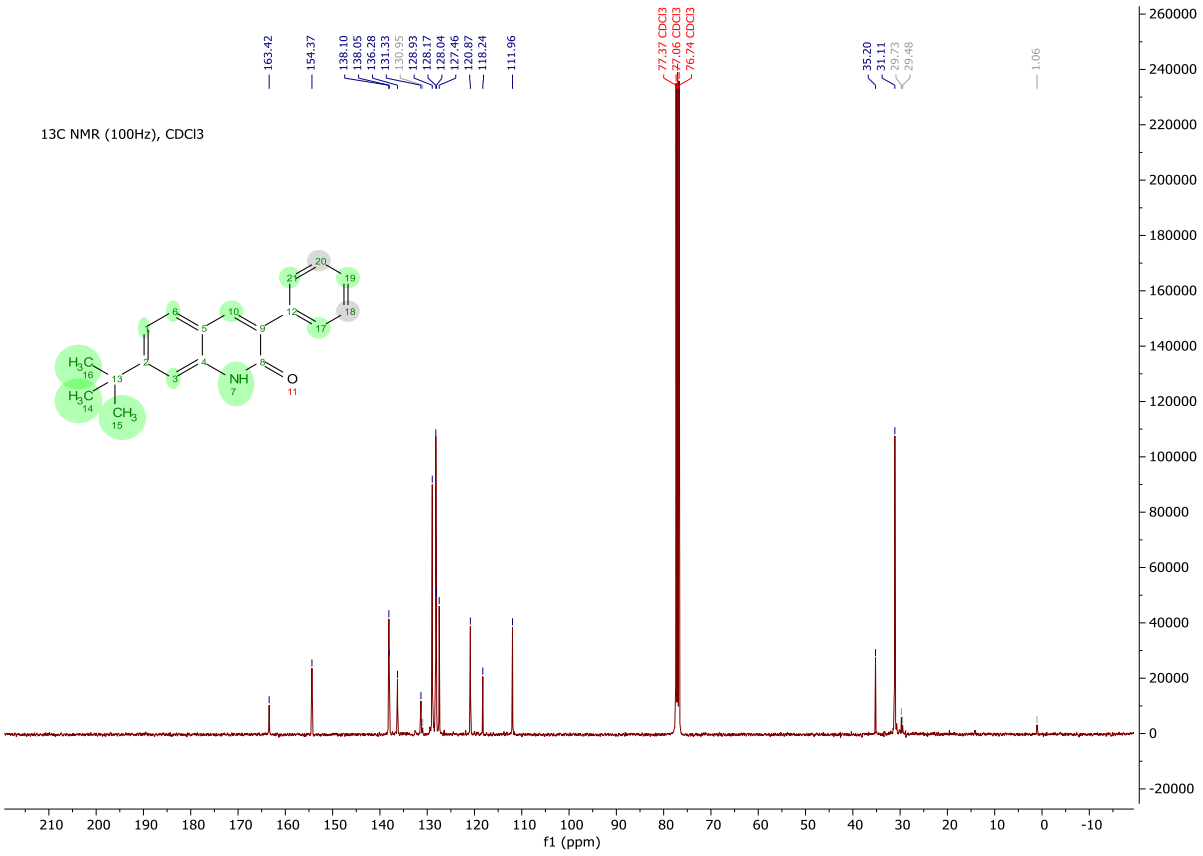

7-Methoxyquinolin-2(1*H*)-one (Compound 4I)

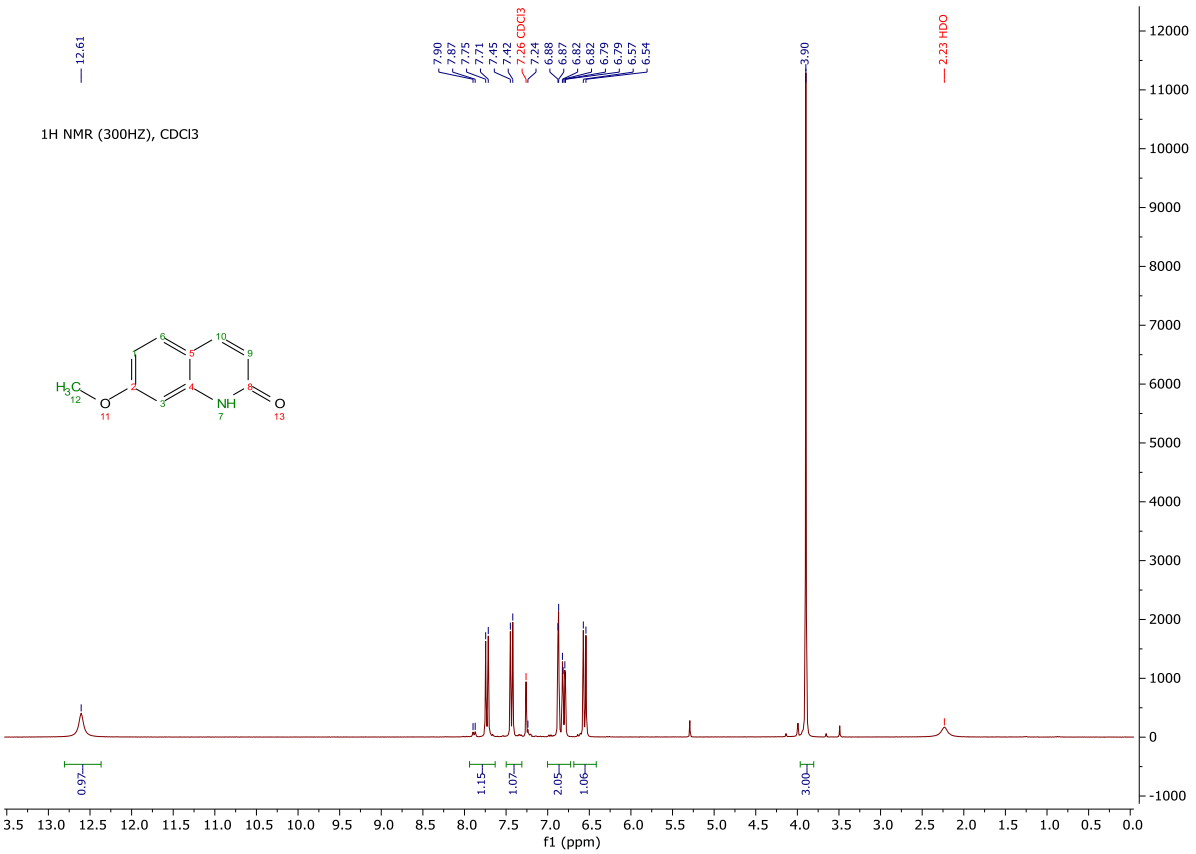
12.61
7.90
7.87
7.75
7.71
7.45
7.42
7.26 CDCl3
7.24
6.88
6.87
6.82
6.82
6.79
6.79
6.57
6.54
3.90
2.23 HDO
1H NMR (300HZ), CDCl3
H3C
12
O
11
2
3
4
NH
7
5
6
8
9
10
O
13
0.97
1.15
1.07
2.05
1.06
3.00
f1 (ppm)